Lung-Targeted Receptor Occupancy by Drug Inhalation: an Experimental and Computational Evaluation

by

Elin Boger

A thesis submitted for the degree of

Doctor of Philosophy in Engineering

University of Warwick, School of Engineering

May 2016

"*We shall not cease from exploration, and the end of all our exploring will be to arrive where we started and know the place for the first time*"
T.S. Eliot

Table of contents

List of figures

List of tables

Acknowledgements

So many people have been instrumental in the completion of this PhD project and I am forever grateful for their support. First and foremost I would like to thank my main supervisor Dr Markus Fridén, who guided me, not only scientifically but also personally, towards becoming a more senior scientist. I am very grateful for all our discussions and I keep to be stunned by your insightfulness. Thanks also for finding the delicate balance of initially setting much time aside for supervision to gradually decrease the guidance to ensure that I would develop into an independent researcher. I would also like to thank my academic supervisors Dr Michael Chappell and Dr Neil Evans for their invaluable guidance and support throughout my studies. My co-supervisors Dr Pär Ewing and Prof Margareta Hammarlund-Udenaes have both been important discussion partners during the journey of this PhD.

I would like to express my sincere gratitude to the Marie Curie FP7 People ITN European Industrial Doctorate (EID) [Project No.316736] for funding this research.

I would also like to express my appreciation to everyone at RIA DMPK at AstraZeneca for creating a friendly and warm working environment where laughter is as important as science. Many scientists at AstraZeneca have provided important guidance and support for completing this research and some names stand out. I would like extend my sincere gratitude to Susanne Arlbrandt, Dr Britt-Marie Fihn, Kajsa Claesson, Louise Hammarberg, Marie Johansson and Gina Hyberg for their invaluable contributions to the *in vivo* studies. I cannot emphasise enough how impressed I am by your laboratory skills. Another contribution, which indeed constituted a step-change for this project, was the improved bioanalytical methodology for FP conducted by Dr Anders Lundqvist. That particular analysis enabled the important validation of the developed model's ability to predict the

systemic PK and I am deeply grateful for this contribution. Sara Johansson and Annica Jarke are acknowledged for their help with formulating nanosuspensions of FP and budesonide for the PK studies. I would also like to thank Anders Wigenborg for controlling and operating the inhalation system as well as setting time aside to explain to me how it works. Furthermore, I would like to thank Dr Jan Westergren, Dr Ulrika Tehler and Dr Ulf Eriksson for fruitful discussions.

I was exceptionally fortunate to have Erica Bäckström sitting next to me at AZ, being the best possible office neighbour! Besides having great (and perhaps a bit geeky) scientific discussions on inhalation pharmacokinetics, we have laughed enough to extend our lives by several years. Thanks for being awesome!

I would also like to thank each and everyone of the Biomedical Superheroes for making my time in the UK a great experience. In particular I would like to thank Magnus Trägårdh and Linnéa Bergenholm. Magnus has, despite his perhaps slightly overly optimistic attitude, been a great support for me on several levels. I have learned a lot from our various discussions, but first and foremost thanks for being a great friend. Linnéa, thanks for sharing your seemingly endless energy, optimism and for making everyday life much more fun. Once my knee gets better, I'm sure we will climb Mount Everest!

My friends and family have been very supportive, understanding and encouraging during this PhD journey. Most importantly, you have done what you do best; been yourself and I am just so happy to be surrounded by you guys! In particular, I would like to thank mum, dad, Frida and "stor-Oskar". Thanks for your endless support and for always being there for me.

I also want to take the opportunity to thank my gym and my running routes for providing exceptional tools for effectively controlling the fluctuating stress levels of

a PhD student. I am confident that I have never been stronger than I am at the time of writing.

And last but not least, I would like to thank Oskar. Clearly, no words are worthy to describe how grateful I am to have you in my life and for how you have supported me during this journey. Thanks for everything –you make me complete.

Declaration

This thesis is submitted to the University of Warwick in support of my application for the degree of Doctor of Philosophy. It has been composed by myself and has not been submitted in any previous application for any degree apart from the experiments described in sections '3.2.1.2 Tracer identification *in vitro*' and '3.2.1.4 Evaluation of tracer dose' which was previously submitted for a master's degree. The experiment described in section '3.2.1.5 Evaluation of nonspecific binding' was done whilst I was employed at AstraZeneca R&D. The mathematical modelling of the aforementioned data was all performed as part of this project. This thesis has not been submitted for a degree at any other university.

Where any of the content presented in this thesis is the result from collaborative research this is clearly stated in the text such that it is possible to ascertain how much of the work is my own.

Parts of this thesis have been published by the author:

Journal articles:

Boger, E., Ewing, P., Eriksson, U.G., Fihn, B.M., Chappell, M., Evans, N. & Fridén, M. (2015). A novel *in vivo* receptor occupancy methodology for the glucocorticoid receptor: towards an improved understanding of lung PK/PD. The *Journal of Pharmacology and Experimental Therapeutics*, 353(2), 279-287.

Boger, E., Evans, N., Chappell, M., Lundqvist, A., Ewing, P., Wigenborg, A. & Fridén, M. (2016). A systems pharmacology approach for prediction of pulmonary

and systemic pharmacokinetics and receptor occupancy of inhaled drugs. *CPT: Pharmacometrics & Systems Pharmacology*, 5(4), 201-210.

Conferences:

Boger, E., Evans, N., Chappell, M., Lundqvist, A., Ewing, P., Wigenborg, A. & Fridén, M. A systems pharmacology approach for prediction of pulmonary and systemic pharmacokinetics and receptor occupancy of inhaled drugs, PKUK Conference 2015: Programme and Abstract Book. *PKUK Conference 2015*, Chester, UK, 18-20 November 2015.

Fridén, M., Boger, E., A Systems Pharmacology Approach for Prediction of Systemic and Pulmonary PK for Inhaled Drugs. Oral presentation at *QSP Europe*, Basel, Switzerland, 29 April, 2015

Fridén, M., Boger, E., Towards estimation of unbound drug concentrations in the lung: utility of lung slices and target occupancy methodologies. Oral presentation at *Phys Chem Forum*, Uppsala, Sweden, January 29, 2015

Boger, E., Evans, N., Chappell, M., Lundqvist, A., Ewing, P., Wigenborg, A. & Fridén, M., Development of a PBPK model with lung disposition – towards an increased understanding of PK and PK/PD for inhaled drugs. Presented at *AstraZeneca's Modelling and Simulation Symposium*, Mölndal, Sweden, 17-18 December, 2014

Fridén, M., Boger, E., Glucocorticoid receptor occupancy and PBPK-PD models for inhalation. Oral presentation at *AstraZeneca modeling and simulation symposium*, Mölndal, Sweden, 17 December 2014

Boger, E., Ewing, P., Eriksson, U.G., Fihn, B.M., Chappell, M., Evans, N. & Fridén, M. Development and application of a novel pulmonary *in vivo* receptor occupancy methodology for the glucocorticoid receptor, PKUK Conference 2014: Programme and Abstract Book. *PKUK Conference 2014*, Bath, UK, 5-7 November 2014.

Boger, E., Ewing, P., Eriksson, U.G., Fihn, B.M., Chappell, M., Evans, N. & Fridén, M. Development and Application of a Novel Pulmonary in vivo Target Occupancy Methodology for the Glucocorticoid Receptor. Presented at *AAPS*, San Diego, USA, 2-6 November, 2014

Boger, E., Ewing, P., Eriksson, U.G., Fihn, B.M., Chappell, M., M., Evans, Jirstrand, M., Hammarlund-Udenaes & M., Fridén M. Development of a novel pulmonary *in vivo* target occupancy methodology for the glucocorticoid receptor. Oral presentation at *AstraZeneca Modelling & Simulation Symposium*, Alderley Park, 3-4 December 2013

Boger, E., Ewing, P., Eriksson, U.G., Fihn, B.M., Chappell, M., M., Evans, Jirstrand, M., Hammarlund-Udenaes & M., Fridén M. Development of a novel pulmonary *in vivo* target occupancy methodology for the glucocorticoid receptor, PKUK Conference 2013: Programme and Abstract Book. *PKUK Conference 2013*, Harrogate, UK, 1-2 November 2013.

Abstract

Inhalation is attractive for treating respiratory diseases since it offers an opportunity to achieve lung-selectivity, i.e. high local and low systemic levels of unbound drug. Nevertheless, evaluation and prediction of the former is challenging for reasons including: 1) the unbound blood concentration cannot be assumed to reflect the free lung target site exposure after inhalation, 2) it is not possible directly measure unbound drug concentrations locally in the lung, and 3) pulmonary drug disposition is known to be a complex interplay between numerous processes. This thesis therefore aims to increase the understanding of how different drug- and formulation-specific properties relate to the free target site exposure to inhaled drug. This was done by: 1) developing and subsequently applying an experimental methodology for measuring pulmonary and systemic occupancy of a receptor targeted by inhaled drugs, and 2) developing a rat physiologically-based pharmacokinetic (PBPK) model, which mechanistically describes underlying processes of pulmonary drug disposition. Experimental studies provided data on the time-course of the PK and receptor occupancy after intravenous (IV) and inhaled drug delivery of fluticasone propionate (FP). The binding kinetics parameters, which were estimated from data generated after IV-dosing, were used as input parameters to the developed model together with other properties specific to FP. The model accurately described the PK and receptor binding for several IV-doses. Predictions were consistent with the observations from inhalation studies, confirming that FP has a dissolution rate-limited absorption and highlighting that drug in solid state does not contribute to receptor binding. As the model is mechanistic, it can assess how different drug- and formulation-specific properties, or combinations thereof, give rise to lung-selectivity. Specific findings include lung-selectivity possibly being unattainable in well-perfused lung regions and that slow drug-receptor dissociation can provide lung-selectivity. Hence, the model lends itself to guiding the design of inhaled compounds and formulations.

List of abbreviations

ADME	Absorption, distribution, metabolism and excretion
ANOVA	Analysis of variance
AUC	Area under the curve
BAL	Broncho-alveolar lavage
BDP	Beclomethasone dipropionate
B_{max}	Receptor density
$C_{control}$	Tissue concentration of tracer in drug-naïve control animals
C_{ELF}	Total drug concentration in the epithelial lining fluid
CL	Clearance
CL_b	Blood clearance
CL_p	Plasma clearance
C_{lung}	Total drug concentration in the lung
$C_{nonspec}$	Nonspecific tissue concentration of tracer
COPD	Chronic Obstructive Pulmonary Disease
C_p	Total drug concentration in the plasma
C_s	Solubility
$C_{spec,max}$	Maximum specific tissue concentration of tracer
C_{spleen}	Total drug concentration in the spleen
C_{test}	Tissue concentration of tracer in test animals
CYP	Cytochrome P450
D	Diffusion coefficient
d_a	Aerodynamic diameter
d_g	Geometric diameter

ED_{50}	Dose giving 50% efficacy
E_H	Hepatic extraction ratio
ELF	Epithelial lining fluid
F	Bioavailability
f_{abs}	Fraction absorbed from the gastroinstestinal tract
FaSSIF	Fasted-state small intestinal fluid
FDA	Food and Drug Administration
FEV	Forced expiratory volume
f_{gut}	Fraction that escapes gut extraction
f_h	Fraction that escapes hepatic extraction
FP	Fluticasone propionate
f_{tb}	Target-bound fraction
f_u	Fraction unbound in plasma
$f_{u,fluid}$	Unbound fraction in the ELF or the nasal lining fluid
$f_{u,h}$	Fraction unbound in lung homogenate
GI	Gastrointestinal
GR	Glucocorticoid receptor
ICS	Inhaled corticosteroids
ID	Total inhaled dose
IT	Intratracheal
IV	Intravenous
K_d	Dissociation constant
K_{off}	Dissociation rate constant
K_{on}	Association rate constant
K_p	Tissue-to-plasma partition coefficient

$K_{p,u}$	Tissue-to-unbound plasma partition coefficient
LADME	Liberation, absorption, distribution, metabolism and excretion
LC-MS/MS	Liquid chromatography tandem mass spectrometry
LDD	Lung deposited dose
LLE	Liquid liquid extraction
LLOQ	Lower limit of quantification
log$D_{7.4}$	The logarithm of the ratio of concentrations of a compound (unionized+ionized) between octanol and water buffered to pH 7.4
log*P*	The logarithm of the ratio of the concentrations of a compound (unionized) between octanol and water
MCC	Mucociliary clearance
MMAD	Mass Median Aerodynamic Diameter
MTBE	Methyl-tertbutyl ether
ODE	Ordinary differential equation
P	Permeability
P_{app}	Apparent permeability
PBPK	Physiologically-based pharmacokinetic
PD	Pharmacodynamics
PEF	Peak expiratory flow
PET	Positron emission tomography
PK	Pharmacokinetics
RO_{ave}	Weighted average of receptor occupancy in the central and peripheral lung

RO_c	Receptor occupancy in the central lung
RO_p	Receptor occupancy in the peripheral lung
RO_{spleen}	Receptor occupancy in the spleen
SPE	Solid phase extraction
Stk	Stokes number
TI	Therapeutic index
V_d	Apparent volume of distribution
V_{dss}	Steady state volume of distribution
$V_{u,lung}$	Unbound lung volume of distribution
ρ	Density

Chapter 1 Introduction

Inhalation is an attractive route of administration that has been employed for more than 2000 years [1]. Delivery of drug directly to the diseased target organ has been associated with advantages such as a rapid onset of action and a higher and more sustained local tissue concentration [2]. The latter offers an opportunity to increase the therapeutic index (TI), which often is defined as the ratio of the dose that causes a toxic response to the dose that produces the desired, therapeutic effect in 50% of the population [3]. The TI can be increased by achieving lung-selectivity and thereby fulfil the aim of locally acting inhaled drugs, i.e. to obtain high drug concentrations at the lung target site whilst the systemic concentrations are kept at a minimum [4]. In order to minimise the systemic exposure, and thus systemic side-effects, drug discovery typically aims to develop inhaled drugs with high hepatic clearance to obtain a rapid elimination and to avoid absorption from the gastrointestinal (GI) tract [5].

However, assessment and prediction of lung-selectivity has so far proven to be elusive. Collection of relevant exposure measurements is recognised as a challenge both within clinical and preclinical research. Since the appearance of drug in the systemic circulation is the result of pulmonary absorption, unbound drug concentrations in plasma ($C_{u,p}$) cannot be assumed to reflect the unbound target site concentration in the lung [2]. In contrast, this assumption can generally be held as valid for systemically acting drugs. This constitutes a challenge for evaluation of locally acting inhaled drugs since $C_{u,p}$ usually forms the basis for establishing a quantitative relationship between the drug exposure (pharmacokinetics - PK) and the

drug effect (pharmacodynamics - PD), commonly referred to as a PK/PD-relationship.

To date, it is not possible to measure the unbound, and thus pharmacologically active, target site concentrations locally in lung tissue. In a preclinical setting, the lungs can be collected by destructive sampling at several time points after inhalation of drug, where destructive sampling implies that the animal is euthanized during the process of sampling (i.e. only one sample/animal). Drug concentrations are subsequently measured in lung tissue homogenates, providing a time profile of total lung concentrations where the lung, despite its heterogeneous nature, is reflected as one anatomical entity. Moreover, the homogenisation process severely distorts data interpretation by dissolving solid drug particles [6]. Indeed, the establishment of PK/PD-relationships based on total lung concentrations is known to be more challenging for poorly soluble compounds [7]. This can be attributed to a large, but quantitatively unknown, fraction of the deposited drug still being undissolved when the lung is dissected, meaning that it could not have contributed to the pharmacological effect. As receptor occupancy is driven by the unbound drug concentration at the target site, such measurements would clarify the PK, as well as the PK/PD, after topical administration. Developing an experimental methodology for measuring receptor occupancy of an inhaled target would thus bring us one step closer towards understanding the time course of free target site exposure to inhaled drugs. Yet another dimension would be added if such a methodology not only allowed for measurements of receptor occupancy in the lung, but also in another organ, which thus could be used as a reference organ for the systemic exposure of drug after inhalation. Studies utilising such a methodology would not only provide results, which inherently contain information about the local target site exposure, but

also provide a quantitative readout of the degree of lung-selectivity that was achieved by inhalation. The latter information can thus be obtained by comparing the pulmonary and the systemic receptor occupancy.

Data on local and systemic receptor occupancy would thus inherently contain information about the fate of an inhaled drug and thereby be informative about the underlying processes in this system. While this doubtlessly would provide one piece of the puzzle, these measurements alone would not be sufficient enough to build a deeper mechanistic understanding and thereby enabling predictions of how the extent and time course of the free target site exposure to inhaled drug would be affected by changes in drug- and/or formulation-specific properties (*e.g.* the solubility and the particle size distribution). Hence, it would still remain challenging to identify rational strategies for: 1) the chemical design of inhaled compound series, 2) the inhaled formulation design for clinical studies, and 3) targeting appropriate dose ranges for clinical studies utilising the inhaled route.

To understand why predicting the fate of an inhaled drug is held as particularly challenging, we need to consider the complexity of pulmonary drug disposition. This can be illustrated by considering some of the events that follow inhaled drug delivery. In preclinical inhalation studies, rodents are generally exposed via nose-only inhalation, where a substantial deposition of drug particles will occur in the nose [6]. Drug deposited in the lung and the nose will both be subject to a self-cleansing mechanism called mucociliary clearance (MCC), which transports drug particles towards the pharynx where they are eventually swallowed [8]. Accordingly, the resulting plasma PK is a result of parallel absorption from the lung, the nose and the GI-tract [9,10]. Nevertheless, predicting regional drug concentrations in the lung is even more demanding since pulmonary drug disposition involves numerous

processes including regional drug deposition, dissolution of solid drug particles and MCC. Furthermore, additional complexity comes from the heterogeneous nature of the organ with distinct differences between the tracheobronchial and alveolar regions [11]. An integrated understanding, which takes the mechanistic processes as well as the organ heterogeneity into account, would thus be desirable.

Simulation models have previously been used to predict the systemic exposure of inhaled drugs in humans. Hochhaus and Weber [12] developed a compartmental simulation tool, in which the lung was divided into two subcompartments representing the central and peripheral region, respectively. The model also included features such as MCC and drug dissolution described by rate constants [12]. Chaudhuri *et al*. used GastroPlus™ to predict the systemic PK of budesonide [13]. The simulated plasma profiles of both models proved to agree well with experimental data. These simulation studies thus aimed at characterising the systemic and not the local exposure. There has also been research focusing on predicting the local exposure to inhaled drug. A simulation study by Hochhaus *et al*. evaluated lung-selectivity in terms of pulmonary and systemic receptor occupancy [14]. However, those simulations relied on a very simple model structure where the lung was described by a single compartment and the receptor binding by a static model. Furthermore, the drug dissolution was non-mechanistically described by a single rate constant. Thus the simple model structure and the incorporation of only a few, empirically described drug disposition processes cannot provide a sufficiently detailed description of the system to understand the *interplay* between different processes and thereby *e.g.* make inferences on the optimal design of inhaled compounds and/or formulations. Even so, despite its simplicity, the model by

Hochhaus *et al*. could *e.g.* identify that lung-selectivity is attained during the dissolution process.

Nevertheless, a *mechanistic* model predictive of local tissue concentrations combined with measurements such as receptor occupancy for validation is currently lacking. Such a model would be necessary to elucidate the highly complex processes involved in pulmonary drug disposition [15]. Clearly, some of these processes will be affected by pulmonary diseases [16]. For instance, simulations have proposed that the drug deposition will be enhanced at the sites of airway narrowing in asthmatic patients [17]. Whilst this research focuses on healthy lungs, it opens up for later research to evaluate how the pathophysiology of a given disease might affect processes of pulmonary drug disposition and thereby the local lung concentrations.

In this thesis, a mechanistic and physiologically-based rat inhalation PK and receptor occupancy model is developed. The presented model provides the pharmaceutical industry with a novel systems modelling tool for understanding how the free target site exposure to inhaled drug relates to different drug- and formulation-specific properties and thereby enables informed decisions on *e.g.* the chemical and formulation design.

1.1 Aims and objectives

The aim of this thesis is to increase the understanding of how the level and time course of free lung target site exposure to inhaled drug relate to different drug- and formulation-specific properties. Therefore the objectives of this thesis are to:

1. Continue and complete an ongoing development of an *in vivo* receptor occupancy methodology for an inhaled target, the glucocorticoid receptor (GR).
2. Apply the developed *in vivo* receptor occupancy methodology to characterise and compare the time course of receptor occupancy after intravenous- and inhaled drug delivery.
3. Characterise the binding kinetics of a GR agonist using the intravenous route.
4. Develop a mechanistic, mathematical framework to predict the time course of target site exposure to unbound drug and receptor occupancy after inhalation, taking into account the physiology of the species and processes judged to be important for pulmonary drug disposition.
5. Apply the developed model to understand what drug- and formulation-specific properties, or combinations thereof, that give rise to lung-selectivity in terms of local and systemic receptor occupancy.

1.2 Thesis outline

This thesis will lead up to the development of a mechanistic and physiologically-based inhalation PK model, which subsequently is used to gain an understanding of how different drug- and/or formulation-specific properties can (or cannot) give rise to lung-selectivity. As detailed below, this aim can be obtained by conducting the research in a stepwise manner.

Chapter 2 introduces relevant background information, which has been divided into two main categories: inhalation PK and modelling, respectively. The focus of the former category is primarily on processes that are unique for pulmonary drug disposition, but it also covers *e.g.* lung anatomy, preclinical inhalation models and

general PK concepts. Clearly, it is crucial to build an understanding about these different subcategories as it will provide the foundation for the model development and the subsequent validation.

Chapter 3 presents the development of an *in vivo* receptor occupancy methodology for an inhaled target (the GR) in rats. As outlined in the introduction, such measurements will inherently contain information about the free target site exposure to inhaled drug, which cannot be directly measured. The developed methodology is subsequently evaluated by testing its ability to demonstrate a dose-receptor occupancy relationship as well as to characterise the time course of receptor occupancy after intravenous administration of a GR agonist (fluticasone propionate, FP).

In chapter 4, the developed experimental methodology is applied to study the time course of receptor occupancy and the PK after nose-only exposure of FP as well as after intravenous administration of another GR-agonist (budesonide). Mathematical modelling is subsequently used to estimate the unknown *in vivo* binding kinetics parameters for both compounds using the data generated from intravenous dosing.

Chapter 5 describes the development of a physiologically based pharmacokinetic (PBPK) model, which places emphasis on mechanistically describing the underlying processes of pulmonary drug disposition. Here it also becomes clear that chapter 4 serves two important purposes. Firstly, it provides estimates of the binding kinetics parameters K_{on} and K_{off}, which are then used as input parameters to the presented model. Secondly, the receptor occupancy measurements as well as the PK from the nose-only exposure studies can used for model validation purposes. The ability of the model to mechanistically describe PK and the receptor binding after intravenous and inhaled drug delivery is thus evaluated using FP as a test compound. The developed

PBPK model is subsequently used to explore various aspects of pulmonary drug disposition, including how the interplay between different drug- and formulation-specific properties can produce lung-selectivity.

The overall project conclusions and recommendations for future research are discussed in chapter 6.

Chapter 2 Background

2.1 Introduction

This thesis is set out to explore how the target site exposure to inhaled drug relates to different drug- and formulation-specific properties. Ultimately, this will lead up to the development of a new systems model, which is built by formulating mathematical descriptions of the system based on the current understanding of pulmonary drug disposition and rodent physiology. Such a model can be evaluated using drug- and formulation-specific properties as input parameters and subsequently be validated using different experimental measurements. Clearly, developing such a model requires knowledge about several different areas including inhalation pharmacokinetics (PK) and modelling.

This chapter, which aims to introduce relevant background information, has therefore broadly been divided into two main sections: inhalation PK and modelling, respectively. The focus of the former section is primarily on processes that are unique for pulmonary drug disposition, but it also covers *e.g.* lung anatomy, preclinical inhalation models and general PK concepts. The latter section will introduce various modelling techniques and concepts that are useful for this thesis such as physiologically-based pharmacokinetic (PBPK) modelling.

2.2 Inhalation pharmacokinetics

2.2.1 General background to inhalation

The ability to deliver drug specifically to its site of action has made inhalation an attractive route of administration for respiratory diseases. This feature has been associated with advantages such as a rapid onset of action and a higher and more

sustained local tissue concentration [2]. The latter can lead to an increased therapeutic index by achieving lung-selectivity and thus fulfilling the aim of locally acting inhaled drugs, i.e. to obtain high unbound drug concentrations at the lung target site while the systemic (unbound) concentrations are kept at a minimum [4]. Clearly, the unbound lung target site concentrations are expected to drive the desired pharmacological effect, whereas the unbound systemic concentration might exert unwanted systemic side-effects [18]. Inhalation is therefore generally held as the optimal route of administration of the first-line therapy for asthma [19] and chronic obstructive pulmonary disease (COPD) [20].

Nevertheless, the large absorptive surface area of the lung has also led to widespread interest in using inhalation as an alternative route of administration for the systemic delivery of drug. Furthermore, relative to oral administration, inhalation might significantly reduce pre-systemic metabolism since the lung is expected to have a lower metabolic capacity than the GI-tract [21]. These features thus serve to illustrate why inhalation might be advantageous for systemic drug delivery. Expressed differently, the utility of using inhalation for both lung-targeted drug treatment and systemic drug delivery are two sides of the same coin. Hence, we need to understand what combinations of drug- and formulation-specific properties are beneficial for either creating a lung-selective drug exposure or for systemic drug delivery.

2.2.2 Lung anatomy

This subsection aims to provide a short overview of the lung anatomy and to introduce fundamental terms, which will be used in this thesis.

The respiratory system is often divided into two different regions: the conducting airways and the respiratory airways. As can be understood from the terminology, one important function of the conducting airways (nose, pharynx, larynx, trachea, bronchi and nonalveolized bronchioles) is to conduct inhaled air into the respiratory airways (respiratory bronchioles, alveolar ducts and alveolar air sacs) where gas-exchange takes place [22].

There are two different circulatory systems in the lung: bronchial and pulmonary circulation, which supply the conducting and the respiratory airways, respectively [23]. The primary function of the pulmonary circulation is to carry deoxygenated blood from the heart to the alveoli for gas-exchange. It is a circulation system connected in series with the systemic circulation and it receives the entire cardiac output [24]. The bronchial circulation, on the other hand, is part of the systemic circulation and a fraction of the cardiac output thus supplies the conducting airways with oxygen and nutrients [23].

According to an alternative division of the respiratory system, three different regions can be defined: the extrathoracic region, the tracheobronchial region and the alveolar region. The extrathoracic region then refers to the respiratory tract proximal to the trachea (i.e. the nose, pharynx and larynx). The tracheobronchial region is also referred to as the ‘lower airways’, consisting of the airways that conduct air from the larynx to the alveolar region. Expressed differently, anatomically this region starts at the trachea and stops at the end of the terminal bronchioles [25].

The human airways show a bifurcation pattern starting at the trachea (generation 0), which divides into the left and right main stem bronchi (generation 1), which in turn undergo bifurcations into additional bronchi (generation 2) [26]. The branching pattern continues in this manner until the last generation has been reached, which is

illustrated in fig. 2.1a from [11]. There are several different anatomical models for the lung, which differ to some extent in *e.g.* the total number of airway generations (n = 23-26) [27]. In contrast to humans, rat airways follow a monopodial (asymmetric) branching [22]. This different branching pattern has been an important factor to consider *e.g.* when developing realistic particle deposition models for rats. Models that have been constructed for describing the lung anatomy also serve to highlight one of the main features of the organ: its large surface area. Clearly, this feature is of great importance for gas-exchange.

The lung is considered to be a complex and heterogeneous organ [28] with distinct regional differences. Moving from the trachea to the alveolar region, both the type of epithelium and its thickness will change. In humans, the thickness of the epithelium decreases from 58 μm in the bronchi to 0.1-0.2 μm in the alveoli [11]. In rats, the bronchi epithelium thickness is 13 μm [29]. Likewise, there are also distinct differences in both the composition and the thickness of the lung wall [30]. The same principle applies for the epithelial lining fluid (ELF), which is a thin fluid layer that covers the epithelial surface. The ELF also becomes thinner throughout the lung; ranging from 8 μm in the human bronchi and gradually decreasing until reaching a final value of 0.07 μm in the alveoli [11]. The heterogeneity of the lung epithelium and the decreasing thickness of the ELF are both illustrated in fig 2.1b from [11]. The ELF is slightly acidic (pH 6.6) and mainly consists of water (96%), salts, phospholipids, protein and mucins [4]. Its composition is held to vary between different lung regions. Nevertheless, this information is incomplete due to the technical challenges associated with sampling the ELF from different regions [31].

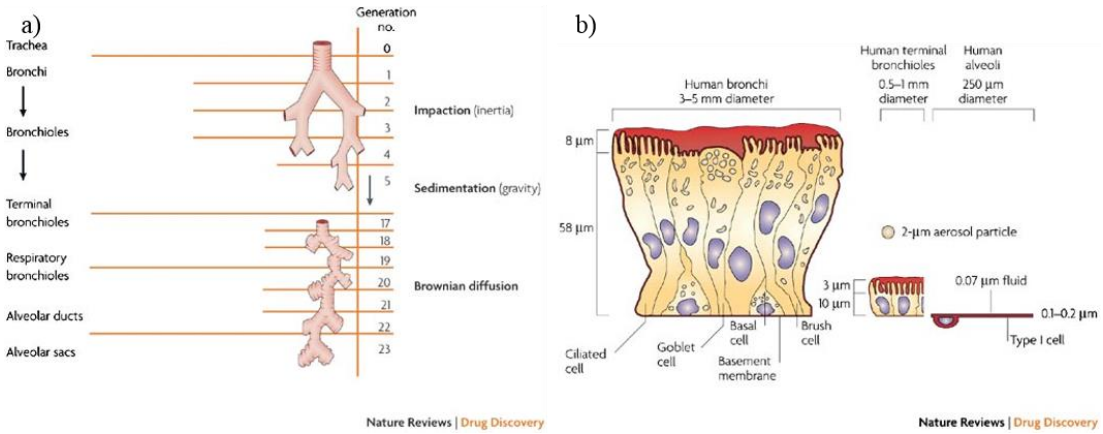

Figure 2.1 Illustration of the lung heterogeneity. a) Illustration of the bifurcation pattern in the human lung; starting at the trachea (generation 0), each bifurcation gives rise to a new generation. b) Illustration of how the thickness of the epithelial cells, which are drawn at their relative sizes, decreases when moving distally from the bronchi to the alveoli. The figure also demonstrates that the same pattern applies for the epithelial lining fluid (darker orange colour). Both figures are taken from [11] with permission.

2.2.3. Pharmacokinetics and pharmacodynamics

This subsection aims to provide an overview of pharmacokinetics (PK) and pharmacodynamics (PD) as well as to introduce terms that are commonly used within the field.

PK can in general terms be described as "what the body does to the drug" [32]. A drug undergoes several different processes once it has entered the body and the PK of a drug is therefore often defined by its absorption, distribution, metabolism and excretion (ADME). If liberation (L) of the drug from its pharmaceutical form is seen as a separate step from absorption, the acronym LADME is used instead [33]. Absorption refers to the process by which unchanged drug moves from the site of administration (*e.g.* the GI-tract) to the site of measurement within the body (*e.g.* the venous blood) [34]. Absorption includes, but is not limited to, oral absorption. Bioavailability (F) is a term that is often used in the context of absorption. F

describes the extent of drug absorption and is defined as the fraction of the administered dose that reaches the systemic circulation in an unchanged form [35]. *F* following oral absorption can be written as

$$F = f_{gut} \times f_{abs} \times f_{h}. \quad (2.1)$$

That is, *F* accounts for the fraction absorbed from the GI-tract (f_{abs}), the fraction that escapes from gut (f_{gut}) and hepatic extraction (f_h). The f_{gut} of a drug can be caused by luminal degradation, efflux transporters and/or gut metabolism. The fraction of absorbed drug that has escaped gut extraction (i.e. $f_{abs} \times f_{gut}$) will initially enter the liver via the portal vein, where a fraction of the drug can be metabolised prior to reaching the systemic circulation. The hepatic extraction ratio, E_H, thus accounts for the so-called hepatic first-pass extraction and is dependent on the extent of metabolism in the liver [36]. E_H can also be written as

$$E_H = 1 - f_h. \quad (2.2)$$

The process by which a drug is reversibly transferred from one location to another within the body is referred to as distribution [37]. The rate and extent of distribution of a particular drug to various organs is dependent on several factors including binding within blood and tissue, lipid solubility and regional blood flow [35]. At equilibrium, the extent of distribution in the body is described by the apparent volume of distribution (V_d), which is calculated by

$$V_d = \frac{A_b}{C_p}\ , \qquad (2.3)$$

where A_b is the amount of drug in the body and C_p is the plasma concentration of the drug [34]. Expressed differently, V_d can be seen as a theoretical volume that would have been required to obtain the drug concentration that was measured in plasma given the amount of drug in the body.

The amount of drug in the body will decline with time as a result of drug elimination, which can take place via two different processes: metabolism and excretion. Metabolism, which describes an enzyme-catalysed conversion of a drug into its metabolites [35], can take place in several organs. Nevertheless, the liver has the highest metabolic capacity and is therefore generally the major site for metabolism [37]. Metabolism, or biotransformation, can be divided into two different phases. Phase I involves enzymatic reactions that change the parent compound by oxidation, reduction or hydrolysis. The resulting metabolite may or may not be pharmacologically active. The role of phase I is generally to create derivatives amenable to phase 2 biotransformation, in which the molecules undergo conjugation reactions. Phase 2 makes the molecule more hydrophilic and thus more easily excreted. Excretion describes the different processes by which a molecule or its metabolite is eliminated from the body. The major excreting organ is the kidney [35]. An essential term within the field of PK that is used for evaluating the elimination of drug is clearance (*CL*), which relates the drug concentration (*C*) to the rate of elimination (RoE) [34]:

$$\text{RoE} = CL \times C\,. \qquad (2.4)$$

If C refers to the plasma or blood concentration of drug, CL describes either the plasma or blood clearance, respectively (the concentration in these two biological matrices are not necessarily equal) [37].

Another concept worthwhile introducing is the area under the curve (AUC), which is the definite integral of the plasma/blood concentration of drug as a function of time ($C(t)$) in the interval $[a, b]$, i.e.

$$AUC = \int_a^b C(t)dt\,. \qquad (2.5)$$

Generally, one of the two following time intervals are used: [0, 24] or [0, ∞] h.

PD can be described as "what the drug does to the body" [32]. More formally, in [38] it is defined as "the study of the biologic effects resulting from the interaction between drugs and biologic systems". Hence, PK describes the drug-concentration time course that follows after administration of a certain dose and PD describes the pharmacological effect that results from a certain drug concentration.

Clearly, it is important to understand the link between PK and PD, which can be done by PK/PD-modelling. PK/PD-models aim to describe the effect-time course that results from administration of a certain drug dose [39]. Such models can be of great value both in drug discovery and drug development. Preclinically, they can, for instance, be used to select the most promising drug candidate to test in humans. PK/PD-modelling has several applications in drug development, including assisting in the design of clinical trials by, for instance, selecting an optimal dose and sampling scheme [40]. Over recent years, the discipline has progressed from using empirical functions to purely describe the observed data to utilising mechanism-based PK/PD-modelling. As opposed to just describing the data, the latter aims to

quantitatively describe the underlying principles of the pharmacology, of the physiology and of the pathology. By virtue of relying on actual mechanisms, such models are expected to have a better predictive capability [41].

2.2.4 Systemic and local PK after inhaled drug delivery

Figure 2.2 from [42] shows a schematic representation of the PK for an orally inhaled drug. In patients, inhalation devices are used to deliver the drug directly to the lung whilst animal studies typically rely on tidal breathing. After inhalation, a large fraction of the dose will deposit in the mouth and the pharynx. Given that this portion of the dose is not completely rinsed out of the mouth by the patient, it may be swallowed and reach the GI-tract. The swallowed dose will thus be treated by the body as an oral dose with the potential of being absorbed from the GI-tract. Absorbed drug that escapes first-pass metabolism in the liver will reach the systemic circulation in an unchanged form, potentially increasing the risk of systemic side-effects [18]. A fraction of the delivered dose will deposit in the lung, where it will have to be dissolved in the ELF prior to absorption to the pulmonary/systemic circulation [15]. The deposited drug will also be subject to a self-cleansing mechanism called mucociliary clearance (MCC), which acts by transporting particles from the airways towards the pharynx, where they subsequently can be swallowed and reach the GI-tract [8]. Although not included in figure 2.2, solid drug particles deposited in the alveolar region may be phagocytosed by alveolar macrophages. However, this is a slow process that might take weeks or months to complete [43]. Accordingly, given that the drug is orally bioavailable, the resulting plasma PK is a result of parallel absorption from the lung and the GI-tract.

Hence, the total amount of drug that will reach the systemic circulation after inhalation will be dependent on the absorption from both the GI-tract and the lung as well as on the ability of the lung to remove the substance. The latter includes clearance in terms of MCC or macrophage uptake as well as metabolic processes. However, the lung has low levels of metabolising enzymes. In fact, the total cytochrome P450s (CYP) content constitutes only 1% of the corresponding value in the liver. Thus, the lung is only expected to play a minor role in the metabolism process compared with the liver. Interestingly, the relatively low metabolic capacity combined with the large surface area of the lung has also lead to a widespread interest in using inhalation for the systemic delivery of drugs [7]. In these instances, the lung is seen as an entry port to the systemic circulation rather than as the target organ for the pharmacological effect.

In contrast, when the pulmonary route is used for direct treatment of disease localised in the lung, the focus is on improving the benefit-safety ratio by maximising the pulmonary and minimising the systemic unbound drug exposure [45]. From the description above, it becomes clear that the level of pharmacologically active drug in the lung will be the result of several complex and simultaneously occurring processes including, but not restricted to, MCC, the dissolution rate of solid particles (if applicable) and flux to/from the systemic circulation.

In order to minimise the systemic exposure, and thus the systemic side-effects, drug discovery typically aims to develop inhaled drugs with high hepatic clearances and low oral bioavailabilities in order to obtain rapid elimination and to avoid absorption from the GI-tract [5]. Nevertheless, achieving lung-selective drug exposure after inhalation is not a trivial task. The large surface area, good

vascularisation and thin alveolar epithelium offer the potential for rapid absorption into the systemic circulation [46]. Indeed, with the exception of intravenous (IV) administration, inhalation is the fastest route for systemic drug delivery of small molecules. This is particularly prominent for small lipophilic molecules, where the absorption half-life is approximately 1-2 minutes [21]. Several strategies for enhancing lung retention have therefore been explored, which will be described in section 2.2.5.4.

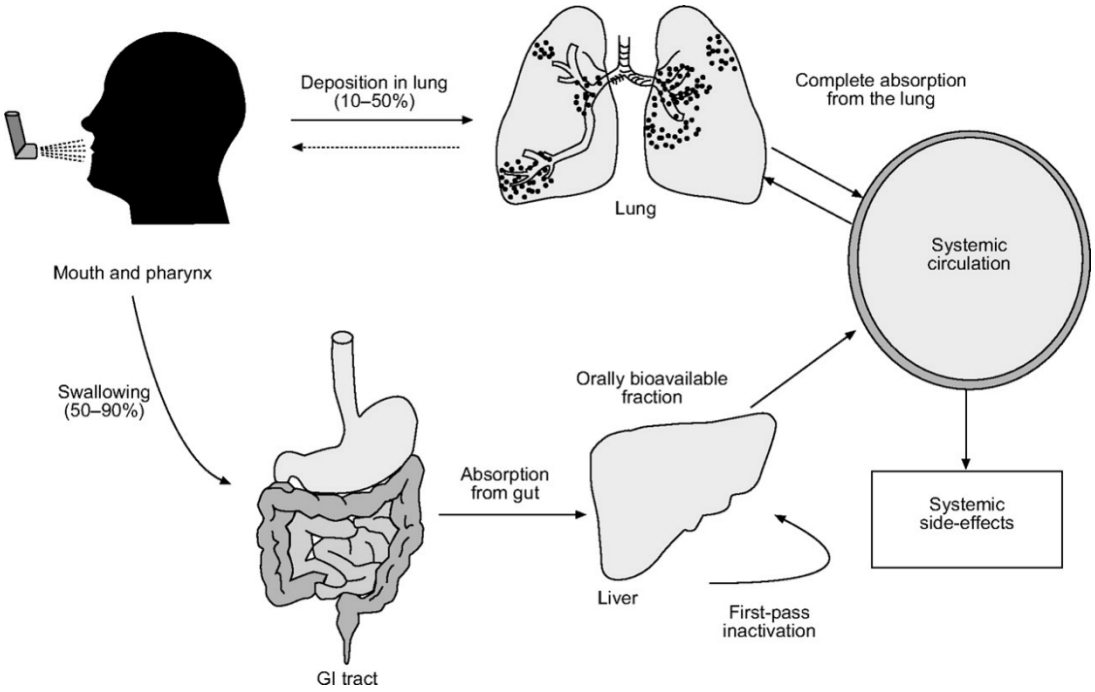

Figure 2.2 Schematic representation of the fate of an orally inhaled drug from [42] with permission.

2.2.4.1 Dose-response for inhaled corticosteroids

Inhaled corticosteroids (ICS) are considered to be the most effective medication used for controlling asthma [47]. Indeed, the Global Initiative for Asthma (GINA) recommends low doses of ICS to be used as controller medication for asthma [48]. The clinical effect of ICS can be measured using several different outcomes including peak expiratory flow (PEF), use of rescue β_2-agonists [47] and forced

expiratory volume (FEV) [49]. Meta-analyses of clinical studies investigating the effect(s) of ICS in asthma have shown that although ICS demonstrate a clinical benefit versus placebo, the dose-response curve for efficacy measurements is relatively flat. This is in contrast to the dose-response curve for side-effects, which has been reported to be steep [49,50]. However, due to paucity of data, the meta-analysis described in [50] could not investigate the effect of dose on systemic side-effects such as hypothalamo-pituitary axis function. The analysis instead focused on local side-effects related to deposition of ICS in the oropharynx. In [49] a steep dose-response relationship was found for local side-effects and one of the included studies reported significantly lower cortisol levels (systemic side-effect) after a high dose of fluticasone propionate. References [47] and [51] also state that there is a steep dose-response curve for systemic side-effects. Overall this implies that only a small clinical benefit is expected from increasing the clinical ICS doses whilst the risk of side-effects is considerably increased.

2.2.5 Pulmonary drug disposition after inhalation

2.2.5.1 Pulmonary drug dissolution and absorption

Compared with other routes of administration, there is only limited information on the absorption of inhaled drugs. Generally, the epithelium is considered to constitute the main barrier for absorption from the airway lumen [11]. It is worth noting that the thickness of this cell barrier varies throughout the lung, starting at about 60 μm thick columnar epithelia in the bronchi and then decreases along the lung generations until reaching a final thickness of about 0.2 μm in the alveoli [4]. Due to differences both in thickness and blood perfusion, regional differences in absorption rates might be expected in different areas of the lung [15].

Drug molecules are absorbed across the epithelium both via passive and active transport mechanisms. The process by which a molecule moves from a point with higher concentration (*e.g.* the ELF) to a point with a lower concentration (*e.g.* the submucosa) is referred to as passive diffusion. The drug transport of lipophilic compounds across the cellular barriers is generally considered to rely on transcellular diffusion, whereas hydrophilic compounds appear to rely on paracellular diffusion [4]. Hydrophilic compounds can also be actively transported across cells [52] and over the recent years there has been an increased interest in the role of drug transporters in the lung [53]. Nevertheless, evaluation of the role of drug transporters on pulmonary drug disposition does not fall within the scope of this thesis. Experiments have shown that lipophilic compounds are rapidly absorbed from the lung (absorption half-lives ranging from seconds to a few minutes), whereas hydrophilic compounds are absorbed more slowly (absorption half-lives of about 1 hour). Interestingly, the absorption half-life did not appear to be dependent on log*P* other than enabling the identification of two distinct groups in the data: hydrophilic (log$P < 0$) and lipophilic (log$P > 0$). Another interesting finding was that within the molecular weight range of 100-1000 Da there was no discernible trend of the pulmonary absorption rate being size-dependent [21].

Before drug absorption can take place, the solid drug particles must firstly dissolve in the ELF. The pulmonary dissolution rate will depend on different properties of the drug, the formulation and the system (i.e. physiological and anatomical characteristics). One important property is the solubility, which will depend on *e.g.* the compound and the composition of the dissolution medium (i.e. the ELF). The measured solubility will therefore be different depending on the choice of dissolution medium. Although fluids have been specifically developed to mimic the ELF,

so-called simulated lung fluids, the lung has unique features that are considered difficult to replicate *in vitro* [54]. To date, development of *in vitro* dissolution methods predictive of the *in vivo* situation is therefore an ongoing challenge. Moreover, as will be discussed in depth in section 2.2.5.4, a commonly used strategy for enhancing lung retention is to develop poorly soluble drugs. Previous research aiming to predict the *in vivo* dissolution rate in the GI-tract based on measurements of the aqueous solubility have found poor *in vitro-in vivo* correlation for poorly soluble compounds [55], which emphasises the need to choose a bio-relevant dissolution medium for this particular compound class.

As mentioned in section 2.2.2, the total volume of ELF available for dissolving the deposited drug particles is small. Moreover, the thickness of ELF gradually decreases along the lung generations from 5 μm centrally [56] to 0.07 μm in the alveolar region [11]. This suggests that the dissolution rate might be higher centrally. Nevertheless, due to the complexity of the system other factors could actually lead to the opposite behaviour [4].

As pulmonary drug dissolution has been speculated to be the rate-limiting process for several inhaled compounds [15], there is a recognised need for further research in this area.

As mentioned in section 2.2.4, the lung has a metabolic capacity that is low relative to the corresponding capacity of the liver. For most inhaled compounds, pulmonary metabolism is therefore not expected to largely influence the extent of pulmonary absorption. However, the possible impact of metabolism in the target organ needs to be considered on a drug-specific basis. This can be exemplified by the drug beclomethasone dipropionate (BDP), which is rapidly metabolized by esterases in the lung to its active metabolite 17-beclomethasone monopropionate [57].

The effect of pulmonary metabolism of different ICS has been investigated *in vitro* in human precision-cut lung slices [58]. In this experiment, lung slices were incubated with different ICS including FP and BDP for several hours to monitor the concentrations of parent compound and metabolites over time. FP was shown to be metabolically stable in this test system, i.e. no metabolites were found in the incubation medium. In contrast, the levels of BDP decreased over time and metabolites were detected in the medium. Hence, whilst some compounds might unaffected by pulmonary metabolism, this study emphasises the importance of considering the impact of this process on a drug-specific basis.

2.2.5.2 Regional drug deposition

After drug inhalation, the particles/droplets will deposit in different regions throughout the lung, which is generally referred to as the pulmonary deposition pattern. The optimal site for deposition is often reasoned to be dependent on the drug target. For instance, delivery of drug to a lung region devoid of the receptor of interest might result in a suboptimal response to the drug treatment [59]. As mentioned in the previous section, absorption rates of drug might be expected to vary throughout the lung [15]. Hence, different deposition patterns may be desired depending on the aim of the treatment and/or knowledge of the target location. It is therefore of interest to be able to predict the regional deposition pattern of inhaled particles and particle deposition modelling is used for this purpose.

The deposition of inhaled particles depends on several factors including: 1) the anatomy of the respiratory tract, 2) the respiratory physiology, and 3) the physics of aerosol particles. All of these factors need to be considered in mathematical deposition models. Due to the complexity of these factors, most models make

simplifying assumptions related to *e.g.* the structure of the respiratory tract, the airflow rate and the breathing pattern [60].

In short, an anatomical model is used to provide a geometric description of the airway structure. A commonly used anatomical model type is the so-called "single-path" model. In this model type, all airways in a given airway generation have identical dimensions. This feature leads to identical pathways of the inhaled particles travelling from the nose to the alveoli. Expressed differently, all pathways can be represented by a single path [61]. Two important respiratory parameters used as input for predicting regional particle deposition are the breathing frequency (f_{br}), i.e. the number of breaths per minute, and the tidal volume (V_T), i.e. the volume of air that is inspired in a single breath during normal breathing conditions. Both f_{br} and V_T depend on the level of physical activity [61], which thus will have an impact on the deposition pattern. Another important parameter is the particle velocity (u), which will decrease distally throughout the lung. As a result of the lower velocities in the distal parts, particles have longer mean residence times peripherally.

One of the most important parameters for determining regional drug deposition is the aerodynamic diameter (d_a) of the aerosol particle [59]. The d_a is defined as the diameter of a unit density sphere that would have the same aerodynamic behaviour as the particle in question. The d_a can be calculated by

$$d_a = d_g \sqrt{\frac{\rho_p}{\chi}}, \qquad (2.6)$$

where d_g is the geometric diameter of the particle, ρ_p is the density of the particle and χ is a dynamic shape factor that can be used if d_a needs to be modified to account for

shape irregularity. That is, the value χ depends on the shape of the particle; *e.g.* χ is 1.00 and 1.08 for spheres and cubes, respectively [62]. Expressed differently, particles with the same d_a can have different shapes and densities.

There are several mechanisms by which a particle can be forced to leave the stream of inhaled air and deposit in the airways. Three main mechanisms are: 1) inertial impaction, 2) gravitational sedimentation, and 3) Brownian diffusion [61]. Each of these mechanisms will be described below and they are graphically illustrated in figure 2.3, which is taken from [63].

As a result of inertia, a particle may not be able to follow the air streamline when the curvature of the airway is changing, but it instead continues along its initial trajectory. The Stokes number (*Stk*) is a dimensionless parameter that can be used to characterise inertial impaction. *Stk* is the ratio of the particle's relaxation time t_r (the time it takes for a particle to reach equilibrium with a new set of forces acting on it, i.e. the time it takes to respond to the changes in the local flow) to the time taken to flow past an obstacle. *Stk* can therefore be seen as a measure of how rapidly a particle can adjust to changes in the flow field. A small *Stk* implies that the particle closely follows the streamlines while a large *Stk* implies that the particle takes a longer time to adjust to the flow distortion; i.e. it might deviate from the streamline and deposit due to its inertia [64]. If the characteristic length of the obstacle is set to the radius of the airway (D_i/2), the *Stk* can be calculated by [65,66]

$$Stk_i = \frac{t_r u_i}{0.5 D_i} = \frac{\rho_0 d_a^2 u_i}{9 \eta D_i}, \qquad (2.7)$$

where Stk_i is Stokes number in generation i, ρ_0 is the unit particle density (1 g/cm^3), d_a is the aerodynamic diameter, η is the viscosity of air and D_i is the diameter of the

airway in generation *i*. From eq. 2.7 it is thus evident that large particles with high velocities will have higher *Stk* and thus be more prone to inertial impaction. Hence, it follows that inertial impaction is most effective for large particles in the upper airway generations [61].

Deposition due to gravity is referred to as gravitational sedimentation. Deposition by this mechanism is *e.g.* dependent on the residence time in the airway (t_i) and the gravitational settling velocity (v_g), which can be calculated as

$$v_g = t_r g = \frac{\rho_0 d_a^2 g}{18\eta}, \tag{2.8}$$

where ρ_0 is the unit particle density (1 g/cm^3) and g is the acceleration due to gravity. From eq. 2.8 it is clear that v_g increases rapidly with particle size as it is proportional to the square of d_a. However, eq. 2.8 is only valid for larger particles unless the Cunningham slip correction factor (C_d) is used. Therefore, eq. 2.8 can be rewritten as [65,66]

$$v_g = \frac{\rho_0 d_a^2 g C_d}{18\eta}, \tag{2.9}$$

with [65]

$$C_d = 1 + \frac{\lambda}{d_a}\left(2.514 + 0.8e^{-0.55\frac{d_a}{\lambda}}\right), \tag{2.10}$$

where λ is the mean free path of air molecules. As the deposition efficiency by gravitational sedimentation increases with t_i and v_g [67], deposition by this

mechanism is important for larger particles in the distal lung regions where t_i is longer.

The third deposition mechanism that is generally accounted for by deposition models is Brownian diffusion. When fine particles are suspended in air, collisions with the surrounding gas molecules will cause the particles to wobble randomly. This random motion of particles suspended in a gas is referred to as Brownian motion and it may cause a particle to randomly deviate from the streamline and deposit on the airway wall [60]. As the Brownian diffusion coefficient (D_{mol}) is inversely proportional to the particle size, this mechanism is particularly important for smaller particles. D_{mol} is calculated as [65,66]

$$D_{mol} = \frac{k_B T C_d}{3\pi\eta d}, \tag{2.11}$$

where k_B is the Boltzmann constant and T is the absolute temperature. Like gravitational sedimentation, a prolonged t_i increases the probability of deposition by this mechanism. Brownian diffusion is thus the predominant deposition mechanism for smaller particles in the alveolar region [61].

Several different analytical equations have been published for calculating the deposition probability by each of these three mechanisms in cylindrical airways [61]. As can be understood from the description of each mechanism above, the probability of particle deposition by each mechanism will vary over the different lung generations. The resulting deposition probability of a particle in generation i (P_i) is given by [68]

$$P_i = 1-(1-DE_{im,i})(1-DE_{s,i})(1-DE_{d,i}), \quad (2.12)$$

where $DE_{im,i}$, $DE_{d,i}$ and $DE_{s,i}$ are the probabilities of particle deposition by inertial impaction, Brownian diffusion and gravitational sedimentation, respectively. When eq. 2.12 is combined with the inhaled air volume passing through each generation *i* as well as the fraction of particles already deposited in the preceding lung generations, the particle deposition in generation *i* (DE_i) can be calculated during the inhalation phase. The value of DE_i can be calculated for each of the three stages of a breath: inhalation (DE_i^{in}), breath-holding (DE_i^{b}) and exhalation (DE_i^{ex}) [66]. The total deposition (DE_i^{tot}) during a breath is subsequently given by

$$DE_i^{tot} = DE_i^{in} + DE_i^{b} + DE_i^{ex}. \quad (2.13)$$

Some models developed for rats exclude the breath-holding phase since this interval is short compared to the breathing-phase [65]. Generally, the particle deposition is reported for larger lung regions rather than an individual lung generation. The deposition in a lung region (DE_{region}) between region *j* and *k* is then defined as

$$DE_{region} = \sum_{i=j}^{k} (DE_i^{in} + DE_i^{b} + DE_i^{ex}). \quad (2.14)$$

The resulting deposition fraction in a certain region (DF_{region}) is subsequently obtained by dividing the amount of deposited drug in a predefined region (eq. 2.14) by the amount inhaled.

Several computational models have been developed for predicting regional drug deposition both in humans [61] and rodents [65,66,69,70].

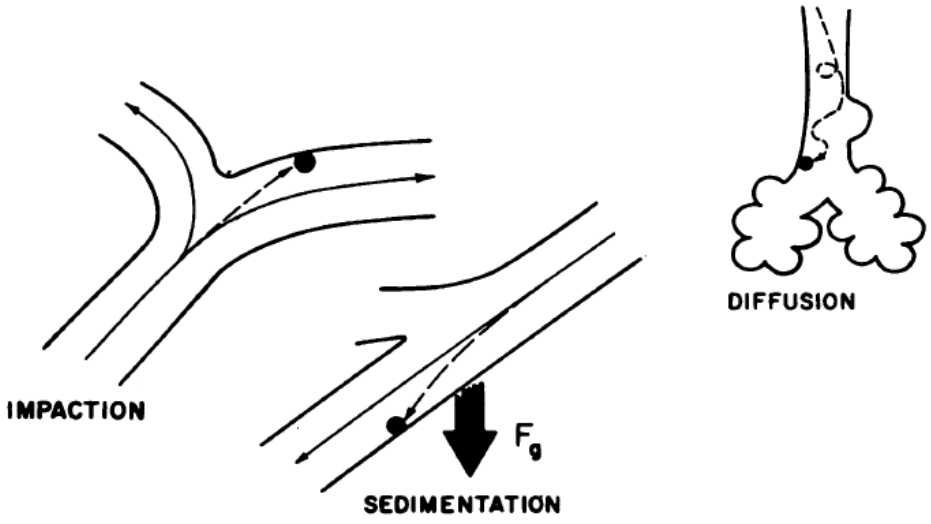

Figure 2.3 Drug deposition mechanisms. Drug can deposit in the respiratory tract by different mechanisms including inertial impaction, gravitational sedimentation and Brownian diffusion. The figure is taken from [63].

2.2.5.3 Mucociliary clearance and macrophage clearance

Since the primary physiological function of the lung is gas exchange, it follows that this organ must be in constant contact with the external environment and it will thus be exposed to inhaled particles such as dust and bacteria. As a result, several innate defence mechanisms have evolved to protect the body from potential threats that might enter the body via the airways [71]. One of the most important defence mechanisms is the mucociliary clearance (MCC), which acts by transporting particles from the airways toward the pharynx, where they subsequently may be swallowed and reach the GI-tract [8]. Interestingly, the velocity of MCC has been shown to be independent of particle properties such as size, shape and charge [72]. Obviously, this clearance mechanism will also be effective for inhaled drugs. As ciliated cells are responsible for clearing particles from the airways, inhaled drugs will be

subjected to MCC in the ciliated parts of the airways (unless the particles are readily dissolved) [73]. Consequently, MCC can reduce the pulmonary bioavailability after inhalation and this effect is expected to be more pronounced for slowly dissolving drugs.

MCC is primarily associated with the tracheobronchial region [74], however, there is another innate defence mechanism in the peripheral parts of the lung. Solid drug particles deposited in the alveolar region may be phagocytosed by alveolar macrophages. Nevertheless, this is a slow process that might take weeks or months to complete [43]. It is hypothesised that some of these macrophages might migrate to the ciliated terminal bronchioles, where they are subsequently cleared from the lung via MCC [74].

2.2.5.4 Strategies for enhancing lung retention

Regardless of route of administration, it is crucial to develop drugs with appropriate effect duration. Clearly, there are no general rules defining either the desired level or the duration of effect of a drug, but these need to be evaluated on a case-by-case basis for each drug target and disease. Nevertheless, it is often desirable to have an efficacious response throughout the entire dose interval. Once-daily is generally the preferred dosing regimen since this is convenient for the patient. As a result, it is important to design locally acting inhaled drugs such that sufficiently high concentrations can be obtained throughout the entire dosing interval . As previously described in section 2.2.4, depending on drug properties, inhaled drugs might be rapidly absorbed to the systemic circulation. Achieving a sustained lung exposure is therefore not a trivial task and several different strategies have been explored for enhancing lung retention of inhaled drugs.

One commonly used strategy to prolong the pulmonary residence time is to develop drugs with a low solubility in order to reduce the dissolution rate. Indeed, a low aqueous solubility has been demonstrated to give a prolonged lung retention preclinically . Two poorly soluble inhaled compounds are fluticasone propionate (FP) and BDP. Clinical data have shown that the average pulmonary absorption time of FP (5-7 h) is considerably longer compared with more soluble ICS such as budesonide and triamcinolone acetonide (2.9 and 1 h, respectively) [11]. The prolonged absorption time has been suggested to be caused by the slow dissolution of FP [75]. Moreover, the absorption across membranes is a rapid process for lipophilic ICS, which further strengthens the hypothesis of dissolution rate-limited absorption [76]. This approach is thus well-known for yielding high lung concentrations as well as a prolonged lung retention. Even so, there are potential caveats with this strategy. One important factor to bear in mind when considering using this approach is that undissolved drug cannot elicit a pharmacological response. Moreover, solid drug particles will be removed by MCC . Hence, this is a strategy that elucidates the importance of understanding the complex interplay between different pulmonary processes; more research is needed to understand what compound- and formulation-specific properties are required for this strategy to be advantageous.

Another approach that is commonly used to obtain lung retention is to chemically design the inhaled compounds to be bases. Cooper *et al*. [7] showed that the ion class strongly influences lung retention. A comprehensive data set was generated preclinically, where the amount of drug remaining in the lung was monitored after intratracheal instillation of dissolved compounds belonging to different ion classes. The researchers noted that the compounds could be broadly grouped by ion class: 1) neutral, acidic and zwitterionic compounds tended to have a generally short

pulmonary half-life ($t_{½,lung}$), 2) basic compounds had an intermediate $t_{½,lung}$, and 3) di-bases had a long $t_{½,lung}$. One potential explanation for this phenomenon is lysosomal trapping. The working hypothesis is that basic compounds are sequestered in lysosomes, i.e. this organelle can be seen as a subcellular drug reservoir which then acts like a slowly eluting pool. Lysosomal trapping has been demonstrated to take place *in vitro* in lung slices [77]. However, to the best of my knowledge, the kinetics of this process has not yet been characterised in the literature.

The lung retention of the ICS budesonide is held to rely on a completely different mechanism. Reversible fatty acid esterification of the molecule has been found to take place intracellularly, which results in an intracellular reservoir of inactive drug. The ester, budesonide-oleate, will then be hydrolysed back to its active form as the intracellular concentration of free budesonide decreases. The ester is thus suggested to act like an intracellular depot of budesonide, which would prolong lung retention of the molecule. This reasoning may be supported by the following observations: 1) the esterification is a rapid process, 2) a large fraction of the molecules (70-80%) was found to be in the esterified form in the central airways after intratracheal administration of the compound [78], and 3) preclinical PK-studies have shown that similar tissue concentrations of budesonide-oleate and budesonide are obtained after IV-administration and inhalation of the parent compound [79].

Another approach that has been speculated to drive lung- and effect duration is a slow dissociation rate from the receptor. Some inhaled drugs are held to have this property, *e.g. in vitro* experiments have shown a slow drug-receptor dissociation rate for FP. Högger and Rohdewald state that the long half-life of the drug-receptor complex might provide a scientific rationale for the dosing interval of FP. However, they also emphasise that *in vitro* dissociation rates are not necessarily translatable to

the *in vivo* situation [80]. Nevertheless, in order to use this strategy it is crucial to understand if sufficiently high unbound concentrations can be obtained at the lung target site prior to the drug is being absorbed to the systemic circulation and/or cleared from the lung.

To summarise, several different strategies can be used for enhancing lung retention of inhaled drugs. From the literature review it is also clear that a more thorough mechanistic understanding is desirable to enable informed decisions about the choice of strategy.

2.2.6 Preclinical inhalation studies

2.2.6.1 Inhalation pharmacokinetic studies in drug discovery

In drug discovery, several different methodologies can be employed for studying pulmonary drug delivery. These can roughly be divided into two different categories: exposure methods and direct dosing methods.

Exposure methods rely on creating a controlled atmosphere of drug exposure. Depending on how the test animals are exposed to the drug atmosphere, such systems fall into different subcategories of whole-body exposure, nose-only exposure, head-only exposure and specialised exposure methods. In this section, the first two categories will be introduced.

In whole-body exposure, the test animal is placed in a chamber with a controlled atmosphere of drug exposure. The methodology thus resembles environmental or work-place exposure of potentially toxic vapours. The animals can be housed either individually or in groups [81]. This methodology is straightforward from an experimental perspective. Nevertheless, results from such studies might be difficult to interpret since the entire animal is exposed to drug, which inevitably will lead to

contamination of the fur. This has the potential to confound the results in two different ways. Firstly, in conjunction with blood sampling, there is a risk of the samples being contaminated by drug from the fur. Secondly, as a result of the animal cleaning process, the test subjects are likely to swallow compound from the contaminated fur. The latter might cause substantial oral absorption of the drug. In drug discovery, nose-only exposure studies are therefore generally favoured . In contrast to whole-body exposure, such systems are designed to minimise fur- and skin exposure of drug by only exposing the nose to the drug atmosphere. This can be obtained by keeping each animal in a separate tube, which has an adjustable back restraint preventing the animal from backing out. The tube is open at one end to a chamber containing aerosolised compound. Thus, the opening has been designed such that only the nose will protrude into the chamber. Nose-only exposure systems are well suited for rodents, such as the rat, since they are obligate nasal breathers. Furthermore, in comparison with whole-body exposure systems, a lower amount of compound is required for conducting an inhalation study [81]. Perhaps the biggest challenge associated with exposure methods in general is that the lung deposited dose (*LDD*) cannot be directly measured, but instead needs to be estimated, which will be discussed in detail in section 2.2.6.2.

In contrast to exposure methods, direct dosing via intratracheal (IT) instillation offers the advantage of delivering a known amount of compound directly into the lung. Moreover, much less compound is needed for such studies, making it attractive for early drug discovery projects. IT-instillation is generally performed by inserting a catheter into the trachea of an anesthetised animal. A small volume of the test compound, either as solution or suspension, is subsequently injected through the catheter into the lungs [81]. Clearly, there are distinct differences between exposure

methods and instillation. Whereas exposure methods provide a natural route of entry to the lung, IT-instillation is an invasive delivery method. One of the most important disparities between these two methods is the distribution of particles. As opposed to exposure methods, which produce a relatively homogenous distribution of particles throughout the lung, IT-instillation tends to result in a denser distribution centrally compared to the peripheral regions as the drug is injected specifically at the site where the opening of the catheter resides (i.e. in the central region). These regional differences can have an impact on *e.g.* doses to certain cells and lung regions as well as on the degree and site of systemic absorption. Another important aspect to bear in mind is that IT-instillation bypasses deposition in the upper respiratory tract, i.e. above the site of drug delivery. Moreover, prior to delivering a drug via the IT route, it is important to carefully consider the choice of the instillation volume as well as the vehicle used to solubilise or suspend the compound. A too large instillate volume can potentially cause a too rapid mechanical clearance from the lung due to coughing, which clearly would have an impact on the pulmonary PK. It is also important to ensure that the vehicle does not have an influence on either the PD or the PK [82].

Regardless of the experimental methodology used to study pulmonary drug delivery in a preclinical setting destructive sampling is a necessity in order to obtain measurements of lung concentrations. That is, the animal is euthanized in conjunction with sampling and only one sample is obtained from each test subject. Expressed differently, *n* animals are needed to create a concentration-time profile of *n* observations. Interindividual variability in PK-parameters is thus expected to be seen in such profiles. Equally important, variability in the delivered dose is expected from inhalation PK studies that utilise exposure methods. Cooper *et al*. suggest that a

majority of the variability seen in such PK-studies can be attributed to interindividual variability in the inhaled dose rather than in the PK parameters [7].

2.2.6.2 Dose estimation

As opposed to *e.g.* oral and intravenous drug delivery where the given dose is easily controlled, dose estimation after inhalation is very complex. The same degree of control can essentially be achieved in a preclinical setting if the drug is directly instilled in the lung via the trachea (direct dosing methods). However, as mentioned in the previous subsection, techniques such as IT-instillation generally generate a less homogenous dose distribution throughout the lung.

In order to achieve a more uniform distribution in a preclinical setting, drugs can be inhaled from a chamber that contains a cloud of material (exposure methods). The total inhaled dose (*ID*) is defined as the total amount of drug that is inhaled by the animal, whereas the lung deposited dose (*LDD*) is defined as the actual amount of drug that is deposited in the lung. *ID* and *LDD* are calculated accordingly:

$$ID = \frac{C \times RMV \times D}{BW} \tag{2.15}$$

and

$$LDD = \frac{C \times RMV \times D \times DF}{BW} = ID \times DF\,, \tag{2.16}$$

where *C* is the concentration of substance in the air (mg/L), *RMV* is the respiratory minute volume (L/min), *D* is the duration of exposure (min), *BW* is the body weight (kg) and *DF* is the deposition fraction of the particles [83]. As can be seen from eqs.

2.15-2.16, several assumptions must be made in order to estimate *LDD* such as a consistent breathing pattern throughout the dosing period.

From eqs. 2.15-2.16 it is also clear that *C* is a key value for calculation of *LDD*. To enable calculation of *C*, a filter is included in the inhalation system setup. Air/compound is extracted to the filter at a predefined flow rate throughout the duration of exposure, *D*. The amount of drug collected on the filter (m_{filter}) is subsequently quantified using, for instance, liquid chromatography-tandem mass spectrometry (LC-MS/MS) and *C* is then calculated as

$$C = \frac{m_{filter}}{fr \times D} \quad , \tag{2.17}$$

where *fr* is the filter flow rate [7].

It is well-known that different aerodynamic diameters have different deposition probabilities in different lung regions, i.e. *DF* will be dependent on the particle size distribution. Prior to preclinical inhalation studies, this distribution is generally characterised using a cascade impactor, which provides a discrete aerodynamic particle size distribution. By using this discrete distribution and the *DF* corresponding to each particle size range, the total *DF* can be calculated for the batch used in a particular study. In the absence of such data, a default value of *DF* of 10% is generally used for deposition in rodent lungs [7]. 10% is also the conservative *DF* used for inhalation rodent studies by the Food and Drug Administration (FDA) [84]. An alternative approach to determining *LDD* is to quantify the amount of drug in the lung at the end of the exposure period. Under certain circumstances this method may represent *LDD*. However, the following criteria need to be met: 1) the inhalation period is short, 2) the pulmonary absorption that takes place from the start of the

exposure until the sampling of the lung is negligible, and 3) potential pulmonary metabolism of the parent compound is negligible. If any of these criteria are not met, then there is a substantial risk of underestimating *LDD* . Given that several compounds are rapidly absorbed to the systemic circulation [21], this method is inappropriate for numerous inhaled drugs. An alternative approach is to determine the area under the curve (AUC) in blood/plasma following inhalation. By comparing the AUC generated after inhalation of an unknown *LDD* with an AUC from a known dose, *e.g.* obtained from IV-dosing, it is possible to calculate *LDD*. Nevertheless, this approach also has its limitations. Firstly, if a poorly soluble drug is delivered, then the drug is likely to be transported away from the lung by MCC, which would lead to a reduction in the AUC relative to IV-delivery of the same dose. Secondly, drug absorption from the GI-tract would increase the AUC after inhaled drug delivery leading to overestimation of *LDD*. Thirdly, it is essential to assume a negligible first-pass pulmonary extraction . Consequently, much prior information of the PK of the drug candidate is needed to confidently rely on this approach.

To summarise, dose estimation is not straightforward after inhalation and the method used for estimating *LDD* should be chosen with care based on prior knowledge of the drug.

2.2.6.3 Exposure measurements

This subsection aims to provide an overview of the different exposure measurements that are often collected in preclinical inhalation PK-studies. This text also aims to underline potential limitations/challenges associated with the different measurements.

The PK-properties of inhaled compounds are routinely investigated by measurements of total lung concentrations (C_{lung}) and plasma concentrations (C_p). It is worth mentioning that measurements of C_p generally put high demands on the analytical sensitivity due to low C_p-values . This can primarily be attributed to two features: 1) inhalation doses are typically low, and 2) inhaled drug candidates tend to have a high clearance. For this reason, it can be very challenging to properly characterise the systemic PK after inhalation.

After inhalation, appearance of drug in plasma is a downstream event that follows after pulmonary absorption [2]. The C_p-profile is thus expected to inherently contain information on the pulmonary absorption, the events preceding the absorption as well as on the systemic PK.

It is generally accepted that the unbound drug concentration at the target site drives the pharmacological effect, a theory that often is referred to as 'the free drug hypothesis' [85]. For systemically acting drugs, the unbound plasma concentrations are usually assumed to reflect the free target site concentration. However, since the appearance of drug in the systemic circulation is the result of pulmonary absorption, unbound concentrations in plasma cannot be assumed to reflect the free target site concentration in the lung [2]. This constitutes a challenge since unbound plasma concentrations usually form the basis for establishing PK/PD-relationships.

As previously mentioned, it is possible to measure C_{lung} in a preclinical setting. To obtain such measurements, lungs are collected by destructive sampling at several time points after IT-instillation or exposure inhalation. In most studies, the entire lung is dissected and homogenised. Drug concentrations are subsequently measured in lung tissue homogenates, providing a time profile of C_{lung} where the organ is erroneously reflected as one anatomical entity. Moreover, the homogenisation

process also severely distorts the data interpretation by disrupting the normal compartmentalisation (*e.g.* lysosomal trapping) and by dissolving solid drug particles [6]. Indeed, the establishment of PK/PD-relationships based on total lung concentrations is known to be more challenging for poorly soluble compounds . Great caution should thus be exercised when interpreting such data, especially for the latter compound class.

As opposed to measurements of the fraction unbound in plasma (f_u), it is challenging from a technical point of view to measure the fraction unbound in lung tissue ($f_{u,lung}$) . Perhaps even more important, the information obtained from measuring the fraction unbound in a heterogeneous organ, such as the lung, should not be used in the same manner as f_u since it is unlikely that one value would be reflective of the entire organ. Expressed differently, $f_{u,lung}$ cannot be used to convert a measured total organ concentration (i.e. C_{lung}) into *one* unbound lung target site concentration. Nevertheless, two different *in vitro* methodologies have previously been employed for measuring the unbound fraction in lung homogenate ($f_{u,h}$): equilibrium dialysis and ultra-filtration. It is well-known that measurements obtained from these two methods potentially are confounded due to the necessity to homogenise the lung tissue, which disrupts the normal compartmentalisation of the cells and thereby can release drug that was entrapped in lysosomes and/or other endosomal compartments [77,84]. This experimental caveat needs to be taken into account when interpreting data and it is particularly prominent for basic compounds. Since lysosomes are acidic organelles, basic compounds are expected to be trapped in these cellular compartments due to a higher proportion of the molecules being charged in the acidic environment of the lysosome (pH 4-5) as compared to the cytosol (pH 7.4). Furthermore, the lung is a lysosome-rich tissue [86] and lysosomal

trapping might therefore be even more pronounced in this tissue. To overcome this potential experimental caveat, a lung slice methodology was developed, by virtue of using freshly prepared rat lung slices, the compartmentalisation of the lung tissue is kept intact. This can therefore be considered as a better *in vitro* system for studying the extent of lung tissue distribution. The lung slice methodology provides measurements of the unbound lung volume of distribution ($V_{u,lung}$). If $V_{u,lung}$ and $1/f_{u,h}$ differ from unity, the deviation is likely to be caused by the investigated substance being trapped in lysosomes and/or displaying carrier-mediated transport. Indeed, a systematic deviation from unity has been demonstrated for several basic compounds [77].

A procedure called bronchoalveolar lavage (BAL) is occasionally also used for preclinical PK-investigations to estimate the drug concentration in the epithelial lining fluid (ELF). This technique does not allow for direct measurements of ELF alone, but it is retrieved indirectly by repeated instillation of sterile saline. That is, technically the saline is diluted by an unknown volume of ELF. Thus a meaningful quantification of the drug concentration in this fluid would require determination of the volume of ELF obtained by BAL [84]. As urea diffuses freely throughout the body, the concentration of urea is expected to be the same in plasma and ELF. By using this knowledge, simultaneous measurements of urea in both fluids enables calculation of the dilution factor. However, diffusion of urea into the BAL fluid during the instillation has shown to confound this calculation in a time-dependent matter. It has therefore been suggested that the volume of ELF obtained from using this correction method should be referred to as an apparent volume of ELF [87]. Consequently, such measurements should also be interpreted with care.

Hence, there are several limitations with the different exposure measurements currently used to characterise the PK and PK/PD of inhaled drugs. Clearly, under many circumstances the utility of using the described exposure measurements for establishing PK/PD-relationships for locally acting inhaled drugs can be questioned. This problem is also reflected by the sparse scientific literature within the area of inhaled drugs, where the focus instead is typically on systemic effects driven by systemic exposure [88,89,90]. A few studies quantitatively link the pulmonary PK to the local effect by relating ELF concentrations to minimum inhibitory concentrations of antibiotics. This is, however, not following topical, but systemic, administration [91,92]. Interestingly, a PK/PD-analysis by Hochhaus *et al*. suggested that cardiac side-effects, but not the local pulmonary effects, could be described by the plasma PK after inhalation. The analysis instead implied that the free concentrations of drug were higher at the target site in the lung as compared to the plasma thus indicating a lung-selective drug exposure [93].

To conclude, the lack of exposure measurements that are relevant from a PK/PD perspective significantly hampers basic PK/PD understanding for locally acting inhaled drugs. Besides, due to the heterogeneous nature of the lung, the unbound concentration cannot be expected to be homogenous throughout the entire organ. Further research within this field is thus an important avenue for drug discovery as well as drug development.

2.3 Modelling

2.3.1 Empirical compartmental modelling (PK)

In the field of pharmacokinetics, empirical compartmental models are often used to describe the concentration time-profiles that follow after drug administration. In

short, a compartmental model consists of a finite number of subunits that are called compartments. Each of these compartments is assumed to consist of homogenous and well-mixed material. These compartments can interact with each other via the flow of material from one compartment to another. Furthermore, they can also interact with the external environment. Linear, time-invariant compartmental models are often used in the field of pharmacokinetics. The term 'time-invariant' means that the parameters of the system do not change over time [94]. The general form of such a system with n compartments is given by:

$$\frac{dx_i}{dt} = \sum_{\substack{j=1 \\ j \neq i}}^{n} k_{ji} x_j - \sum_{\substack{j=1 \\ j \neq i}}^{n} k_{ij} x_i - k_{i0} x_i + u_i(t), \qquad (2.18)$$

where x_i is the amount of drug in compartment i ($i \in \{1, ..., n\}$), k_{ji} is the rate constant from compartment j to compartment i, k_{ij} is the rate constant from compartment i to compartment j, k_{i0} is the elimination rate constant from compartment i to the external environment (i.e. the outflow from the system) and $u_i(t)$ is the input to compartment i [95]. In general, elimination is assumed to take place directly and exclusively from the central compartment [96]. That is, if the central compartment is referred to as compartment 1, $k_{i0} = 0$ for $i > 1$. Furthermore, the input is often limited to the central compartment, i.e. $u_i(t) = 0$ for $i > 1$. Eq. 2.18 is represented conceptually by the diagram in fig. 2.4.

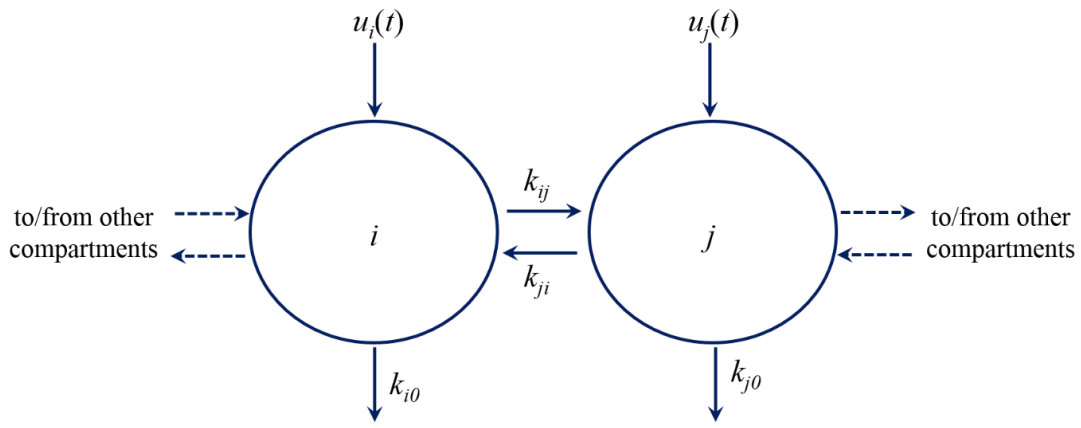

Figure 2.4 Two compartments of a compartmental system as described by eq. 2.18.

PK-studies will generally provide measurements of drug concentration and not the amount of drug. The introduction of an additional parameter is therefore required: the volume of distribution *V*. Given that the measurements are assumed to reflect drug concentrations in the central compartment, the model output *y* that will be compared with the observations is as follows:

$$y = \frac{x_1}{V_1}. \qquad (2.19)$$

In pharmacokinetics, an empirical compartmental model rarely has more than 3 compartments ($n \leq 3$). The following terminology will henceforth be used for pharmacokinetic compartmental models: 1-compartment model ($n = 1$), 2-compartment model ($n = 2$) and so on. The physiological interpretation of *e.g.* a 2-compartment model is that drug distributes between a central compartment ($i = 1$) and a peripheral compartment ($i = 2$), where the latter consists of tissues into which drug distributes more slowly. It is worth mentioning that the choice of *n* is normally

dependent on the available data. That is, the number of compartments is chosen to fit the concentration-time data of a particular drug [96].

Due to the simplicity of the 2-compartment model, it is suitable for illustrating two different parameterisation options: 1) micro-constants (k_{10}, k_{12}, k_{21} and V_1), and 2) physiological parameters (CL, V_1, CL_d and V_2). Both options are graphically illustrated by fig. 2.5:

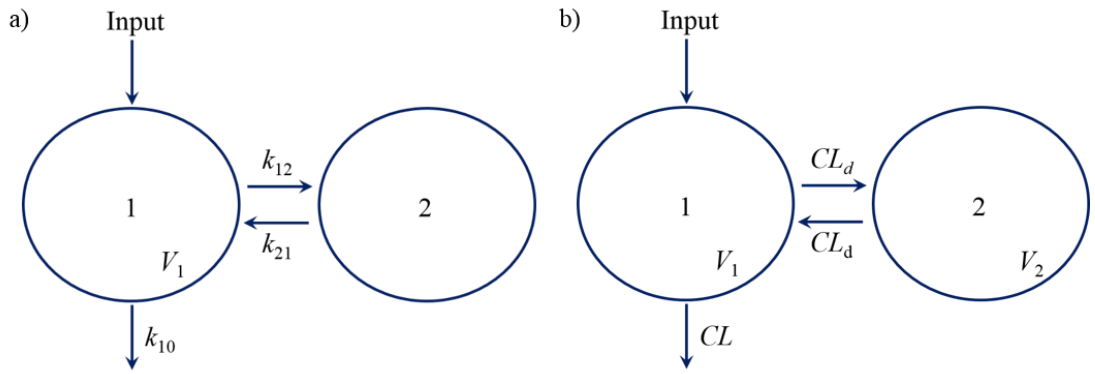

Figure 2.5 A 2-compartment model parameterised using a) micro-constants (k_{10}, k_{12}, k_{21} and V_1), and b) physiological parameters (CL, V_1, CL_d and V_2).

It can be argued that the advantage of the latter parameterisation option (fig. 2.5b) is that the parameters have a physiological meaning. Clearly, CL corresponds to clearance, which was described in section 2.2.3. V_1 and V_2 represent the volumes of the central and peripheral compartments, respectively, CL_d corresponds to the intercompartmental distribution between plasma and tissue, which might comprise *e.g.* perfusion, diffusion, active transport and partitioning [97]. In this thesis, the physiological parameterisation has been used.

2.3.2 Physiologically based PK models

Within drug discovery, there is generally much information gathered about individual drug candidates. In order to guide PK decisions physicochemical, *in vitro* and/or structural properties are characterised. In addition, at later stages, emphasis is put on studying *in vivo* PK of the compounds. Empirical compartmental models are often used for analysing *in vivo* studies as described in the previous section. These models are indeed very useful for many purposes, including characterisation of *in vivo* PK and guidance of future study design. However, by virtue of being empirical, these models cannot accommodate prior information on either the compound or the physiology. This feature restricts their ability to predict the PK for compounds with slightly different properties or to use such models for extrapolation to different physiological conditions [55]. Hence, although much information is available only a small fraction is used in the model development.

As opposed to the empirical compartmental models, physiologically-based pharmacokinetic (PBPK) models aim to integrate the current knowledge of physiological processes with physicochemical properties and/or other available information about the drug candidate in order to simulate complex biological processes. The level of detail is dependent on several factors, including nature and knowledge of the process(es) studied and the level of complexity needed reach a predictive capability. Hence, these models aim to provide a mechanistic understanding of the system by mathematically describing the relevant processes and integrating prior information on the drug. This approach carries advantages and there are several examples of when they have been used to provide new insights into important biological processes [98]. As observed PK-profiles are the result of several underlying processes, they can be said to carry subtle information on different

mechanisms driving the PK. Any discrepancies between the predicted and observed outcomes may therefore be informative as they can provide insights into mechanisms that have not been accounted for by the model. As such, PBPK models can be used for hypothesis generation, to design experiments aimed at supporting/rejecting the hypothesis and to answer key questions in drug discovery and development projects [99].

Traditionally, PBPK models have been said to consist of a structural model and two distinctive groups of input parameters: 1) system-specific input parameters, such as blood flows and organ volumes that are specific for the investigated species, and 2) drug-specific input parameters, such as permeability, clearance and binding kinetics parameters that are unique for each investigated drug. The structural model comprises a compartmental representation of organs and tissues connected by the blood flow [100], where each compartment is represented by a discrete tissue volume perfused uniformly by its specific blood flow [101]. A schematic representation of a typical whole body PBPK model is shown in figure 2.6.

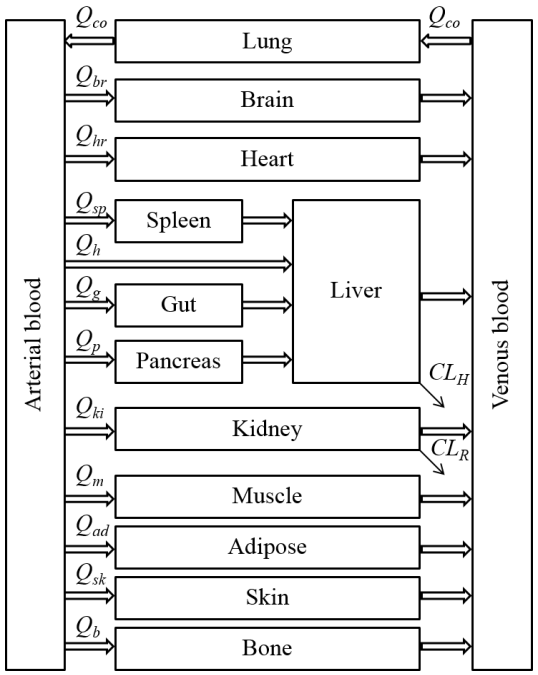

Figure 2.6 A schematic representation of a typical whole-body physiologically based pharmacokinetic (PBPK) model adapted from [102].

For compartment *i*, the rate of change of quantity within the organ is described as [103]

$$V_i \frac{dC_i(t)}{dt} = Q_i \left(C_A(t) - \frac{RC_i(t)}{K_{p,i}} \right), \quad C_i(0) = 0, \tag{2.20}$$

where V_i is the tissue volume, C_i is the drug tissue concentration, Q_i is the blood flow to the tissue, C_A is the arterial drug concentration, R is the blood/plasma ratio and $K_{p,i}$ is the tissue-plasma partition coefficient.

The drug distribution into a tissue can be described as either perfusion rate-limited (eq. 2.20) or permeability rate-limited. The former tends to apply for small lipophilic compounds for which the tissue barrier does not present a barrier for diffusion. Hence, the blood flow to the tissue becomes the rate-limiting step for the distribution

process. In contrast, permeability rate-limited distribution might be feasible for describing the distribution of large polar molecules where permeability across the cell membrane constitutes the rate-limiting step [104].

A group of important drug-specific input parameters for the distribution is the K_p-values, defining the ratio of drug concentration between tissue and plasma at equilibrium. Previously, K_p-values were obtained by time-consuming animal studies where *in vivo* steady-state tissue and plasma drug concentration data were collected. Today there are several *in silico* methodologies for prediction of the tissue to unbound plasma partition coefficients ($K_{p,u}$-values) in the literature that are derived from a mechanistic understanding of the tissue composition as well as the physicochemical properties of the compound. The methodology suggested by [105] has been found to have good predictive capabilities [106]. In short, this method utilises a mechanistic equation that incorporates drug dissolution in tissue water and partitioning into neutral lipids and neutral phospholipids. For acids, neutrals and very weak bases it also takes binding to extracellular proteins into account. Compound-specific input parameters for this equation are unbound fraction in plasma (f_u), the partition coefficient of unionised drug (P) and, if applicable, pK_a [105]. Thus, $K_{p,u}$ is predicted by

$$K_{p,u} = \frac{X \times f_{IW}}{Y} + f_{EW} + \left(\frac{P \times f_{NL} + (0.3P + 0.7) \times f_{NP}}{Y} \right) + \left(\frac{1}{f_u} - 1 - \frac{P \times f_{NL,P} + (0.3P + 0.7) \times f_{NP,P}}{Y} \right) \times \frac{[PR]_T}{[PR]_P}, \quad (2.21)$$

where f_{EW}, f_{IW}, f_{NL} and f_{NP} are fractional tissue volumes for extracellular water, intracellular water, neutral lipids and neutral phospholipids, respectively. The ratio

$[PR]_T/[PR]_P$ refers to the tissue to plasma ratio of albumin or lipoprotein (albumin is used for acids and very weak bases, whereas lipoprotein is used for neutral compounds). The definitions of X and Y depend on the compound class as described in [105], *e.g.* for neutral compounds both equal 1 due to the lack of ionisation.

A compartment can represent a part of an organ, an organ or several organs lumped together. They are generally described as homogenous, well-stirred compartments. For tissues described by permeability rate-limited distribution, the tissue is often subdivided into two well-stirred spaces [107]. As the complexity of the model increases with the number of compartments, only compartments critical for characterising the system should be included [98]. Consequently, there are several examples in the literature of reduced models where tissues with similar perfusion rates have been lumped together in order to reduce this number and the overall complexity of the model [108,109].

For the inhaled route of administration, a third group of input parameters should be added: formulation-specific input parameters, such as the particle size distribution. This parameter is of importance for describing the input signal to the system (the deposited dose), which is more complex than other routes of administration.

2.3.3 Structural identifiability and parameter estimation

This section aims to provide a short overview of parameter estimation and structural identifiability. Briefly, parameter estimation aims to, given a model structure and some sampled experimental data, find a set of model parameters θ which is thought to have generated the data. This is usually done by minimising (or maximising) a cost function (sometimes referred to as an objective function), which quantifies how well the model and the set of parameters θ fit the sampled data.

In this section, we will only consider cases where the optimisation process relies on finding the minimum of a cost function. Clearly, the cost function best suited for the optimisation will depend on the nature of the problem investigated. A commonly used cost function is the sum of squared errors, a so called least squares approach. This approach is performed as follows: consider the observation function

$$y(t,\theta), \tag{2.22}$$

which depends on time t and a set of parameters θ. An experiment is conducted, providing a sampled data vector (experimental data) $\hat{y}$ at n time points, which we hope to describe using the model $y(t,\theta)$. According to the least squares approach, the best parameter estimates are defined as those which minimise the sum of the squared differences between the model output $y(t,\theta)$ and the observations $\hat{y}$, i.e.

$$\sum_{i=1}^{n}\left(y_i(t_i,\theta)-\hat{y}_i(t_i)\right)^2 . \tag{2.23}$$

This is commonly known as ordinary least squares. The differences between the model output $y(t,\theta)$ and the observations $\hat{y}$ are referred to as the residuals. Ordinary least squares assumes that all observations are equally reliable and thus should be treated equally. However, if the standard deviation σ_i of the experimental error is not expected to be constant but instead *e.g.* is proportional to the magnitude of each observation $\hat{y}_i$ and the data span over several orders of magnitudes, this assumption might not be valid. Weighted least squares can then be applied by multiplying each

residual by a weight proportional to the inverse of the standard deviation $w_i = 1/\sigma_i$ to form:

$$\sum_{i=1}^{k} \frac{\left(y_i(t_i,\theta) - \hat{y}_i(t_i)\right)^2}{\sigma_i^2} \,. \tag{2.24}$$

In the case of the standard deviation σ_i being proportional to the magnitude of the sampled data, it is natural to use the inverse sampled data as weights. This could be done by using either the sampled data $\hat{y}$, or if the model is deemed more reliable, the model output $y(t,\theta)$ in which case:

$$w_i = \frac{1}{y(t_i,\theta)} \,. \tag{2.25}$$

Given that the function $y(t,\theta)$ is nonlinear, nonlinear regression is used to find the set of parameters θ that minimises the cost function. In contrast to linear regression, where the unique solution can be found by solving a set of linear equations, nonlinear regression requires more advanced search methods. An optimisation algorithm, *e.g.* a gradient descent algorithm, is used to find the minimum of the cost function. In this context another important difference between linear and nonlinear models should be highlighted. A gradient descent method will follow the gradient of the cost function to a point where small changes to the set of parameters θ no longer improve the cost. Such a point is known as a *local* minimum. The cost function of a general nonlinear model might have several local minima, and the gradient descent method will follow the gradient from an initial set of parameter estimates and find one of these. Hence, it

will be unknown if it is the "best", *global* minimum. The linear model on the other hand will only have one minimum, which is then the global minimum.

Importantly, for parameter estimates to be meaningful, the aim of parameter estimation needs to be extended: the aim is to find a set of *uniquely identifiable* parameters θ that minimises (or maximises) an *appropriately chosen* cost function. From this revised aim, it is clear that structural identifiability is a prerequisite for parameter estimation. Briefly, a model is said to be structurally identifiable if it is possible to uniquely determine all model parameters under ideal circumstances with an error-free, continuous set of observations [110,111]. In case of a non-identifiable model, several combinations of parameters will produce identical input-output behaviours. Hence, whilst a non-identifiable model might well describe the data, the parameter values estimated from such model should be interpreted very cautiously.

2.3.4 Sensitivity analysis

A sensitivity analysis can be used to quantify how "sensitive" the output of a system is to changes in *e.g.* parameter values, initial conditions or inputs [112]. Such analyses can be useful for several reasons. One important application is to understand which parameters are the most influential on the outcome/response of the system. Such information can be useful *per se* to gain a better understanding of the input-output behaviour of the system. Moreover, if it is possible to minimise the uncertainty of one/some of the input parameters, information from a sensitivity analysis can be useful for prioritising which input parameter(s) to choose in order to reduce the uncertainty of the output the most [113]. It can also be useful for optimal experimental design by *e.g.* identifying sampling times that would generate informative data, which is crucial for parameter estimation accuracy.

When implementing larger simulation models, a sensitivity analysis can also be an important part of the model verification process; by detecting unexpected input-output behaviours, potential bugs in the model code can be detected. Another possible application is model simplification, which can be done by identifying, and subsequently possibly removing, redundant parameters that do not have any effect on the output.

In this section, the focus will be on so-called local sensitivity analysis techniques of systems that can be written on the following general form as in [112]:

$$\frac{dy}{dt} = f(y, \theta), \tag{2.26}$$

where y is an n-dimensional vector of state variables, θ is a p-dimensional vector of parameters and the independent variable is time, t.

The sensitivity of a state variable, y_i, to a parameter, θ_j, can be expressed by the following sensitivity function [112]:

$$S(t) = \frac{\partial y_i(t)}{\partial \theta_j}. \tag{2.27}$$

If the analytical solution of eq. 2.26 is known, its partial derivatives (eq. 2.27) may also be solved analytically. However, this is rarely the case and numerical methods are therefore generally used to approximate the sensitivity function (eq. 2.27). By a local sensitivity analysis, it is implied that eq. 2.27 is evaluated around one fixed value of the parameter θ_j. These methods utilise the so-called one-at-a-time (OAT) techniques, meaning that the parameters are varied one at a time while the other parameters are kept at their baseline (nominal) values. One commonly used

technique is the so-called finite difference method, which approximates the partial derivative defined in eq. 2.27. Eq. 2.27 can also be defined accordingly (forward difference considered) [112]:

$$\frac{\partial y}{\partial \theta_j} = \lim_{\Delta\theta_j \to 0} \frac{y(t, \theta_j + \Delta\theta_j) - y(t, \theta_j)}{\Delta\theta_j}. \qquad (2.28)$$

As can be seen from the definition above, eq. 2.28 is only valid if an infinitesimal small perturbation of the parameter θ_j is considered; i.e. $\Delta\theta_j \rightarrow 0$. This has important implications for the finite difference method, which is implemented as follows [112]:

$$\frac{\partial y}{\partial \theta_j} \approx \frac{y(t, \theta_j + \Delta\theta_j) - y(t, \theta_j)}{\Delta\theta_j}. \qquad (2.29)$$

Hence, to ensure that eq. 2.29 is equivalent to the former equation (eq. 2.28), it is required that $\Delta\theta_j$ is small. The factor by which the nominal parameter value is multiplied is generally referred to as the perturbation factor ξ. Theoretically, eq. 2.28 will only be equivalent to eq. 2.29 if ξ approaches 0. Nevertheless, numerically this can never be achieved as the limited precision of the calculations would then give rise to numerical inaccuracies. ξ should thus be chosen to be as small as possible while still maintaining numerical accuracy [112].

For interpretation purposes, it is generally more convenient to investigate the normalised sensitivity. One approach that for instance is used in Berkeley Madonna™ is [114]:

$$S(t) = \frac{y(t, \theta_j + \Delta\theta_j) - y(t, \theta_j)}{\Delta\theta_j / \theta_j} = \frac{y(t, \theta_j + \Delta\theta_j) - y(t, \theta_j)}{\xi}. \qquad (2.30)$$

2.4 Summary

Chapter 2 provides a summary of the relevant and necessary theoretical background that was used in this thesis for designing, performing and interpreting experiments as well as to develop and apply mathematical models. The latter category includes modelling of the *in vivo* binding kinetics of two corticosteroids and the development of a mechanistic *in silico* model for predicting the systemic PK, the local tissue concentrations as well as the resulting receptor occupancy after inhalation.

Chapter 3 Development of an *in vivo* receptor occupancy methodology

3.1 Introduction

One of the main findings of the literature review was that researchers investigating pharmacokinetics via the inhaled route face the tough challenge of not being able to directly measure unbound drug concentrations locally in the lung tissue. Furthermore, the appearance of drug in the blood is a downstream event that follows from absorption of inhaled drug from the lung [2]. As a result, the unbound drug concentration in the blood cannot be assumed to reflect the unbound drug concentration at the target site in the lung . Clearly, this constitutes a challenge for the understanding of PK/PD-relationships for locally acting inhaled drugs. As receptor occupancy is driven by the unbound drug concentration at the target site, such measurements would clarify the PK- and PK/PD-evaluation of locally acting inhaled drugs and provide a quantitative estimate of target engagement in the target organ. Receptor occupancy methodologies amenable to targets of inhaled drugs, such as the glucocorticoid receptor (GR), are therefore desired.

Inhaled corticosteroids have been stated to constitute the cornerstone of asthma treatment [115]. The pharmacological effect of this compound class is mediated by binding to the cytoplasmic GR, which forms a dimer and translocates to the nucleus, where it either binds to sites on the DNA called glucocorticoid responsive elements (transactivation) or interacts with transcription factors (transrepression) [116]. Hence, it was proposed at an early stage that receptor-binding properties could be important in order to link the PK to the PD for this compound class [117]. Indeed,

more recently PK/PD-relationships for receptor/gene-mediated effects of intravenously administered corticosteroids were described in the liver [118].

Estimates of drug occupancy are typically obtained by assessing the number of free binding sites using a tracer ligand that, when administered at a sufficiently low dose, binds with high affinity and specificity to the target of interest. A tracer for the GR amenable to *in vivo* occupancy studies has not been previously reported, although numerous attempts have been made to develop positron emission tomography (PET) radiotracers for this receptor [119]. Receptor occupancy of the GR has been measured in the rat using *ex vivo* binding assays where the tracer is incubated with the tissue sample after collection from the animal [120,121]. Receptor occupancy profiles generated from this methodology were shown to be similar after intravenous (IV) and intratracheal instillation of an aqueous solution of triamcinolone acetonide [120].

While *in vitro* and *ex vivo* binding assays rely on radiolabelled tracer ligands, tracer analysis by liquid chromatography tandem mass spectrometry (LC-MS/MS) offers advantages including simultaneous determination of occupancy and drug concentration. Furthermore, tracer quantification with LC-MS/MS is made without interference of metabolites [122], a feature that is of particular interest for *in vivo* receptor occupancy studies where the tracer is administered to the animal.

Based on the properties of several inhaled drugs, it can be reasoned that a fully *in vivo* based receptor occupancy methodology would carry advantages over *ex vivo* binding assays for the study of inhalation drugs. This reasoning is primarily based on the anticipated risk of additional particle dissolution and thus subsequent formation of drug-receptor complexes post-sacrifice during the processing steps of tissues, which could lead to overestimation of pulmonary occupancy if the tracer is added *ex*

vivo. As several inhaled corticosteroids are poorly soluble compounds, and hence are retained in a solid state in the lung for a considerable time period after inhalation, the advantage of *in vivo* tracer administration is perhaps even more pronounced for this drug class and route of administration. Moreover, the reliability of *ex vivo* binding assays has been questioned since dissociation of drug from receptors during incubations could lead to underestimation of occupancy [123,124].

One objective of this PhD thesis was therefore to complete the ongoing development of an *in vivo* receptor occupancy methodology for an inhaled target (the GR).

Identification of tracer molecules is perhaps the most challenging step and this often constitutes a bottle-neck in the development of receptor occupancy methodologies for new targets. Successful tracers have been shown to have a high target-bound fraction (f_{tb}). A mathematical model, which describes f_{tb} as a function of the unbound target site concentration (C_u) has been proposed by Fridén *et al*. [125]:

$$f_{tb} = \frac{1}{1 + \frac{V_{u,brain}(K_d + C_u)}{B_{max}}} \quad , \qquad (3.1)$$

where $V_{u,brain}$ is a measurement of the nonspecific binding in brain tissue, K_d denotes the affinity of the tracer to the target and B_{max} denotes the target density in the brain. Although this model was initially developed for brain targets, it is applicable for all tissues. Tracer molecules are typically given at low doses with resultingly low C_u. If $C_u << K_d$, eq. 3.1 simplifies accordingly to give:

$$f_{tb} = \frac{1}{1 + \frac{K_d V_{u,brain}}{B_{\max}}}. \qquad (3.2)$$

Hence, given that successful tracer molecules have been shown to have high f_{tb} [125], eq. 3.2 points at three important properties for functioning tracer molecules: 1) a high affinity of the tracer to the target (affinity=1/K_d), 2) a low degree of nonspecific binding ($V_{u,brain}$), and 3) a high expression of the target (B_{max}). Needless to say, the third property should already be considered when choosing the target of interest. If B_{max} is considered to be sufficiently high, the choice of potential tracer candidates to take forward to experimental evaluation should be based on the two first properties. According to eq. 3.2, molecules with a low product of K_d and $V_{u,brain}$ (or the corresponding measurement for the tissue of interest) should thus be favoured. An additional important property, which is not covered by eq. 3.2, is a high bioanalytical sensitivity to enable quantification of low tracer concentrations.

This chapter will describe the development of a novel *in vivo* receptor occupancy methodology for the GR, which was accepted for publication in the Journal of Pharmacology and Experimental Therapeutics [126].

3.2 Tracer identification and development of an *in vivo* protocol

The following subsection describes the sequence of steps taken for developing an *in vivo* receptor occupancy methodology for an inhaled target with respect to the tracer identification *in vitro* as well as the *in vivo* protocol development.

The experiments described in sections ‘3.2.1.2 Tracer identification *in vitro*’ and ‘3.2.1.4 Evaluation of tracer dose’ were performed during my master’s thesis. The experiment described in section ‘3.2.1.5 Evaluation of nonspecific binding’ was done

whilst employed at AstraZeneca R&D Gothenburg. In contrast to the data collection described in the aforementioned three sections, which was done prior to the PhD studies, modelling of the data generated from experiments described in sections '3.2.1.4 Evaluation of tracer dose' and '3.2.1.5 Evaluation of nonspecific binding' was performed as part of this PhD project.

The author was responsible for the design and the execution of all studies. All studies but one were carried out by the author alone: during the *in vivo* part of the PK-study assistance was received from Dr Markus Fridén at AstraZeneca R&D Gothenburg.

3.2.1 Methods

3.2.1.1 Chemicals and animals

Chemicals. Bovine serum albumin fraction v was purchased from Roche (Penzberg, Germany), KCl, $MgSO_4$, HEPES, $NaHCO_3$, NaOH, glucose, N,N-dimethylacetamide, dexamethasone, 5,5-diethyl-1,3-diphenyl-2-iminobarbituric acid and polyethylene glycol 400 were obtained from Sigma-Aldrich (St. Louis, MO, USA). NaCl, $CaCl_2$, KH_2PO_4 and ascorbic acid were purchased from Merck (Darmstadt, Germany). Fluticasone propionate, R-budesonide, compound 1 (fig. 3.1a), and compound 2 (fig. 3.1b) were synthesised by chemists at AstraZeneca R&D Gothenburg. Compound 1 and 2 were discovered as part of a collaboration between AstraZeneca and Bayer HealthCare in the field of selective glucocorticoid receptor modulators. Chemicals were of analytical grade and all solvents of HPLC grade.

a)

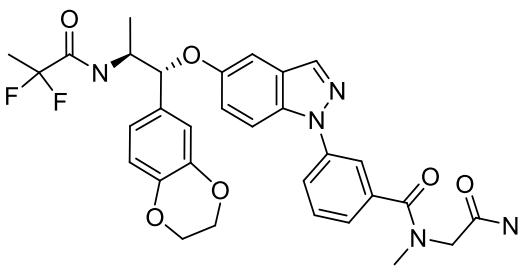

1

b)

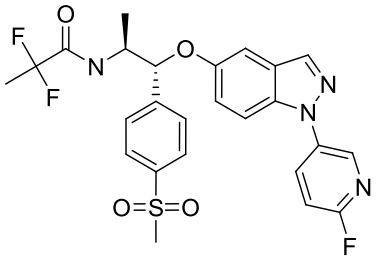

2

Figure 3.1 Chemical structures for a) compound 1 (EC_{50} = 0.153 nM, log$D_{7.4}$ = 2.5), and b) compound 2 (EC_{50} = 0.476 nM, log$D_{7.4}$ = 2.9)

Animals. Male Wistar Han rats (Harlan, Horst, the Netherlands) weighing 275 to 325 g were used for the *in vitro* and the *in vivo* studies. The animals were group-housed at 18-22 ºC under a 12:12 h light/dark cycle with free access to food and water for at least five days prior to the experiments. The studies were approved by the Animals Ethics Committee of Gothenburg (234-2011, 190-2010 and 71-2013). Studies were carried out in accordance with the *Guide for the Care and Use of Laboratory Animals* as adopted and promulgated by the US National Institutes of Health.

3.2.1.2 Tracer identification *in vitro*

AstraZeneca's internal chemical library has numerous of molecules that bind to GR and thus could be tested as potential tracer candidates. Experimental evaluation of all compounds would thus not be feasible. A rational approach was applied in order to narrow down the search space of molecules to enable identification of molecules with a higher probability of success. As described in section 3.1, compounds with a

low product of K_d and $V_{u,brain}$ (or the corresponding measurement describing the nonspecific binding in the tissue of interest) are more likely to be successful tracer molecules. Needless to say, the added value of making this search is highly dependent on the choice of criteria. The database contains results from numerous tests, it is thus important to identify a test that gives information about the properties (i.e. K_d and nonspecific binding). Furthermore, to minimise exclusion of promising compounds, a commonly used test must be chosen such that several compounds have been evaluated with this particular test.

A high lipophilicity is known to be associated with a high degree of nonspecific binding; lipophilicity, as expressed by log$D_{7.4}$, was therefore chosen to represent the nonspecific binding. The *in vitro* potency (EC_{50}) from a reporter gene assay system determining the transrepression activity [127] was used as a surrogate for the dissociation constant (K_d). Compounds were ranked by their differences between $-\log(EC_{50})$ and log$D_{7.4}$ as a large difference indicates a compound with a high potency and a low degree of nonspecific binding in tissue; i.e. a combination predicted to give a high value for f_{tb} according to eq. 3.2, which has been shown to be an important property for successful tracer molecules [125].

Based on this criterion a first selection of compounds was made and these were evaluated for the degree of nonspecific binding in slices of agarose-inflated rat lungs using a methodology described in [77]. Two compounds with low measured values of EC_{50} and low degree of nonspecific binding were subsequently identified from this selection. To experimentally determine f_{tb} for these compounds *in vitro*, lung slices were incubated at subnanomolar concentrations of the potential tracer either in the absence (n = 3 to 6) or presence of excess of R-budesonide (100 nM, n = 3 to 6). Lung slice concentrations of the tracer candidate from incubations with excess R-

budesonide corresponded to the nonspecific binding ($C_{slice,nonspec}$) and the concentrations from incubations containing only the tracer candidate gave the total binding ($C_{slice,total}$). f_{tb} was calculated using equation 3.3, given by

$$f_{tb} = \frac{C_{slice,total} - C_{slice,nonspec}}{C_{slice,total}} \quad , \qquad (3.3)$$

and these values, as well as the analytical sensitivity, were subsequently used for ranking of the compounds. A more detailed description of the evaluation of tracer candidates *in vitro* is provided in the master's thesis written by the author [128].

3.2.1.3 Studies for *in vivo* protocol development

In general terms, *in vivo* receptor occupancy is measured by tracer administration, usually via the intravenous route, and subsequent quantification of tracer concentration in the tissue(s) of interest. Receptor occupancy is reflected by the difference between tissue tracer concentrations in treated animals and drug-naïve control animals.

As was mentioned in section 3.1, successful tracers have been shown to have a high f_{tb}-value. From eq. 3.1, it can be seen that a low C_u of tracer is key to obtaining a high value for f_{tb}. A low tracer dose is therefore used to achieve this goal as well as to ensure that the tracer only binds to a small portion of the available binding sites. Hence, this is important to certify that the measured tissue tracer concentration will be sensitive to changes in occupancy by the drug.

The maximum concentration of tracer is derived from drug-naïve control animals and is denoted by $C_{control}$, which represents the sum of the nonspecific ($C_{nonspec}$) and the maximum specific binding of tracer (i.e. the receptor-bound concentration,

$C_{spec,max}$) and corresponds to 0% occupancy (i.e. all receptors are available to the tracer). $C_{nonspec}$ thus has to be taken into account to enable estimation of the level of specific tracer binding to derive the occupancy by drug from the tracer concentration measured in animals pre-treated with test compound (C_{test}). A second group of animals is therefore dedicated to determination of $C_{nonspec}$. These animals are pre-treated with a high dose of another ligand, with the purpose of occupying all receptors of interest, prior to the tracer administration. Hence, the lower tissue concentration of tracer measured in these animals is only reflective of $C_{nonspec}$ and is assigned to a value of 100% occupancy. To summarise, three different groups of animals are included in *in vivo* receptor occupancy methodologies: 1) drug-naïve control animals ($C_{control}$), 2) animals dedicated to determination of the nonspecific binding ($C_{nonspec}$), and 3) animals treated with test compound (C_{test}). The measured tissue concentrations of tracer in the drug-naïve control animals and the treated animals can be described accordingly:

$$C_{control} = C_{nonspec} + C_{spec,\max} \tag{3.4}$$

$$C_{test} = C_{nonspec} + C_{spec,\max}(1 - RO) \tag{3.5}$$

An appropriate time period, a so-called post-tracer survival interval, is needed after tracer administration for the tracer to bind the receptor and for the nonspecific binding to decrease so that a high ratio of total-to-nonspecific binding is achieved [129].

Consequently, once a promising tracer candidate has been identified, several tracer doses, and sometimes also post-tracer survival intervals, are tested in order to

develop experimental procedures that yield a high ratio of total-to-nonspecific binding.

3.2.1.4 Evaluation of tracer dose

Three dose levels of the tracer candidate compound 1 were assessed (40, 400 and 4000 nmol/kg, respectively). Henceforth, compound 1 will be referred to as the tracer. At each dose level the animals were divided into two groups in order to investigate if $C_{control}$ was distinguishable from $C_{nonspec}$. A post-tracer survival interval of 30 minutes was tested since it has proven successful for several *in vivo* receptor occupancy methodologies [130,131]. For determination of tissue concentrations of tracer, the animals were injected via the tail vein with their group specific dose of tracer (n = 3). Animals dedicated to determination of $C_{nonspec}$ were pre-treated with a high IV-dose of compound 2 via the tail vein 30 minutes prior to the tracer administration (compound 2, 5.0 µmol/kg, n = 2, n = 3 and n = 2 for the 40, 400 and 4000 nmol/kg dose groups, respectively). A high dose of compound 2 was used as pre-treatment since it is a highly potent compound (transrepression EC_{50} = 0.476 nM) with a long half-life in blood, and was thus expected to give a high occupancy over a long time period. This study was complemented with an additional dose level (4 nmol/kg, n = 3) using an identical protocol except that the animals dedicated to the determination of $C_{nonspec}$ were pre-treated with dexamethasone (20 mg/kg, n = 3). The vehicle used for all three compounds was N,N-dimethylacetamide, polyethylene glycol 400 and water (1:1:1, w/w/w). Thirty minutes after administration of the tracer candidate, a blood sample was taken and the lung was dissected for concentration determination.

3.2.1.5 Evaluation of nonspecific binding

To confirm that only nonspecifically-bound tracer remained after pre-treatment with compound 2, $C_{nonspec}$ was measured after pre-treatment with dexamethasone (20 mg/kg, n = 3). Dexamethasone was injected via the tail vein 30 minutes prior to IV-administration of tracer (40 nmol/kg). Thirty minutes after the tracer administration, a terminal blood sample was collected and the lung was dissected for concentration determination.

3.2.1.6 PK-study

The plasma PK of a low tracer dose (30 nmol/kg) was investigated over the first 30 minutes after IV-administration of the tracer, i.e. over the so called post-tracer survival interval. This experiment thus aimed to characterise the PK over this time period. As *in vivo* receptor occupancy methodologies benefit from low tracer doses and the bioanalytical sensitivity allowed for using a slightly lower tracer dose than the one used in section 3.2.1.5, a tracer dose of 30 nmol/kg was selected. All animals (n = 8) were anaesthetised by inhalation of isoflurane shortly before the tracer administration. A heparinised catheter was inserted in *arteria femoralis*, the tracer was subsequently injected via the tail vein (30 nmol/kg). Blood samples (100-150 µL/sample) were then repeatedly collected directly in Microvette® 300 LH tubes (Sarstedt, Nürnbrecht, Germany) from the arterial catheter at the following time points: 2, 5, 10, 15, 20, 25 and 30 min. The animals were maintained under inhalation anaesthesia during the entire study and were then euthanized in conjunction with the last sample by cutting the abdominal aorta.

3.2.1.7 Evaluation of tracer function in other organs

To investigate the functionality of the tracer in various organs, $C_{control}$ and $C_{nonspec}$ were compared in several organs. Animals dedicated to measurements of $C_{nonspec}$ were pre-treated intravenously with dexamethasone (20 mg/kg, n = 5) prior to tracer administration, whereas animals dedicated to measurements of $C_{control}$ did not receive any pre-treatment (n = 5). Dexamethasone was injected via the tail vein 30 minutes prior to IV-administration of tracer (30 nmol/kg). All animals were sacrificed 30 minutes after tracer administration, a terminal blood sample was collected and organs (lung, liver, brain, kidney and spleen) were dissected for concentration determination.

3.2.1.8 General procedures and final protocol for *in vivo* receptor occupancy measurements

The tracer, compound 1, was given intravenously via the tail vein (30 nmol/kg). Animals dedicated to determination of $C_{nonspec}$ had been pre-treated intravenously with dexamethasone (20 mg/kg) 30 minutes prior to the tracer administration. In contrast, animals set aside for determination of $C_{control}$ did not receive any pre-treatment. Animals were anaesthetised by inhalation of isoflurane during the administration(s) and were then allowed to wake up. Anaesthesia during tail vein administrations was made a standard procedure since the tail is sensitive. In conjunction with the termination, the rats were anesthetised once more by inhalation of isoflurane. The fur was rinsed with 70% ethanol and laparotomy was conducted. Heparin (2000 IU) was injected into *vena cava*, a terminal blood sample was collected (3-4 mL) in a heparinised tube from the abdominal aorta and the rat was subsequently euthanized by cutting the abdominal aorta. The terminal blood sample

was taken 30 minutes after the tracer administration. The diaphragm was then removed and the apex was incised along its transverse axis. The pulmonary circulation was perfused by room-tempered bovine serum albumin solution (40 mL, 2.5% bovine serum albumin) via the pulmonary artery in order to clear the tissue of blood. The heart and lung were removed from the thorax *en bloc*. The trachea was dissected from the lung and a predefined section of the spleen (~200 mg) was dissected. The lung and spleen samples were weighed and stored separately in tissue tubes and Eppendorf tubes respectively at - 20 ºC until sample handling and analysis, a detailed description of these procedures is provided in section 3.2.1.10. Receptor occupancy was then calculated for each animal (eq. 3.6, section 3.2.1.9).

3.2.1.9 Calculation of receptor occupancy

Receptor occupancy calculations are made for each animal using a previously established method [130,131,132,133] described below:

$$\text{Receptor occupancy}\,(\%) = 100 \times \left(1 - \frac{Ratio_t - 1}{Ratio_c - 1}\right), \qquad (3.6)$$

where

$$Ratio_t = \frac{C_{test}}{C_{nonspec}} \qquad (3.7)$$

and

$$Ratio_c = \frac{C_{control}}{C_{nonspec}}. \qquad (3.8)$$

$Ratio_t$ refers to the ratio of total tracer concentration in tissue from animals treated with test compound (C_{test}) divided by the mean value of $C_{nonspec}$ obtained from the

group of animals pre-treated with a high dose of another ligand. $Ratio_c$ represents the ratio of $C_{control}$ to $C_{nonspec}$, where $C_{control}$ is the mean value of the total tissue concentration of tracer obtained from a drug-naïve control group. Accordingly, when $Ratio_t$ is equal to $Ratio_c$ this corresponds to an occupancy of 0% and when the $Ratio_t$ is 1 (i.e. the tracer concentration in the treated animal is equal to $C_{nonspec}$) to an occupancy of 100%.

3.2.1.10 Analytical procedures

Sample handling. The blood samples were collected in heparinised tubes which were centrifuged for 10 minutes at 4000g (Rotanta 46R, Hettich, Germany). The plasma samples were subsequently transferred to Eppendorf tubes and stored at -20 ºC until analysis.

The tissue tubes containing lung samples were separately flash-frozen in liquid nitrogen and then immediately placed into Covaris CryoPrep™ (Covaris Inc., Woburn, Massachusetts, USA) for pulverisation. This freeze-fracture-procedure was repeated until pulverisation was judged as being sufficient, generally three times. The pulverised samples were then transferred to separate glass tubes and Ringer-buffer was added to each lung sample (4.0 mL). Covaris E210 and SonoLab software v.4.2.0 (intensity 10.0, cycles 1000, treatment time 180 s, bath degree 40 °C) were used for dissolution of the samples.

Predefined parts of the liver, brain, spleen and kidney were weighed in Eppendorf tubes and homogenised in 3 volumes of distilled water (w/v) with an ultrasonic probe. The samples were stored at -20 ºC until analysis.

Analytical methods. Concentrations of tracer and FP in tissues and plasma were quantified using reversed phase LC-MS/MS with the electrospray ionization source

set in positive mode. The LC-system used was LC Agilent 1200 Series gradient pump (Agilent Technologies, Waldbronn, Germany), a CTC autosampler (CTC Analytics, Zwingen, Switzerland), a HALO C18 column (30×2.1 mm, 2.7 µm, Advancedmaterialtechnology) and an Agilent 6460 detector (Santa Clara, CA, USA). Gradient elution over 1.5 minutes time with acetonitrile and 0.2% formic acid and a flow rate of 0.7 mL/min was performed.

Protein precipitation was used for all samples except lung homogenates. A defined volume (50 µL) of each sample was added in triplicate to a NUNC 96-deepwell plate (Nalge Nunc International, Rochester, NY) and was then protein precipitated by addition of cold acetonitrile containing 0.2% formic acid and 100 nM of 5,5-diethyl-1,3-diphenyl-2-iminobarbituric acid as internal standard (200 µL) to each sample. After two minutes of mixing with a VWR VX-2500 Multi-Tube Vortexer (VWR International west Chester, Pennsylvania, USA) and 20 minutes of centrifugation at 4000 rpm at 4 ºC (Centrifuge 5810 R Eppendorf, Hamburg, Germany) the supernatants (75 µL) were transferred to a new plate, where each sample was diluted by addition of 0.2% formic acid (75 µL). The diluted samples were then injected (20 µL) to the HPLC system.

Liquid-liquid extraction was performed before analysis of the lung homogenates. A certain volume (50 µL) of each sample was added in triplicate to glass vials to which a carbonate buffer pH 10 (50 mM Na_2CO_3, 50 mM $NaHCO_3$) containing 100 nM of 5,5-diethyl-1,3-diphenyl-2-iminobarbituric acid as internal standard was added (50 µL). Each sample was extracted with methyl-tertbutyl ether (MTBE, 600 µL). After sealing the vials with silicon cover, the vials were shaken horizontally for 5 minutes (150 min^{-1}, Edmund Bühler Swip, POCD Scientific, Artarmon, Australia), followed by 15 minutes of mixing with a VWR VX-2500 Multi-Tube Vortexer (speed 5,

VWR International west Chester, Pennsylvania, USA). A defined volume of the upper organic layer (450 µL) was then transferred to glass vials, which were vaporised to dryness with a Techne Sample Concentrator (Techne Incorporated, Staffordshire, UK) during approximately 20 minutes. Samples were reconstituted in 33% acetonitrile and 0.2% formic acid in water (150 µL) and placed in an ultrasonic bath (5210 Branson, Gemini, Apeldoorn, the Netherlands) for 10 minutes. Except from the sample preparation technique of the lung homogenates, the analytical procedure was identical to the one applied for the other samples.

The compounds were quantified using Mass Hunter Workstation Software for Quantitative Analysis (Agilent Technologies Inc., Santa Clara, CA, USA). A standard curve was created for each sample type: plasma, lung, spleen, liver, brain and kidney. The standard curve samples contained a biological matrix, not to be confused with the mathematical term, (blank plasma, blank lung homogenate, blank spleen homogenate, blank liver homogenate, blank brain homogenate and blank kidney homogenate, respectively) in a 1:9 volume ratio in order to match the samples. The highest point of the standard curve was always followed by two injections of blank matrix in order to clean the system and avoid possible contamination. The LLOQ of the tracer was 0.10 nM in all investigated matrices except for the brain homogenate, which had a LLOQ of 0.35 nM. The LLOQ of FP was 1.4, 2.1 and 8.6 nM in lung homogenate, spleen homogenate and plasma, respectively. Corticosterone plasma levels were analysed using an ELISA-kit (ab108821, Abcam, Cambridge, UK).

3.2.1.11 Statistical analysis

Statistical comparisons between two groups were made using a two-tailed, unpaired Student's t-test. The level of significance was set at $p \leq 0.05$. Data are presented as mean ± standard deviation and precision of the estimated parameters is presented as standard errors.

3.2.1.12 Modelling of tissue concentrations of tracer

The four different tracer doses were evaluated by a modelling approach where the tissue concentration of tracer was assumed to consist of two parts: 1) linear nonspecific binding determined by the plasma tracer concentration (C_p) and a partitioning constant for nonspecific binding ($K_{p,ns}$), and 2) nonlinear binding to the target determined by C_p, the dissociation constant (K_d) and the receptor density (B_{max}), given by:

$$C_{control} = C_p K_{p,ns} + \frac{B_{\max} C_p}{K_d + C_p} \tag{3.9}$$

and

$$C_{nonspec} = C_p K_{p,ns}. \tag{3.10}$$

The model was implemented in MATLAB R2013a (Mathworks Inc., Natick, MA, USA) with fitting performed using nonlinear least squares (*lsqnonlin*) and iterative reweighting using predicted data. The default optimisation algorithm of '*lsqnonlin*' was used (the trust region-reflective algorithm). In case of several local minima within the expected parameter space, an exhaustive search was conducted in MATLAB to ensure that the optimization algorithm had not converged to a local

minimum. The sum of squares was evaluated at 450^3 combinations of parameter values, where B_{max} varied between 0.1 and 40 nM, $K_{p,ns}$ varied between 0.1 and 10 and K_d varied between 0.1 and 30 nM.

A sensitivity analysis was performed to investigate how the function responds to small perturbations of the parameters over a broad range of C_p (0.1-10000 nM). Only the function describing $C_{control}$ (eq. 3.9) was considered since $C_{nonspec}$ (eq. 3.10) is a component of that function. The sensitivities were generated by considering the partial derivatives of the output Y with respect to each parameter x_i and these were calculated keeping all other parameters fixed at their assigned values (x_0), i.e.

$$\left.\frac{\partial Y}{\partial x_i}\right|_{x_0} \tag{3.11}$$

The partial derivatives were solved analytically to give:

$$\frac{\partial C_{control}}{\partial K_{p,ns}} = C_p, \tag{3.12}$$

$$\frac{\partial C_{control}}{\partial K_d} = -\frac{B_{\max} C_p}{\left(C_p + K_d\right)^2} \tag{3.13}$$

and

$$\frac{\partial C_{control}}{\partial B_{\max}} = \frac{C_p}{C_p + K_d}. \tag{3.14}$$

3.2.2 Results

3.2.2.1 Tracer identification *in vitro*

Fifteen GR binders were selected from AstraZeneca's internal chemical library on the basis of having large numerical differences between the values of $-\log(EC_{50})$ and $\log D_{7.4}$. Based on the measured nonspecific binding in lung slices and the analytical sensitivity a refined selection of two compounds was made. The chemical structures of compounds 1 and 2 are shown in figure 3.1. Incubation of lung slices in the absence and presence of excess of R-budesonide resulted in statistically significant differences between $C_{slice,total}$ and $C_{slice,nonspec}$ for both compounds. f_{tb} was calculated to be 0.56 ± 0.071 and 0.48 ± 0.069 for compound 1 and 2, respectively. f_{tb} and analytical sensitivity were subsequently used for ranking. Based on these criteria, compound 1 was identified as the most promising tracer candidate.

3.2.2.2 Evaluation of tracer dose

As illustrated in figure 3.2, which shows $C_{control}$ and $C_{nonspec}$ for each tracer dose, there was a separation between $C_{control}$ and $C_{nonspec}$ at the second lowest dose level (40 nmol/kg). $C_{control}$ was 9.2 ± 2.1 nM and $C_{nonspec}$ was 3.8 ± 0.32 nM, resulting in a $C_{control}/C_{nonspec}$ ratio of 2.4, corresponding to a value for f_{tb} of 0.59. The ratio between $C_{control}$ and $C_{nonspec}$ decreased with ascending tracer doses (2.4, 1.5 and 1.3 for 40, 400 and 4000 nmol/kg, respectively). $C_{nonspec}$ was below the lower limit of quantification (LLOQ) at the lowest dose level (4 nmol/kg) and therefore the ratio could not be calculated. $C_{nonspec}$ was proportional to C_p and thus they were found to be highly correlated ($r^2 = 0.99$).

The dependence of $C_{control}$ and $C_{nonspec}$ on C_p was captured by the model. Parameter estimates and standard errors for the model are presented in table 3.1. The

correlations between the estimated parameters are presented in table 3.2. The correlation between B_{max} and K_d was found to be reasonably high (0.886). Whilst $K_{p,ns}$ had a high parameter precision, the confidence intervals for B_{max} and K_d were somewhat wider. Thus, some caution should be exercised when interpreting these two parameter estimates.

In the exhaustive search, the minimum cost function was found at the following parameter values: $K_{p,ns}$ = 0.761, B_{max} = 21.2 nM and K_d = 10.4 nM. The same minimum was thus found when using nonlinear least squares (the trust region-reflective algorithm as the optimisation algorithm) and the exhaustive search algorithm, which confirms that the global minimum had been found within the investigated parameter space.

A partial derivative based sensitivity analysis was performed as described in section 3.2.1.12 and the results are presented in figure 3.3a-c. The plot of $\partial C_{control}/\partial K_d$ as a function of C_p (fig. 3.3a) indicates that samples from the two intermediate dose groups (40 and 400 nmol/kg) were informative with respect to K_d. In contrast, at the C_p resulting from the highest and the lowest dose group (4000 and 4 nmol/kg, respectively), a change in K_d only had a minor effect on the output. As can be seen from eq. 3.14 and fig. 3.3b, the influence of B_{max} on the output becomes more pronounced with increasing C_p until $C_p >> K_d$ when the maximum value of $\partial C_{control}/\partial B_{max}$ has been reached (i.e. $\partial C_{control}/\partial B_{max}$ tends towards 1 as $C_p >> K_d$). Eq. 3.15 shows that $\partial C_{control}/\partial K_{p,ns}$ equals C_p (fig. 3.3c), i.e. the higher C_p the more pronounced is the effect of $K_{p,ns}$ on the output.

By using the developed model and its final parameter estimates, the ratio $C_{control}/C_{nonspec}$ could be simulated for a range of C_p-values of tracer. According to the simulations, the ratio consistently increased with lower C_p-levels of tracer (fig. 3.4).

A ratio of 3 was judged to be a sufficiently high ratio, which occurred when C_p < 3.5 nM. As the C_p-data used for constructing this model had been collected 30 min after IV-administration, the 2-compartment model that had been parameterised to describe the PK of the tracer (section 3.2.2.4) could be used to evaluate what intravenous dose that would yield a C_p of 3.5 nM at t = 30 min. It was found that this situation corresponded to a tracer dose of approximately 55 nmol/kg or less. These model predictions combined with information about the analytical sensitivity could then be used for identifying an appropriate tracer dose. The lowest tracer dose that could be reliably quantified by LC-MS/MS was chosen (30 nmol/kg).

Table 3.1 Parameter estimates from modelling of tissue concentrations of tracer, which was assumed to consist of two parts: 1) linear nonspecific binding determined by the plasma tracer concentration (C_p) and a partitioning constant for nonspecific binding ($K_{p,ns}$), and 2) non-linear binding to the target determined by C_p, the dissociation constant (K_d) and the receptor density (B_{max}).

Parameter	**Estimate**
$K_{p,ns}$	0.76 ± 0.021
B_{max} (nM)	21 ± 8.1
K_d (nM)	10 ± 6.2[a)]

[a)] K_d is estimated from total C_p, if corrected for plasma protein binding K_d is 0.21 ± 0.12 nM.

Precision of the estimates is expressed as standard errors. The root mean square error for this fit was 1.2 nM.

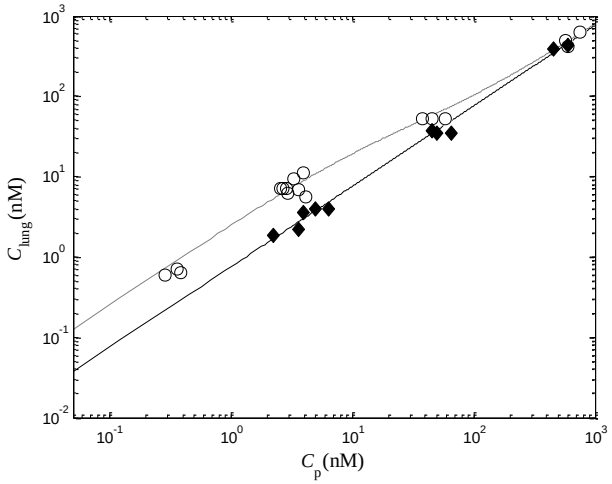

Figure 3.2 Evaluation of total (white circles) and nonspecific (black diamonds) lung concentration of tracer after IV-administration of four different tracer doses (4, 40, 400 and 4000 nmol/kg) to rats. Animals dedicated to determination of nonspecific binding were pre-treated with a glucocorticoid receptor binder 30 minutes before tracer administration.

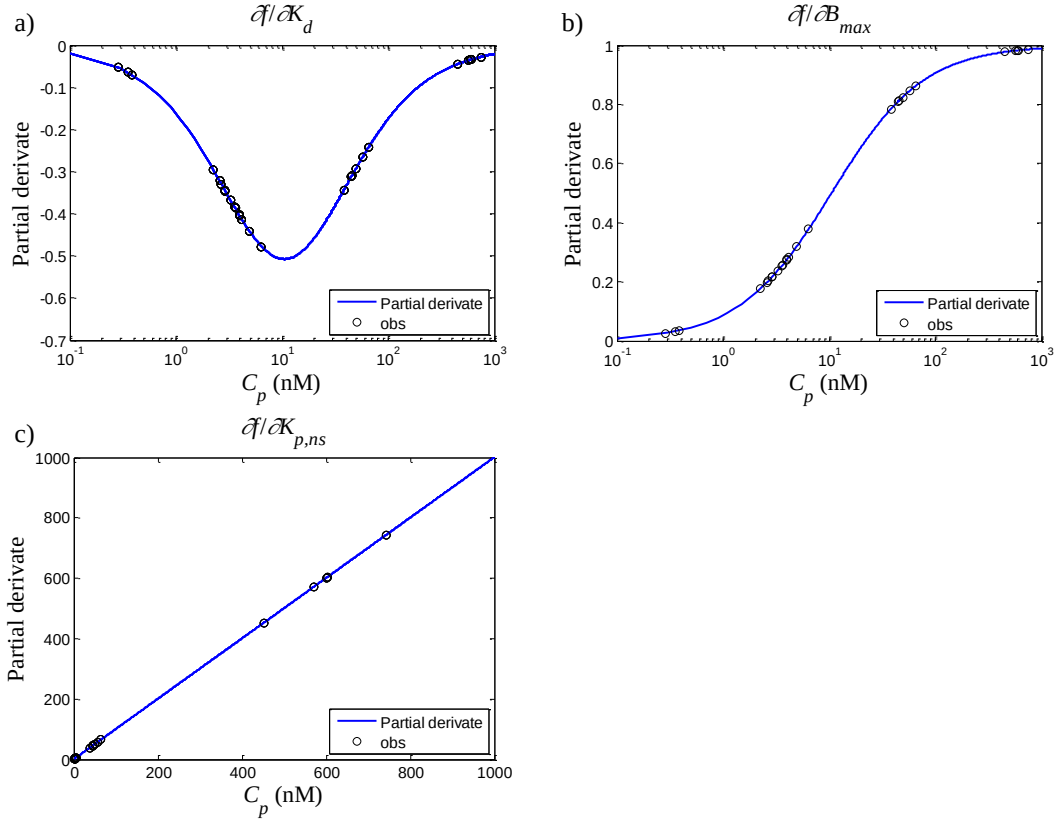

Figure 3.3 A sensitivity analysis was performed by considering the partial derivatives (eqs. 3.12-3.14, blue lines) of the output $C_{control}$ (eq. 3.9) with respect to each of the estimated parameters: a) the dissociation rate constant (K_d), b) the receptor density (B_{max}), and c) the partitioning constant for nonspecific binding ($K_{p,ns}$). The plasma concentrations (C_p) at which observations were made are illustrated by open circles.

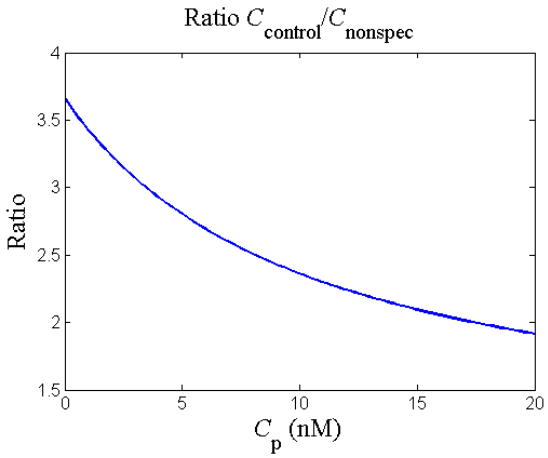

Figure 3.4 Model simulations of the ratio between total ($C_{control}$) and nonspecific ($C_{nonspec}$) lung concentration of tracer as a function of plasma concentration (C_p).

Table 3.2 Estimated correlation matrix of the parameter estimates.

	$K_{p,ns}$	B_{max}	K_d
$K_{p,ns}$	1	-0.487	-0.396
B_{max}	-0.487	1	0.886
K_d	-0.396	0.886	1

3.2.2.3 Evaluation of nonspecific binding

The same degree of nonspecific binding remained when dexamethasone replaced compound 2 as the pre-treatment drug; i.e. $C_{nonspec}/C_p$ was of the same magnitude (0.76 ± 0.12 and 0.69 ± 0.11 after pre-treatment with dexamethasone and compound 2, respectively). As in section 3.2.1.4, $C_{nonspec}$ was proportional to C_p (r^2 = 0.99).

3.2.2.4 PK-study

A 2-compartment model with a multiplicative error model was used to describe the plasma PK of the tracer. A graphical illustration of the model (fig. 2.5b) is included in section 2.3.1. The model was implemented in Phoenix™ WinNonlin® 6.3.0 (Pharsight, Sunnyvale, CA). The compartmental model equations are given by

$$V_1 \frac{dC_1}{dt} = -Cl \times C_1(t) - Cl_2 \times \left(C_1(t) - C_2(t)\right), \quad C_1(0) = \frac{D}{V_1}, \tag{3.15}$$

$$V_2 \frac{dC_2}{dt} = Cl_2 \times \left(C_1(t) - C_2(t)\right), \quad C_2(0) = 0. \tag{3.16}$$

where D is the dose, C_1 is the concentration in the central compartment, CL is the clearance, V_1 is the volume of the central compartment, C_2 is the concentration in the peripheral compartment, CL_2 is the intercompartmental clearance and V_2 is the

volume of the peripheral compartment. The observations and the model fit are shown in figure 3.5a. The estimates and the precision of the parameters are summarised in table 3.3. As can be seen in fig. 3.5b, the weighted residuals were randomly distributed around zero when a multiplicative error model was used.

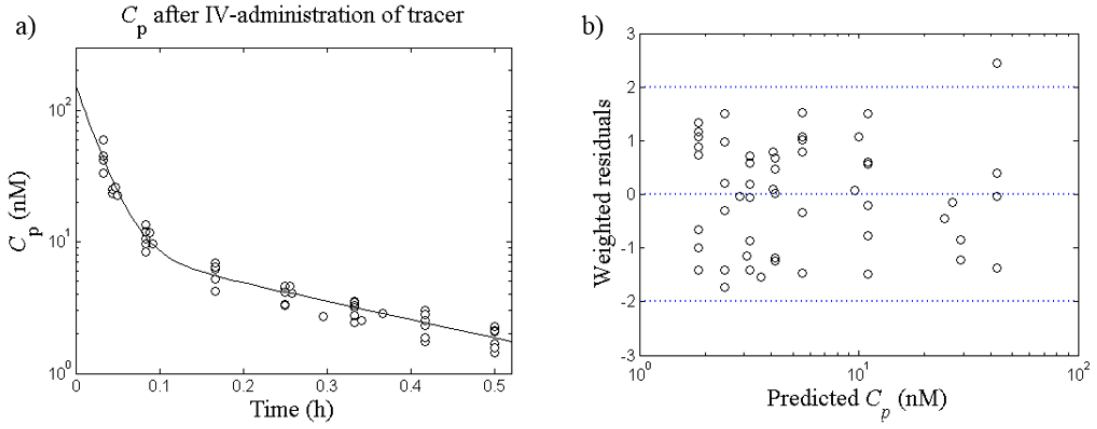

Figure 3.5 Characterisation of the plasma pharmacokinetics (PK) of the tracer. a) The plasma concentration (C_p) after IV-administration of the tracer (30 nmol/kg, n = 8). A 2-compartment model was used to describe the plasma PK (solid line). b) Weighted residuals plotted against the predicted C_p.

Table 3.3 Parameter estimates from PK-modelling of tracer.

Parameter	Estimate
V_1 (L/kg)	0.19 ± 0.037
V_2 (L/kg)	0.56 ± 0.075
CL (L/h/kg)	4.8 ± 0.30
CL_2 (L/h/kg)	3.1 ± 0.43

Precision of the estimates is expressed as standard errors.

3.3.2.5 Evaluation of tracer function in other organs

There were statistically significant differences between $C_{control}$ and $C_{nonspec}$ in the lung, liver, spleen and kidney (table 3.4). The difference was especially pronounced in the lung and in the spleen ($p < 0.001$). All brain samples were below the LLOQ. The ratio of $C_{control}/C_{nonspec}$ in the spleen was found to be higher than the

corresponding ratio in the other investigated organs and the spleen was thus selected to be used as a reference organ for the systemic exposure.

Table 3.4 Total and nonspecific tracer concentrations ($C_{control}$ and $C_{nonspec}$, respectively) measured in lung, liver, spleen, kidney and brain. $C_{nonspec}$ is measured in animals pre-treated intravenously with dexamethasone (20 mg/kg, n = 5) and $C_{control}$ is obtained from drug-naïve control animals (n = 5). Asterisks denote statistical significance between $C_{control}$ and $C_{nonspec.}$

	$C_{control}$ (nM)	$C_{nonspec}$ (nM)
Lung	10 ± 1.4	2.8 ± 0.53***
Liver	1.4 ± 0.41	0.77 ± 0.20*
Spleen	16 ± 1.6	2.8 ± 0.44***
Kidney	20 ± 4.4	14 ± 3.4*
Brain	<LLOQ	<LLOQ

LLOQ: Lower limit of quantification; *Significant at the 0.05 probability level **Significant at the 0.01 probability level ***Significant at the 0.001 probability level

3.3 Application of the methodology

In order to evaluate the developed methodology, the well-established drug fluticasone propionate (FP), which is known to be a selective high-affinity GR agonist [134], was used to assess the ability of the method to: 1) establish a dose-receptor occupancy relationship, and 2) study the time course of receptor occupancy. The intravenous route of administration was favoured versus other routes since it provides the lowest possible interindividual variability in lung tissue exposure.

The author was responsible for the design and the execution of both studies described in section 3.3.1. The dose-receptor occupancy study was done by the author alone. For the *in vivo* work of the time profile study, the author was assisted by Susanne Arlbrandt and Dr Britt-Marie Fihn at AstraZeneca R&D Gothenburg. Both studies were conducted during the PhD studies.

3.3.1 Method

3.3.1.1 Dose-receptor occupancy relationship

The dose-receptor occupancy relationship for FP was assessed by measuring GR occupancy 1.5 hours after IV-administration of three escalating doses of FP: 20 nmol/kg (n = 4), 150 nmol/kg (n = 6) and 750 nmol/kg (n = 6). Prior to both the administration of FP and tracer, plasma samples were taken for measurements of corticosterone in order to investigate if the endogenous ligand was a potential source of variability. To allow for interindividual differences in plasma corticosterone, the IV-administrations of FP were spread out over the time course of a day (8 a.m. – 7 p.m.). One group of animals was pre-treated with dexamethasone via the IV-route (20 mg/kg) 30 minutes prior to tracer administration (n = 6), whereas the animals dedicated to determination of the maximum tissue tracer concentration did not receive any pre-treatment (n = 8). Receptor occupancy was calculated for each animal treated with FP according to eq. 3.6 (section 3.2.1.9).

3.3.1.2 Receptor occupancy time profile

The time course of receptor occupancy was studied after IV-administration of FP (90 nmol/kg). As detailed in section 4.2.1, the choice of the IV-dose was based on the ED_{50} of FP in a preclinical PD-model. Tracer was administered intravenously at the following time points after drug administration: 0.5, 1, 2, 4, 7, 24 and 48 hours (3 animals/time point). Receptor occupancy was calculated for each animal according to eq. 3.6 (section 3.2.1.9).

3.3.1.3 Statistical analysis

One-way analysis of variance (ANOVA). A one-way analysis of variance (ANOVA) was used to determine whether there was a statistically significant difference between any of the mean values of the five different groups in the dose-receptor occupancy study.

An ANOVA compares the mean values of a dependent variable between different groups that are categorised by an independent variable. In this case the dependent variable is the tracer concentration in the lung or in the spleen and the independent variable is the group (i.e. the three FP-dose groups, the group of animals pre-treated with dexamethasone and the group of drug-naïve control animals). That is, an ANOVA tests the following null hypothesis (H_0)

$$H_0 : \mu_1 = \mu_2 = ... = \mu_n , \qquad (3.17)$$

where μ_i is the mean value of group i and n is the total number of groups. H_0 is violated if there is a statistically significant difference between at least two of the group means. Three assumptions should be met in order to make an ANOVA: 1) the dependent variable should have a normal distribution within each group, 2) the data should have equal variances in each group, and 3) the observations should be independent. This statistical test is known to be robust against modest violations of the normality assumption. The second assumption regarding homogeneity of variances can be tested using Levene's Test [135].

Importantly, an ANOVA does not give any information on which specific groups are statistically significantly different from each other. A significant result should therefore be followed up by a *post-hoc* test in order to find where the difference(s)

exist. If the assumption regarding equal variances is met, Tukey's honestly significant difference test can be used [135].

One-way ANOVA using MATLAB. The data were initially tested for equality of variances using Levene's test, which tests the null-hypothesis that the variances are equal. The null-hypothesis was considered to be violated if $p \leq 0.05$, this level of significance applies to all statistical tests in this section. A MATLAB-script for Levene's test was obtained from [136]. Provided that the null-hypothesis was not violated, an ANOVA was carried out.

An ANOVA was conducted in MATLAB using the command '*anova1*' for both lung and spleen tracer concentrations. Provided that the null-hypothesis was rejected, a *post-hoc* test was performed using the command '*multcompare*' with the information in the '*stats*' structure as input. The '*stats*' structure had been obtained from the ANOVA-analysis and it contained the information needed for a *post-hoc* analysis. Tukey's honestly significant difference test was selected.

3.3.1.4 Modelling of the dose-receptor occupancy relationship

A nonlinear E_{max}-model with a baseline (eq. 3.18) was used to describe the dose-receptor occupancy relationship, using

$$C_i = C_{nonspec} + C_{spec,\max} \times \left(1 - \frac{D}{D + ED_{50}}\right) \qquad (3.18)$$

where C_i is the tissue tracer concentration in animal i, $C_{nonspec}$ is the nonspecific binding, $C_{spec,max}$ is the maximum specific binding, D is the dose and ED_{50} is the dose which gives 50% occupancy at 1.5 hours. A high dose (10000 nmol/kg) was assigned

to the animals pre-treated with dexamethasone (n = 6) and D was set to 0 for drug-naïve control animals (n = 8).

An exhaustive-search algorithm was used to obtain initial estimates for $C_{nonspec}$, $C_{spec,max}$ and ED_{50} for the subsequent parameter estimation. This was done by evaluating the sum of squares at 150^3 combinations of parameter values for both data from the lung and the spleen. For the lung, $C_{nonspec}$ varied between 0 and 6 nM, $C_{spec,max}$ varied between 2 and 12 nM and ED_{50} varied between 10 and 60 nmol/kg. For the spleen, $C_{nonspec}$ varied between 0 and 6 nM, $C_{spec,max}$ varied between 2 and 14 nM and ED_{50} varied between 20 and 80 nmol/kg.

The parameter estimation was implemented in MATLAB R2013a using nonlinear least squares (*lsqnonlin*), which minimised the difference between the measured and the predicted C_i. The default optimisation algorithm of '*lsqnonlin*' was used (trust region-reflective algorithm). $C_{control}$ for drug-naïve control animals was then calculated as follows

$$C_{control} = C_{spec,\max} + C_{nonspec} \ . \qquad (3.19)$$

A sensitivity analysis was performed to investigate how the function responds to changes in the parameters over a broad dose range (0.1-1000 nmol/kg). The sensitivities were generated by considering the partial derivatives of the output C_i with respect to each parameter x_i and these were calculated whilst keeping all other parameters fixed at their assigned values (x_0) as described by eq. 3.11 (section 3.2.1.12). That is, the following partial derivatives were generated:

$$\frac{\partial C_i}{\partial C_{nonspec}} = 1, \tag{3.20}$$

$$\frac{\partial C_i}{\partial C_{spec,\max}} = 1 - \frac{D}{D + ED_{50}} \tag{3.21}$$

and

$$\frac{\partial C_i}{\partial ED_{50}} = \frac{C_{spec,\max} D}{(ED_{50} + D)^2}. \tag{3.22}$$

The analysis was implemented using the MATLAB symbolic math toolbox.

3.3.2 Results

3.3.2.1 Dose-receptor occupancy relationship

A dose-dependent decrease in tracer concentrations was observed in the lung and the spleen, which is illustrated in figures 3.6a and 3.6b, respectively. An ANOVA was used to determine whether there was a statistically significant difference between any of the mean values for the five different groups. The statistical analysis resulted in a rejection of the null-hypothesis for both measured tissue concentrations of tracer ($F(4,25) = 75.52$, $p = 1.38\times10^{-13}$ and $F(4,25) = 107.42$, $p = 2.29\times10^{-15}$ for the lung and the spleen tracer concentrations, respectively).

The results of the two *post-hoc* tests of all possible pairings of the groups are summarised in tables 3.5 and 3.6. Table 3.5 contains the results of the analysis in which the lung tracer concentration was the dependent variable, whereas the analysis of the spleen tracer concentration is presented in table 3.6.

Table 3.5 shows that the mean values of the lung tracer concentration in the control group and the lowest dose group (20 nmol/kg, FP) were statistically significantly

different from the mean values for all other groups. It also shows that the differences between the mean values of all dose groups were statistically significant. The difference between the mean values of the highest dose group (750 nmol/kg, FP) and the group pre-treated with dexamethasone was not statistically significant, neither was the difference between the intermediate dose group (150 nmol/kg) and the group pre-treated with dexamethasone.

As can be seen in table 3.6, the *post-hoc* test for the spleen tracer concentrations shows that differences in group mean values were statistically significant for all combinations except for the highest dose group (750 nmol/kg, FP) and the group pre-treated with dexamethasone.

Table 3.5 *Post-hoc* test for the lung tracer concentrations.

	Control	20 nmol/kg	150 nmol/kg	750 nmol/kg	Dex
Control	NA	$p \leq 0.05$	$p \leq 0.05$	$p \leq 0.05$	$p \leq 0.05$
20 nmol/kg	$p \leq 0.05$	NA	$p \leq 0.05$	$p \leq 0.05$	$p \leq 0.05$
150 nmol/kg	$p \leq 0.05$	$p \leq 0.05$	NA	$p \leq 0.05$	X
750 nmol/kg	$p \leq 0.05$	$p \leq 0.05$	$p \leq 0.05$	NA	X
Dex	$p \leq 0.05$	$p \leq 0.05$	X	X	NA

The level of significance was set at $p \leq 0.05$. X indicates that the difference between two mean values was not statistically significant.

Table 3.6 *Post-hoc* test for the spleen tracer concentrations.

	Control	20 nmol/kg	150 nmol/kg	750 nmol/kg	Dex
Control	NA	$p \leq 0.05$	$p \leq 0.05$	$p \leq 0.05$	$p \leq 0.05$
20 nmol/kg	$p \leq 0.05$	NA	$p \leq 0.05$	$p \leq 0.05$	$p \leq 0.05$
150 nmol/kg	$p \leq 0.05$	$p \leq 0.05$	NA	$p \leq 0.05$	$p \leq 0.05$
750 nmol/kg	$p \leq 0.05$	$p \leq 0.05$	$p \leq 0.05$	NA	X
Dex	$p \leq 0.05$	$p \leq 0.05$	$p \leq 0.05$	X	NA

The level of significance was set at $p \leq 0.05$. X indicates that the difference between two mean values was not statistically significant.

A dose-receptor occupancy relationship was thus observed after IV-administration of FP (fig. 3.7). As can be seen in fig. 3.7, IV-administration resulted in receptor occupancies of similar magnitude in both investigated organs. An E_{max}-model with a baseline captured how tissue concentrations of tracer depend on the dose of FP. Parameter estimates and standard errors obtained from the model are presented in table 3.7. ED_{50} was estimated to be 47 ± 8.6 nmol/kg. Concentration data from the lung and the spleen were initially modelled separately. When the data sets were modelled separately, they gave overlapping 95% confidence intervals of ED_{50} (34 [13-52] and 53 [27-79] nmol/kg for the lung and the spleen, respectively). Since the models provided overlapping 95% confidence intervals for ED_{50} and no difference in ED_{50} is expected for these two organs after IV-dosing, co-modelling of both data sets was instead applied in order to achieve a more reliable estimate of ED_{50}. As can be

seen in the correlation matrix (table 3.8), none of the estimated parameters were found to be highly correlated.

As can be seen from eqs. 3.19-3.21, the partial derivatives with respect to $C_{nonspec}$ and $C_{spec,max}$ are identical for concentration data from the spleen and the lung, whereas $\partial C_i/\partial ED_{50}$ will have different magnitudes for the two organs as $C_{spec,max}$ is included in the numerator (eq. 3.21). The sensitivity analysis showed that $\partial C_i/\partial C_{nonspec}$ is constant and all observations thus provided similar information for this parameter regardless of FP dose (fig. 3.8a). This is expected as $C_{nonspec}$ should be unaffected by receptor occupancy and thus also unaffected by the dose of the test compound. In contrast, the function was most sensitive to $C_{spec,max}$ as the dose approached 0 (fig. 3.8b), which is also in line with the expectations as the specific binding decreases with increasing doses of test compound and drug-naïve animals should thus be most informative with respect to this parameter. $\partial C_i/\partial ED_{50}$ had a bell-shaped curve and the function was most sensitive to changes in ED_{50} in the proximity to ED_{50} (fig. 3.8c-d). For all parameters, the sensitivity analysis showed that observations had been made in informative regions of the dose range.

Although the measurements of corticosterone, both before the administration of FP (27-330 µg/L) and tracer (25-260 µg/L), varied between the animals, no relationship between corticosterone and estimated receptor occupancy was observed in the treated animals. This is shown in a representative graph (fig. 3.9).

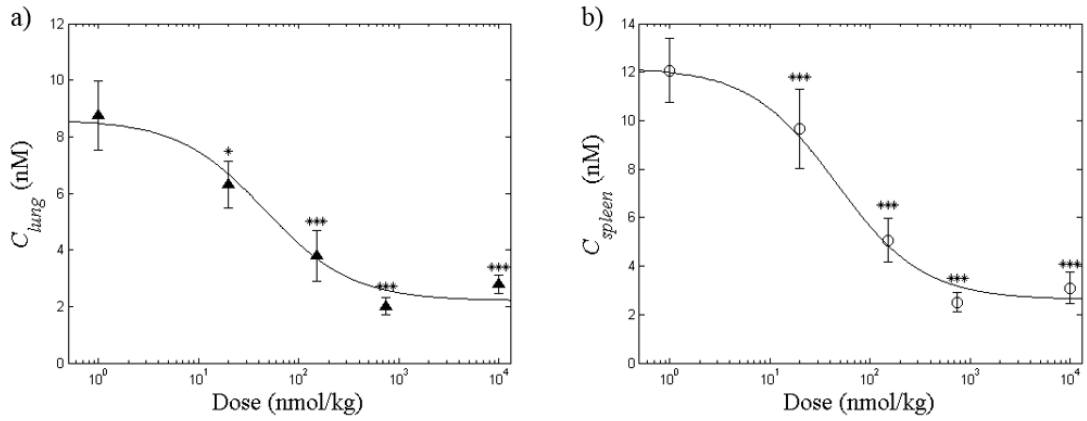

Figure 3.6 Tissue tracer concentration in a) the lung, and b) the spleen after IV-administration of three escalating doses of fluticasone propionate to rats (20, 150 and 750 nmol/kg). Drug-naïve control animals as well as animals pre-treated with dexamethasone (20 mg/kg) were also in the study to account for maximum and nonspecific tracer concentration, respectively. The solid line represents the model fit (eq. 3.17). Asterisks denote statistical significance between treated animals and drug-naïve control animals (n = 8), which are also included in the graph. *Significant at the 0.05 probability level **Significant at the 0.01 probability level ***Significant at the 0.001 probability level

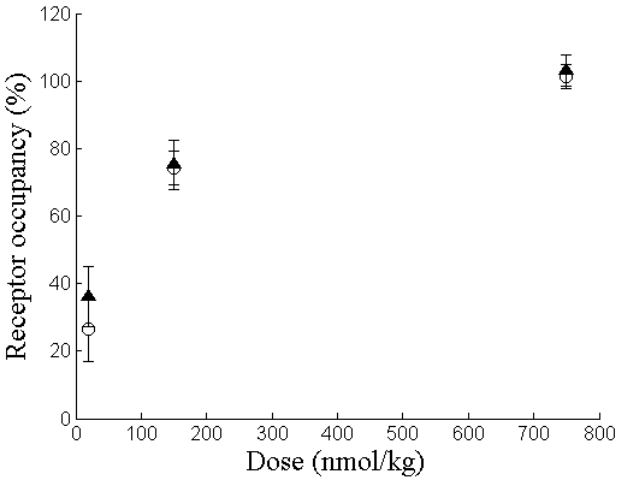

Figure 3.7 Dose-receptor occupancy relationship: receptor occupancy in the lung (black triangles) and the spleen (white circles) measured 1.5 hours after IV-administration of escalating doses of fluticasone propionate to rats (20, 150 and 750 nmol/kg).

Table 3.7 Parameter estimates from the modelling of the dose-receptor occupancy relationship, in which the tracer concentration was described with a nonlinear E_{max}-model with a baseline.

Parameter	**Estimate**
$C_{nonspec,lung}$ (nM)	2.2 ± 0.28
$C_{spec,max,lung}$ (nM)	6.4 ± 0.44
$C_{nonspec,spleen}$ (nM)	2.6 ± 0.30
$C_{spec,max,spleen}$ (nM)	9.6 ± 0.44
ED_{50} (nmol/kg)	47 ± 8.6

Precision of the estimates is expressed as standard errors. The root mean square error for this fit was 0.99 nM.

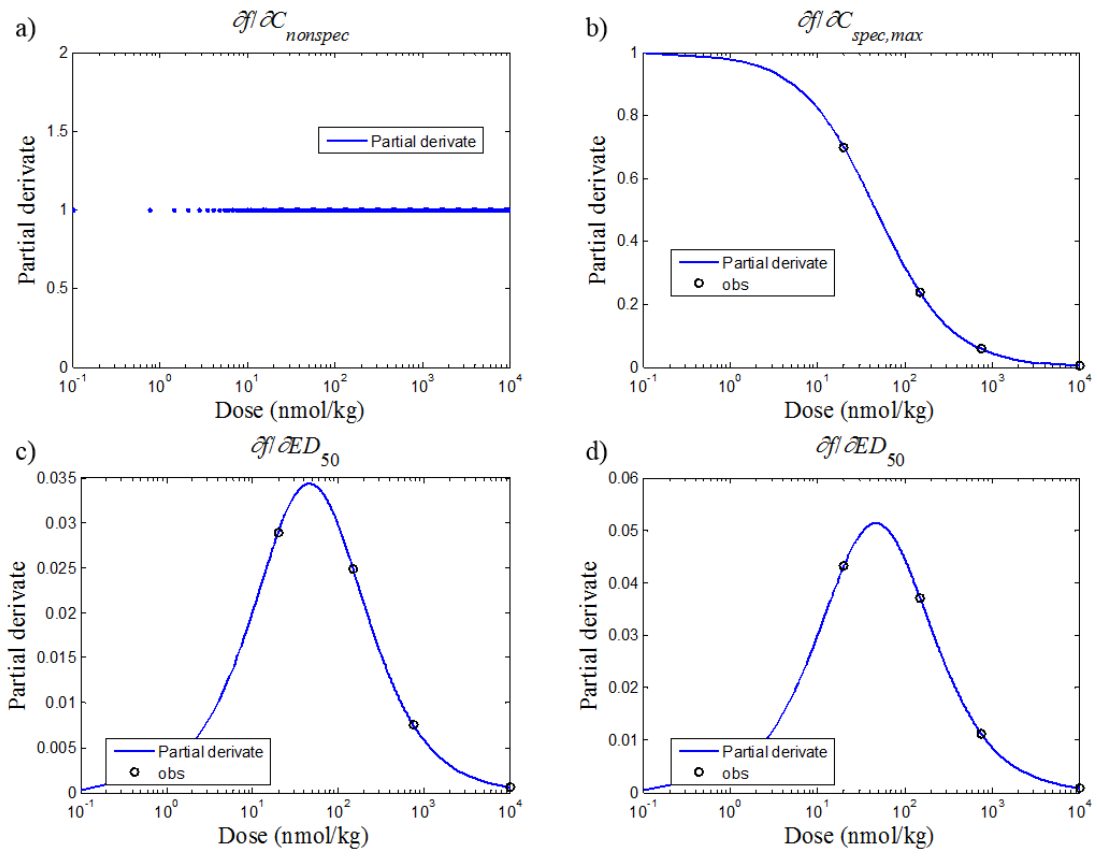

Figure 3.8 A sensitivity analysis was performed by considering the partial derivatives of the output C_i with respect to: a) $C_{nonspec}$, b) $C_{spec,max}$, c) ED_{50} (using parameter estimates specific for the lung) and d) ED_{50} (using parameter estimates specific for the spleen).

Table 3.8 Estimated correlation matrix of the parameter estimates

	$C_{spec,max,spleen}$	ED_{50}	$C_{nonspec,spleen}$	$C_{spec,max,lung}$	$C_{nonspec,lung}$
$C_{spec,max,spleen}$	1	0.0751	-0.657	0.00380	-0.0270
ED_{50}	0.0751	1	-0.498	0.0503	-0.359
$C_{nonspec,spleen}$	-0.657	-0.498	1	-0.0251	0.179
$C_{spec,max,lung}$	0.00380	0.0503	-0.0251	1	-0.686
$C_{nonspec,lung}$	-0.0270	-0.359	0.179	-0.686	1

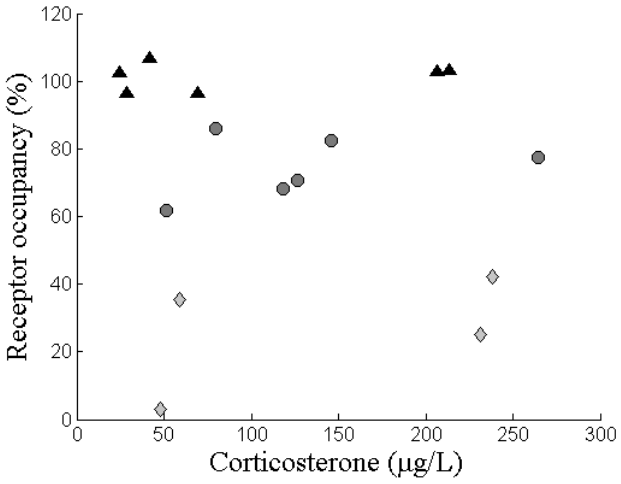

Figure 3.9 Corticosterone and receptor occupancy: receptor occupancy in the lung 1.5 hours after IV-administration of three different doses of fluticasone propionate: 20 nmol/kg (diamonds), 150 nmol/kg (circles) and 750 nmol/kg (triangles), respectively. No relationship was observed between receptor occupancy and plasma corticosterone measurements made before the IV-administration of tracer.

3.3.2.2 Receptor occupancy time profile

As can be seen in figure 3.10, a high initial receptor occupancy was observed, which was followed by a time-dependent decline between 0.5 and 7 h. Receptor occupancy in the spleen had returned to baseline within seven hours after dosing, whereas there still remained some drug occupancy in the lung. The occupancy profiles initially followed each other closely, while the occupancy was estimated to be slightly higher in the lung at t = 4 and 7 h after IV-administration of FP.

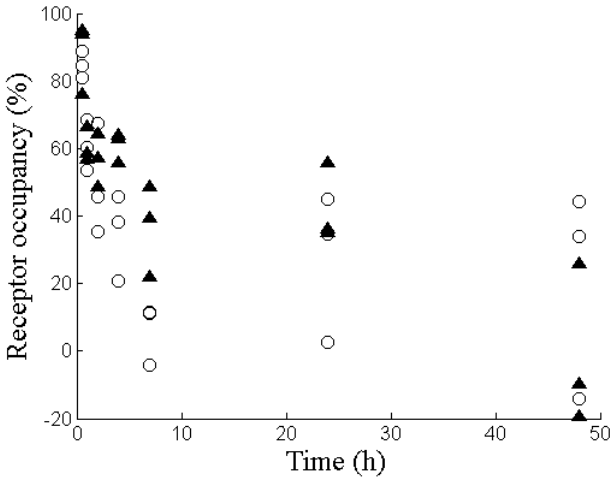

Figure 3.10 Time course of receptor occupancy in the lung (triangles) and the spleen (circles) after intravenous administration of fluticasone propionate to rats (90 nmol/kg).

3.3.2.3 Concentration-receptor occupancy relationship in the spleen

When data from both studies (sections 3.3.2.1 and 3.3.2.2) were used, a relationship between occupancy in the spleen and the spleen concentration of FP was observed (fig. 3.11). Since the analytical sensitivity for FP in the lung tissue was not equally good, the corresponding graph could not be created for the lung.

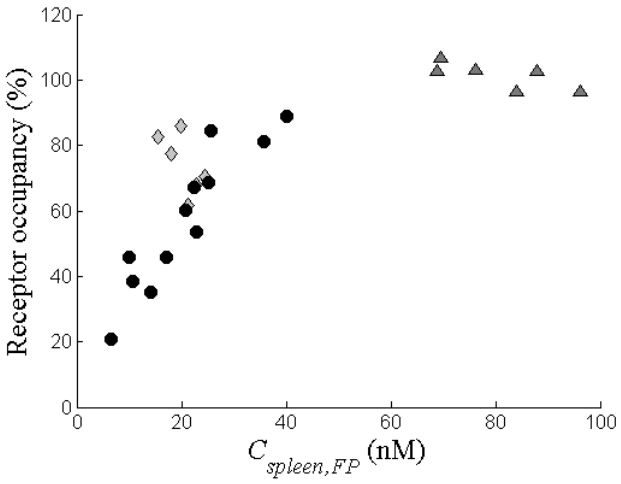

Figure 3.11 A relationship between receptor occupancy in the spleen and spleen concentrations of fluticasone propionate ($C_{spleen,FP}$) was observed. Each data point corresponds to the receptor occupancy of an individual animal and data were taken from two different studies where FP was administered as an IV-bolus. In the first study, occupancy was measured 1.5 hours after IV-administration of different doses of FP: 150 nmol/kg (diamonds) and 750 nmol/kg (triangles), respectively. In the second study, the time course of occupancy was studied after administration of 90 nmol/kg (circles). All animals from the two studies where $C_{spleen,FP}$ > LLOQ are included in the graph.

3.4 Discussion

This chapter presents the development of the first methodology that is capable of simultaneous measurements of both pulmonary and systemic *in vivo* occupancy of GR. It is novel both in terms of measuring GR occupancy strictly *in vivo* and by the analytical technique used for tracer quantification (LC-MS/MS).

Identifying a tracer molecule is a prerequisite for developing a receptor occupancy methodology for a new target and this is indeed recognised as a challenging task. As highlighted in section 3.2.1.2, AstraZeneca's internal library contains numerous compounds with affinity for the GR, which thus theoretically could be considered as potential tracer candidates. However, it would not be feasible to experimentally evaluate each candidate and a rational approach was thus needed to narrow down the search space and select compounds with a higher probability of success as GR tracers. Potential tracer candidates were therefore selected based on molecular and pharmacological properties as suggested by Fridén *et al*. [125]. This strategy proved to be successful and one of these compounds, which had demonstrated a high f_{tb} *in vitro* and a sufficiently high analytical sensitivity, was brought forward to *in vivo* evaluation. The *in vivo* studies showed that it was a successful tracer for the GR in lung tissue as an appropriate ratio of $C_{control}/C_{nonspec}$ was obtained at a low tracer dose (30 nmol/kg, IV). As expected, this ratio was demonstrated to decrease with higher tracer doses since the relative contribution of $C_{nonspec}$ increases with higher tracer exposure (fig. 3.2). This behaviour was captured by a model, which described the receptor- and nonspecifically-bound tracer concentrations as a function of C_p (eqs. 3.9-3.10). Simulations of this model evaluated at its final parameter estimates showed that the ratio $C_{control}/C_{nonspec}$ consistently increased with lower C_p-levels of tracer (fig. 3.4). Thus, an appropriate tracer dose should be low while still ensuring that the resulting tissue tracer concentrations exceed the LLOQ. By combining PK-model predictions with information about the analytical sensitivity, a low tracer dose that could be reliably quantified by LC-MS/MS was selected (30 nmol/kg). A post-tracer survival interval of 30 minutes was tested since it is commonly used in other preclinical *in vivo* receptor occupancy methodologies [130,131]. As it proved to give

an appropriate ratio of total-to-nonspecific binding, this post-tracer survival interval was chosen. It was also shown that normal variation of corticosterone plasma concentrations had no relevant impact on the estimates of occupancy after drug administration (fig. 3.9).

There is no tissue devoid of GR that can be used as a reference region to estimate nonspecific tissue binding for the tracer. Instead the nonspecifically-bound tracer concentration must be estimated in separate animals. As expected, it was shown that $C_{nonspec}$ was proportional to C_p. The partitioning constant for nonspecific binding ($K_{p,ns}$) was of the same magnitude when high doses of two structurally different GR binders, a steroid and a selective non-steroidal GR agonist respectively, were used as pre-treatment. Based on these results the tested IV-dose of dexamethasone (20 mg/kg) was considered an appropriate pre-treatment for measurements of $C_{nonspec}$.

The possibility of extending the methodology by including a reference organ for the systemic exposure after inhalation was explored by evaluating the functionality of the GR-tracer in several organs. The ratio of total-to-nonspecific tracer concentrations was found to be considerably higher in the spleen as compared to the other tested organs (including the lung). From a methodological point of view, a higher ratio of total-to-nonspecific tracer concentration allows for more reliable receptor occupancy measurements. Accordingly, the experimental methodology provides slightly more accurate measurements of receptor occupancy in the spleen. Furthermore, the spleen is known to be a highly perfused organ, which is a desired property of a reference organ for systemic exposure. Due to the rapid perfusion, a fast equilibrium between the unbound drug concentrations in plasma and tissue can be expected (given a perfusion rate-limited drug distribution). This property also contributed to the choice of reference organ.

Once the experimental procedures had been established, the developed methodology was evaluated by assessing its ability to establish a dose-receptor occupancy relationship and to study the time course of receptor occupancy. Fluticasone propionate was selected as test compound based on its pharmacological properties; a high selectivity and high affinity for the GR [134].

As expected from a dose-receptor occupancy evaluation, a dose-dependent decrease in tracer concentrations was observed both in the lung and the spleen (fig. 3.6a-b). This behaviour was captured by a model and the ED_{50} was estimated to be 47 nmol/kg. A partial derivative based sensitivity analysis suggested that informative doses had been used in the study. In summary, the methodology proved capable of demonstrating a dose-receptor occupancy relationship.

GR occupancy had previously not been determined after IV-administration of FP. Nevertheless, based on its high potency the highest dose level (750 nmol/kg) was expected to give a high occupancy. In fact, complete occupancy was observed in both organs. It should not be possible to exceed 100% occupancy but as $C_{nonspec}$ is obtained from a separate group of animals, interindividual variability can explain why some estimates were slightly higher than 100%. Measurements of occupancy were therefore made in treatment groups of 4-6 animals to reduce the impact of interindividual variability.

The time course of receptor occupancy was captured in the lung and the spleen after IV-dosing of FP (90 nmol/kg). A high initial occupancy was followed by a relatively rapid decline, where the occupancy had returned to 0% in the spleen within 7 hours after dosing (fig. 3.10). This is in line with the behaviour observed after IV-administration of another corticosteroid, triamcinolone acetonide, where the level of free receptors was found to return to baseline within six hours using an *ex vivo*

binding assay [120]. The estimated occupancy 24 hours after dosing was higher than after 7 hours and is most likely not reflective of the drug-receptor interaction. Rather, this observation may reflect the dynamics of the GR with a drug-induced down-regulation of the receptor population, which has been demonstrated to take place after GR agonist exposure both *in vitro* and *in vivo* [137]. Either way, the estimated occupancy can be viewed as a reflection of free binding sites.

One of the advantages of utilising LC-MS/MS for tracer quantification is that such methodologies also allow for simultaneous quantification of drug concentrations in the same sample. Hence, total organ concentrations of FP had been measured in the spleen and the lung in both studies. When the results from these two studies were combined, a relationship between GR occupancy in the spleen and total spleen concentrations appeared (fig. 3.11). Interestingly, a plateau of occupancy (100%) was reached at a total tissue concentration of 40 nM, which is in close proximity to the measured GR density in the spleen (31 nM) [138]. It is also noted that the rise in occupancy below 40 nM showed a linear behaviour, these two indices suggest that a large fraction of the tissue concentration constitutes of receptor-bound rather than nonspecifically-bound drug; i.e. the results point towards FP having a high f_{tb} in the spleen. As the analytical sensitivity of FP was not equally good in lung homogenates, it could not be investigated whether the same relationship was present in the lung (several samples were below the LLOQ).

By applying this methodology, a dose-receptor occupancy relationship was established and the time course of occupancy was captured after IV-administration of FP, a well-known GR agonist. This gives confidence in the methodology, which henceforth can be used as a tool to increase the fundamental understanding of inhalation PK and PK/PD by studying receptor occupancy after inhalation of GR

modulators. In chapter 4, the developed methodology will be used for this very purpose.

3.5 Summary

Chapter 3 presents the development and the subsequent evaluation of an *in vivo* receptor occupancy methodology for an inhaled target: the GR. The developed methodology is novel both in terms of being fully *in vivo*-based and by utilising LC-MS/MS for tracer quantification.

A refined selection of potential tracer candidates was made based on molecular and pharmacological properties as suggested by Fridén *et al*. [125]. One of these compounds, which had a demonstrated high f_{tb} *in vitro* and a sufficiently high analytical sensitivity, was brought forward for *in vivo* evaluation. The *in vivo* studies showed that it was a successful tracer for the GR in lung tissue as an appropriate ratio of $C_{control}/C_{nonspec}$ was obtained at a low tracer dose (30 nmol/kg, IV) after a post-tracer survival interval of 30 minutes. The possibility of simultaneously estimating receptor occupancy in a reference organ for the systemic exposure was explored by evaluating the functionality of the selected tracer molecule in other organs as judged by the ratio of $C_{control}/C_{nonspec}$. Based on this criterion and the high splenic perfusion rate, the spleen was considered to be an appropriate reference organ.

Once the experimental *in vivo* protocol had been finalised, the developed methodology was evaluated by assessing its ability to establish a dose-receptor occupancy relationship and to characterise a time course of receptor occupancy. Both studies used a selective, high-affinity GR agonist as test compound (FP). As expected from a dose-receptor occupancy evaluation utilising the IV-route, a dose-

dependent decrease in tracer concentrations was observed (fig. 3.6a-b) and the occupancies were of similar magnitude in both organs (fig. 3.7). Hence, the methodology proved capable of demonstrating a dose-receptor occupancy relationship after IV-administration. The dose-dependency was described by a mathematical model and the ED_{50} was estimated to be 47 nmol/kg. A partial derivative based sensitivity analysis suggested that informative doses had been selected for the study. In the time course study, the highest receptor occupancy observation was made at the first time point (t = 30 min). The peak was followed by a relatively rapid decline and the receptor occupancy had returned to 0% in the spleen within 7 hours after dosing (fig. 3.10).

Besides being a selective and high-affinity GR-agonist, FP has interesting properties from an inhalation PK perspective. These properties will be discussed in more detail in chapter 4, in which the developed methodology is used for studying receptor occupancy after nose-only exposure of this compound.

Chapter 4 Temporal relationship between target site exposure and receptor occupancy

4.1 Introduction

As highlighted in chapter 3, contemporary experimental methodologies do not allow for direct measurements of unbound drug concentrations locally in the lung tissue. Since receptor occupancy is driven by the unbound drug concentration at the target site, such measurements would clarify the PK- and PK/PD-evaluation of locally acting inhaled drugs. The *in vivo* receptor occupancy methodology, the development of which was described in chapter 3, could thus be used for this purpose. Fluticasone propionate (FP) was selected as a test compound for various reasons. Firstly, it is a well-established drug that is broadly used in the clinic, for example for the treatment of asthma [48]. Secondly, it is a highly selective and potent glucocorticoid receptor (GR) agonist [79]. Thirdly, its lung retention is held to rely on its low solubility and thus slow dissolution rate [4]. Although a low solubility is a commonly used strategy for achieving lung retention after inhalation, more in-depth knowledge is needed to better understand potential benefits and limitations of this strategy. As measurements of total lung concentrations (C_{lung}) after inhalation does not distinguish between solid and dissolved drug, preclinical inhalation studies of poorly soluble compounds are held to be exceedingly difficult to interpret. Furthermore, the complex interplay between *e.g.* dissolution, mucociliary clearance and permeation into lung tissue makes the interpretation even more challenging. The third property is thus clearly the most interesting one from an inhalation PK perspective. When switching focus from the pulmonary to the systemic PK, it becomes clear that FP, and several other inhaled corticosteroids, has properties strategically chosen to minimise the systemic exposure following inhalation: a high clearance and a low oral bioavailability [18]. In

summary, characterisation of the receptor occupancy of FP after nose-only exposure has the potential to yield interesting information about inhalation PK.

In contrast to drug delivery via the inhaled route, the unbound plasma concentration (C_u) is generally assumed to reflect the target site concentration after IV-administration of drug. This is based on the assumption that unbound drug freely distributes between blood and tissues, hence at equilibrium the C_u and the unbound drug concentration in tissues (C_{uT}) will be the same (the 'free drug hypothesis'). Assuming that the drug of interest has a perfusion rate-limited drug distribution, i.e. membranes do not present a barrier to distribution but the rate determining step is the blood flow to the tissue, the tissue distribution half-life ($t_{½,distr}$) can be calculated from the distribution rate constant k_T accordingly [139]:

$$k_T = \frac{\text{Rate of leaving}}{\text{Amount in tissue}} = \frac{Q_i C_{vein}}{V_i K_p C_{vein}} = \frac{Q_i}{V_i K_p}, \quad (4.1)$$

$$t_{½,distr} = \frac{\ln 2}{k_T}, \quad (4.2)$$

where Q_i is the flow to tissue i, C_{vein} is the venous concentration of drug, V_i is the volume of tissue i and K_p is the tissue-to-plasma partition coefficient. Parameters specific for the spleen were used to investigate whether it would be feasible to assume that measurements of C_u would be representative of the unbound drug concentration in the spleen. By setting Q_{spleen} to 1.485 L/h/kg (cardiac output, Q_{CO} = 20.77 L/h/kg [140] and the spleen receives 7.15% of Q_{CO} [141]), V_{spleen} to 2 mL/kg [142] and K_p to *e.g.* 2.5, eq. 4.2 gives a $t_{½,distr}$ of 8.4 s. Hence, the C_u can be assumed to be reflective of the unbound drug concentration in the spleen. This has interesting implications; given that receptor occupancy is measured in the spleen, the more

easily accessible C_u can be used to mathematically describe the relationship between target site exposure and receptor occupancy after IV-administration. Expressed differently, such studies would enable characterisation of the *in vivo* binding kinetics by estimating the association rate constant (K_{on}) and the dissociation rate constant (K_{off}). The binding kinetics of several GR agonists have previously been characterised in *in vitro* systems. However, data generated from an *in vitro* system are not necessarily translatable to the *in vivo* situation. In fact, results from previous work have indicated that this might be the case. In an *in vitro* system, the K_{off} of the corticosteroid triamcinolone acetonide was experimentally determined to be 5.5×10^{-4} min^{-1}, which corresponds to a dissociation half-life of 21 h [143]. In contrast, when an *ex vivo* binding assay was used to monitor receptor occupancy following an IV-dose of triamcinolone acetonide to rats (22 µg), the level of free receptors initially declined rapidly after dosing, but was then found to return to baseline already within six hours after dosing [120]. Hence, studies with triamcinolone acetonide as a model drug suggest a disconnection between the *in vitro* and the *in vivo* situation with respect to the dissociation half-life. To gain further understanding of inhaled corticosteroids, it would thus be interesting to characterise the *in vivo* binding kinetics for this compound class. Ultimately, if estimates of K_{on} and K_{off} subsequently could be incorporated into a mechanistic *in silico* model used for predicting the local tissue concentrations after inhalation, measurements of receptor occupancy after inhalation would provide the first opportunity for validating such predictions.

This chapter will describe the experiments and the mathematical modelling used to characterise the *in vivo* binding kinetics after IV-administration of FP and budesonide. It also comprises the experiments used for studying the inhalation PK as well as the receptor occupancy after nose-only exposure of FP.

4.2 Receptor occupancy studies after IV-administration

The time course of receptor occupancy was studied after IV-administration of FP and budesonide. The experimental details and the results from the study with FP are described in sections 3.3.1.2 and 3.3.2.2, respectively, whereas the budesonide study is described in this subsection.

4.2.1 Choice of IV-dose

As the IV-studies aimed to characterise the binding kinetics of the two compounds, it was essential to choose a dose that would significantly perturb the system and thereby enable receptor occupancy measurements over an extended time period. It was reasoned that data from preclinical PD-studies could be used to find an appropriate dose. Since both compounds are usually administered via the inhaled route, previous research at AstraZeneca has focused on characterising the compounds after inhalation. Due to a lack of efficacy data after IV-administration, inhalation PD-studies were used to guide the dose setting. Both compounds had been investigated in an animal model that is used internally at AstraZeneca to evaluate the local pulmonary effects as well as the systemic side-effects of glucocorticoid receptor (GR) binders in rats. This animal model is *e.g.* described in [144]. In these studies, the effect is studied for several different lung deposited doses (*LDD*). This enables estimation of $ED_{50,}$ i.e. the *LDD* giving 50% efficacy. Since the intention was to perturb the system such that the receptors would be occupied several hours after drug administration, it was reasoned that the IV-dose should be several-fold higher than the ED_{50} to increase the chances of achieving this goal. Clearly, the IV-dose cannot be too high as that might jeopardise the well-being of the animals. The IV-dose was

therefore set to be 7.5 times ED_{50}, which corresponded to 90 and 167 nmol/kg for FP and budesonide, respectively.

4.2.2 IV-study, budesonide

The author was responsible for designing, coordinating, performing as well as analysing the receptor occupancy IV-studies. Three additional researchers from AstraZeneca R&D Gothenburg assisted the author with the *in vivo* aspects of the budesonide study: Dr. Britt-Marie Fihn, Kajsa Claesson and Louise Hammarberg.

Animals. Male Wistar Han rats (Harlan, Horst, the Netherlands) weighing 260 to 300 g were used for the IV-study with budesonide. The animals were group-housed at 18-22 ºC under a 12:12 h light/dark cycle with free access to food and water for at least five days prior to the experiments. The studies were approved by the Animals Ethics Committee of Gothenburg (71-2013).

Study protocol. The animals were anaesthetised by inhalation of isoflurane during both drug- and tracer administration. Budesonide was administered via the tail vein (167 nmol/kg) and the animals were then allowed to wake up. Tracer was subsequently administered via the tail vein at the following time points after drug administration: 0.5, 1, 2, 4, 7, 24 and 48 h (3 animals/time point). Animals dedicated to determination of $C_{nonspec}$ had been pre-treated with an IV-dose of dexamethasone (20 mg/kg) 30 minutes prior to the tracer administration (n = 6). In contrast, animals set aside for determination of $C_{control}$ did not receive any pre-treatment prior to tracer administration (n = 7). A detailed experimental protocol for the *in vivo* receptor occupancy methodology as well as the sample handling is provided in section 3.2.1.8.

4.2.3 Analytical procedures

The sample handling as well as the analytical procedures used for the GR-tracer are described in detail in section 3.2.1.10.

4.2.4 Results

As can be seen in fig. 4.1, the receptor occupancy in the lung (RO_{lung}) and the spleen (RO_{spleen}) were of similar magnitudes after IV-administration of budesonide. The receptor occupancy was initially high and then rapidly returned to baseline within 4 hours after dosing.

One animal, which was dosed with tracer at t = 4 h (where t = 0 h assigns the time point of drug administration), was excluded from the study since the apex was not incised along its transverse axis prior to perfusion of the lung. Due to this experimental error, water assembled in the lung causing the lung weight to increase by more than 100%. It was therefore judged as inappropriate to include measurements from this animal.

The data generated in this study was subsequently used for characterising the *in vivo* binding kinetics by mathematical modelling, which is described in section 4.4.

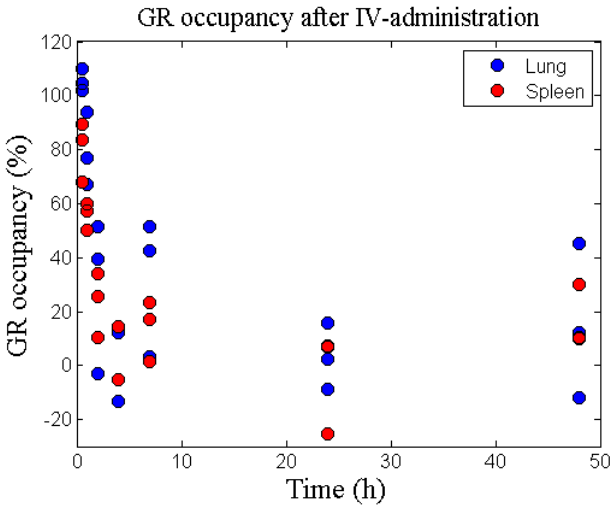

Figure 4.1 Glucocorticoid receptor (GR) occupancy was measured in the lung (blue circles) and the spleen (red circles) after IV-administration of budesonide (167 nmol/kg) to rats.

4.3 Pharmacokinetic studies

To enable modelling of the *in vivo* binding kinetics, the plasma pharmacokinetics (PK) of FP and budesonide were characterised using the same IV-doses as in the receptor occupancy studies. As the experimental data showed that *dRO*/*dt* was high during the initial part of the study, emphasis was placed on characterising the initial part of the plasma PK-profile by designing a study with frequent sampling at early time points.

FP is known to be challenging from a bioanalytical perspective and in the previous LC-MS/MS analyses the analytical sensitivity in plasma was recognised as very poor with a lower limit of quantification (LLOQ) above 5 nM. An improved analytical methodology was therefore set up in collaboration with Dr. Anders Lundqvist at AstraZeneca R&D Gothenburg. Due to the poor analytical sensitivity with the previously employed LC-MS/MS methodology, several plasma samples were still judged to be at high risk of falling below the LLOQ after an IV-dose of 90 nmol/kg. Hence, to ensure that it would be possible to quantify the plasma concentrations of

FP over several hours following drug administration an additional higher dose level was included in the PK-study (1000 nmol/kg).

4.3.1 Preparation of dose solutions

FP and budesonide were prepared as nanosuspensions at AstraZeneca's R&D facility in Gothenburg by Sara Johansson and Annica Jarke according to the following two experimental protocols. In this study, nanosuspensions were favoured over the previously used vehicle with N,N-dimethylacetamide, polyethylene glycol 400 and water (1:1:1, w/w/w) due to newly discovered issues with possible animal discomfort during the tail-vein administration.

Fluticasone propionate. Glass-ware and utensils were cleaned with 70% ethanol. 20 mL of the vehicle (Polyvinylpyrrolidone *K30*/SDS, 0.2%/0.25 mM) was prepared by mixing polyvinylpyrrolidone *K*30 (1 mL), 50 mM SDS (0.1 mL) and purified water (18.9 mL). A stock solution of 33.33 mM in DMA (stock A) was prepared by dissolving FP (4.05 mg) in DMA (243 µL). Subsequently, a second stock solution of 3 mM (stock B) was prepared by diluting stock A (33.33 mM, 18 µL) with DMA (182 µL).

The nanosuspension for the higher dose level was prepared by precipitating stock A (33.33 mM, 60 µL) in vehicle (1940 µL), resulting in a final concentration of 1.0 mM. The nanosuspension for the lower dose level was prepared by precipitating stock B (3 mM, 60 µL) in vehicle (1940 µL), resulting in a final concentration of 90 µM. Hence, the concentrations of both nanosuspensions were prepared such that the dose volume should be 1 mL/kg. The particle size was determined by fibre-optic detection and quasi-electric light-scattering (FOQELS); 371.7 and 297.8 nm for the

1.0 mM and 90 µM nanosuspensions, respectively. Both suspensions were stored in room temperature under stirring until dosing.

Budesonide. The vial and the magnetic stirrer were cleaned using 70% ethanol. Budesonide was weighed (57 mg) and vehicle (2% Pluronics F127, 510 µL) was added to the substance. The slurry was put on stirring over-night. The milling vessel was cleaned with 70% ethanol prior to the start of wet milling (4×30 min at 700 rpm with 15 minutes intermission). A washing step with 5% filtered mannitol was then applied (filtered through a 22 µm filter). The process resulted in a final particle size of 186 nm. The suspension was diluted with 5% filtered mannitol providing a final concentration of 167 µM so that the dose volume should be 1 mL/kg. The suspension was stored in room temperature until dosing.

4.3.2 *In life* pharmacokinetic study

The surgeries and the PK-study were performed at AstraZeneca R&D Gothenburg. The surgeries were performed by Marie Johansson and Gina Hyberg. The PK-study was led, designed and coordinated by the author, who also actively took part in the experimental study. Three additional researchers assisted the author in the experimental parts of the PK-study: Dr. Britt-Marie Fihn, Marie Johansson and Gina Hyberg.

Animals. Male Wistar Han rats (Harlan, Horst, the Netherlands) weighing 290 to 350 g were used for the PK-study. The animals were group-housed at 18-22ºC under a 12:12 h light/dark cycle with free access to food and water for at least five days prior to the experiments. The studies were approved by the Animals Ethics Committee of Gothenburg (71-2013).

Study protocol. Jugular vein catheterisation was performed on 11 rats to enable repeated blood sampling. The surgery was followed by four days of recovery before the start of the PK-study. On the day of the study, the functionality of the vein catheters was tested both by injecting saline solution and by taking a blood sample. Three catheters did not pass the test and those animals were therefore not included in the study, leaving eight animals for the PK-study. A nanosuspension of the drug was administered as an IV-bolus (1 mL/kg) to the three different dose groups accordingly: 1) 167 nmol/kg budesonide (n = 3), 2) 90 nmol/kg FP (n = 2), and 3) 1000 nmol/kg FP (n = 3). Blood samples were repeatedly collected from the catheter over 8 hours following drug administration (t = 1, 3, 5, 10, 15, 30, 60, 120, 240 and 480 min). An additional time point was included for budesonide at t = 24 h. No sample was taken for FP at t = 24 h as the drug concentration was expected to be below the LLOQ. The animals were euthanized by injection of pentobarbital (200 mg/kg) after the last blood collection.

Sample handling. The blood samples were collected in heparinised tubes which were centrifuged for 10 minutes at 4000g (Rotanta 46R, Hettich, Germany). The plasma samples were subsequently transferred to Eppendorf tubes and stored at -20ºC until analysis.

4.3.3 Analytical procedures

The plasma samples were analysed at AstraZeneca R&D Gothenburg by Dr. Anders Lundqvist according to the following experimental protocols, which were written in collaboration with Dr. Lundqvist. Both the analytical methodology for FP and budesonide provided an improved analytical sensitivity, i.e. a lower LLOQ, as compared to the previously used methodologies. The improved methodologies

provided a LLOQ in plasma of 0.04 and 0.10 nM for FP and budesonide, respectively.

4.3.3.1 Analytical procedures for fluticasone propionate

Sample preparation. A Solid Phase Extraction (SPE) procedure was used for preparation of the FP plasma samples. Briefly, aliquots of 100 µL plasma samples were pipetted to a 96-well plate and 125 µL Zinc sulphate (0.2 M) was added to each well. The plate was sealed and vortexed for 1 minute and then centrifuged for 5 min at 4000 rpm. The supernatants (200 µL) were loaded on an Bond Elute C18 SPE plate (Agilent Technologies Inc., Wilmington, DE, USA), preconditioned with 200 µL acetonitrile, methanol and water, respectively and a vacuum was then applied. The wells were washed with 200 µL water and then 200 µL of 20% methanol water solution. FP was eluted from the plate by 300 µL of 90% acetonitrile water solution and evaporated to dryness under nitrogen flow. The extracts were reconstituted with 125 µL of 40% acetonitrile water solution prior analysis by LC-MS/MS.

LC-MS/MS conditions. Separation was carried out on a Kinetex C18, 2.6 µm, 50×2.1 mm column (Phenomenex, CA, USA) at 45 °C, connected to a LC-20 AD binary pump (Shimadzu Scientific Instruments, MD, USA) delivering a flow rate of 0.4 mL/min. Mobile phases A and B consisted of 0.02% ammonium hydroxide in water and 50% acetonitrile in methanol, respectively. Gradient elution was applied using a linear gradient of 35-95% mobile phase B from 0.2 to 1.5 minutes, held at 95% for 1 minute and returned to initial conditions in one step. Sample storage and injection was performed by a CTC PAL HTC-xt autosampler (CTC Analytics, Zwingen, Switzerland) keeping the samples conditioned at 12 °C. The mass spectrometric detection was carried out by a Sciex API 5000 triple quadrupole

(Applied Biosystems, MDS Sciex, Toronto, Canada) operating under positive ESI in SRM mode. The *m/z* transition for FP was 501.2 > 293.2. Instrument control, data acquisition and data evaluation were performed using Analyst 1.6.

4.3.3.2 Analytical procedures for budesonide

Sample preparation. A liquid liquid extraction (LLE) procedure was used for preparation of budesonide plasma samples. Briefly, aliquots of 50 µL plasma samples were pipetted to glass tubes placed in a 96-well plate followed by addition of 50 µL carbonate buffer, pH 10. Methyl-tertbutyl ether (MTBE, 600 µL) was added to create a two phase condition. The plate was sealed and shaken for 20 minutes and then centrifuged for 5 min at 2000 rpm. The upper organic layer (550 µL) was transferred to a new set of glass tubes and evaporated to dryness under streaming nitrogen. The extracts were reconstituted with 150 µL of 50% acetonitrile water solution prior analysis by LC-MS/MS.

LC-MS/MS conditions. Separation was carried out on a Kinetex C18, 2.6 µm, 50×2.1 mm column (Phenomenex, CA, USA) at 45 °C, connected to a LC-20 AD binary pump (Shimadzu Scientific Instruments, MD, USA) delivering a flow rate of 0.5 mL/min. Mobile phases A and B consisted of 10 mM ammunium acetate/0.2% acetic acid and methanol/0.2% acetic acid, respectively. Gradient elution was applied using a linear gradient of 45-97% mobile phase B from 0.1 to 1.0 minutes, held at 97% for 0.7 minute and returned to initial conditions in 0.3 min. Sample storage and injection (10 µL) was performed by a CTC PAL HTC-xt autosampler (CTC Analytics, Zwingen, Switzerland) keeping the samples conditioned at 12°C. The mass spectrometric detection was carried out by a Sciex API 5000 triple quadrupole (Applied Biosystems, MDS Sciex, Toronto, Canada) operating under negative ESI in

SRM mode. The *m/z* transition for the acetate adduct of budesonide was 489.4 > 357.2. Instrument control, data acquisition and data evaluation were performed using Analyst 1.6.

4.3.4 Modelling of plasma pharmacokinetics

All plasma samples were above the LLOQ except for the samples collected at the last time point in the budesonide PK-study (t = 24 h). The LLOQ for budesonide and FP were 0.1 nM and 0.04 nM, respectively.

A 3-compartment model with a multiplicative error model was used to describe the plasma PK after IV-administration of FP (90 nmol/kg, n = 2) and budesonide (167 nmol/kg, n = 3). This model has been proven to be structurally identifiable [94]. An additive error model was also tested. A naïve-pooled data approach was used, i.e. the observations were treated as if they came from one individual. The models were implemented in Phoenix™ WinNonlin® 6.3.0 (Pharsight, Sunnyvale, CA), which minimised the exact negative log-likelihood using a quasi-Newton algorithm. The compartmental model equations describing the process were given by

$$V_1 \frac{dC_1}{dt} = -ClC_1 - Cl_2(C_1 - C_2) - Cl_3(C_1 - C_3), \quad C_1(0) = \frac{D}{V_1} \tag{4.3}$$

$$V_2 \frac{dC_2}{dt} = Cl_2(C_1 - C_2), \quad C_2(0) = 0 \tag{4.4}$$

$$V_3 \frac{dC_3}{dt} = Cl_3(C_1 - C_3), \quad C_3(0) = 0 \quad . \tag{4.5}$$

The model is graphically illustrated by figure 4.2. The plasma profiles and the model fits are shown in figure 4.3a-b and the estimated PK-parameters are presented in table 4.1. The correlation matrices for the parameter estimates are presented in tables 4.2 and 4.3 for FP and budesonide, respectively. Plots of weighted residuals resulting from using either multiplicative or additive error models are shown in fig. 4.4a-d. As can be seen in fig. 4.4a, the weighted residuals were randomly distributed around zero when a multiplicative error model was used for FP. A small trend was noted in the residuals at two time points for budesonide when a multiplicative error model was used (fig. 4.4c). However, they were judged to provide a sufficiently good description of the data. In contrast, the weighted residuals systematically increased with increasing values of the predicted plasma concentration when an additive error model was used (fig. 4.4b and 4.4d). Expressed differently, a fan-shaped pattern appeared in the residual plot, which indicated that an additive error model was inappropriate to use for both data sets.

Table 4.1 Estimated pharmacokinetic parameters for fluticasone propionate (FP) and budesonide (mean ± SE)

Parameter	**FP**	**Budesonide**
V_1 (L/kg)	0.63 ± 0.16	0.49 ± 0.13
V_2 (L/kg)	9.0 ± 3.5	1.3 ± 0.78
V_3 (L/kg)	2.8 ± 1.0	0.44 ± 0.10
CL_1 (L/h/kg)	11 ± 1.0	3.0 ± 0.19
CL_2 (L/h/kg)	2.1 ± 0.63	0.15 ± 0.035
CL_3 (L/h/kg)	5.8 ±1.6	4.3 ± 1.8

Abbreviations: V_1=volume of distribution in the central compartment; V_2=volume of distribution in the slowly equilibrating compartment; V_3=volume of distribution in the rapidly equilibrating compartment; CL_1=clearance; CL_2=slow distribution clearance; CL_3=rapid distribution clearance

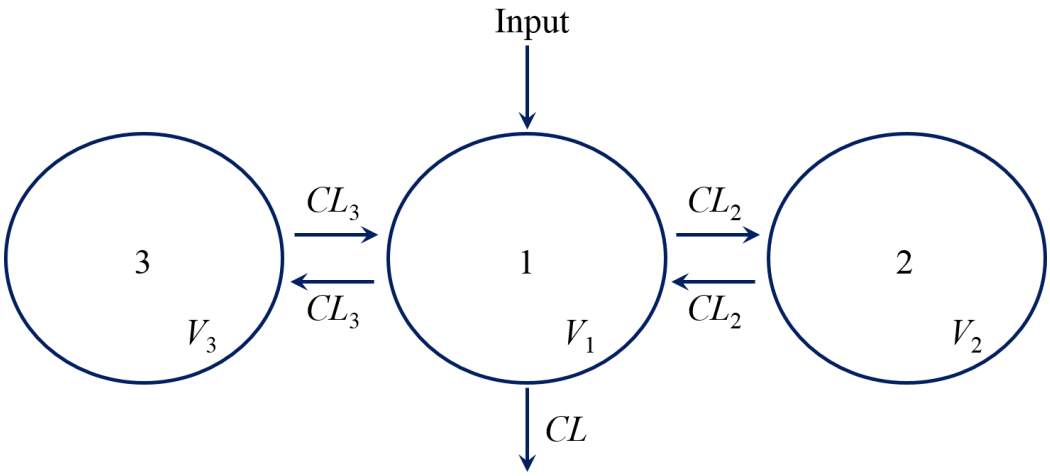

Figure 4.2 Graphical illustration of a 3-compartment model.

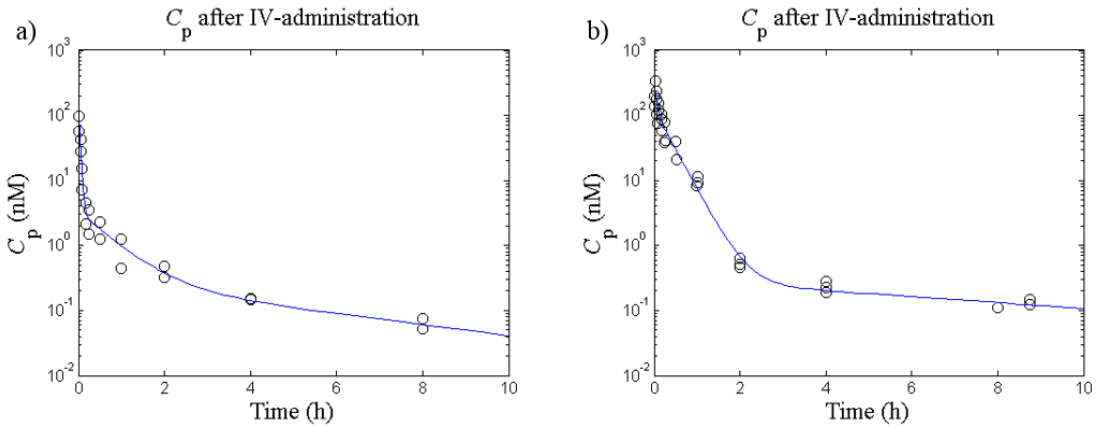

Figure 4.3 Plasma concentration (C_p) after intravenous (IV) administration of a) fluticasone propionate to rats (90 nmol/kg, n = 2), and b) C_p after IV-administration of budesonide to rats (167 nmol/kg, n = 3). Observed data are indicated by circles and the model fit by a solid line.

Table 4.2 Estimated correlation matrix for the parameters obtained from modelling of the pharmacokinetics of fluticasone propionate.

	V_1	V_2	V_3	CL	CL_2	CL_3
V_1	1	0.41	0.55	0.82	0.45	0.71
V_2	0.41	1	0.57	0.23	0.036	0.52
V_3	0.55	0.57	1	0.35	-0.28	0.80
CL	0.82	0.23	0.35	1	0.62	0.62
CL_2	0.45	0.036	-0.28	0.62	1	0.13
CL_3	0.71	0.52	0.80	0.62	0.13	1

Table 4.3 Estimated correlation matrix for the parameters obtained from modelling of the pharmacokinetics of budesonide.

	V_1	V_2	V_3	CL	CL_2	CL_3
V_1	1	0.11	-0.75	0.50	0.27	-0.63
V_2	0.11	1	0.038	0.053	0.89	-0.06
V_3	-0.75	0.038	1	0.061	0.043	0.72
CL	0.50	0.05	0.061	1	0.39	-0.19
CL_2	0.27	0.89	0.043	0.39	1	-0.12
CL_3	-0.63	-0.06	0.72	-0.19	-0.12	1

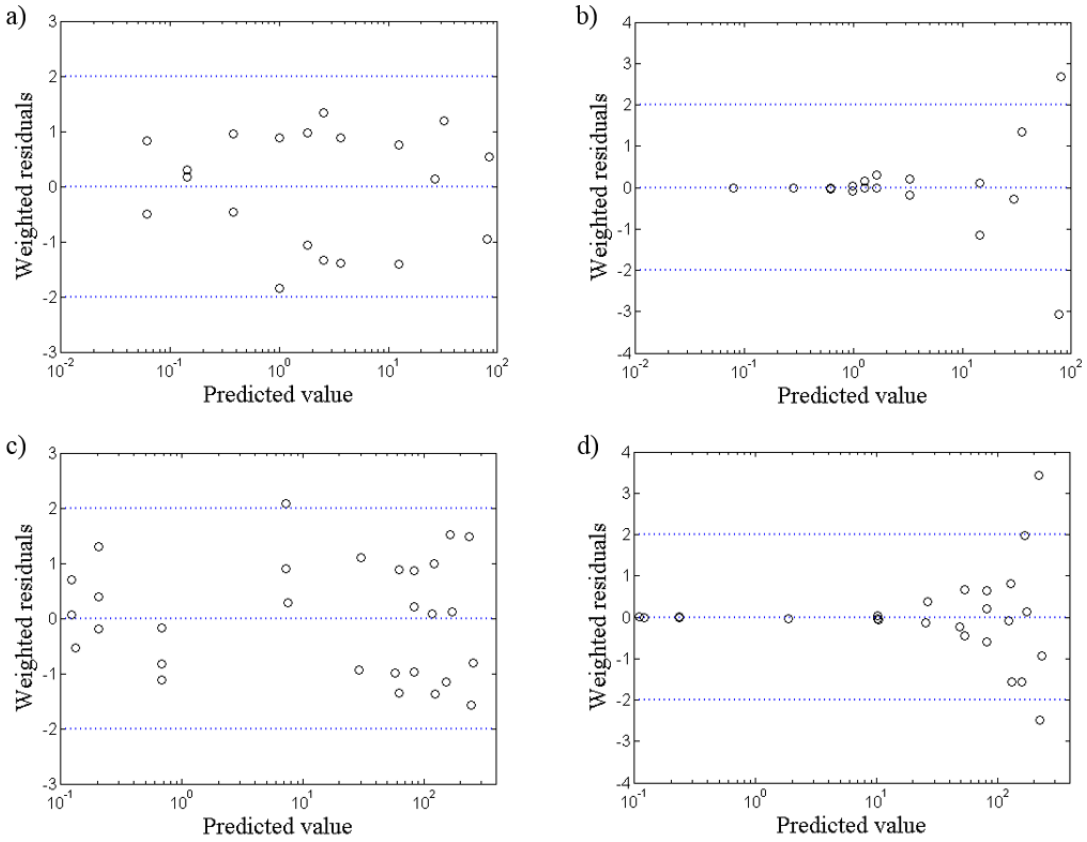

Figure 4.4 Weighted residuals plotted against the predicted plasma concentration using different error models: a) multiplicative error model, fluticasone propionate (FP), b) additive error model, FP, c) multiplicative error model, budesonide, and d) additive error model, budesonide.

4.4 Modelling of binding kinetics

4.4.1 Characterisation of binding kinetics

As described in section 4.3.4, a 3-compartment model with a multiplicative error model was used to describe the plasma PK after IV-administration of FP (90 nmol/kg) and budesonide (167 nmol/kg). The compartmental model equations were given by eqs. 4.3-4.5 and the estimated PK-parameters were presented in table 4.1. The unbound drug concentration in plasma (C_u) was calculated from eq. 4.6, where f_u is the fraction unbound in plasma and C_1 is the drug concentration in the central compartment given below:

$$C_u(t) = f_u C_1(t). \qquad (4.6)$$

The receptor density (B_{max}) in the spleen has previously been measured and found to be 31.5 nM [138]. The concentration of the receptor-drug complex *(RD*) could therefore be calculated from the spleen GR occupancy data, which were favoured for modelling purposes as this organ had a higher ratio of total-to-nonspecific tracer binding and thus allowed for more accurate occupancy estimations [126].

For both compounds a high initial occupancy was observed after IV-administration, which then returned to baseline within 7 and 4 h after dosing for FP and budesonide, respectively. The estimated occupancy at 24 h after dosing of FP was higher than after 7 h, which, most likely, is not reflective of the drug-receptor interaction. Rather, the observation may reflect the dynamics of the glucocorticoid receptor with a drug-induced downregulation of the receptor population, which has been demonstrated to take place after administration of GR agonists both *in vitro* and *in vivo* [137]. Receptor occupancy data from $0 < t \leq 7$ and $0 < t \leq 4$ h were therefore

used for parameter estimation for FP and budesonide, respectively. Within these two time intervals, two receptor occupancy observations had been calculated as negative (-4.0 and -5.3%). Negative receptor occupancy is not possible from a theoretical point of view; however, since the maximum tracer concentration is obtained from a separate group of animals, interindividual variability can explain why these two estimates were slightly lower than 0%. As the receptor occupancy cannot be lower than 0%, these two values were set to zero in the modelling data set.

The binding kinetics was described accordingly:

$$\frac{dRD(t)}{dt} = K_{on}C_u(t)(B_{\max} - RD(t)) - K_{off}RD(t), \quad RD(0) = 0 \qquad (4.7)$$

$$K_d = \frac{K_{off}}{K_{on}}, \qquad (4.8)$$

where K_d is the dissociation constant, K_{on} is the association rate constant and K_{off} is the dissociation rate constant. As opposed to the PK model, an additive error model was used for the binding kinetics.

Both the PK- and the binding kinetics models were implemented in Phoenix™ WinNonlin® 6.3.0 (Pharsight, Sunnyvale, CA). "The Naïve pooled engine" was used, i.e. the observations were treated as if they came from one individual. This engine minimises the exact negative log-likelihood by using a quasi-Newton algorithm. The default ODE-solver was used for the PK-model (matrix exponential). A stiff ODE-solver was used for the binding kinetics model. The estimated binding kinetics parameters are presented in table 4.4. The observations and the corresponding model fit are shown in figure 4.5a and 4.5b for FP and budesonide, respectively.

The estimated correlation matrices for FP and budesonide are presented in table 4.5 and 4.6, respectively. A negative correlation between K_{off} and K_d was found (-0.76 and -0.74 for FP and budesonide, respectively). The optimisation was restarted several times with different sets of initial estimates to check whether it converged to the same estimates. The optimisation algorithm was found to converge to same solution when a broad range of initial estimates were used.

An exhaustive search was subsequently performed in MATLAB to ensure that the global minimum had been found within the expected parameter space. The sum of squares was evaluated at 360000 combinations of parameter values. For FP, K_{on} varied between 1 and 100 L/nmol/h and K_{off} varied between 0.05 and 5 h^{-1}. For budesonide, K_{on} varied between 0.1 and 100 L/nmol/h and K_{off} varied between 0.05 and 10 h^{-1}. The parameter values were selected from a logarithmic scale to ensure that the search was not biased to the large regions.

In the exhaustive search for FP, the lowest cost function was found at 33.8 L/nmol/h and 0.510 h^{-1} for K_{on} and K_{off}, respectively. For budesonide, the lowest cost function was found at 1.13 L/nmol/h and 1.31 h^{-1} for K_{on} and K_{off}, respectively. Hence, the exhaustive search showed that the global minimum had been found for both compounds within the defined parameter space. The two exhaustive searches are graphically illustrated in figures 4.6a and 4.6b.

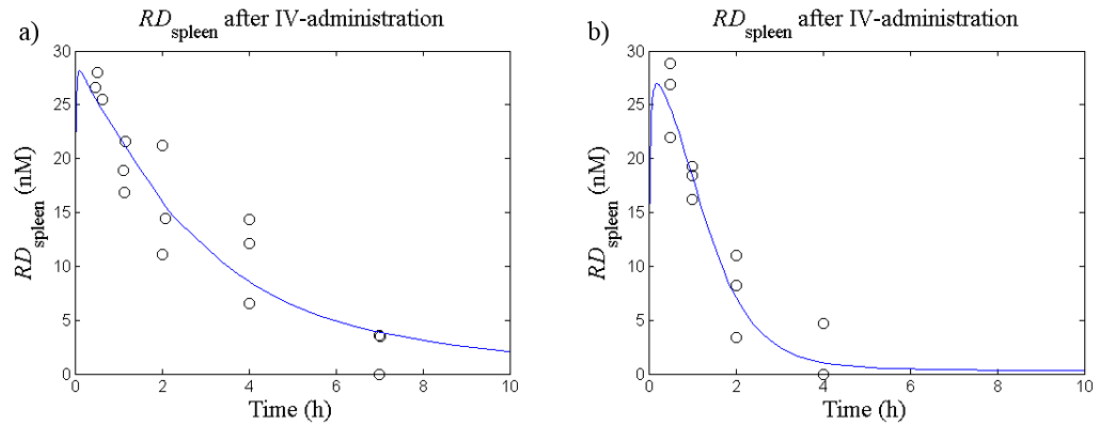

Figure 4.5 Concentration of receptor-drug complex in the spleen (RD_{spleen}) after intravenous (IV) administration of a) fluticasone propionate (90 nmol/kg, n = 3/time point) and b) budesonide (167 nmol/kg, n = 3/time point). Observed data are indicated by circles and the model fit by a solid line.

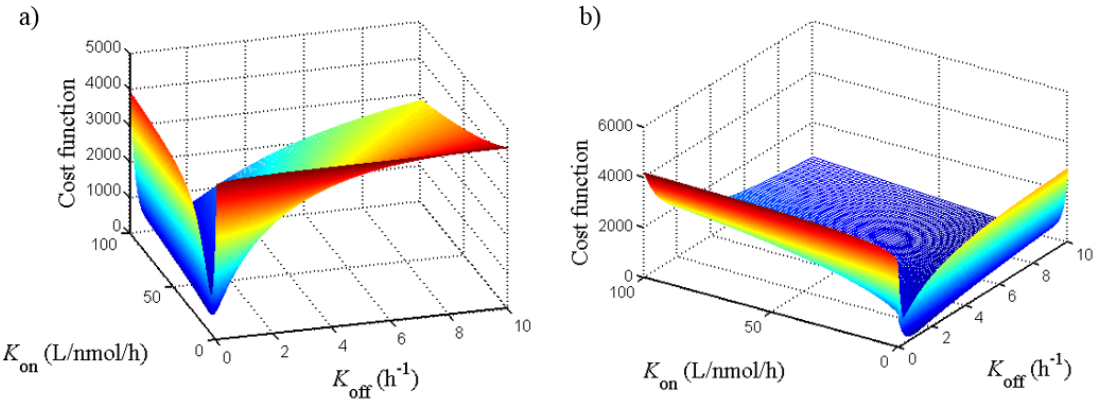

Figure 4.6 An exhaustive search was performed for a) fluticasone propionate, and b) budesonide by evaluating the cost function (the sum of squares) at 360000 different combinations of parameter values. These two exhaustive searches confirmed that the global minimum had been found within the expected parameter space.

Table 4.4 Estimated binding kinetics parameters for fluticasone propionate (FP) and budesonide (mean ± SE)

Parameter	**FP**	**Budesonide**
K_d (nM)	0.015 ± 0.0045	1.2 ± 0.34
K_{off} (h^{-1})	0.51 ± 0.17	1.3 ± 0.39
K_{on} (L/nmol/h)	34 ± 20	1.12 ± 0.62

Abbreviations: K_d = dissociation constant; K_{off} = dissociation rate constant; K_{on} = association rate constant

Table 4.5 Estimated correlation matrix for the parameters estimates obtained from modelling of the binding kinetics of fluticasone propionate.

	K_d	K_{off}
K_d	1	-0.76
K_{off}	-0.76	1

Table 4.6 Estimated correlation matrix for the parameters estimates obtained from modelling of the binding kinetics of budesonide.

	K_d	K_{off}
K_d	1	-0.74
K_{off}	-0.74	1

4.4.2 Sensitivity analysis

A sensitivity analysis was performed by considering the partial derivatives of the output *RD* with respect to each estimated binding kinetics parameter p_i. That is, each partial derivative was evaluated at the final parameter estimate. Phoenix™ WinNonlin® 6.3.0 computed a numerical approximation of the partial derivatives accordingly

$$\frac{\partial RD}{\partial p_i} = \frac{RD(p_i + \Delta) - RD(p_i)}{\Delta}, \qquad (4.9)$$

where p_i is K_d or K_{off} (K_{on} was a secondary parameter) and Δ is the increment multiplied by the final parameter estimate (Δ = 0.00001). That is, all other parameters but p_i were kept at their nominal values in the calculations.

The plots showing $\partial RD/\partial K_d$ over time (figs. 4.7a and 4.7c for FP and budesonide, respectively) indicate that small changes in K_d would have a profound effect on *RD* directly after IV-dosing, *i.e.* this is an effect that coincides with the peak in the drug

plasma concentration. This was especially pronounced for FP. In general, with the exception of a small bump, this parameter became less influential over time. Hence, the sensitivity analysis shows that observations made at early time points had the largest influence on the estimation of K_d. From a mathematical point of view, if the studies were to be repeated they would benefit from a sampling scheme with more frequent sampling at early time points, given that the purpose was to obtain a good estimate of K_d. Nevertheless, in general the sampling scheme used was informative with respect to K_d. However, at the last time point included in the modelling data set of budesonide (t = 4 h), the analysis showed that K_d only had a minor effect on the output *RD*.

Figures 4.7b and 4.7d show the $\partial RD/\partial K_{off}$ over time for FP and budesonide, respectively. Again, the analysis shows that the output *RD* was sensitive to small changes in the investigated parameter (K_{off}) directly after dosing. $\partial RD/\partial K_{off}$ had the same behaviour for both compounds and it changed sign from positive to negative over the investigated time course. For FP, *RD* was very sensitive to changes in K_{off} at approximately t = 3 h, whereas the output would have been less sensitive to changes in the parameter at later time points. For budesonide, the corresponding nadir occurred at approximately t = 1.8 h.

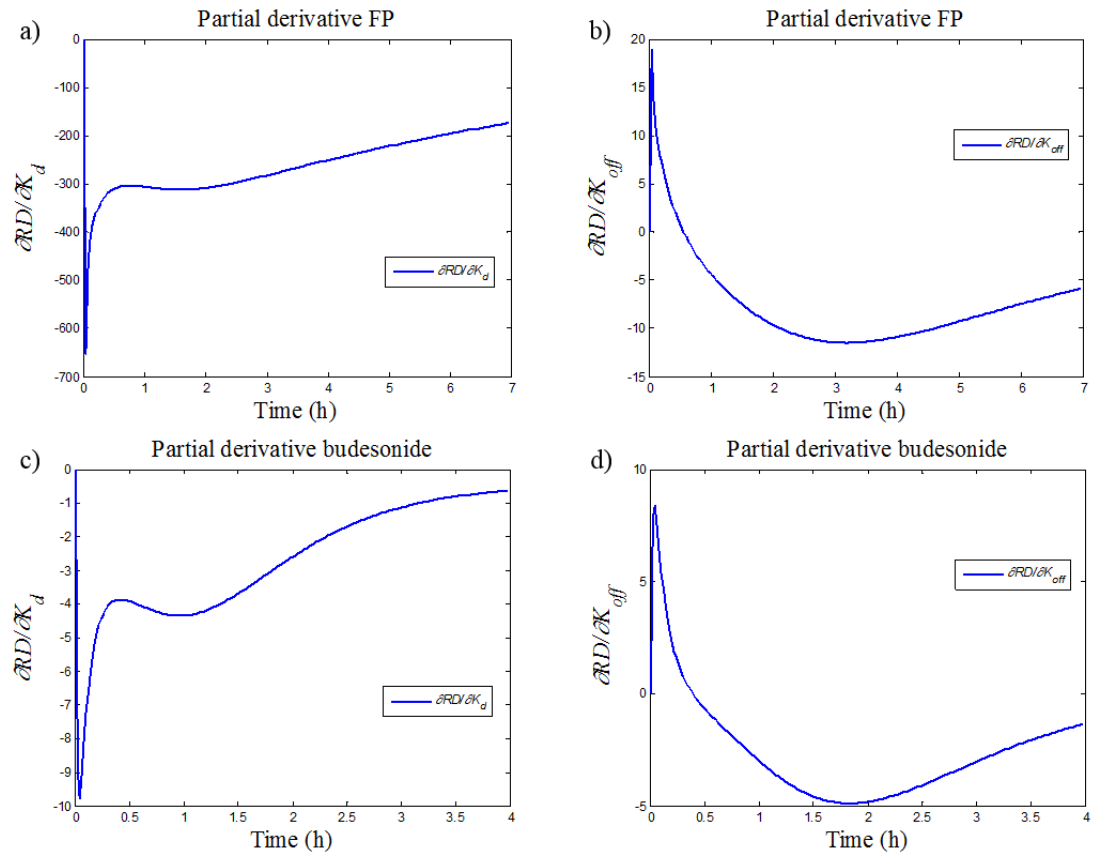

Figure 4.7 Sensitivity analysis was performed by considering the partial derivatives of the output RD with respect to the estimated binding kinetics parameters K_d and K_{off}. This was done for both the study comprising fluticasone propionate (FP) and budesonide.

4.5 Receptor occupancy studies after nose-only exposure

The time course of receptor occupancy after nose-only exposure was studied for FP. The experimental details as well as the results are included in this subsection.

4.5.1 Nose-only exposure studies

In the inhalation studies, the rats were nose-only exposed to dry powder of FP. In nose-only exposure studies, each rat is restrained in a separate tube that is open at one end to a chamber containing aerosolised compound [145]. The inhalation system was controlled and operated by Anders Wigenborg, AstraZeneca R&D Gothenburg. Otherwise, the author (Elin Boger) was responsible for designing, coordinating,

performing as well as analysing the studies. The bioanalysis with respect to FP in the plasma samples was done by Dr. Anders Lundqvist. Three additional researchers from AstraZeneca R&D assisted the author in the *in vivo* parts of the studies: Dr Markus Fridén, Dr Britt-Marie Fihn and Susanne Arlbrandt. The subsection describing the inhalation system is written in collaboration with Anders Wigenborg.

Animals. Male Wistar Han rats (Harlan, Horst, the Netherlands) weighing 250 to 375 g were used for the inhalation studies. The animals were group-housed at 18-22ºC under a 12:12 h light/dark cycle with free access to food and water for at least five days prior to the experiments. The studies were approved by the Animals Ethics Committee of Gothenburg (71-2013).

Study protocol. The time course of receptor occupancy was studied after nose-only exposure of FP. The inhalation study was performed twice using the same experimental setup. The two studies are henceforth referred to as study 1 and study 2.

The following precautions were taken to reduce the stress for the animals: 1) all animals were accustomed to nose-only exposure, including the restrainer tubes, prior to the study, 2) they were accustomed to human contact prior to the study, 3) the animals were weighed the day before the study, and 4) they were carefully moved to the laboratory several hours before the start of the study.

The GR occupancy after nose-only exposure was investigated over 48 hours (t = 1, 2, 4, 7, 24 and 48 h, n = 3 and n = 4 per time point in study 1 and 2, respectively) with additional PK-measurements at earlier time points (t = 45 and 75 min, n = 2 per time point). The maximum tracer concentration was obtained from drug-naïve control animals and the nonspecific tracer concentration from animals that had been pre-treated intravenously with dexamethasone (n = 6, 20 mg/kg) 30 min prior to tracer administration. The drug-naïve control animals from the two studies were

pooled (n = 14). In conjunction with euthanization, a terminal blood sample was taken from the abdominal aorta and organs (lung and spleen) were collected for quantification of the GR-tracer and drug concentrations.

Details concerning receptor occupancy calculations, the inhalation system, dose estimation and bioanalytical procedures are described under their respective headings.

Calculation of receptor occupancy and propagation of error. Receptor occupancy was calculated by the ratio method (eq. 4.10) [130,131,132,133] which includes three different measurements: 1) the tissue tracer concentration obtained from treated animals (T), 2) the nonspecific tracer concentration obtained from animals pre-treated with a high IV-dose of dexamethasone (N), and 3) the maximum tracer concentration obtained from drug-naïve control animals (C). Propagation of error was used to account for the effect of the uncertainty of each experimental measurement on the calculated receptor occupancy, i.e.

$$RO = 100 \times \left(1 - \frac{Ratio_t - 1}{Ratio_c - 1}\right), \tag{4.10}$$

where

$$Ratio_t = \frac{T}{N} \tag{4.11}$$

and

$$Ratio_t = \frac{C}{N}. \tag{4.12}$$

By inserting eqs. 4.11 and 4.12 into 4.10, the function can be simplified accordingly to yield:

$$RO = 100 \times \left(1 - \frac{\frac{T-N}{N}}{\frac{C-N}{N}} \right) = 100 \times \left(1 - \frac{T-N}{C-N} \right) \quad (4.13)$$

The simplified equation is used for calculation of partial derivatives with respect to each measurement (eqs. 4.15-4.17), which then can be inserted into the formula for propagation of error assuming independent variables (eq. 4.14), so that

$$\sigma_{RO} = \sqrt{\left(\frac{\partial RO}{\partial T} \right)^2 \times {\sigma_T}^2 + \left(\frac{\partial RO}{\partial N} \right)^2 \times {\sigma_N}^2 + \left(\frac{\partial RO}{\partial C} \right)^2 \times {\sigma_C}^2}, \quad (4.14)$$

where

$$\frac{\partial RO}{\partial T} = -\frac{100}{C-N}, \quad (4.15)$$

$$\frac{\partial RO}{\partial N} = \frac{100}{C-N} + \frac{100 \times (N-T)}{(C-N)^2} = \frac{100 \times (C-T)}{(C-N)^2}, \quad (4.16)$$

and

$$\frac{\partial RO}{\partial C} = -\frac{100 \times (N-T)}{(C-N)^2}. \quad (4.17)$$

Inhalation system. FP was formulated as a micronized dry powder and was compressed to a pellet, from which a dry particle aerosol could subsequently be produced using a Wright Dust Feeder mechanism (L. Adams Ltd, London, UK).

The inhalation system used for nose-only exposure studies can be considered to consist of two basic parts: an airflow and a dosing tower with a dry powder

generator. The airflow can further be described as two separate flows: 1) an airflow into the dosing tower, through the generator, and 2) a flow out of the dosing system.

The incoming air is mixed with the dry powder in a generator prior to entering into the tower, and therefore acts as both a carrier for the active compound and provides fresh air for the animals to breathe. The outflow of air/compound runs through the animal breathing ports and the bottom of the tower, where the excess is extracted. The driving force for this is provided by a vacuum with a slightly lower flow than the incoming air.

The dosing tower usually consists of two concentric cylinders. The outer cylinder is in direct contact with the animals through the dosing openings, communicating with the inner cylinder that serves as a container for compound/air mixture. Since the flow of air into the tower and the amount of substance generated is known, the concentration in the inner cylinder of the tower can be calculated. The concentration of delivered compound is measured online while dosing, using an aerosol monitor (Casella Microdust-Pro-Aerosol-Monitoring, Bedford, UK) connected to a computer with a software specifically developed for controlling inhalation dosing (MIVIS, developed by Flexura AB, Sweden). MIVIS is one of the systems used to regulate the dosing rate. This also means that the rate of the generation of powder and/or the duration of dosing can be changed during the study if deemed necessary.

Some losses occur due to coating of the internal walls of the tower and for particles with high kinetic energy, by impacting with the base of the tower. In either case, these particles will not be inhaled by the animals. The actual concentration of the compound in the aerosol and an estimate of the amount delivered to each animal can be calculated by sampling at one of the animal ports. Air/compound is extracted to a filter at a pre-defined flow during the time of dosing using a vacuum and the

compound is collected onto a filter for later analysis. This procedure ensures that the amount of drug on the filter reflects the concentration of compound exposed to the animals. The equations used for estimating the lung deposited dose are provided in the next section.

Estimation of the lung deposited dose. A filter was included in the Wright Dust Feeder during dosing to enable estimation of *LDD* for each study according to eq. 4.18. A detailed description is provided in . The *LDD* is determined by:

$$LDD = \frac{CC \times RMV \times D \times DF}{BW} \tag{4.18}$$

where *RMV* is the respiratory minute volume (eq. 4.19), *BW* is the mean body weight (0.344 and 0.270 kg in FP study 1 and FP study 2, respectively), *D* is the duration of exposure (7.25 and 8.64 min in FP study 1 and 2, respectively), *DF* is the deposition factor (eq. 4.20) and *CC* is the chamber concentration of drug (eq. 4.21), where

$$RMV\ (\text{L/min}) = 4.19 \times BW(g)^{0.66}, \tag{4.19}$$

$$DF = \sum_{i=1}^{8} (f_i f_{p,i} + f_i f_{c,i}) \tag{4.20}$$

and

$$CC = \frac{m_{filter}}{fr \times D} \tag{4.21}$$

where f_i is the mass fraction of particles of size class i where $i \in \{1, \ldots, 8\}$, $f_{p,i}$ and $f_{c,i}$ are the fractions of peripheral and central deposition for particles of size class i

extracted from [65] (aerodynamic diameter considered), m_{filter} is the amount of drug on the filter and *fr* is the filter flow rate (0.25 L/min).

The particle size distribution was determined using a 7-stage Mercer cascade impactor (model 02 110, In-tox Products, USA). In short, a cascade impactor has several impactors with decreasing cut-off sizes in series. As each stage has its own removable collection plate, the amount of compound collected at each stage can subsequently be determined either by gravimetric analysis or by liquid chromatography tandem mass spectrometry (LC-MS/MS) analysis. The impactor used in these studies provided a discrete particle size distribution with eight different particle sizes. LC-MS/MS analysis was employed for quantifying the amount of compound collected at each stage and the same analytical method was also used for quantification of m_{filter}. Analytical details are provided in section 3.2.1.10 and the sample handling is described in section 4.5.2. The particle size distribution is presented in table 4.7. Using this particle size distribution and eq. 5.6, the lung deposition fraction was calculated to be 10.3%, which is close to the deposition fraction used by the FDA for rat inhalation studies (10%) [84].

The *LDD* was estimated to be 12.8 and 9.75 nmol/kg in study 1 and 2, respectively. Since identical experimental procedures were applied and the drug concentrations in lung and plasma were indistinguishable between the two studies (figs. 4.8a and 4.8b), it was reasoned that the same *LDD* had been delivered. The average value of the two estimated *LDD* values was therefore used (11.3 nmol/kg), which was judged to be a reasonable estimate of *LDD* given the average amount of drug recovered in the lungs collected at the earliest time points (6.5 ± 1.8 nmol/kg for $45 \leq t \leq 75$ min).

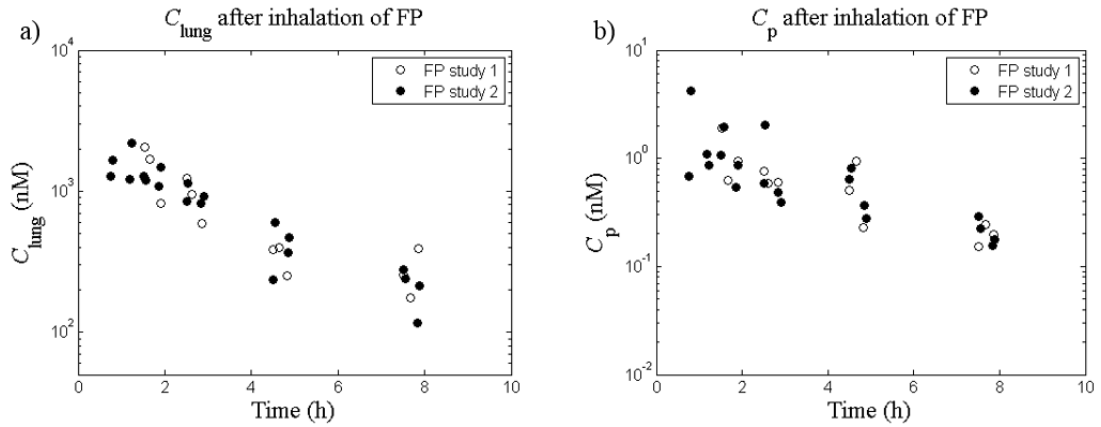

Figure 4.8 a) Total lung concentrations (C_{lung}) and b) plasma concentrations (C_p) after inhalation of fluticasone propionate (FP) in study 1 (white circles) and study 2 (black circles).

4.5.2 Analytical procedures

The analytical procedures used for quantifying FP and the GR-tracer in lung homogenates, spleen homogenates and plasma have been described in detail previously in section 3.2.1.10. The analytical procedures used for quantifying FP in plasma was described in section 4.3.3.1.

Sample preparation and analytical procedures connected to the filter analysis. To enable estimation of the *LDD*, the amount of drug collected by a filter (m_{filter}) during the inhalation period needed to be quantified. The filter was placed in a jar of appropriate size immediately after inhalation. On the day of analysis, ethanol (4 mL) was added to the filter and the jar was placed in an ultrasonic bath (5210 Branson; Gemini, Apeldoorn, The Netherlands) for 20 minutes. Dimethyl sulfoxide (4 mL) was then added to the sample to ensure that all of the substance was dissolved. A certain volume of the resulting solution (1 mL) was filtered through 0.2 µm Acrodisc® syringe filter (Pall Corporation, Ann Arbor, Mich.) to remove filter particles prior to further treatment. The filtered solution was diluted by a factor of 35 by transferring a predetermined volume (20 µL) to a vial containing 40% acetonitrile

and 0.2% formic acid in water (680 µL). The resulting solution was added in triplicate to a NUNC 96-deep well plate (Nalge Nunc International, Rochester, NY). The samples were then injected (20 μL) to a high-performance liquid chromatography system, a detailed description of the bioanalysis is provided in section 3.2.1.10.

Except for the filtering step, the same sample handling procedure was applied to the samples collected from the 7-stage Mercer cascade impactor. The impactor samples were diluted by a factor of 15 by transferring a predetermined volume (50 µL) to a vial containing 40% acetonitrile and 0.2% formic acid in water (700 µL). The amount of drug collected at each stage and the corresponding mass fraction were subsequently calculated. The result is presented in table 4.7 below:

Table 4.7 Characterisation of particle size distribution of fluticasone propionate. The table shows the amount of drug and the corresponding mass fraction collected at each stage by a 7-stage Mercer cascade impactor.

Stage	**Geometric midpoint (µm)**	**Amount (µg)**	**Mass fraction**
1	6.0	3.63	0.17
2	3.9	6.29	0.30
3	2.4	5.45	0.26
4	1.5	3.68	0.18
5	0.92	1.53	0.073
6	0.59	0.190	0.0091
7	0.39	0.0678	0.0032
8	0.20	0.0729	0.0035
Total		20.9	1

4.5.3 Results

As can be seen in fig. 4.9**,** the RO_{lung} was generally slightly higher than RO_{spleen} after nose-only exposure of FP. The highest receptor occupancy observation was not made at the first time point, but the measured occupancy peak occurred at t = 4 h. The receptor occupancy had returned to 0% at t = 48 h.

The drug concentration was quantified in plasma, lung homogenates and spleen homogenates from the inhalation studies. The drug concentration-time profiles are shown individually for each of the biological matrices in fig. 4.10a-c. All three profiles are shown in fig. 4.10d. All samples collected at t = 24 and 48 h were below the LLOQ. Furthermore, all spleen homogenates samples from t = 8 h were below the LLOQ.

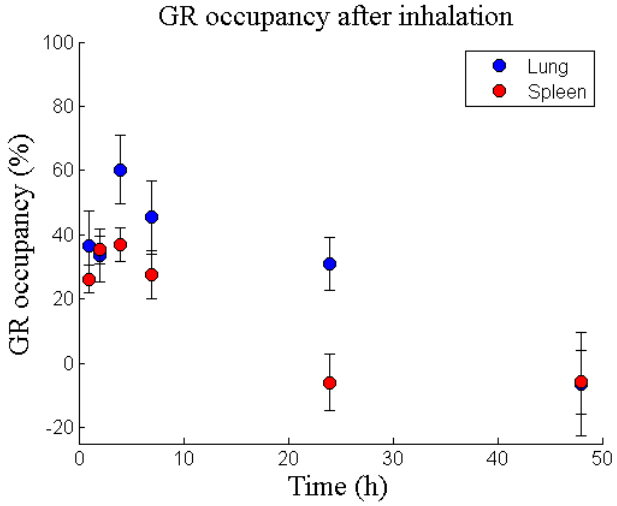

Figure 4.9 Glucocorticoid receptor (GR) occupancy in the lung (blue circles) and the spleen (red circles) after nose-only exposure of fluticasone propionate, n = 7 per time point, lung deposited dose = 11.3 nmol/kg.

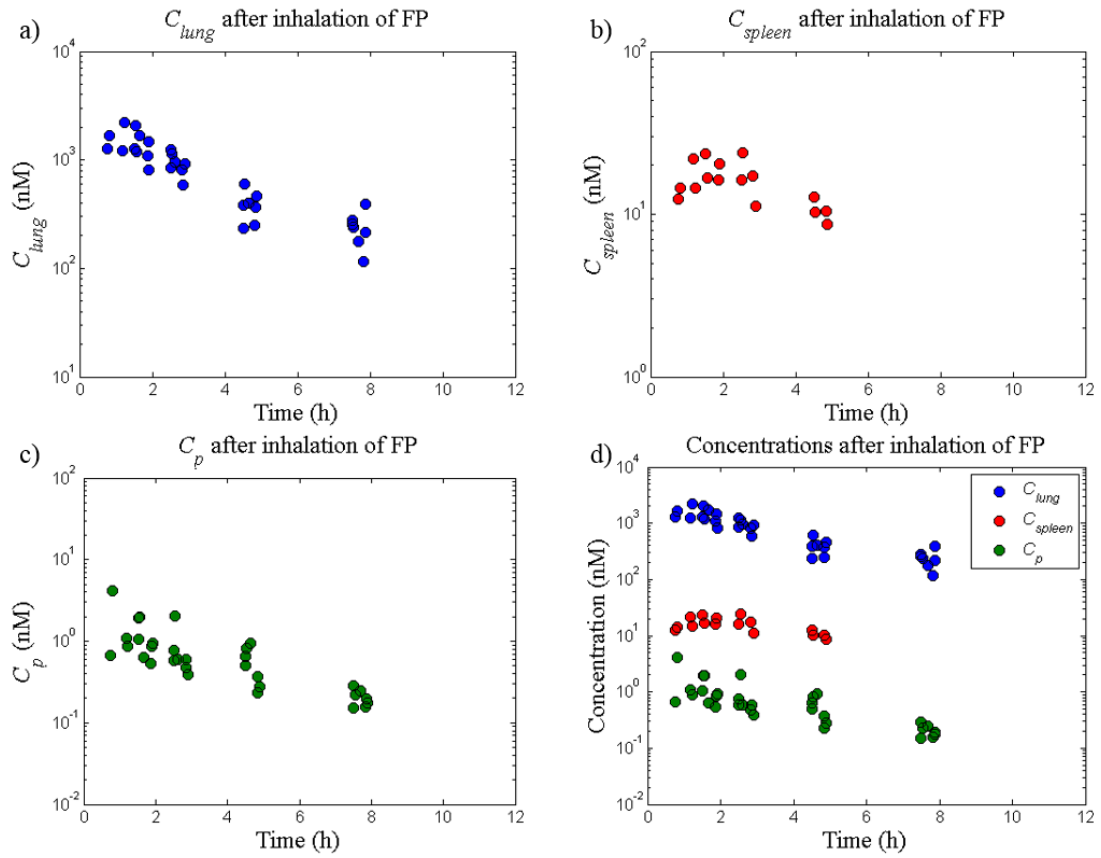

Figure 4.10 Drug concentration profiles after nose-only exposure after nose-only exposure of fluticasone propionate (FP). Drug concentrations were quantified in lung homogenates (C_{lung}, blue circles), spleen homogenates (C_{spleen}, red circles) and blood plasma (C_p, green circles). The lung deposited dose was 11.3 nmol/kg. Destructive sampling was applied, i.e. the animals were sacrificed in conjunction with the sampling.

4.6 Discussion

The studies aimed at characterising the receptor occupancy following IV-dosing of FP and budesonide were found to give results similar to those previously reported after IV-administration of another corticosteroid (triamcinolone acetonide) [120]: a high initial receptor occupancy, which then returned to baseline within 4-7 hours after dosing (4, 4 and 7 h for triamcinolone acetonide, budesonide and FP, respectively). As with triamcinolone acetonide, these results would not have been expected based on the binding kinetics parameters previously reported from *in vitro*

experiments with dissociation half-lives of 21 h [143], 10 h [80] and 4.6 h [146] for triamcinolone acetonide, FP and budesonide, respectively. These results, combined with earlier research [120], thus suggest a disconnection between the *in vitro* system used for studying binding kinetics and the *in vivo* situation. However, the cited *in vitro* experiments were conducted at temperatures that were low relative to the rodent's body temperature, which could explain the deviation between the *in vitro* and the *in vivo* situation.

As pointed out in section 4.4.1, the estimated receptor occupancy 24 hours after IV-dosing of FP was higher than after 7 hours, which is most likely not reflective of the drug-receptor interaction. Rather, the observation may reflect the dynamics of the GR with a drug-induced down-regulation of the receptor population, which has been demonstrated to take place after GR agonist exposure both *in vitro* and *in vivo* [137]. Furthermore, observations from earlier time points revealed that the receptor occupancy had returned to baseline within 7 hours after the IV-injection. The observations made at 24 and 48 h after dosing were therefore not included in the data set for parameter estimation. Similarly, since receptor occupancy had returned to baseline within 4 hours after dosing of budesonide, observations made at $t > 4$ h were not judged to provide any information on the binding kinetics and were thus not used for parameter estimation purposes.

Based on the receptor occupancy profiles obtained from the IV-studies, it can be concluded that the chosen doses were sufficiently high to significantly perturb the system and thus enable receptor occupancy measurements over several hours. Hence, mathematical modelling could subsequently be applied to estimate the *in vivo* binding kinetics parameters (K_{on} and K_{off}), where an exhaustive search confirmed that

the minimum had been found by the optimisation algorithm (within the expected parameter space as defined in section 4.4.1).

The PK-data from the nose-only exposure studies (fig. 4.10) followed a pattern expected from a poorly soluble inhaled drug: a large amount of drug remained in the lung over several hours after inhalation whereas only low drug levels could be detected in plasma. Furthermore, the plasma profile was flat as compared to the corresponding profile resulting from IV-dosing, which indicates a slow absorption of drug to the systemic circulation. This PK-behaviour can thus potentially be explained by a dissolution rate-limited absorption.

The measured receptor occupancy peak occurred at t = 4 h, which possibly, at least partly, could be explained by a slow dissolution process. The receptor occupancy was generally slightly higher in the lung than in the reference organ for systemic exposure (the spleen) after nose-only exposure (fig. 4.9). It is worth noting that the low degree of lung-selectivity reflected by receptor occupancy measurements was consistent with data from a preclinical PD-model, in which the local and systemic effects are studied after nose-only exposure of GR modulators. In short, as described by Källström *et al.* [147] this PD-model relies on inducing pulmonary inflammation by Sephadex, which will be reflected by an increased lung weight. The local effect of the test compound is subsequently determined by lung weight changes, whereas the systemic effect is determined by quantifying thymic involution. Interestingly, FP was found to have a therapeutic ratio of approximately 1 in this PD-model [148].

In chapter 5, the estimates of K_{on} and K_{off} will be incorporated into a mechanistic *in silico* model developed for predicting the systemic PK, the local tissue concentrations as well as the resulting receptor occupancy after inhalation. In contrast to traditional PK/PD-models, this model will not rely on a top-down

approach where an appropriate model structure (empirical or mechanistic) is chosen and the included parameters are optimised to minimise an objective function (*e.g.* the deviation between predicted and observed data as described by the sum of squares). Instead, the model structure will be based on the current understanding of pulmonary drug disposition as well as on the rodent physiology and the input parameters will be obtained from experimental data and literature sources. By subsequently comparing model predictions from this systems model to observed data, the current understanding of the system can be evaluated. For the first time, receptor occupancy observations from an inhalation study will be used for validating predictions of the local, and not only the systemic, exposure following topical administration. Any discrepancy can be informative with respect to the existing knowledge of underlying mechanisms and assumptions. If proven to be predictive, the model can be used to *e.g.* generate hypotheses, explore scenarios that currently cannot be tested experimentally and to provide a framework for a facilitated translation from animal to human.

4.7 Summary

This chapter presented a sequence of research activities undertaken for characterising the *in vivo* binding kinetics of the two GR agonists FP and budesonide. The two drugs were given at sufficiently high IV-doses to perturb the system such that receptor occupancy could be monitored over several hours (fig. 4.5a-b). For the first time, the binding kinetics parameters for these two substances could be estimated based on *in vivo* data. Parameter estimation was performed in Phoenix™. An exhaustive search algorithm implemented in MATLAB subsequently confirmed that the minimum objective function had been found by the optimisation algorithm

(within the expected parameter space). The receptor occupancy and the PK were studied after nose-only exposure of FP (11.3 nmol/kg, *LDD*). The PK-data showed high levels of unabsorbed drug in the lung following inhalation with low resulting plasma levels. The receptor occupancy was generally slightly higher in the lung than in the reference organ for systemic exposure (the spleen) and the data suggested a late occupancy peak at approximately 4 h after dosing.

The estimates of the binding kinetics parameters K_{on} and K_{off} will be used as drug-specific input parameters for a mechanistic *in silico* model in chapter 5 that was developed as part of this thesis. The receptor occupancy measurements as well as the PK from the nose-only exposure studies will be used for model validation purposes.

Chapter 5 A mechanistic inhalation PBPK model for prediction of local and systemic PK and receptor occupancy

5.1 Introduction

Even though inhalation is an attractive route of administration that has been employed for more than 2000 years [1], inhalation pharmacokinetics is still recognised as a challenging research area. As discussed in depth in chapters 3 and 4, the challenges are partly related to the difficulties of getting relevant exposure measurements. Furthermore, pulmonary drug disposition of inhaled drugs is known to be a complex interplay between numerous processes including *e.g.* regional drug deposition, particle dissolution and mucociliary clearance (MCC). Additional complexity comes from the heterogeneous nature of the organ with distinct differences between the tracheobronchial and the alveolar regions [11]. Lung targeting by inhalation in terms of the free target site concentration and the resulting local receptor occupancy is therefore notoriously difficult to predict.

While some of the aforementioned processes have been thoroughly characterised on an individual basis, a step-change in the understanding of inhalation pharmacokinetics could be gained if we also understood the *interplay* between these different processes in a physiological context. Significant progress towards achieving this goal can be made by developing a physiologically-based pharmacokinetic (PBPK) model, which places emphasis on lung disposition for inhaled drugs by mathematically describing these fundamental processes. However, such a mechanistic model predictive of local tissue concentrations combined with measurements such as receptor occupancy for validation is currently lacking. The recently generated data on local and systemic receptor occupancy after inhalation of

fluticasone propionate (FP) in combination with the estimates of its binding kinetics parameters (K_{on} and K_{off}) thus provide an opportunity to validate such predictions. Furthermore, data on drug concentrations in different biological matrices will also be available for model validation.

Expressed differently, a new mathematical framework can be built by formulating mathematical descriptions of the system based on the current understanding of pulmonary drug disposition and rodent physiology. Once the model structure is in place, it can be evaluated by using drug- and formulation-specific parameters, obtained from experimental data or literature sources, as input parameters. In this context, it is worth mentioning that the approach used to evaluate this model type, i.e. a systems model, is different from the approach used to evaluate standard PK/PD-models. Since systems models are built based on the current understanding of a system, any discrepancy between model predictions and observations can be informative with respect to the existing knowledge of underlying mechanisms and assumptions [149]. That is, a discrepancy may for example be due to a mechanism that is unaccounted for by the model structure or not fully understood.

If the model is proven to be predictive, it can be used to generate hypotheses and explore scenarios that have not been tested experimentally. Another useful feature of PBPK models is that they can separate physiological system- from drug-/formulation-specific properties, which carries several advantages including the possibility to explore how different drug- and formulation-specific properties, or combinations thereof, relate to important endpoints such as the lung-selectivity of a drug treatment. Such information could for instance be used to guide: 1) the design of chemical series in the early phases of drug discovery, and 2) the choice of drug formulations for clinical trials.

This chapter will describe the development of a mechanistic rat PBPK model including lung disposition, in which knowledge of the system (physiology) is integrated with drug- and formulation-specific properties. The developed model is subsequently used to theoretically explore different aspects of pulmonary drug disposition after single as well as repeated inhaled dosing.

5.2 Development of a PBPK model including lung disposition

5.2.1 Model structure

5.2.1.1 Structural model

A mechanistic PBPK model including lung disposition was developed and implemented in MATLAB R2013a (Mathworks Inc., Natick, MA, USA). Within PBPK modelling, tissues with similar properties are commonly lumped together to reduce the complexity of the model [109]. Focus is instead put on organs that are judged as important for the processes which are being studied in the particular model. Thus, for inhalation purposes the lung, the nose and the gut were included. The first two organs were included as inhaled drug particles will deposit both in the lung and the nose after nose-only exposure [65,66]. The gut was included to account for oral absorption of drug that has been transported to the pharynx by the mucociliary clearance and subsequently swallowed to reach the gut [8]. The rationale for including the spleen was to enable model validation with regard to both measurements of receptor occupancy and tissue concentrations. As perfusion rate is an important feature for drug distribution, the remaining tissues were lumped together into either richly or poorly perfused tissues. The adipose tissue was described separately from the other poorly perfused tissues since it may have a much higher partition coefficient for lipophilic compounds. Accordingly, the included

organs were as follows: nose, lung, gut, spleen, liver, richly perfused tissues, poorly perfused tissues and adipose tissue. The structural model is illustrated in figure 5.1a. Blood flows and volumes of the included tissue compartments are presented in table 5.5 in section 5.2.2.3.

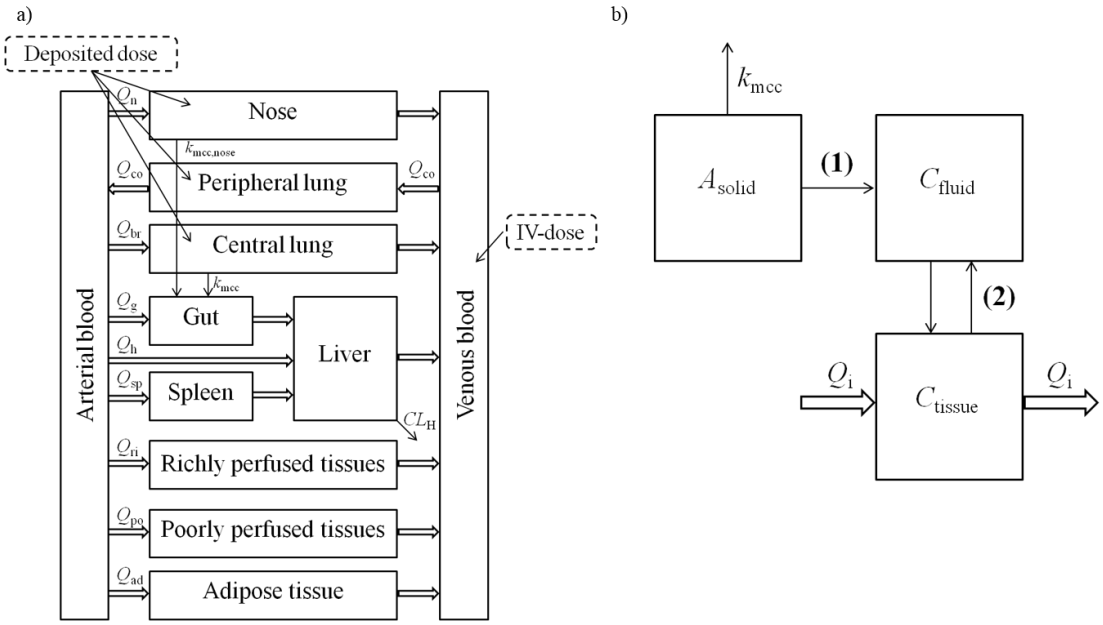

Figure 5.1 Schematic representation of the developed PBPK model. a) Structural model of the whole-body PBPK model, and b) compartmental representation of the central lung, peripheral lung and the nose: solid drug (A_{solid}), dissolved drug in the epithelial- or nasal lining fluid (C_{fluid}), and drug in tissue (C_{tissue}). In the nose and the central lung, solid particles are transported away by mucociliary clearance (k_{mcc}). Drug particles are dissolved in the lining fluid (1), once dissolved drug may permeate through the epithelial membrane to the tissue (2).

Due to anatomical and physiological differences the lung was divided into a tracheobronchial and alveolar region. One of the main differences between these two regions is the blood flow. The alveolar region, in which the gas-exchange takes place, is perfused by the entire cardiac output via the pulmonary circulation. The lung parenchyma, on the other hand, is perfused by arterial blood via the bronchial circulation which constitutes approximately 1-2% of the cardiac output [150]. The

thickness of the epithelial lining fluid (ELF) is also known to gradually decrease along the lung generations [151], as is the thickness of the epithelium [11]. The latter property is expected to give rise to permeability differences across the lung. Interestingly, studies by Gerde *et al*. showed that the highly lipophilic substance BaP was rapidly absorbed through the thin alveolar epithelium [152], whereas the absorption through the tracheobronchial epithelium was several-fold slower [153]. Hence, these studies point towards the importance of treating the lung as a heterogeneous organ.

Each of the two lung regions was in turn divided into three separate compartments (fig. 5.1b). The same compartmental representation was used for the nose: 1) undissolved drug (A_{solid}), 2) dissolved drug in the epithelial or nasal lining fluid (C_{fluid}), and 3) drug in tissue (C_{tissue}). The tracheobronchial region is perfused by the bronchial blood flow (Q_{bronch}), the alveolar region by the entire cardiac output (Q_{CO}) and the nose by the nasal blood flow (Q_{nose}). The compartmental representation of the nose and the two lung regions is shown in figure 5.1b. The system-specific input parameters for the nose and lung are summarised in table 5.6 in section 5.2.2.3. Once the drug has dissolved (see section 5.2.1.3) it may permeate through the epithelial membrane to the tissue according to:

$$\frac{dQ}{dt} = PA_{surf}(C_{fluid}(t)\, f_{u,fluid} - \frac{C_i(t)}{K_{p,u,i}}), \qquad (5.1)$$

where dQ/dt is the molar flow of drug (nmol/h), P is the permeability, A_{surf} is the surface area, $f_{u,fluid}$ is the unbound fraction in the lining fluid, C_i is the tissue concentration of drug and $K_{p,u,i}$ is the tissue-to-unbound plasma partition coefficient. A detailed description of the prediction of $K_{p,u}$-values as well as the subsequent

calculations of K_p-values is provided in section 5.2.2.1. The *in vitro* apparent permeability across CaCo2-monolayers was measured and used as the parameter *P* (tables 5.3 and 5.4 in section 5.2.2.1).

Perfusion rate-limited distribution was assumed to apply for all tissues. For compartment *i*, the rate of change of quantity of drug within the organ was described as [103]

$$V_i \frac{dC_i(t)}{dt} = Q_i\left(C_A(t) - \frac{RC_i(t)}{K_{p,i}}\right), \quad C_i(0) = 0\,, \tag{5.2}$$

where V_i is the tissue volume, C_i is the drug tissue concentration, Q_i is the blood flow to the tissue, C_A is the arterial drug concentration, R is the blood/plasma ratio and $K_{p,i}$ is the tissue-to-plasma partition coefficient.

5.2.1.2 Particle size distribution, regional deposition and mucociliary clearance

Inhaled drug particles can be deposited in the extrathoracic, tracheobronchial and alveolar region. This model neglects deposition in the pharynx and the larynx, hence only nasal deposition is considered in the extrathoracic region. Henceforth, the tracheobronchial and alveolar regions are referred to as the central and the peripheral lung, respectively.

Several models have been developed for prediction of regional particle deposition in rat lungs [65,66,69,154]. By extracting the regional deposition fraction for the relevant aerodynamic diameters from [65], the number of deposited particles can be calculated based on the deposition fraction and the mass fraction of the relevant particle size class via:

$$N_{j,i}(0) = \frac{f_i f_{j,i} ID}{A_{j,i}(0)}, \qquad (5.3)$$

where $N_{j,i}$ is the number of particles of size i in region j, f_i is the mass fraction of particles of size i, $f_{j,i}$ is the deposition fraction of particle size i in region j, ID is the total inhaled dose and $A_{j,i}(0)$ is the amount of drug in a particle of size i in region j at $t = 0$ (nmol/particle). The aerodynamic diameters are obtained from the impactor measurements. Assuming spherical particles, the geometric diameter (d_g) can calculated from the aerodynamic diameter (d_a):

$$d_g = d_a \sqrt{\frac{\chi}{\rho}}, \qquad (5.4)$$

where ρ is the density of the particle and χ is the dynamic shape factor of the particle ($\chi = 1$ for spheres). The initial geometric radii ($r_1, \ldots, r_8$), i.e. prior to particle dissolution, are presented in tables 5.3 and 5.4 in section 5.2.2.1. $A_{j,i}(t)$ can subsequently be obtained from the geometric radius of particle i in region j ($r_{j,i}$) and ρ (nmol/dm^3):

$$A_{j,i}(t) = V_{j,i}(t)\rho = \frac{4\pi r_{j,i}(t)^3}{3}\rho. \qquad (5.5)$$

Given that the mass fractions of different aerodynamic diameters ($f_1, \ldots, f_8$) had been measured using an impactor, the fraction of central ($f_{c,1}, \ldots, f_{c,8}$) and peripheral deposition ($f_{p,1}, \ldots, f_{p,8}$) had been extracted from [65] and the lung deposited dose

(*LDD*) was obtained from filter analysis (see section 4.5.1), it follows that *ID* can be calculated accordingly:

$$DF = \sum_{i=1}^{8} (f_i f_{p,i} + f_i f_{c,i}) \tag{5.6}$$

and

$$LDD = ID \times DF = ID \sum_{i=1}^{8} (f_i f_{p,i} + f_i f_{c,i}) \tag{5.7}$$

so

$$ID = \frac{LDD}{\sum_{i=1}^{8} (f_i f_{p,i} + f_i f_{c,i})} \quad , \tag{5.8}$$

where *DF* is the total lung deposition fraction.

The nasal deposition fractions ($f_{n,1}$, …, $f_{n,8}$) had also been extracted from [65]. $N_{j,i}(0)$ could thus be calculated for particle size *i* in each of the three considered regions (eq. 5.3). Due to MCC, $N_{j,i}$ was described to decline exponentially:

$$N_{j,i}(t) = N_{j,i}(0) \times e^{-kmcc,j \times t}, \tag{5.9}$$

where $N_{j,i}(0)$ is the number of particles of size *i* in region *j* at $t = 0$ (eq. 5.3) and $k_{mcc,j}$ is MCC in region *j*. MCC in the central lung ($k_{mcc,lung}$) was estimated from [155] as described in section 5.2.2.3 and MCC in the nose ($k_{mcc,nasal}$) was extracted from [156]. MCC in the peripheral lung was assumed to be negligible, since it has been primarily associated with the tracheobronchial region [74]. Clearance by macrophage uptake was not accounted for in this model since it has been reported to be a slow

process [41]. However, in case of repeated dosing of compounds with very slow dissolution rates, it might be worthwhile considering extending the model by also incorporating this process. Consequently, $N_{j,i}$ in the peripheral region is constant. The total amount of solid drug in region j ($A_{solid,j}$) for all particle size classes ($i \in \{1, ..., 8\}$) is thus as follows:

$$A_{solid,j}(t) = \sum_{i=1}^{8} N_{j,i}(t) A_{j,i}(t). \tag{5.10}$$

Since the following relationship applies

$$\frac{A_{j,i}(t)}{A_{j,i}(0)} = \frac{V_{j,i}(t)\rho}{V_{j,i}(0)\rho} = \frac{\frac{4\pi r_{j,i}(t)^3}{3}\rho}{\frac{4\pi r_{j,i}(0)^3}{3}\rho} = \left(\frac{r_{j,i}(t)}{r_{j,i}(0)}\right)^3, \tag{5.11}$$

$A_{j,i}(t)$ can be obtained from

$$A_{j,i}(t) = A_{j,i}(0)\left(\frac{r_{j,i}(t)}{r_{j,i}(0)}\right)^3. \tag{5.12}$$

Inserting eq. 5.12 in eq. 5.10 gives

$$A_{solid,j}(t) = \sum_{i=1}^{8} N_{j,i}(t) A_{j,i}(0)\left(\frac{r_{j,i}(t)}{r_{j,i}(0)}\right)^3. \tag{5.13}$$

Drug removed by MCC is transported to the gut, where the bioavailable fraction subsequently can be absorbed into the systemic circulation. The ODE governing the mass transport by MCC of solid drug particles from the nose and the central lung to the gut is given by

$$\frac{dA_{gut}}{dt} = k_{mcc,lung} \times A_{solid,c}(t) + k_{mcc,nasal} \times A_{solid,n}(t) \tag{5.14}$$

where the subscripts *c* and *n* assign central lung and nose, respectively. Since the oral bioavailability (*F*) determines the degree of absorption from the gastrointestinal (GI) tract, only the bioavailable fraction of solid drug particles will be transported to the gut absorption compartment (A_{gut}). The ODE governing mass transfer of A_{gut} is thus obtained by also accounting for *F* and the absorption to the systemic circulation. By inserting eqs. 5.9 and 5.13, it follows that

$$\frac{dA_{gut}}{dt} = k_{mcc,lung}\sum_{i=1}^{8}\left(FN_{c,i}(0)A_{c,i}(0)e^{-kmcc,lung\times t}\left(\frac{r_{c,i}(t)}{r_{c,i}(0)}\right)^3\right) + k_{mcc,nasal}\sum_{i=1}^{8}\left(FN_{n,i}(0)A_{n,i}(0)e^{-kmcc,nasal\times t}\left(\frac{r_{n,i}(t)}{r_{n,i}(0)}\right)^3\right) - k_a A_{gut} \quad (5.15)$$

where k_a is the absorption rate constant and *F* is defined as

$$F = f_{gut}\times f_{abs}\times f_h. \quad (5.16)$$

That is, *F* accounts for the fraction absorbed from the GI-tract (f_{abs}), the fraction that escapes gut (f_{gut}) and hepatic extraction (f_h) [36]. For both investigated substances, fluticasone propionate (FP) and budesonide, f_{abs} and f_{gut} were set to be 1. For budesonide, f_h was calculated as

$$f_h = 1 - E_H = 1 - \frac{CL_B}{Q_{h,tot}}, \quad (5.17)$$

where E_H is the hepatic extraction ratio, CL_B is the blood clearance and $Q_{h,tot}$ is the total hepatic blood flow,

$$Q_{h,tot} = Q_h + Q_{sp} + Q_g \ , \qquad (5.18)$$

where Q_h is the hepatic blood flow, Q_{sp} is the spleen blood flow and Q_g is the gut blood flow. Due to the high CL_B of FP, f_h for FP was set to 0. Clearly, since FP is a poorly soluble compound, it can be argued that its f_{abs} most likely is less than 1. However, as the high CL_B leads to a negligible F (caused by $f_h = 0$), the value of f_{abs} will not affect the outcome of the simulations and it was therefore arbitrarily set to 1.

Similarly, as F was set to 0 for FP, no absorption will take place from the GI-tract and the value of k_a is thus irrelevant. Orally administered budesonide has been reported to be rapidly absorbed in rats [157], its k_a was therefore set to be high (5 h^{-1}) to reflect the rapid absorption process.

5.2.1.3 Dissolution of drug

Drug particles are dissolved in the ELF or in the nasal lining fluid, which is modelled by the Nernst-Brunner equation [158,159]:

$$\frac{dQ_{diss}}{dt} = \frac{4\pi r(t)^2 D(C_s - C_{fluid}(t) f_{u,fluid})}{h}, \qquad (5.19)$$

where h is the thickness of the boundary layer of solvent at the surface of the dissolving particle. Empirical evidence suggests that h is of the order of r for particles with $r < 30$ µm, h has therefore previously been set equal to r when $r < 30$ µm [160]. Eq. 5.19 can thus be simplified as

$$\frac{dQ_{diss}}{dt} = 4\pi r(t) D\left(C_s - C_{fluid}(t)\, f_{u,\,fluid}\right), \qquad (5.20)$$

where dQ_{diss}/dt is the rate of dissolution (nmol/h), D is the diffusion coefficient, C_s is the solubility of the drug, C_{fluid} is the concentration of drug in the ELF or the nasal lining fluid and $f_{u,fluid}$ is the unbound fraction in the ELF or the nasal lining fluid.

According to [4], the ELF is slightly acidic (pH 6.6) and mainly consists of water (96%), salts, phospholipids, protein and mucins. Although there is a dispute about the presence of albumin in ELF, it cannot be excluded that the investigated compounds are bound to other proteins in the ELF. However, experimental methodologies need to be developed in order to experimentally determine $f_{u,fluid}$. As it is currently not possible to do this, $f_{u,fluid}$ was assumed to be 1. The same assumption was made in a recently published paper by Gaohua *et al*. [161], which presented a model intended for simulating drug concentrations in the ELF following systemic administration of antituberculosis drugs.

There are eight different particle sizes in the model, hence the ODE describing the change of concentration in C_{fluid} in region j will be as follows:

$$V_{fluid,\,j}\frac{dC_{fluid,\,j}}{dt} = \sum_{i=1}^{8}\left(N_{j,i}(t) 4\pi r_{j,i}(t) D(C_s - C_{fluid,\,j}(t)\, f_{u,\,fluid})\right) - PA_{surf,j}\left(C_{fluid,\,j}(t)\, f_{u,\,fluid} - \frac{C_j(t)}{K_{p,u,\,j}}\right), \qquad (5.21)$$

where the latter term describes the flux of drug to/from the systemic circulation (eq. 5.1). The function $r(t)$ will change over time accordingly:

$$\frac{dr}{dt} = -\frac{D}{\rho r(t)}\left(C_s - C_{fluid}(t)\, f_{u,\,fluid}\right), \qquad (5.22)$$

where ρ is the density of the particle. Calculation of D is described in section 5.2.2.1. The derivation of eq. 5.22 is included in the following section (5.2.1.4).

Note that the inverse radius term in eq. 5.22 will cause numerical problems for small r, as a sufficiently small step size cannot be achieved. To ensure numerical stability, the inverse radius is assumed to decay exponentially with regard to r for $r \leq r_a$, (r_a = 0.075 µm). The rate of the exponential decay is chosen such that the function remains continuous at r_a.

However, simply switching between these two functions at $r = r_a$ can lead to numerical instability, since the derivative of this new function is discontinuous at r_a. This can be solved by adding yet another switching point r_b, such that the new numerically stable version of the inverse radius switches between three functions:

$$f(r) = \begin{cases} -k_0 r & r \leq r_a \\ g(r) & r_a < r \leq r_b \\ -1/r & r > r_b \end{cases}, \qquad (5.23)$$

where $g(r)$ is a function which should ensure that $f(r)$ and its first order derivative remains continuous.

In this thesis, a circular segment is used for $g(r)$, in order to create a smooth transition. The radius and position of the circular segment are defined such that the continuity conditions just posed hold. In other words $g(r)$ is defined as

$$g(r) = y_0 - \sqrt{s_0^2 - (r - x_0)^2}\,, \qquad (5.24)$$

where y_0 and x_0 define the centre co-ordinates and s_0 the radius of the circle segment. Note that the exponential decay factor k_0 is chosen together with these to ensure

continuity. Setting r_b = 0.15 µm provided a sufficiently smooth transition. Therefore eq. 5.22 is replaced by the following equation, with $f(r)$ defined by eq. 5.23 and $g(r)$ by eq. 5.24:

$$\frac{dr}{dt} = \frac{D}{\rho} f(r)(C_s - C_{fluid}(t) f_{u,fluid}) \tag{5.25}$$

5.2.1.4 Derivation of the change of radius equation

The radius, r, changes over time as described in eq. 5.22. A step-wise description of the derivation of dr/dt is provided in this section.

The dissolution process can be described by the Nernst-Brunner equation [158,159]

$$\frac{dQ_{diss}}{dt} = \frac{4\pi r(t)^2 D(\mathrm{C_s} - C_{fluid}(t) f_{u,fluid})}{h}, \tag{5.26}$$

where h is the thickness of the diffusion layer. Empirical evidence suggests that h is of the order of r for particles with r < 30 µm. Setting $h = r$, eq. 5.26 becomes

$$\frac{dQ_{diss}}{dt} = 4\pi r(t) D(C_s - C_{fluid}(t) f_{u,fluid}). \tag{5.27}$$

Since the radius r changes during dissolution, the mass balance expression for a dissolving particle can be written as follows [162]:

$$\frac{dQ_{diss}}{dt} = -4\pi r(t)^2 \rho \frac{dr}{dt}. \tag{5.28}$$

Eqs. 5.27 and 5.28 are independent of each other, thus equating eqs. 5.27 and 5.28 gives

$$4\pi r(t)D(C_s - C_{fluid}(t)\, f_{u,fluid}) = -4\pi r(t)^2 \rho \frac{dr}{dt}. \quad (5.29)$$

Solving for *dr*/*dt* yields

$$\frac{dr}{dt} = -\frac{D}{\rho r(t)}(C_s - C_{fluid}(t)\, f_{u,fluid}). \quad (5.30)$$

5.2.1.5 Receptor binding

Receptor binding was included in all tissue compartments and was described as

$$\frac{dRD_i(t)}{dt} = \left(K_{on}\left(B_{\max,i} - RD_i(t)\right)\frac{C_i(t)}{K_{p,u,i}} \right) - K_{off} RD_i(t), \quad (5.31)$$

where RD_i is the concentration of the drug-receptor complex in compartment *i*, K_{on} is the association rate constant, $B_{max,i}$ is the receptor density in compartment *i* and K_{off} is the dissociation rate constant.

Receptor occupancy in compartment *i* (RO_i) can be calculated via:

$$RO_i(t) = 100 \times \frac{RD_i(t)}{B_{\max,i}}. \quad (5.32)$$

B_{max} for the spleen was obtained from [138], B_{max} for the lung from section 3.2.2.2 and B_{max} in the other tissue compartments was set to the mean value of B_{max} in five brain regions [163].

Since the lung has been divided into a central and a peripheral compartment, receptor occupancy is predicted for each region individually. The whole-lung can also be considered by using a weighted average based on the occupancy for the two regions (RO_{ave}). The volume fractions of a rat lung consisting of central ($f_{v,c}$) and peripheral lung ($f_{v,p}$) were estimated to be 0.81 and 0.19, respectively (see section 5.2.2.3). RO_{ave} could therefore be calculated via:

$$RO_{ave} = f_{v,c} RO_c + f_{v,p} RO_p . \qquad (5.33)$$

Since the experimental methodology cannot discriminate between central and peripheral occupancy, RO_{ave} corresponds to the observations.

5.2.2 Parameterisation

The input parameters are divided into three categories: 1) drug-specific, 2) formulation-specific, and 3) system-specific input parameters. In this section, the parameterisation of each of these categories will be described.

5.2.2.1 Drug-specific input parameters

All drug- and formulation-specific input parameters for budesonide and FP are summarised in tables 5.3 and 5.4, respectively. The following sections contain information on how the drug-specific input parameters were obtained.

Prediction and measurements of tissue-to-unbound plasma partition coefficients. Tissue-to-unbound plasma partition coefficients ($K_{p,u}$) were predicted using a method described in [105], which has been found to have good predictive capabilities [106]. Since both FP and budesonide are neutral compounds, log$D_{7.4}$ is not expected to be different from log$P$. Log$D_{7.4}$ was therefore used as input together with the unbound plasma fraction (f_u) for prediction of $K_{p,u}$-values. Log$D_{7.4}$ was 4.2 and 2.9 for FP and budesonide, respectively [164]. f_u was 0.016 and 0.09222 for FP and budesonide, respectively [164]. In order to simplify the model structure, richly and poorly perfused organs were lumped together to form one compartment each. The mean value of the predicted $K_{p,u}$-values of the heart and the kidney was used as $K_{p,u,richly}$, whereas $K_{p,u,poorly}$ was defined as the mean value of the predicted K_p-values of the bones and the muscles. All predicted $K_{p,u}$-values are presented in table 5.1.

The unbound lung volume of distribution ($V_{u,lung}$), corresponding to $K_{p,u,lung}$, was measured for FP and budesonide by Dr. Erica Bäckström at AstraZeneca R&D according to the protocol described in [77]. $K_{p,i}$ was subsequently obtained from:

$$K_{p,i} = f_u K_{p,u,i}\,. \qquad (5.34)$$

Neither prediction methodologies nor measurements of $K_{p,u,nose}$ were available, this was therefore set to $K_{p,u,lung}$.

The resulting steady-state volume of distribution (V_{dss}) was calculated from the predicted and measured K_p-values (eq. 5.35) and compared to the observed V_{dss} ($V_{dss,obs}$, eq. 5.36) obtained from modelling of PK-data from *in vivo* studies using:

$$V_{dss} = V_p + \sum_{i=1}^{8} K_{p,i} V_{t,i} \qquad (5.35)$$

$$V_{dss,obs} = V_1 + V_2 + V_3 \qquad (5.36)$$

where V_p is the volume of the plasma and $V_{t,i}$ is the volume of tissue i. The calculated V_{dss} should equal $V_{dss,obs}$. Any discrepancy between the calculated V_{dss} and $V_{dss,obs}$ can be corrected by introducing a K_p-factor (f) given by [99]:

$$f = \frac{V_{dss,obs} - V_p}{\sum_{i=1}^{n} K_{p,i} V_{t,i}} \qquad . \qquad (5.37)$$

Since the K_p-value of the lung was known and the nose was assumed to have the same value, these two values were not corrected by f. The equation was thus written in the following form:

$$f = \frac{V_{dss,obs} - \left(V_p + K_{p,lung}(V_{lung} + V_{nose})\right)}{\sum_{i=1}^{6} K_{p,i} V_{t,i}} \qquad (5.38)$$

All predicted K_p-values were multiplied by f in order to obtain $V_{dss,obs}$. The final K_p-values are presented in table 5.2.

Table 5.1 Tissue-to-unbound plasma partition coefficients ($K_{p,u}$) for budesonide and fluticasone propionate

Tissues	$K_{p,u,Bude}$	$K_{p,u,FP}$
Adipose	206	4083
Bone	15.0	285
Brain	32.5	628
Gut	34.6	657
Heart	15.1	268
Kidney	17.1	309
Liver	18.3	331
Lung	21.9	403
Muscle	10.8	195
Pancreas	35.3	683
Skin	50.3	979
Spleen	10.4	168
Thymus	16.9	312
Poorly[1)]	12.9	240
Richly[2)]	16.1	289

[1)] $K_{p,u,poorly}$ is the mean value of the predicted $K_{p,u}$-values of bone and muscles.[2)] $K_{p,u,richly}$ is the mean value of the predicted $K_{p,u}$-values of the heart and kidney. Abbreviations: Bude=budesonide; FP=fluticasone propionate

Table 5.2 Calculated tissue-to-plasma partition coefficients (K_p) for budesonide and fluticasone propionate (multiplied by the K_p-factor, f, calculated from eq. 5.38)

Tissue	Volume (L/kg)	$K_{p,Bude}$	$K_{p,FP}$	Method
Liver	0.04	1.95	10.4	Rodgers *et al.*
Spleen	0.002	1.10	5.29	Rodgers *et al.*
Poorly[1)]	0.789	1.37	7.86	Rodgers *et al.*
Richly[2)]	0.0388	1.71	9.46	Rodgers *et al.*
Gut	0.0259	3.68	20.7	Rodgers *et al.*
Adipose	0.04	21.9	129	Rodgers *et al.*
Lung	0.00413	2.13	3.41	$V_{u,lung}$
Nose	0.000254	2.13	3.41	$V_{u,lung}$
Venous blood	0.02	*NA*	*NA*	
Arterial blood	0.04	*NA*	*NA*	
f		1.15	1.97	
$V_{dss,obs}$ (L/kg)		2.27	12.5	

[1)] $K_{p,poorly}$ is the mean value of the predicted K_p-values of bone and muscles. [2)] $K_{p,richly}$ is the mean value of the predicted K_p-values of the heart and kidney. Abbreviations: Bude=budesonide; FP=fluticasone propionate; f=K_p-factor; $V_{dss,obs}$=observed steady-state volume of distribution; $V_{u,lung}$=unbound lung volume of distribution

Estimation of the diffusion coefficient. The diffusion coefficient (D) was estimated using the Hayduk-Laudie equation [36]:

$$D = \frac{13.26\times10^{-5}}{\mu^{1.14}\times V_M{}^{0.589}} = \frac{13.26\times10^{-5}}{\mu^{1.14}\times\left(\frac{MW}{\rho}\right)^{0.589}}, \qquad (5.39)$$

where μ represents the viscosity of water (37°C), MW the molecular weight and ρ the density of the particle. The calculated D for budesonide and FP is presented in table 5.3 and 5.4, respectively.

Calculation of blood clearance. The blood/plasma drug concentration ratio (*R*) was determined to be 0.95 and 0.78 for FP and budesonide, respectively [164]. Experimental measurements of *R* were done by Pharmaron® (Pharmaron Beijing, Co. Ltd., Bejing, China). The blood clearance (CL_B) was calculated from the plasma clearance (CL_P) obtained from the PK study described in section 4.3 according to:

$$CL_B = \frac{CL_P}{R} \quad . \tag{5.40}$$

As CL_P was estimated from venous drug concentrations, elimination was set to occur from the venous compartment. Accordingly, CL_B acts on absorbed drug prior to entering the other organs.

Parameter estimation of the solubility. FP is a poorly soluble drug with a measured water solubility of <779.1 nM and a fasted-state small intestinal fluid (FaSSIF) solubility of 3120 nM [164]. FaSSIF is defined as a biorelevant medium. As opposed to buffer, these media better reflect the composition of physiological fluids by, for instance, containing lipids, surfactants and buffers, where the purpose of the latter is to maintain physiological pH [165]. In contrast, budesonide has a higher solubility with an aqueous solubility of 38.56 µM and a FaSSIF solubility of 103.6 µM [164]. Whilst the composition of the FaSSIF (pH 6.5, osmolality 270 ± 10 mOsmol/kg, 3 mM sodium taurochlorate, 0.75 mM lecithin, 28.7 mM KH_2PO_4 and 103.3 mM KCl [166]) is not expected to precisely reflect the composition of the ELF, it clearly serves to illustrate how a biologically relevant medium significantly can change the solubility of a compound.

Since the aqueous solubility of a poorly soluble compound tends to under-predict the *in vivo* dissolution rate [55], the solubility (C_s) of FP, but not budesonide, was estimated.

C_s was estimated as 4530 nM (95% CI [3845-5215] nM) using nonlinear least squares in the MATLAB Curve-Fitting Toolbox, which minimised the sum of squared deviations between observed and predicted total lung concentrations (11.3 nmol/kg, *LDD*). The Levenberg-Marquardt algorithm was used to find the minimum of the cost function. The root mean squared error (RMSE) of the fit was 272 nM. The estimated C_s was thus of the same magnitude as the measured FaSSIF solubility of FP.

The initial estimate was selected from an exhaustive search, in which the sum of squares was initially evaluated for 1000 candidates over a broad search space where C_s ranged from 10^2 to 10^5 nM (fig. 5.2a). The cost function turned out to be locally convex in the explored interval and a minimum was found at 4529.7 nM. The search space was then confined to the proximity of the best solution $C_{s,0}$ ($C_{s,0}$-200 $\leq C_s \leq$ $C_{s,0}$+200 nM), in which 300 candidates were evaluated (fig. 5.2b). The best solution of the confined search was 4530 nM, which was close to the measured FaSSIF C_s (3120 nM). Fig. 5.2c shows simulations of total lung concentrations using the optimised C_s (blue line) and the FaSSIF C_s (dashed line).

Sensitivity analysis of C_{lung} with respect to D and C_s indicated that these two parameters might be indistinguishable (fig. 5.2d), in which case only the product can be estimated. However, calculation of D (eq. 5.39) enables unique determination of C_s. A detailed description of the sensitivity analysis is provided in section 5.3.1.3.

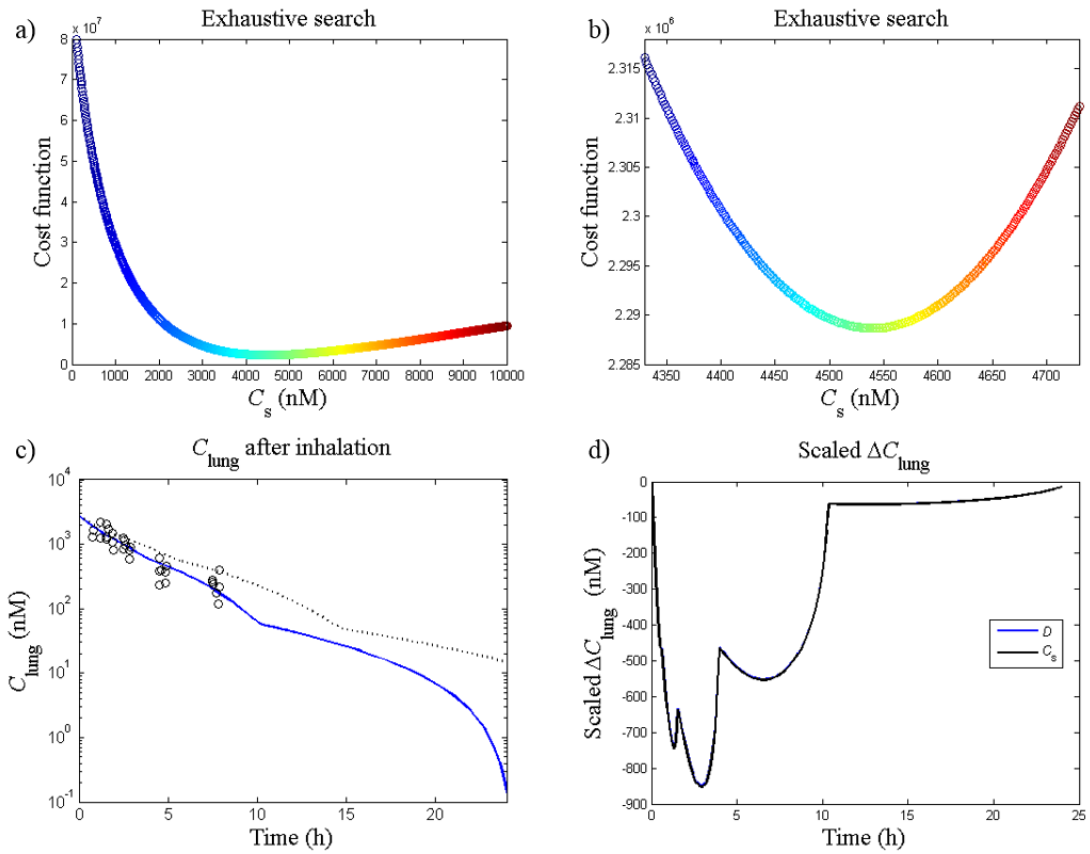

Figure 5.2 Parameter estimation of the solubility (C_s). An exhaustive search was performed to find an initial estimate of C_s. The cost function (sum of squares) was evaluated firstly using a) a broad search space ($10^2 \leq C_s \leq 10^5$ nM), which was followed by b) a confined search space in the proximity to the best solution, obtained from the first exhaustive search. c) Simulations of the total lung concentration of drug (C_{lung}) using the optimised C_s (blue line) and the measured FaSSIF C_s (dashed line). d) Sensitivity analysis: influence of a 0.1% increase in C_s (black line) and the diffusion coefficient (D, blue line) on the dynamic behaviour of C_{lung}.

5.2.2.2 Formulation-specific input parameters

Two different formulation-specific input parameters are used in the model: 1) particle density, and 2) particle size distribution.

Calculation of particle density. The particle density (ρ) was assumed to be the same as the bulk density of the densely compressed pellet used in the inhalation study, which was calculated via:

$$\rho = \frac{m}{V}, \tag{5.41}$$

where m is the mass of substance and V is the volume of the pellet.

Characterisation of particle size distribution. Prior to preclinical inhalation studies, the aerodynamic particle size distribution is typically characterised using a 7-stage Mercer cascade impactor (model 02 110, In-tox Products, USA), providing a discrete particle size distribution with eight different size classes. The analytical procedures applied for the characterisation are described in section 4.5.2.

Table 5.3 Drug- and formulation-specific input parameters for budesonide

Parameter	**Value**
Blood/plasma ratio	0.78
CL_B (L/h/kg)	3.80
CL_P (L/h/kg)	2.96
C_s (nM)*	103.6
D (m^2/s)	2.28×10^{-11}
f_1,...,f_8**	0.047, 0.017, 0.060, 0.19, 0.31, 0.074, 0.15, 0.16
F***	0.22
f_u	0.0922
$f_{u,fluid}$	1
k_a (h^{-1})	5
K_d (nM)	1.16 ± 0.343
K_{off} (h^{-1})	1.30 ± 0.351
K_{on} (L/nmol/h)	1.12 ± 0.621
log$D_{7.4}$	2.9
Molecular weight (g/mol)	430.54
P_{app} (cm/s)	65.9×10^{-6}
ρ (nmol/dm^3)	1.428×10^{9}
V_{dss} (L/kg)	2.27
$V_{u,lung}$ (mL/g lung tissue)	23.1

*FaSSIF solubility. ** $\sum_{i=1}^{8} f_i = 1$ when all decimal places are used. *** $F=f_{abs}\times f_{gut}\times f_h$. Abbreviations: CL_B=blood clearance; CL_P=plasma clearance; C_s=solubility; D=diffusion coefficient; f_1,...,f_8=mass fractions for particle sizes 1,...,8, respectively; F=oral bioavailability; f_{abs}=fraction absorbed; f_{gut}=fraction escaping gut metabolism; f_h=fraction escaping hepatic metabolism; f_u=fraction unbound in plasma; $f_{u,fluid}$=fraction unbound in epithelial or nasal lining fluid; K_d=dissociation constant; K_{off}=dissociation rate constant; K_{on}=association rate constant; P_{app}=apparent permeability; ρ=particle density; V_{dss}=steady-state volume of distribution; $V_{u,lung}$=unbound lung volume of distribution

Table 5.4 Drug- and formulation-specific input parameters for fluticasone propionate

Parameter	**Value**
Blood/plasma ratio	0.95
CL_B (L/h/kg)	11.53
CL_P (L/h/kg)	10.95
C_s (nM)	4530
D (m^2/s)	2.27×10^{-11}
$f_1,...,f_8$*	0.17, 0.30, 0.26, 0.18, 0.073, 0.0091, 0.0032, 0.0035*
F**	0
f_u	0.016
$f_{u,fluid}$	1
K_d (nM)	0.015 ± 0.0045
K_{off} (h^{-1})	0.51 ± 0.17
K_{on} (L/nmol/h)	34 ± 20
log$D_{7.4}$	4.2
Molecular weight (g/mol)	500.6
P_{app} (cm/s)	46.9×10^{-6}
ρ ($nmol/dm^3$)	1.430×10^{9}
V_{dss} (L/kg)	12.5
$V_{u,lung}$ (mL/g lung tissue)	213.4

* $\sum_{i=1}^{8} f_i = 1$ when all decimal places are used. ** $F=f_{abs}\times f_{gut}\times f_h$. Abbreviations: CL_B=blood clearance; CL_P=plasma clearance; C_s=solubility; D=diffusion coefficient; $f_1,...,f_8$=mass fractions for particle sizes 1,...,8, respectively; F=oral bioavailability; f_{abs}=fraction absorbed; f_{gut}=fraction escaping gut metabolism; f_h=fraction escaping hepatic metabolism; f_u=fraction unbound in plasma; $f_{u,fluid}$=fraction unbound in epithelial or nasal lining fluid; K_d=dissociation constant; K_{off}=dissociation rate constant; K_{on}=association rate constant; P_{app}=apparent permeability; ρ=particle density; V_{dss}=steady-state volume of distribution; $V_{u,lung}$=unbound lung volume of distribution

5.2.2.3 System-specific input parameters

The model includes several system-specific input parameters describing the anatomy and physiological processes for the rat. Where possible, anatomical values were obtained from the literature. In the absence of literature values, calculations of parameter missing values were made based on available anatomical data. All system-specific input parameters are summarised in tables 5.5 and 5.6, where the latter specifies parameters for the central lung, peripheral lung and the nose.

Calculation of V_{ELF} and V_{nasal}. The volume of the epithelial lining fluid in the central ($V_{ELF,C}$) and the peripheral lung ($V_{ELF,P}$) as well as the corresponding volume in the nose (V_{nasal}) was calculated accordingly:

$$V_{fluid,i} = A_{surf,i} \times d_i , \qquad (5.42)$$

where $A_{surf,i}$ is the surface area in compartment i and d_i is the thickness of the lining fluid in compartment i. d in the central lung was set to be 5 µm [56], as was d in the nose [167]. Since d is known to gradually decrease along the lung generations [151], a smaller d was used peripherally (0.07 µm, [11]).

Calculation of central and peripheral lung tissue fractions. The volume of region j was calculated from:

$$V_j = A_{surf,j} h_j , \qquad (5.43)$$

where $A_{surf,j}$ is the surface area and h_j is the lung wall thickness of region j. Since limited information on surface areas and lung wall thickness in the different

subregions of the central lung was available, the bronchial wall thickness was assumed to be representative of the entire region. The rationale for choosing the bronchial wall as a representative was that it is thinner than the tracheal- but thicker than the bronchiolar wall. The bronchial (h_c = 29 μm) and alveolar wall thickness (h_p = 1.42 μm) were obtained from [168] and [30], respectively. The central ($f_{v,c}$) and peripheral ($f_{v,p}$) tissue fractions were subsequently calculated using eqs. 5.44 and 5.45, respectively, as follows:

$$f_{v,c} = \frac{V_c}{V_c + V_p}, \tag{5.44}$$

$$f_{v,p} = 1 - f_{v,c}. \tag{5.45}$$

Calculation of nasal mucosa volume. The volume of the nasal mucosa (V_n) was calculated using:

$$V_n = A_{surf,n} h_n, \tag{5.46}$$

where $A_{surf,n}$ is the surface area of the nose and h_n is the average thickness of the nasal epithelium. The average thickness (h_n = 61 μm) was obtained from [169]. Measurements from 60 day-old Sprague Dawley rats were chosen as this was in the proximity of the age range used in the studies (9-11 weeks).

Estimation of mucociliary rate constant. The mucociliary rate constant (k_{mcc}) was estimated using data from [155], where clearance of a tracer from the airway by mucociliary transport was studied in rats after inhalation ($0 \leq t \leq 6$ h, median spray droplet size 4-6 μm) using a single-photon emission computed tomography

(SPECT)-based method. The fraction retained (f_{ret}) was assumed to decline exponentially and MCC was assumed to be negligible in the peripheral region. Hence, a baseline corresponding to the fraction of the total lung dose deposited in the peripheral region (f_0) was introduced as this fraction should not be affected by MCC. There were no data available on the droplet size distribution, the mean value (5 µm) was therefore used for calculation of regional deposition. The peripheral ($f_{p,mcc}$) and central deposition fractions ($f_{c,mcc}$) for particles with an aerodynamic diameter of 5 µm were extracted from [65] and f_0 was calculated accordingly:

$$f_0 = \frac{f_{p,mcc}}{f_{p,mcc} + f_{c,mcc}} \approx 0.2 . \qquad (5.47)$$

The resulting equation for f_{ret} was as follows:

$$f_{ret} = f_0 + (1 - f_0)e^{-k_{mcc} \times t} = 0.2 + 0.8e^{-k_{mcc} \times t} \qquad (5.48)$$

k_{mcc} was estimated as 0.0472 ± 0.0011 h^{-1} using the MATLAB Curve Fitting Toolbox (Mathworks Inc., Natick, MA, USA), corresponding to a half-life of 14.7 h. The observations and model fit are shown in figure 5.3.

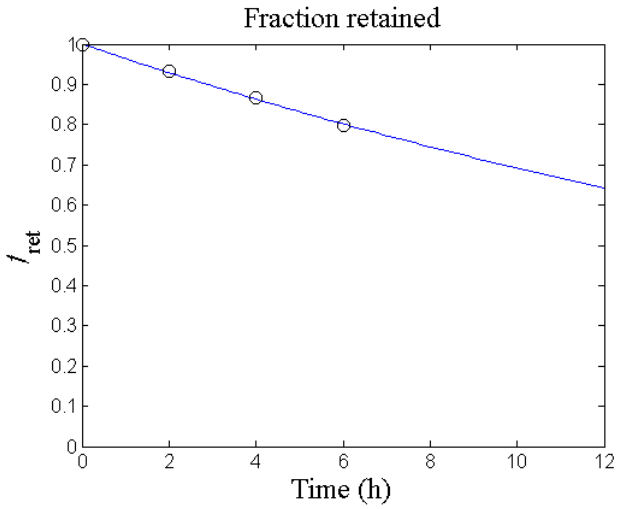

Figure 5.3 Characterisation of mucociliary clearance (MCC): a tracer was administered via inhalation in order to characterise MCC in rats. The retention of the tracer was governed by SPECT-imaging and data are presented as the fraction of tracer retained in the lung (f_{ret}). Observations from [155] are indicated by circles and the model fit by a solid line.

Table 5.5 System-specific input parameters for the rat.

Tissue	**Volume** (fraction of BW)	**Blood flow** (fraction of Q_{CO})
Adipose	0.040[b)]	0.009217[b)]
Gut	0.0259[c)]	0.14[c)]
Liver	0.04[a)]	0.024[c)]
Lung	0.004127[d)]	0.021[c)]/1
Nose	0.000254[e)]	0.0015[f)]
Poorly perfused[*]	1-(the rest)	1-(the rest)
Richly perfused[**]	0.039[a)]	0.5096 [a)]
Spleen	0.002[c)]	0.0715[g)]
Arterial blood	0.02 [a)]	*NA*
Venous blood	0.04 [a)]	*NA*

[*]Poorly perfused = 1 – other organs; [**]Richly perfused = richly perfused + brain + kidney from [a)]; Q_{CO} = cardiac output, 20.77 L/h/kg[a)]; a) [140]; b) [170]; c) [142]; d) Internal AstraZeneca data, han Wistar (n = 100); e) eq. 5.46, section 5.2.2.3; f) [171]; g) [141]

Table 5.6 System-specific input parameters for the central lung, the peripheral lung and the nose.

Parameter	Central lung	Peripheral lung	Nose
Blood flow (fraction of Q_{CO})	0.021[a)]	1	0.0015[b)]
Surface area (dm^2/kg)	3.27[c)]	276.4[d)]	0.416[e)]
Lining fluid volume (µL/kg)	163.6[*]	193.5[*]	20.8[*]
Fraction of tissue volume	0.19[*]	0.81[*]	NA
k_{mcc} (h^{-1})	0.0472	NA	0.2079

[*]Calculations of the lining fluid volume and tissue fractions are provided in section 5.2.2.3;

References: a) [142] b) [171] c) [172] (normalised per kg, 330 g rat, 108 cm^2) d) [173] (normalised per kg, 140 g rat, 3870 cm^2 e) [174] (normalised per kg, 10.4 cm^2, 250 g rat). Abbreviations: Q_{CO}=Cardiac output; k_{mcc}=rate constant for mucociliary clearance

5.3 Application of the developed model

This section focuses on application of the model, firstly in terms of model validation and verification. Administrations via the IV-route and via nose-only inhalation were simulated using drug- and formulation-specific input parameters for FP or budesonide (tables 5.4 and 5.3, respectively). The simulations were subsequently compared with experimental data obtained from work contained in this thesis or from AstraZeneca's internal data base. The source of the data is clearly stated in the text. As FP was used as a model substance in the development of the experimental *in vivo* receptor occupancy methodology, more data were available for that substance. Secondly, emphasis was put on exploring which properties are beneficial for inhaled drugs to advance the understanding of inhalation PK.

The MATLAB built-in solver *ode15s* was used throughout the thesis to numerically solve the system of coupled ODEs in the PBPK model. This solver was chosen since it is suitable for treating stiff problems.

5.3.1 Fluticasone propionate (model validation and verification)

5.3.1.1 Intravenous administration

Administrations via the IV-route (20, 90, 150, 750 and 1000 nmol/kg) were simulated using drug-specific input parameters for FP (table 5.4). The simulations were subsequently compared with experimental data on drug concentrations (plasma, spleen and lung) and receptor occupancy obtained from work contained in this thesis (sections 3.3.2.1, 3.3.2.2 and 4.3).

Model predictions of the plasma profiles as well as the time course of occupancy (figs. 5.4a-b) were consistent with experimental IV-data (90 and 1000 nmol/kg), supporting a perfusion rate-limited distribution of FP and validating the capability to predict plasma PK. As expected from IV-dosing, the predicted occupancy profiles in the two lung regions and the spleen were identical. No occupancy measurements were available for the higher dose. Of note is that the binding kinetics parameters (K_{on} and K_{off}) were obtained from modelling of IV-data (90 nmol/kg). As the model was predictive of the plasma PK for this particular dose, it follows that it should also be predictive of the corresponding receptor occupancy profile. This consistency can thus be regarded as a verification step of the model. A test set independent of the training data set was also available to validate model predictions of occupancy after IV-administration. The model proved to be predictive of the test set, which comprised of receptor occupancy measurements made 1.5 h after three IV-doses of FP (section 3.3.2.1). Simulated occupancies were 27, 64 and 86% for 20, 150 and 750 nmol/kg, respectively. Simulations agreed well with observed data: 27 ± 9.7, 74 ± 5.0 and 100 ± 3.5% for 20, 150 and 750 nmol/kg, respectively.

It was shown that inclusion of the receptor-bound concentration was essential for the predictive capability of both the lung- and the spleen concentrations. This is

illustrated by figure 5.4c-d, showing predictions of tissue concentrations inclusive (solid red line) and exclusive (dashed black line) of receptor binding.

In conjunction with the IV-simulations, it was also verified that mass balance was preserved in the PBPK model. This was done by simulating the cumulative amount of drug cleared from the system (A_{cum}) and subsequently comparing A_{cum} at t = 72 h to the input (90 nmol/kg, IV, fig. 5.4e).

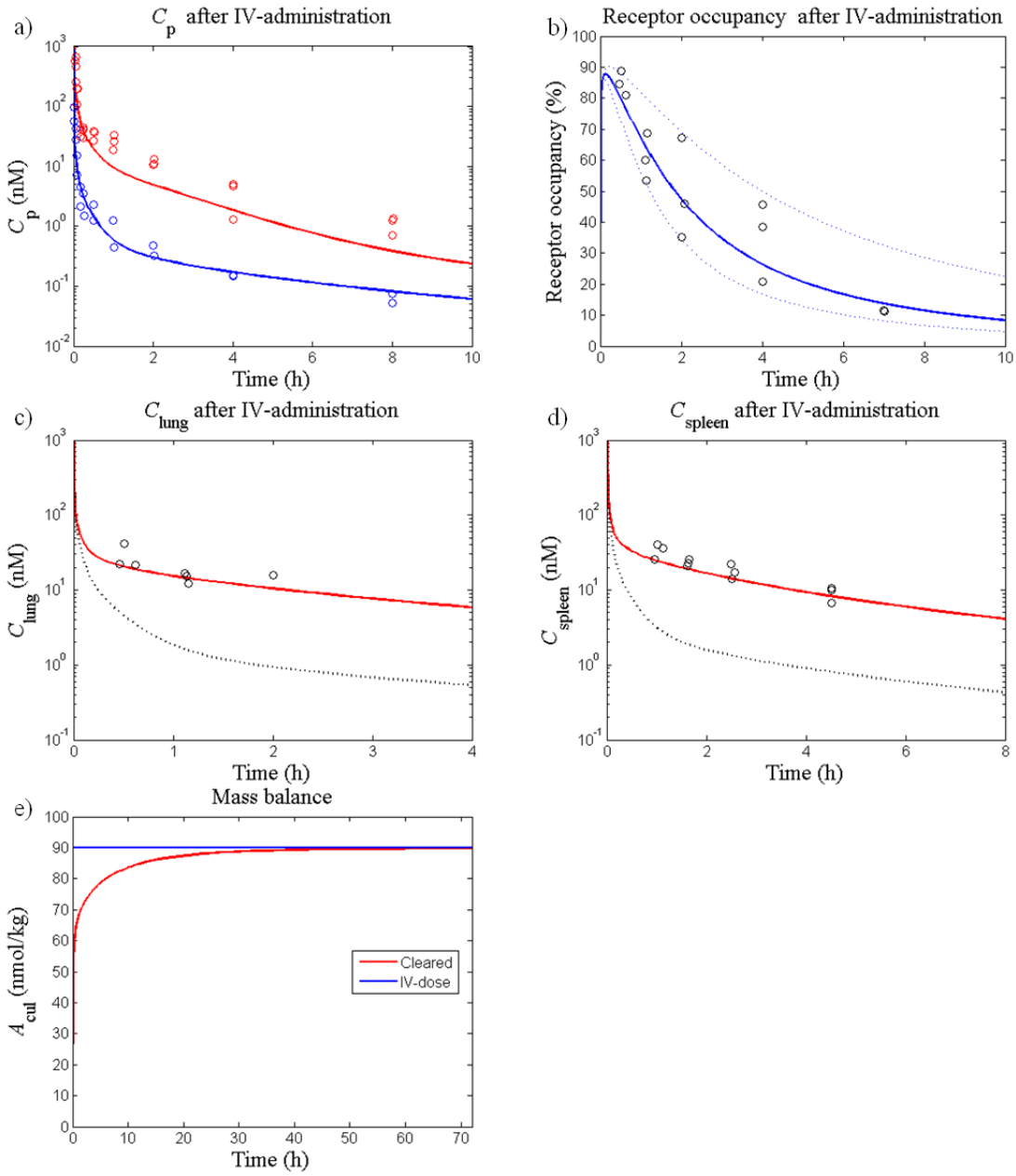

Figure 5.4 Model predictions and observations of fluticasone propionate administered as an IV-bolus to rats. The figures show: a) plasma concentrations (C_p) after IV-administration of 90 (blue line) and 1000 nmol/kg (red line), b) receptor occupancy after IV-administration of 90 nmol/kg (blue line), c) lung concentration (C_{lung}) after IV-administration of 90 nmol/kg (red line) the dashed line shows C_{lung} excluding the receptor-bound concentration, d) spleen concentrations (C_{spleen}) after IV-administration of 90 nmol/kg (red line), the dashed line shows C_{spleen} excluding the receptor-bound concentration, e) verification of preserved mass balance by comparing the cumulative amount cleared (A_{cul}, red line) to the IV-dose (blue line). For the receptor occupancy simulation, a 90% CI was created by a Monte

Carlo simulation which repeatedly sampled random values from a lognormal distribution of the binding kinetics parameters (n = 1000, dashed lines).

5.3.1.2 Nose-only exposure

Nose-only exposures with two different *LDD* (11.3 and 100 nmol/kg) were simulated using drug- and formulation-specific input parameters for FP (table 5.4). Neither particle size distribution nor density was available for the higher *LDD*, it was therefore assumed to have the same formulation-specific properties as the lower dose. Model predictions were subsequently compared with experimental data on drug concentrations (plasma, spleen and lung) and receptor occupancy. Observations from the lower dose (11.3 nmol/kg, *LDD*) were generated as part of this thesis (section 4.5), whereas observations corresponding to the higher dose (100 nmol/kg, *LDD*) were obtained from AstraZeneca's internal data base [164]. The latter data set only contained measurements of total lung concentrations.

Total lung-, plasma- and spleen concentrations were well-predicted by the model after nose-only inhalation (fig. 5.5a-c). In line with the IV-predictions, inclusion of the receptor-bound concentration was necessary for the model's predictive capability of total spleen concentrations (fig. 5.5c). In contrast to the spleen, the relative contribution of the receptor-bound concentration to the total lung concentration was small after inhalation (fig. 5.5d). This difference can be attributed to the large amount of FP retained in a solid state in the lung after inhalation.

The single parameter C_s was estimated from observations made in one inhalation study (11.3 nmol/kg, *LDD*). When the model was tested on another data set (100 nmol/kg, *LDD*), it was shown to be predictive of the total lung concentrations with the exception of the last time point (fig. 5.5a). As the particle size distribution was

not available for the latter study, larger particles could be a possible explanation for the under-prediction seen at 24 h.

Model predictions of the systemic occupancy were consistent with the observations (fig. 5.5e). Comparison of observations and model predictions of pulmonary occupancy was slightly more complex as the experimental methodology cannot distinguish between occupancy in the central and the peripheral lung. RO_{ave} (eq. 5.33), a weighted average of the occupancy accounting for the relative contribution of each region, was found to capture key trends in the data, although a tendency towards under-prediction was noted (fig. 5.5f). Given the uncertainty in $f_{v,c}$ and the slightly lower accuracy of lung occupancy measurements, a whole-lung occupancy prediction that qualitatively captures key features including lung-selectivity and late occupancy peak can be regarded as a good description of the data.

Neither plasma concentrations nor receptor occupancy had been measured following inhalation of the higher dose.

It was noted that, given the particle size distribution of the batch used, the nasally deposited dose was predicted to be approximately six times higher than *LDD* (fig. 5.5g).

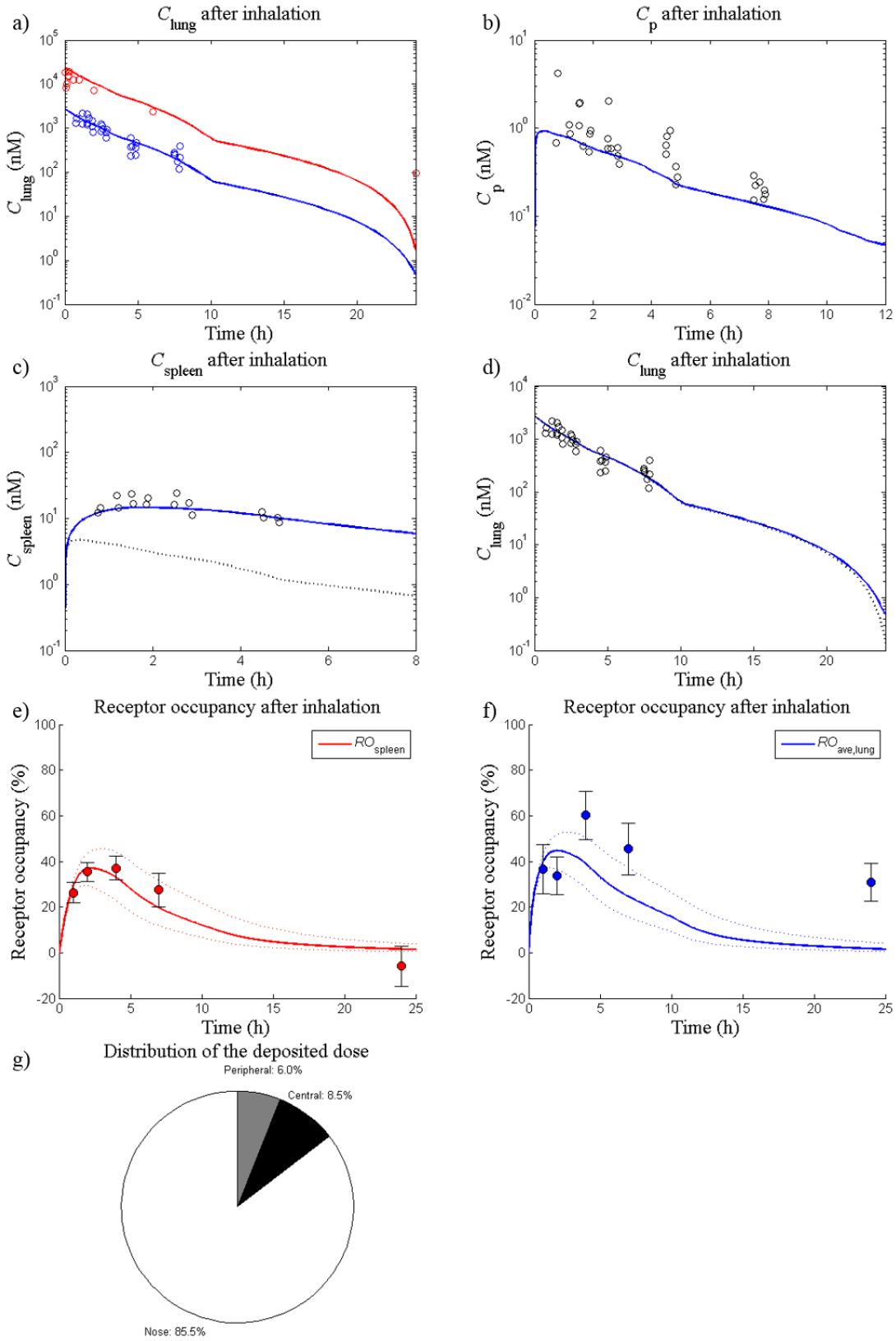

Figure 5.5 Model predictions and observations after nose-only exposure of fluticasone propionate, the figures show: a) total lung concentrations (C_{lung}) after a lung deposited dose (*LDD*) of 11.3 nmol/kg

(blue line) and 100 nmol/kg (red line), b) C_p after a *LDD* of 11.3 nmol/kg (blue line), c) spleen concentration (C_{spleen}) after a *LDD* of 11.3 nmol/kg (blue line), the dashed line shows C_{spleen} excluding the receptor-bound concentration, d) C_{lung} after a *LDD* of 11.3 nmol/kg (blue line), the dashed line shows C_{lung} excluding the receptor-bound concentration, e) receptor occupancy in the spleen after a *LDD* of 11.3 nmol/kg (red line), and f) whole-lung receptor occupancy after a *LDD* of 11.3 nmol/kg (blue line). For each receptor occupancy simulation, a 90% CI was created by a Monte Carlo simulation which repeatedly sampled random values from a lognormal distribution of the binding kinetics parameters (n = 1000, dashed lines). g) Distribution of the deposited dose between the central lung region (black), the peripheral lung region (grey) and the nasal region (white).

5.3.1.3 Sensitivity analysis for fluticasone propionate

A sensitivity analysis was performed to investigate how the dynamic behaviour of the system responds to changes in selected input parameters. The sensitivities were generated by considering the partial derivatives of the output Y with respect to each parameter p_i and these were calculated keeping all other parameters fixed at their nominal values (p_0), i.e.

$$\left.\frac{\partial Y}{\partial p_i}\right|_{p_0} \tag{5.49}$$

Two outputs were investigated: receptor occupancy in the central lung (RO_c) and receptor occupancy in the spleen (RO_{sp}). This was done by firstly simulating the system with all parameters at their nominal values [$f(t,p_0)$]. Subsequently, a simulation was performed after considering a 0.1% increment in the parameter of interest, p_i, [$f(t,p)$] while all other parameters were kept at their nominal values. As mentioned in section 5.3, the MATLAB built-in solver *ode15s* was used to solve the system of coupled ODEs. The choice of integrator accuracy was important to enable

the use of a low perturbation fraction (0.001). An accuracy of 10^{-12} was therefore chosen (i.e. '*RelTol*' in MATLAB was set to 10^{-12}). The sensitivities here were calculated according to the same principle as that is used in, for example, Berkeley Madonna™ and carried out follows:

$$S(t) = p_0 \frac{\partial f(t,p)}{\partial p} = \frac{f(t,p) - f(t,p_0)}{(p - p_0)/p_0}. \qquad (5.50)$$

As expected, the sensitivity analysis (fig. 5.6a-b) showed that the parameters *D* and C_s, both essential for the dissolution process, have a big impact on the dynamic response of RO_c and RO_{sp}. The sensitivity curves with regard to *D* and C_s have several peaks as a result of the dissolution of eight different particle sizes. The change in sign of the derivative of the sensitivity function coincides with the time points when the radius *r* approaches 0. Increasing the bronchial blood flow (Q_{bronch}) had a negative impact on RO_c, whereas RO_{sp} was principally unaffected. RO_{sp} was largely affected by *CL*, whereas this parameter only had a small impact on RO_c. As the extent of nasal absorption is in part determined by $k_{mcc,nasal}$, it follows that RO_{sp} should be sensitive to perturbations in this parameter. This hypothesis was confirmed by the sensitivity analysis, which also verified that $k_{mcc,nasal}$ does not have a big effect on RO_c. The analysis showed that P_{app} had a bigger impact on RO_{sp} than RO_c during the dissolution process. This reflects the effect of P_{app} on the absorption of drug to the systemic circulation as well as the fast equilibration between unbound concentrations in the systemic circulation and the spleen.

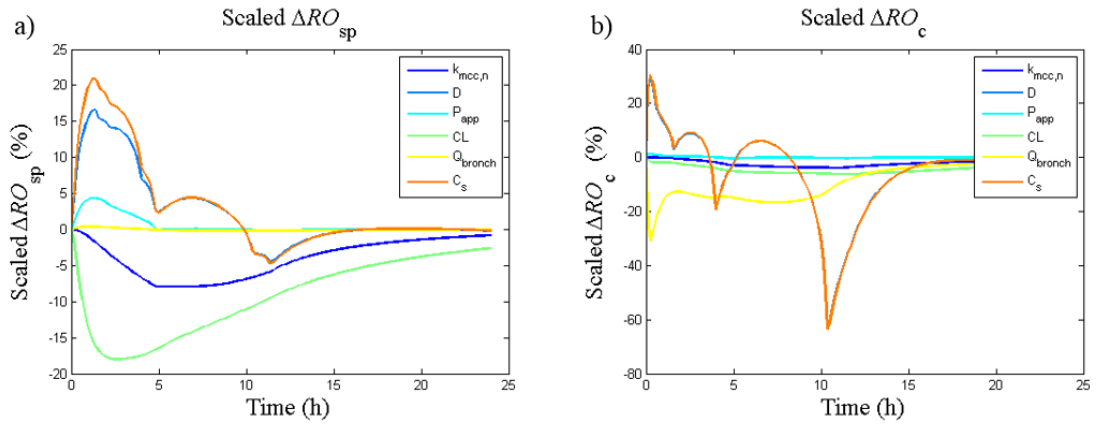

Figure 5.6 Sensitivity analysis. Influence of a 0.1% increase in the values of six different parameters on the dynamic behaviour of a) receptor occupancy in the spleen (RO_{sp}), and b) receptor occupancy in the central lung (RO_c) was investigated. The following parameters were included in the analysis: the mucociliary clearance rate in the nose ($k_{mcc,n}$), the diffusion coefficient (D), the apparent permeability (P_{app}), the clearance (CL), the bronchial blood flow (Q_{bronch}) and the solubility (C_s).

5.3.2 Budesonide

5.3.2.1 Intravenous administration

IV-administration (167 nmol/kg) was simulated using drug-specific input parameters for budesonide (table 5.3). The simulations were subsequently compared with experimental data on drug concentrations (plasma, spleen and lung) and receptor occupancy, i.e. data obtained from work contained in this thesis (section 4.2 and 4.3, respectively).

The initial distribution phase in the plasma profile (t < 1.1 h) was well-captured by the model predictions, whereas a consistent deviation between experimental and predicted C_p was observed at later time points (fig. 5.7a). This discrepancy suggests the presence of a mechanism that is unaccounted for by the model. In fact, reversible fatty acid esterification of budesonide has been demonstrated to take place both *in vitro* [175] and *in vivo* [79]. Earlier research aiming at characterising the PK of budesonide and its ester, budesonide-oleate, showed that budesonide-oleate was

rapidly formed both after IV-administration and inhalation of budesonide in rats [79]. As the resulting budesonide-oleate concentrations were in the proximity of the budesonide concentrations, the formation and subsequent hydrolysis of the ester is likely to have a pronounced effect on the PK of budesonide. The latter hypothesis has also been confirmed via semi-empirical modelling approaches [79,176]. Hence, the current PBPK model structure is not expected to be able to accurately describe the PK of budesonide neither in plasma (fig. 5.7a) nor in tissues (5.7b and 5.7c for the lung and the spleen, respectively).

Further research would have been required to adequately describe the esterification of budesonide in a quantitative manner, which was not considered to fall within the scope of this thesis. However, since budesonide-oleate is rapidly formed in tissues [79], this process may well be reflected in the plasma profile by a rapid initial decline followed relatively flat second phase caused by the ester accumulated in tissues slowly being hydrolysed back to budesonide. This phenomenon is seen in the experimental data (fig. 5.7a), but cannot be captured by the current model structure as it does not account for this process.

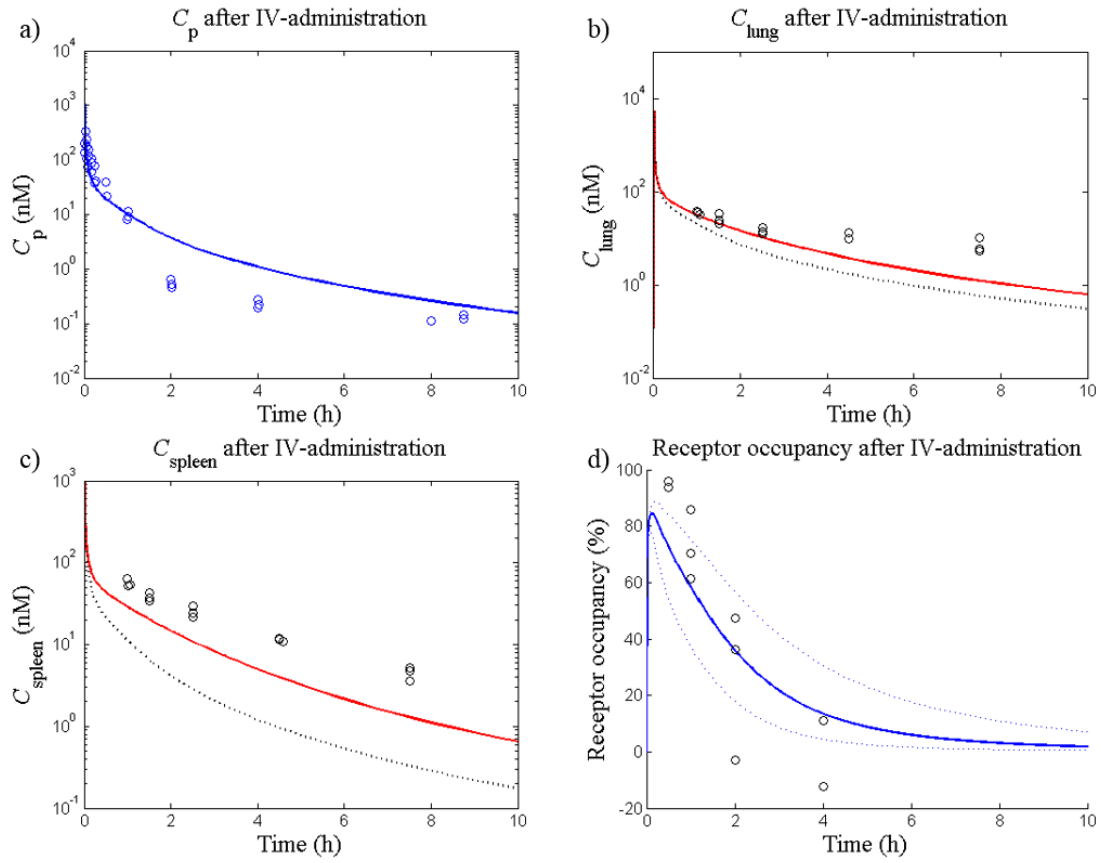

Figure 5.7 Model predictions and observations of budesonide administered as an IV-bolus (167 nmol/kg) to rats. The figures show: a) plasma concentrations (C_p, blue line), b) lung concentrations (C_{lung}, red line), the dashed line shows C_{lung} excluding the receptor-bound concentration, c) spleen concentrations (C_{spleen}, red line), the dashed line shows C_{spleen} excluding the receptor-bound concentration, and d) receptor occupancy (blue line). For the receptor occupancy simulation, a 90% CI was created by a Monte Carlo simulation which repeatedly sampled random values from a lognormal distribution of the binding kinetics parameters (n = 1000, dashed lines)

5.3.2.2 Nose-only exposure

AstraZeneca's internal data base was searched for inhalation PK-studies with budesonide. Three studies were found in which budesonide had been administered as a dry powder [164]. The time profile of C_{lung} had been characterised in all three studies and two studies also comprised measurements of C_p. In two studies, the *LDD* had been determined to be 100 and 127 nmol/kg, respectively by filter analysis (the principles are described in section 2.2.6.2). The *LDD* had not been determined in the

third study. However, since the measured lung concentrations were approximately equal in the aforementioned study and the study with an *LDD* of 100 nmol/kg, the *LDD* of the third study was also assumed to be 100 nmol/kg. For simplicity, the details for each study have been summarised in table 5.7. The formulation-specific parameters (particle size distribution and density) were only available for study 3 and were assumed to be identical across the three studies (table 5.3).

Nose-only exposures with two different *LDD* (100 and 127 nmol/kg) were simulated using drug- and formulation-specific input parameters for budesonide (table 5.3). Model predictions were subsequently compared with experimental data on lung- and plasma concentrations. There was only a small difference between the concentration profiles generated from simulations of the two different *LDD*. The initial drop in C_{lung} was well captured by the model predictions, suggesting that budesonide is rapidly dissolved. However, there was a consistent under-prediction of C_{lung} from approximately 5 h after dosing and onwards (fig. 5.8a). As expected from the deviations between model predictions and observations of C_p after IV-administration, the model could not describe the plasma profile after inhalation (fig. 5.8b). The discrepancy patterns between model predictions and observations were similar for both routes of administration (IV and inhalation), again suggesting the presence of a mechanism that is unaccounted for by the model.

Table 5.7 Details for the inhalation studies with budesonide

Study	Observations	*LDD* (nmol/kg)
1	C_{lung}	100
2	C_{lung}, C_p	127
3	C_{lung}, C_p	100[1)]

Abbreviations: *LDD*=lung deposited dose; C_{lung}=total lung concentrations; C_p=plasma concentrations.

[1)] The *LDD* in study 3 was assumed to be identical to the *LDD* in study 1.

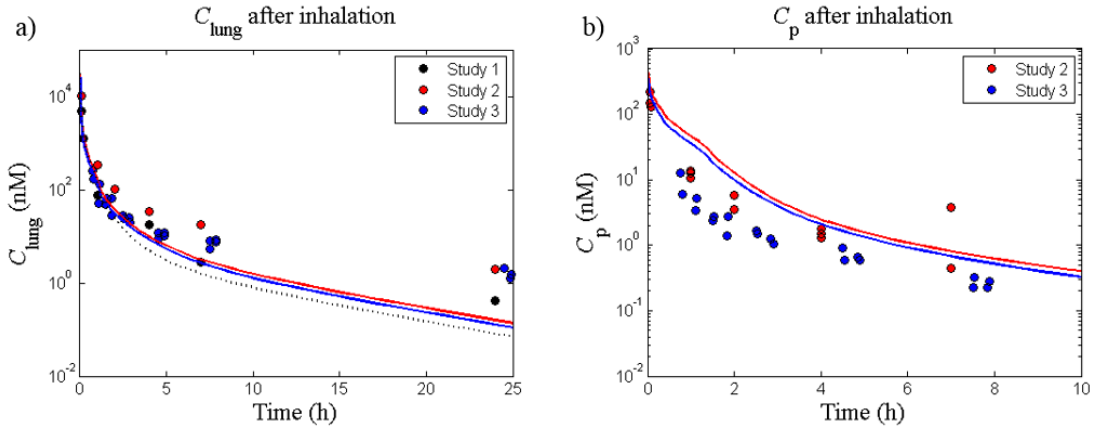

Figure 5.8 Observations and model predictions after nose-only exposure of budesonide. The figures show: a) total lung concentrations (C_{lung}), and b) plasma concentrations (C_p) after a lung deposited dose (*LDD*) of 100 and 127 nmol/kg. Data were taken from three studies with the following colour codes and *LDD*: study 1 (black, *LDD* = 100 nmol/kg), study 2 (red, *LDD* = 127 nmol/kg) and study 3 (blue, *LDD* = 100 nmol/kg). Lines represent model predictions and circles represent observations. C_p was not measured in study 1. The dotted line in a) represents C_{lung} exclusive of the receptor-bound concentration.

5.3.3 Evaluation of concepts for lung-selectivity

This model can distinguish between drug-, formulation- and system-specific properties. As such, it enables assessment of important factors determining lung-selectivity including properties of the molecule, formulation as well as the physiology of the animal species. Hence, this section will focus on exploring what properties are beneficial for inhaled drugs. In addition, it will also address possible

limitations of the animal models currently used for characterisation of inhalation drugs.

5.3.3.1 Definition of lung-selectivity

Lung-selectivity can be defined as the ratio between pulmonary and systemic receptor occupancy, where a ratio of unity implies absence of lung-selectivity. In accordance with the previous line of reasoning, the spleen is used as a reference organ for the systemic exposure. Since the lung is divided into a central and a peripheral region, lung-selectivity can be evaluated for each region individually. Regardless of the scenario simulated, it was noted that lung-selectivity could not be achieved if the peripheral lung was considered as the pulmonary region. A ratio of unity was thus obtained between the occupancy in the peripheral lung (RO_p) and the spleen (RO_{sp}) in this model. This is attributed to the high perfusion rate of this region (entire cardiac output, Q_{CO}), which thus rapidly equilibrates with the systemic circulation. However, under certain circumstances lung-selectivity could be obtained in the central lung after inhalation. Henceforth, the occupancy in the central lung (RO_c) is therefore used as the pulmonary region for evaluation of lung-selectivity. In other words, the criterion for lung-selectivity is fulfilled when

$$\frac{RO_c}{RO_{sp}} > 1. \qquad (5.51)$$

5.3.3.2 Evaluation of drug-, formulation- and system-specific input parameters

In the following simulations, the impact of an individual parameter p_i on the degree of lung-selectivity obtained by inhalation will be evaluated by simulating the system using varying values of p_i while all other parameters (p) are fixed at their assigned

values. Unless otherwise specified, drug- and formulation-specific input parameters for FP (table 5.4) are used for the parameter vector p. For consistency, an *LDD* of 11.3 nmol/kg will be used unless stated otherwise.

The impact of the following drug-specific input parameters on lung-selectivity was evaluated: CL, F, C_s, P_{app} and K_{off}. Furthermore, one formulation- and one system-specific input parameter were investigated: particle size and nasal blood flow (Q_n), respectively. The latter parameter was included to evaluate the contribution of nasal drug absorption following nose-only exposure, which was done by simulating and comparing the plasma PK profile from a base-case scenario (input parameters from tables 5.4-6) to a scenario where Q_n was set to 0. The particle size distribution was investigated by comparing the base-case scenario to one where the particles were evenly distributed between the four smallest size classes, that is $f_i = 0.25$ for $i \in \{5, \ldots, 8\}$ and $f_i = 0$ otherwise.

As can be seen in figure 5.9a, a longer period of lung-selectivity was obtained for a poorly soluble drug (C_s = 2.5 µM) than for a highly soluble drug (C_s = 50 µM). Since the dissolution phase can be prolonged by decreasing C_s (eq. 5.20), a lower C_s resulted in an extended period of lung-selectivity. Nevertheless, a transient concentration gradient created during dissolution of a highly soluble compound (C_s = 50 µM) could also give rise to a prolonged lung-selectivity given a slow K_{off} (fig. 5.9b).

The dissolution rate is not only dependent on C_s. From eq. 5.20 and 5.22 it is evident that the particle size is also important. Moreover, the regional deposition depends on the particle size. Accordingly, given a certain *LDD*, simulations showed that the particle size distribution had an impact on the occupancy profile as well as on the degree of lung-selectivity (fig. 5.9c).

According to the simulations, nasal absorption significantly contributed to the systemic exposure (fig. 5.9d) and decreased the degree of lung-selectivity following nose-only inhalation of FP (fig. 5.9e). Noteworthy is that the nasally deposited dose was predicted to be several-fold higher than *LDD* (fig. 5.5e, section 5.3.1.2).

P_{app}-values are known to differ across laboratories, thus there are no strict cut-off values for P_{app} assigning low, moderate and high permeability, respectively. However, as a benchmark the following permeability ranges are used for CaCo-2 [177]:

- 2×10^{-6} cm/s > P_{app} (low permeability)
- 2×10^{-6} cm/s ≤ P_{app} ≤ 20×10^{-6} cm/s (moderate permeability)
- 20×10^{-6} cm/s < P_{app} (high permeability)

In the simulations P_{app} = 0.2×10^{-6} cm/s and P_{app} = 100×10^{-6} cm/s assigned low and high permeability, respectively. In order to distinguish permeability from other mechanisms of lung retention, the following changes were made in the simulations: 1) drug was administered as a solution directly in the central ELF, and 2) the K_{off} was set to be 10-fold higher than the corresponding value for FP; i.e. K_{off} = 5.1 h^{-1}. Administration of a solution was done by setting the initial central ELF concentration ($C_{ELF,C}$) to

$$C_{ELF,C}(0) = \frac{LDD}{V_{ELF,C}}, \qquad (5.52)$$

where $V_{ELF,C}$ is the volume of ELF in the central lung. As can be seen in figure 5.9f, simulations suggest that a low permeability alone can give rise to a prolonged period of lung-selectivity despite the drug already being dissolved and having a fast K_{off}. However, administration of a dissolved, highly permeable compound with the same properties did not produce any lung-selectivity.

Simulations also showed that *F* was negatively correlated with lung-selectivity, whereas a positive correlation was found for *CL* (simulations not shown).

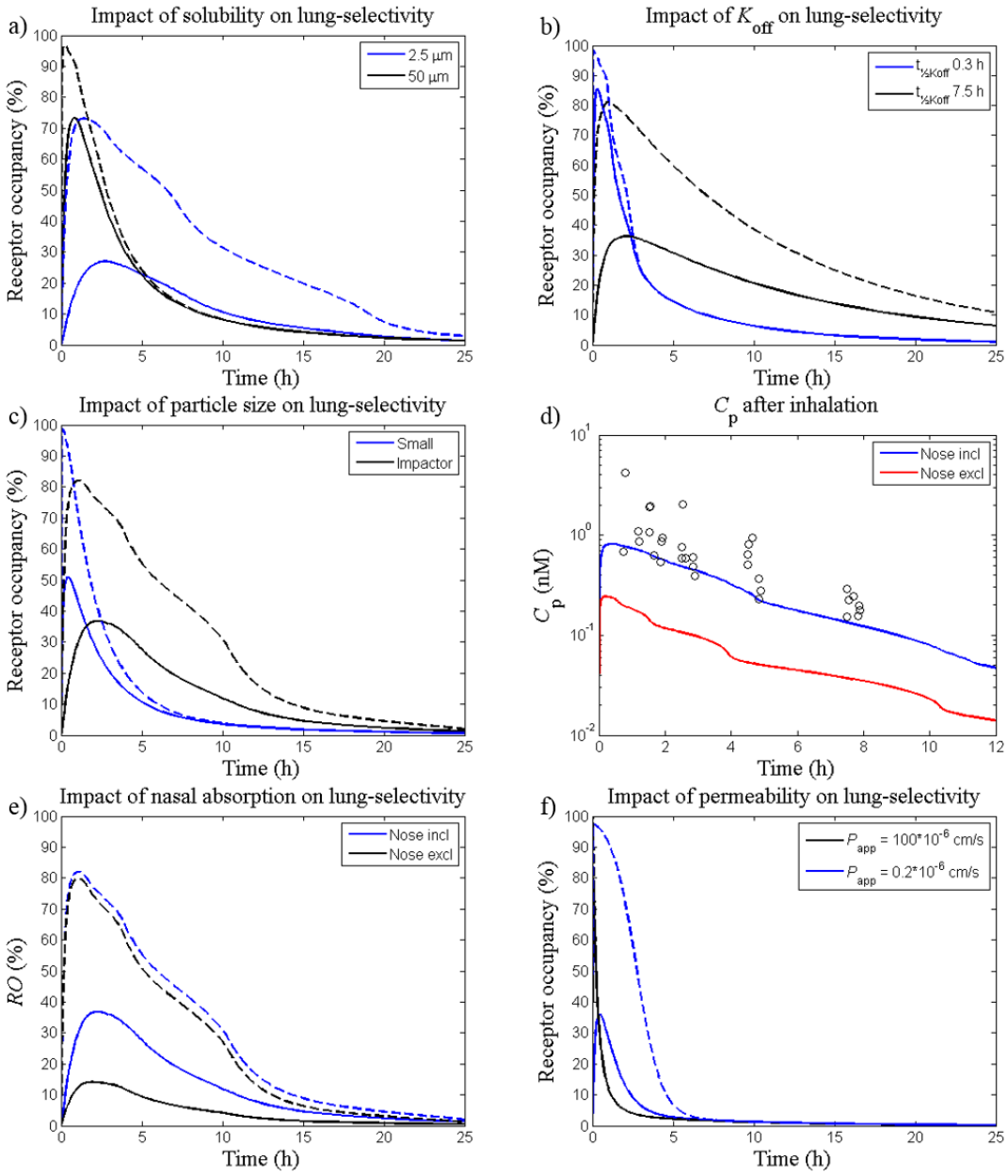

Figure 5.9 The impact of different drug-, formulation- and system-specific properties on lung-selectivity was evaluated by varying the following parameters: a) solubility; C_s = 2.5 µM (blue line) and C_s = 50 µM (black line), b) dissociation rate; $t_{½,Koff}$ = 7.5 h (black line) and $t_{½,Koff}$ = 0.3 h (blue line), c) particle size distribution; f_1, ..., f_8 from table 5.4 (black line) and f_i = 0.25 for i = 5, …, 8 and f_i = 0 otherwise (blue line), d) nasal absorption; nose included (blue line) and nose excluded (red line), e) nasal absorption; nose included (blue line) and nose excluded (black line) and f) permeability; P_{app} = 0.2×10^{-6} cm/s (blue line) and P_{app} = 100×10^{-6} cm/s (black line). Except for subfigure d), which shows predictions (lines) and observations (open circles) of plasma concentrations of fluticasone

propionate (C_p), dashed lines represent receptor occupancy in the central lung and solid lines represent occupancy in a systemic reference organ.

5.3.4 Evaluation of different concepts

5.3.4.1 Intravenous administration versus instillation of dissolved drugs without any pulmonary retention mechanism

With exception of the intravenous route, inhalation is the fastest route of systemic delivery of small molecules. This is particularly prominent for small lipophilic molecules, where the absorption half-life is approximately 1-2 minutes [21]. The model was used to confirm this feature by firstly simulating the plasma profile following instillation of a compound in solution (*LDD*, 20 nmol/kg). This was done by setting the initial concentration in the ELF in the central lung to

$$C_{ELF,C}(0) = \frac{20}{V_{ELF,C}}, \qquad (5.53)$$

where $C_{ELF,C}$ is the drug concentration in the ELF in the central lung and $V_{ELF,C}$ is the volume of the ELF in ditto. An IV-dose matching the instilled dose (20 nmol/kg) was subsequently simulated in order to compare the resulting plasma profile to the corresponding profile obtained after inhalation. As can be seen in fig. 5.10, the resulting arterial concentration profiles from the two administration routes were similar for a drug without any specified pulmonary retention mechanism.

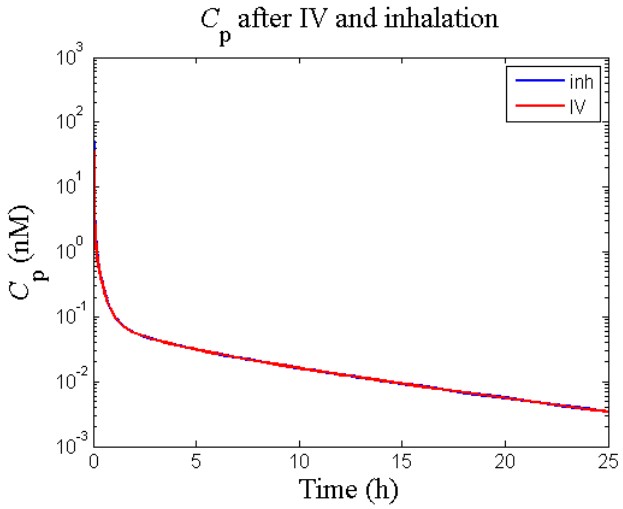

Figure 5.10 Plasma concentration (C_p) profiles were simulated after intratracheal instillation of dissolved drug (20 nmol/kg, blue line) and intravenous (IV) administration (20 nmol/kg, red line).

Despite the similar blood exposure, the inhaled route gave rise to a transient period of lung-selectivity whereas a ratio of unity was obtained after IV-administration. The duration of lung-selectivity is dependent on the binding kinetics of the drug, which was illustrated by simulating RO_{sp} and RO_c for varying values of K_d and K_{off} accordingly: 1) K_d = 15 pM and K_{off} = 0.51 h^{-1}, 2) K_d = 150 pM and K_{off} = 5.1 h^{-1}, and 3) K_d = 1.5 pM and K_{off} = 0.051 h^{-1}.

In the first simulation, the binding kinetics parameters of FP were used (fig. 5.11a-b). Increasing K_d and K_{off} by a factor of 10 led to a significantly shorter period of lung-selectivity (fig. 5.11c-d). In the third simulation, when K_d and K_{off} were decreased by a factor of 10, a prolonged period of lung-selectivity was obtained (fig. 5.11e-f). Needless to say, this method for prolonging the duration of lung-selectivity will be accompanied by a prolonged systemic occupancy profile.

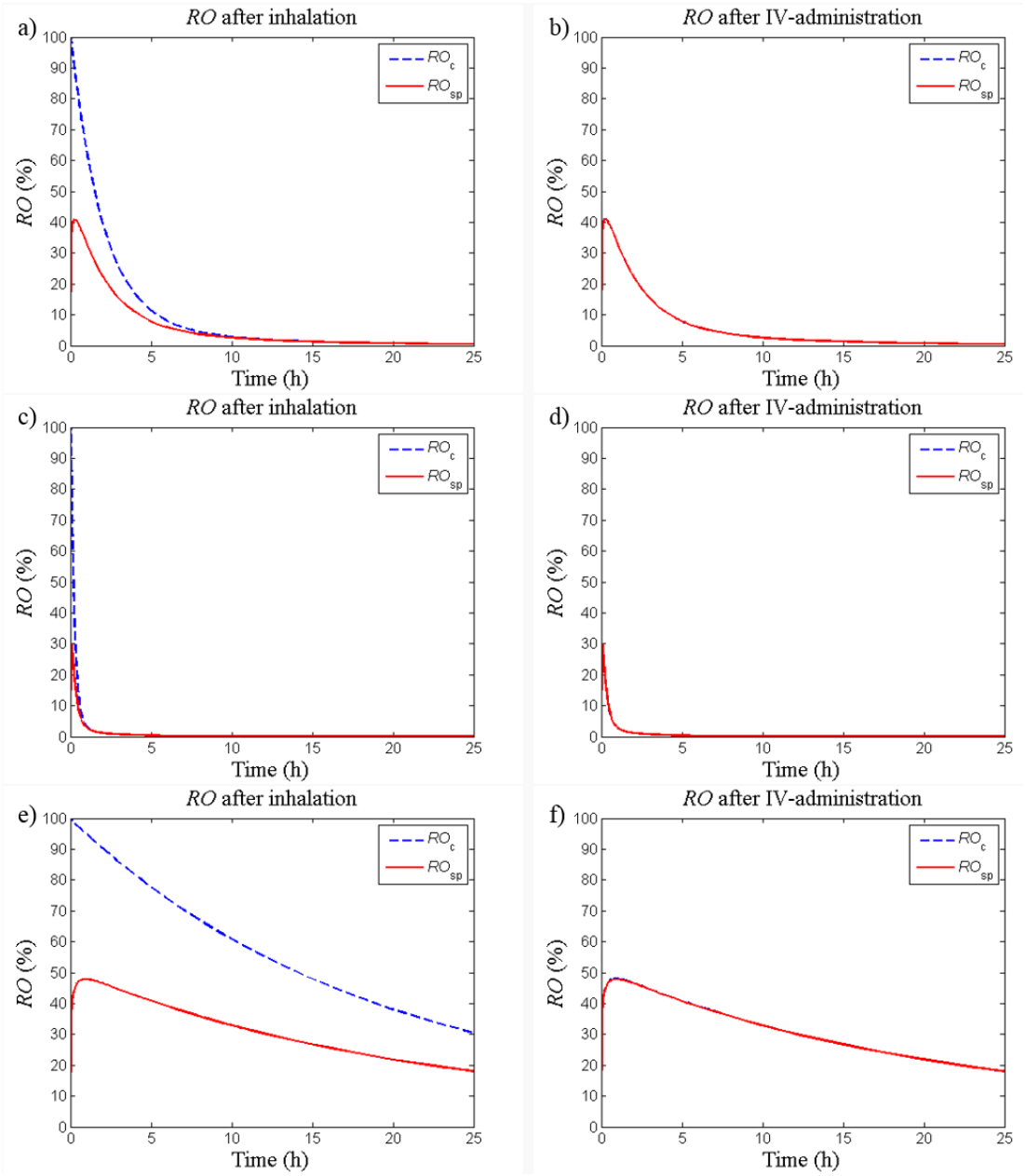

Figure 5.11 Receptor occupancy profiles were simulated after intratracheal instillation of dissolved drug (20 nmol/kg) and intravenous (IV) administration (20 nmol/kg). Receptor occupancy profiles were simulated in the spleen (red line) and the central lung (dashed blue line) using varying values of binding kinetic parameters and different routes of administration accordingly: a) K_d = 15 pM and K_{off} = 0.51 h^{-1}, inhalation, b) K_d = 15 pM and K_{off} = 0.51 h^{-1}, IV, c) K_d = 150 pM and K_{off} = 5.1 h^{-1}, inhalation, d) K_d =150 pM and K_{off} = 5.1 h^{-1}, IV, e) K_d = 1.5 pM and K_{off} = 0.051 h^{-1}, inhalation, and f) K_d = 1.5 pM and K_{off} = 0.051 h^{-1}, IV.

5.3.4.2 Impact of mucociliary clearance on the pharmacokinetics

The impact of MCC on the PK will be dependent on the residence time of the drug in the lung and the nose. As poorly soluble compounds are anticipated to be retained in a solid state for a longer time period than drugs with a high C_s, MCC is expected to have a bigger effect on that compound class. Indeed, the effect of MCC was shown to be more pronounced for poorly soluble drugs. The amount of drug transported by MCC from the nose and the central lung to the gut (A_{mcc}) was simulated for a broad range of C_s (0.01-10^5 nM, 300 steps) after an *LDD* of 10 nmol/kg (*ID*, 97.0 nmol/kg) using drug- and formulation-specific input parameters for FP. A_{mcc} decreased with higher C_s, which can be attributed to the higher dissolution rate as described in eq. 5.20. Accordingly, the percentage of drug removed by MCC tends towards 100% as C_s approaches 0 (fig. 5.12). The model thus suggests that the impact of MCC on the PK is high for compounds with a low C_s and negligible for compounds with a high C_s. This is in line with previous research, which suggests that MCC has a larger impact on slowly dissolving compounds [8].

Expressed differently, these simulations suggest that MCC will act by decreasing the pulmonary bioavailability for poorly soluble drugs. Interestingly, a clinical study showed less systemic side-effects of inhaled FP (poorly soluble compound) in patients with moderately severe asthma as compared to healthy volunteers. However, there was no statistically significant difference between the two groups for the highly soluble compound budesonide [178]. Another clinical study showed a significantly lower bioavailability of inhaled FP in asthmatic patients as compared to healthy volunteers [179]. Since FP has a very low oral bioavailability it is reasonable to assume that this difference is primarily caused by pulmonary absorption. The lower pulmonary bioavailability of inhaled FP in asthmatic patients was suggested to be

caused by a higher central lung deposition of drug in the asthmatic group, which makes the drug particles more prone to clearance by MCC [179]. Indeed, asthmatic patients have been shown to have a higher central deposition of drug [180], which has been suggested to be caused by the airway narrowing in this patient population [179]. To summarise, clinical data also suggest that slowly dissolving drugs are more prone to be cleared by MCC. Since MCC primarily is associated with the tracheobronchial region [74], this effect is expected to be more pronounced after central drug deposition.

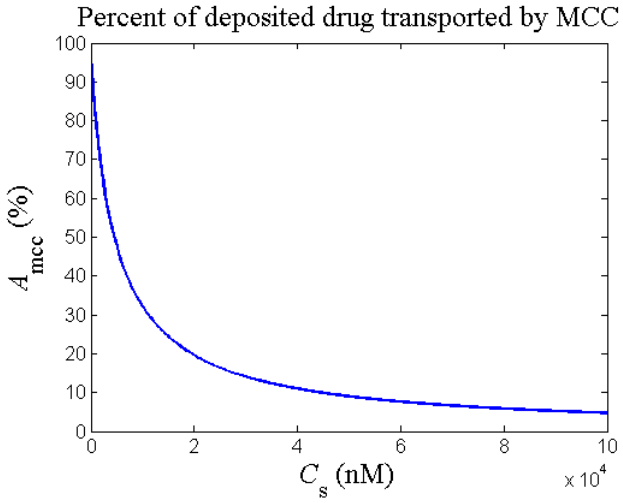

Figure 5.12 Percent of drug particles deposited in the nose and central lung that are removed by the mucociliary clearance (MCC) as a function of solubility (C_s).

5.3.4.3 Evaluation of the impact of permeability on pulmonary absorption

As mentioned in section 2.2.4, inhaled drugs may be rapidly absorbed to the systemic circulation. The pulmonary absorption rate of a dissolved drug is for instance expected to be dependent on the permeability of the compound. In fact, a weak relationship (r^2 = 0.45) between the lung absorption half-life in rats and the measured CaCo-2 permeability has been shown in . It is worth mentioning that only limited information on the experiments is available in the cited publication. Nevertheless, the

authors investigated the correlation between the CaCo-2 permeability and pulmonary absorption half-life ($t_{½,lung}$) after IT-instillation of solutions to rats. Since several of the 19 included compounds were bases, the $t_{½,lung}$ cannot be expected to be explained by permeability alone. Both protonation of the compound in the slightly acidic ELF (pH 6.6 [4]) as well as intracellular lysosomal trapping might be possible mechanisms for prolongation of $t_{½,lung}$. One could argue that the slowness of the lysosome might already be described by the P_{app} obtained from CaCo-2 experiments. However, the cell model's feasibility to capture this mechanism as well as the relative abundance of lysosomes in CaCo-2 and lung epithelial cells remain to be experimentally evaluated prior to confirming or rejecting that hypothesis.

Since only neutral compounds have been explored in this thesis, the current model structure does not account for lung retention caused by basicity and the aim of this thesis is not to theoretically/experimentally explore the mechanisms thereof. Nevertheless, the impact of permeability on pulmonary absorption was theoretically explored to investigate whether the model predictions are in line with the observations made in . In that study, $t_{½,lung}$ was calculated based on measurements of C_{lung}. That approach was subsequently mimicked in this simulation study.

Administration by IT-instillation means that the drug is directly dosed into the lung, i.e. nasal drug deposition is avoided. It has been shown that the pulmonary deposition pattern of drug after IT-instillation is highly dependent upon the technique of the experimentalist [164]. However, IT-instillation tends to result in a higher deposition centrally in the lung . Hence, to mimic this dosing method drug was administered as a solution directly in the central ELF. That is, the initial condition in this compartment was set to

$$C_{ELF,C}(0) = \frac{LDD}{V_{ELF,C}}, \qquad (5.54)$$

where $V_{ELF,C}$ is the volume of the central ELF. *LDD* was set to 10 nmol/kg and *P* varied between 0.1×10^{-6} and 100×10^{-6} cm/s, where 40 values were selected from a logarithmic scale. The system was simulated iteratively for $0 \leq t \leq 25$ h for each value of *P*. For each simulation, the time point at which C_{lung} had decreased to 50% of its value at $t = 0$ was extracted and used as the model prediction of $t_{½,lung}$. Clearly, this value will also be dependent on the systemic PK both in the simulations as well as in the experimental data. This simulation exercise was subsequently repeated with the aim of mimicking a more *homogenous* distribution of drug after IT-instillation, i.e. the initial condition in each of the two ELF compartments was set to $0.5LDD/V_{ELF}$.

It follows that two important assumptions are made in these simulations: 1) the permeability is identical throughout the entire lung (i.e. the measured P_{app} applies for all lung regions, which probably is not true for the alveolar region where a higher permeability is expected), and 2) the CaCo-2 P_{app} equals the effective permeability. Thus, two assumptions were made in areas which still remain to be investigated by future research. Nevertheless, in a theoretical situation where only *P* differs, the model-derived values of $t_{½,lung}$ can be used to evaluate the impact of *P* on pulmonary absorption on a *qualitative level*.

Starting by evaluating the simulations resulting from a central deposition of drug, figure 5.13a shows that $t_{½,lung}$ decreased with a higher permeability. The model predictions thus agreed with the observations made by Cooper *et al*. [7] on a qualitative level. As can be seen in figure 5.13b, model simulations indicate that the

initial profile of the lung PK-profile, which often is referred to as the ‘alpha phase’, would be less steep for poorly permeable compounds.

As expected, lower values of *P* resulted in higher drug concentrations in the ELF (C_{ELF}, fig. 5.13c), which can have interesting implications for drugs with targets localised in the airway lumen. The same pattern, although not as pronounced, was seen for C_{lung} (fig. 5.13b).

Interestingly, despite the assumption of *P* being identical throughout the entire lung, the simulations suggested that the pulmonary PK is largely influenced by the initial deposition pattern. This was particularly prominent when comparing the lung PK-profiles over the first few minutes. After IT-administration of an evenly distributed dose, the model predictions indicated that a particularly rapid pulmonary absorption phase took place during the first few minutes after dosing (fig. 5.13d). However, this pattern was not present when drug administration was restricted to the central lung (fig. 5.13e). The simulations thus suggest that pulmonary absorption is more rapid in the rapidly perfused peripheral lung region. In contrast, a poor *P* appears to be an effective mechanism for lung-retention in the central lung region.

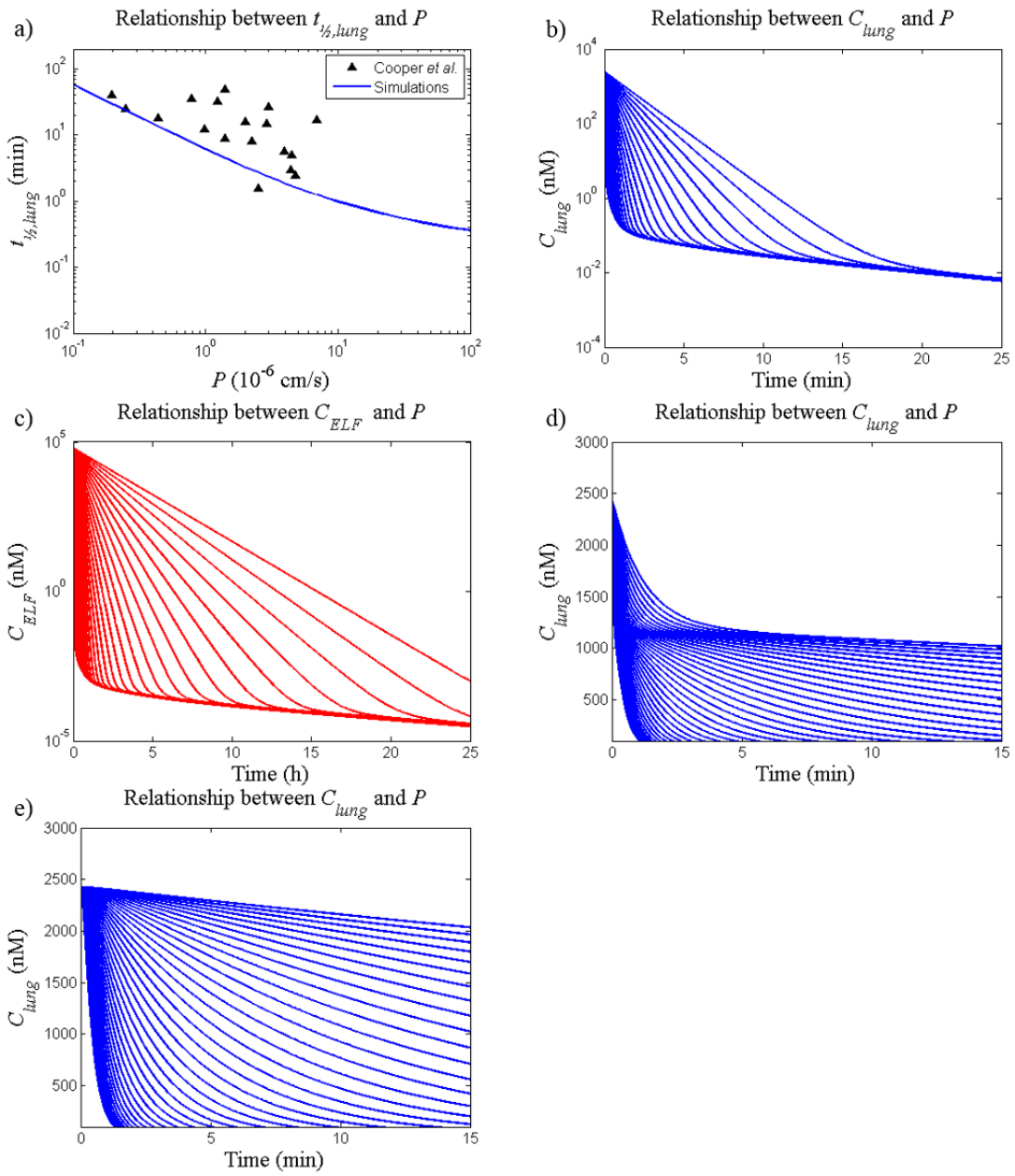

Figure 5.13 The impact of permeability (P) on pulmonary absorption was theoretically explored by simulating pulmonary drug administration of a solution (10 nmol/kg). The dose was either only administered in the central lung region (subfigure a-c and e) or evenly distributed between the central and the peripheral lung (subfigure d). The subfigures show: a) pulmonary absorption half-life ($t_{½,lung}$) for different values of P (blue line), the measurements of $t_{½,lung}$ were obtained from (black triangles), b) total lung concentrations of drug (C_{lung}, blue lines) over 25 h, c) concentration of drug in the epithelial lining fluid (C_{ELF}, red lines), and d-e) C_{lung} (blue lines) focused on the first 15 minutes. The system was simulated iteratively for 40 different values of P, where P varied between 0.1×10^{-6} and 100×10^{-6} cm/s. In subfigures b-e each line corresponds to a simulation using one value of P. The

different lines can be identified by the observation that a lower *P* consistently made the curves less steep.

5.3.4.4 Evaluation of the extent of nasal drug absorption

Under certain conditions, model simulations indicated that extensive nasal drug absorption might be present after nose-only exposure. This is perhaps not surprising as intranasal drug delivery is a common route of drug administration, both for local- and systemic drug delivery. Clearly a high degree of nasal absorption is desired when the aim is to induce systemic effects. Hence, numerous research groups have investigated what factors influence nasal drug absorption. For simplicity, these factors are often divided into three different categories: 1) nasal physiological factors (system-specific parameters), 2) characteristics of the drug (drug-specific parameters), and 3) properties of the formulation (formulation-specific parameters) [181].

System-specific parameters for instance include blood-flow, nasal MCC, enzymatic degradation and transporters [181]. Neither enzymatic degradation nor transporters are included in this model structure. Model simulations showed that a higher nasal MCC and a lower blood-flow decreased the extent of nasal drug absorption (simulations not shown). Noteworthy is that some drugs might cause vasoconstriction and hence decrease the blood-flow. It has been shown that such drugs can inhibit the nasal absorption [182], which thus is in line with the model predictions. If the drug of interest is expected to induce vasodilatation or vasoconstriction, the nasal blood flow can thus be changed in the model to investigate the effect on nasal drug absorption.

Drug-specific parameters include, for instance, solubility and permeability. As the nasal membrane primarily has a lipophilic character, a lower permeability can be

expected from hydrophilic drugs [183]. Conversely, a highly lipophilic drug may have a low water solubility, which would slow down the dissolution rate of drug particles in the aqueous environment in the nose [181]. As such compounds remain in a solid state for a longer time period they are more prone to be removed by the nasal MCC. The extent of nasal drug absorption is thus determined by complex interactions between several different parameters. In order to investigate how changes in the solubility (C_s) and the permeability (P) affect the extent of nasal absorption following nose-only exposure, the system was simulated 625 times using different combinations of these two parameters. More specifically, the cumulative amount of drug absorbed from the nose (A_{nose}) after 24 h was simulated for a broad range of C_s and P after an LDD of 11.3 nmol/kg. C_s varied between 0.1 and 50 µM and P varied between 0.1×10^{-6} and 50×10^{-6} cm/s. The parameter values were subsequently selected from a logarithmic scale. Figure 5.14 shows the interplay between C_s and P.

The same exercise was carried out for the lung. As can be seen in figure 5.15, the impact of C_s and P was less pronounced in the lung. This can primarily be attributed to: 1) $k_{mcc} = 0$ in the peripheral lung region, i.e. all drug deposited in this region will be absorbed as $t \rightarrow \infty$ provided $C_s \neq 0$ and $P \neq 0$, and 2) k_{mcc} is several-fold slower in the central lung as compared to the nose. The second model feature translates to a longer pulmonary- than nasal residence time, i.e. the time during which drug can absorbed will be longer in the lung.

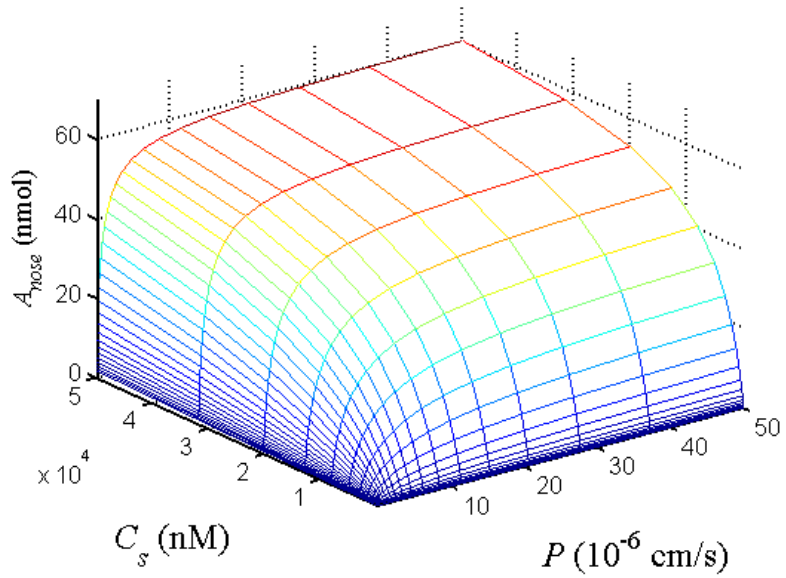

Figure 5.14 The amount of drug absorbed from the nose (A_{nose}) after nose-only exposure was simulated for different combinations of two parameters: permeability (P) and solubility (C_s).

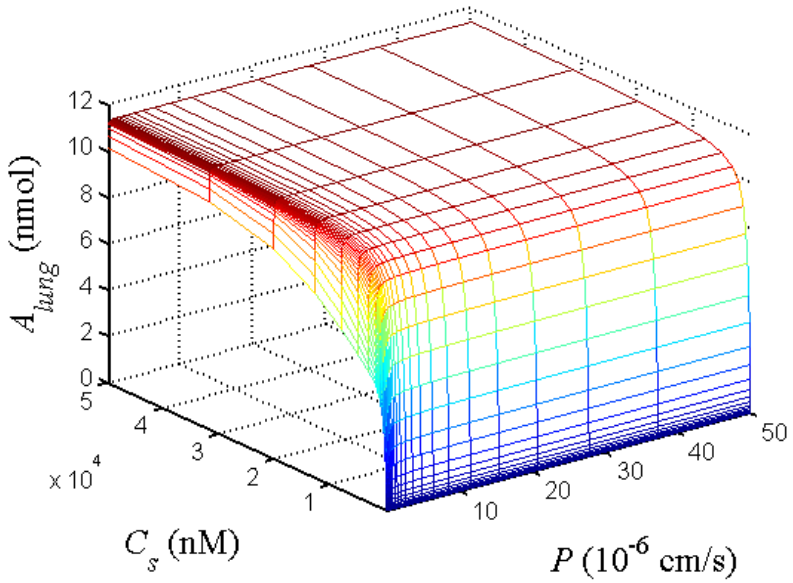

Figure 5.15 The amount of drug absorbed from the lung (A_{lung}) after nose-only exposure was simulated for different combinations of two parameters: permeability (P) and solubility (C_s).

5.3.4.5 Impact of permeability in the central lung

Absorption of dissolved drug from the lung to the systemic circulation is generally assumed to be slower from the tracheobronchial region as compared to the alveolar region. This has been attributed both to the lower blood perfusion and to the thicker airway walls in this region [15]. The proposed differences in regional absorption rates have also been demonstrated experimentally after regional administration of solutions [184,185]. Furthermore, the differences in regional perfusion rates and surface area alone were shown to have a pronounced impact on the pulmonary absorption by a simulation study described in section 5.3.4.3.

In [186], the drug permeability (P) is described as a constant that depends on the diffusion coefficient (D) of the drug in the barrier, the thickness of the barrier (h) and the partition coefficient into the barrier (γ):

$$P = \frac{\gamma D}{h}. \qquad (5.55)$$

Moving from the trachea to the alveolar region, both the type of epithelium and its thickness will change. In humans, the thickness of the epithelium decreases from 58 µm in the bronchi to 0.1-0.2 µm, in the alveoli [11]. In rats, the bronchi epithelium thickness is 13 µm [29]. From eq. 5.55 it thus seems plausible that P will not be constant throughout the lung. Furthermore, it specifies that region-specific knowledge about both γ and h is needed for proper scaling of P in different lung regions. To the best of my knowledge, such data is currently not available. New experimental methodologies would be desired to further investigate this issue. Nevertheless, as the thickness of the epithelium gradually decreases when moving

distally throughout the lung, it is plausible that this gradual decrease in epithelium thickness is also applicable for *P*.

Three different scenarios were simulated in order to investigate what impact a lower *P* in the central lung region would have on the pulmonary drug disposition if the peripheral *P* was kept high. The *LDD* was set to be 100 nmol/kg and the drug- and formulation-specific parameters of FP specified in table 5.4 were used in all three scenarios, whereas P_{app} in the central lung region varied accordingly: 1) P_{app}, 2) $P_{app}/10$, and 3) $P_{app}/100$. That is, the resulting central P_{app} in each of the three simulations was 46.9×10^{-6} cm/s (high *P*), 4.69×10^{-6} cm/s (moderate *P*) and 0.469×10^{-6} cm/s (low *P*), respectively.

As can be understood from eq. 5.1 (the ODE describing the flux to/from the systemic circulation), a lower *P* would result in a slower permeation into the lung tissue. The result of the slower permeation is an increased drug concentration in the ELF (C_{ELF}, fig. 5.16a). As a higher C_{ELF} would slow down the dissolution rate (eq. 5.20) this would in turn lead to an increased retention time of drug in the lung (fig. 5.16b). The latter example thus also serves to demonstrate that *P* is an important parameter for accurately predicting the lung retention of slowly dissolving drugs. The profile of RO_c would also change (fig. 5.16c), whereas the impact on RO_{sp} would be less pronounced (fig. 5.16d). Briefly, according to model simulations a lower *P* in the central lung region might lead to a prolonged lung-retention. A lower *P* would also have an effect on the C_p-profile (fig. 5.16e), where simulations show that *P* is an important parameter for determining both the amplitude of the maximum C_p (C_{max}) and the time point when it occurs (t_{max}).

Considering the regional differences with respect to both the type of epithelium as well as its thickness, differences in *P* are highly likely. As previously mentioned in

section 5.3.4.3, further research is required in this area to increase the understanding of regional pulmonary permeability as well as the feasibility to use different *in vitro* models for the description thereof. The P_{app} obtained from CaCo-2 experiments is more likely to reflect the *P* in the central lung than the peripheral lung owing to the characteristics of the cells. Simulations using the drug- and formulation-specific input parameters for FP (table 5.4) showed that a 100-fold higher *P* in the peripheral region were indistinguishable from the earlier simulations (simulations not shown since they were indistinguishable from fig. 5.5). Hence, the model validation step has not been biased by using the same *P* throughout the lung. Nevertheless, the final model structure presented in this thesis, which also allows for repeated dosing, will have a 100-fold higher permeability in the peripheral lung. The primary rationale for scaling by a factor of 100 is based on the differences in epithelium thickness.

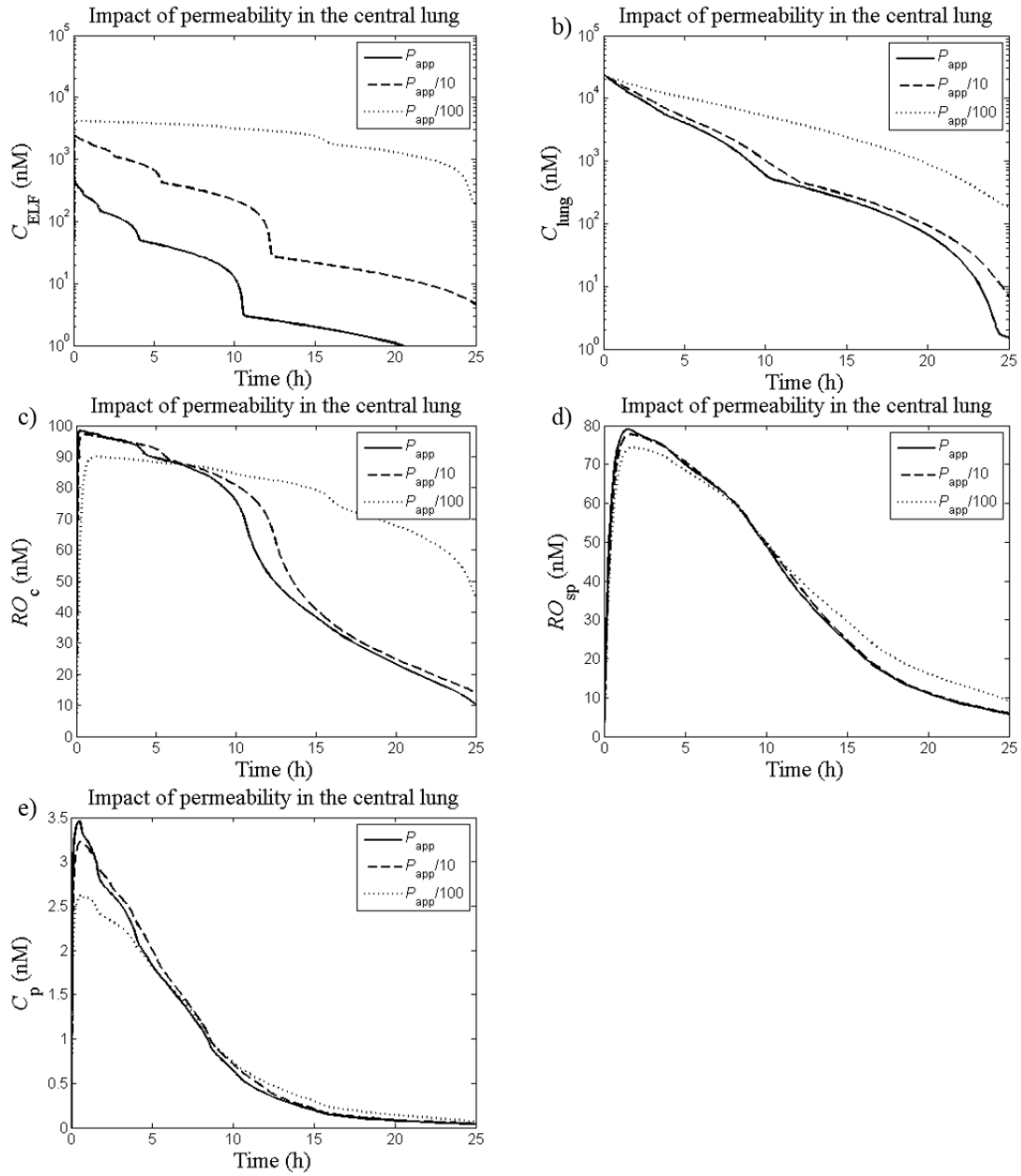

Figure 5.16 Three different scenarios were simulated to investigate what impact a lower permeability in the central lung would have on the pharmacokinetics. The lung deposited dose was set to 100 nmol/kg and the drug- and formulation-specific parameters of FP specified in table 5.4 were used in all three scenario, whereas the apparent permeability (P_{app}) in the central lung varied accordingly: 1) P_{app} (solid line), 2) P_{app}/10 (dashed line), and 3) P_{app}/100 (dotted line). The following model outputs were simulated: a) drug concentration in the epithelial lining fluid (C_{ELF}), b) total lung concentration of drug (C_{lung}), c) receptor occupancy in the central lung (RO_c), d) receptor occupancy in the spleen (RO_{sp}), and e) plasma concentration of drug (C_p).

5.3.5 Repeated dosing

Up until now, the simulations have aimed to explore the fundamental principles for systemic and local pharmacokinetics after inhaled drug delivery. Single dosing has thus been sufficient to address these questions. Nevertheless, in the clinical situation, inhalation is often used to treat chronic diseases such as chronic obstructive pulmonary disease (COPD) and asthma. It is therefore essential to understand the effects of long-term use of inhaled drug therapy. Repeated dosing was thus implemented to enable theoretical investigations of how chronic dosing affects the PK and PK/PD of inhaled drugs. Previously, the regional deposition fractions for the different regions (nose, central lung and peripheral lung) and the relevant aerodynamic diameters have been extracted from Lee *et al*. [65]. To enable simulations of repeated dosing of any particle size classes, the model by Lee *et al*. [65] was implemented in MATLAB and integrated with the lung simulation model. The technical implementation of this deposition model is described in the section 5.3.5.2 below.

5.3.5.1 Technical implementation of repeated dosing

Repeated dosing was implemented in MATLAB by adding a new set of 24 ODEs describing the change of the radius r_{ij} (where $i \in \{1, \ldots, 8\}$ and $j \in \{1, 2, 3\}$) (eq. 5.25) for each dosing occasion k, where $k \in \{1, \ldots, n\}$. That is, $k = 1$ assigns the first dose, $k = 2$ assigns the second dose and so on. The number of states in the PBPK model was updated automatically by having k as an input to the function defining the coupled ODEs.

Except for $k = 1$, the initial conditions for the set of ODEs describing the change of r_{ij} for each dosing occasion k were initially set to 0. The parameter τ was used to

define time span between dosing, which is often referred to as the dosing interval. A for-loop was used to enable simulations of repeated dosing by iteratively solving the coupled ODE-system. The interval of integration for the ODE-solver was set to [(k-1)×τ, k×τ]. At each iteration k, the initial condition for each state y was updated to the solution of y at $t = k\times\tau$. The initial conditions for the set of ODEs describing the change of r_{ij} for the following dosing occasion (k+1) was changed from 0 to the geometric radius corresponding to each particle size class i. The entire code is attached as Appendix A. For clarity, all PBPK model ODEs are summarised in Appendix C.

5.3.5.2 Technical implementation of a deposition model

The deposition model by Lee *et al*. was implemented in MATLAB and the entire code is attached as Appendix B. Details of the model are provided by the authors in the original paper [65] whereas this subsection aims to define the most important equations as well as to specify the breathing conditions and the anatomical model used in the simulations.

The anatomical model structure is presented in table 5.8. To summarise, each lung generation i is described to consist of a number of cylindrical tubes (N_i), which are characterised by a length (L_i), a diameter (D_i), an average angle with gravity (φ_i) and a branching angle (θ_i). In this model, the lung is divided into three regions: 1) the extrathoracic region (i = 1, 2), 2) the tracheobronchial region (i = 3, …, 18), and 3) the alveolar region (i = 19, …, 26). The alveolar region is also characterised by a so-called "effective airway diameter" (D_{eff}), which is added to account for the alveoli volume. In contrast to the airways, the nose is described as an artificial rectangular channel as suggested by Schmid *et al.* [66]. Unless stated differently, the normal

breathing conditions specified by Lee *et al*. were used with a tidal volume (V_T) of 2.6 cm^3 and breathing frequency (f_{br}) of 97.4 min^{-1}. As the anatomical data in table 5.6 refers to a lung at nearly full inflation, the dimensions were scaled to conform to a more realistic average respiration lung volume (*ARLV*). This was done by multiplying L_i and D_i with a factor f_{scale} [65], which was defined as

$$f_{scale} = \left(\frac{ARLV}{TLC} \right)^{1/3} = \left(\frac{FRC + 0.5V_T}{TLC} \right)^{1/3} = \left(\frac{0.4TLC + 0.5V_T}{TLC} \right)^{1/3}, \quad (5.56)$$

where *TLC* is the total lung capacity, *FRC* is the functional residual capacity and V_T is the tidal volume. As can be understood from eq. 5.56, it is assumed that

$$FRC = 0.4TLC \quad (5.57)$$

and

$$ARLV = FRC + 0.5V_T = 0.4TLC + 0.5V_T, \quad (5.58)$$

where *TLC* is calculated as suggested by Yeh *et al*. 1979 [172]:

$$TLC = 0.032BW^{1.05}, \quad (5.59)$$

where *BW* is the body weight in gram. In line with Lee *et al*., the *BW* was set to be 381 g. Thus, given V_T = 2.6 cm^3 and *BW* = 381 g, f_{scale} was calculated to be 0.7825. The length of the last ventilated generation is subsequently adapted such that V_T matches the total volume of the anatomical model [66].

The average inspiratory flow rate (Q_{in}) was calculated as described by Schmid *et al*. [66]

$$Q_{in} = 2V_T f_{br} \ . \tag{5.60}$$

The flow pattern was assumed to be constant (i.e. a square wave flow pattern), the flow rate (Q_i) and the average velocity in each generation i (u_i) were subsequently calculated as [187]

$$Q_i = \frac{Q_{in}}{N_i}, \tag{5.61}$$

and

$$u_i = \frac{Q_i}{A_i}, \tag{5.62}$$

respectively. In eq. 5.62 A_i denotes the cross-sectional area of generation i, i.e.

$$A_i = \begin{cases} L_1 W_1 & i = 1 \\ \pi\left(\frac{D_i}{2}\right)^2 & i \geq 2 \end{cases} \ . \tag{5.63}$$

This model accounts for deposition by three different mechanisms: 1) inertial impaction, 2) gravitational sedimentation, and 3) Brownian diffusion. The deposition probability by inertial impaction (DE_{im}) was calculated according to Zhang *et al.* 1997 [188]:

$$DE_{im,i} = \begin{cases} 0.000654 e^{55.7 Stk_i^{0.954}} \mathrm{Re}_i^{1/3} \sin\theta_i & \text{for } Stk_i < 0.04 \\ (0.19 - 0.193 e^{-9.5 Stk_i^{1.565}}) \mathrm{Re}_i^{1/3} \sin\theta_i & \text{for } Stk_i \geq 0.04 \end{cases} \tag{5.64}$$

with

$$Stk_i = \frac{\rho_0 d_a^2 u_i}{9\eta D_i} \tag{5.65}$$

and

$$\mathrm{Re}_i = \frac{\rho_a D_i u_i}{\eta}, \tag{5.66}$$

where Stk_i is Stokes number in generation i, Re_i is Reynold number of the airflow in generation i, ρ_0 is the unit particle density (1 g/cm^3), d_a is the aerodynamic diameter, u_i is the mean air flow velocity in generation i, η is the viscosity of air and ρ_a is the air density. The deposition probability by gravitational sedimentation (DE_s) was calculated according to Thomas 1958 [67]:

$$DE_{s,i} = \frac{2}{\pi}\left(2\varepsilon(1-\varepsilon^{2/3})^{1/2} - \varepsilon^{1/3}(1-\varepsilon^{2/3})^{1/2} + \arcsin(\varepsilon^{1/3})\right) \tag{5.67}$$

with

$$\varepsilon = \frac{3v_g t_i \sin\varphi_i}{4D_i}, \tag{5.68}$$

$$v_g = \frac{\rho_0 d_a^2 g C_d}{18\eta}, \tag{5.69}$$

and

$$C_d = 1 + \frac{\lambda}{d_a}\left(2.514 + 0.8e^{-0.55\frac{d_a}{\lambda}}\right) \tag{5.70}$$

where v_g is the gravitational settling velocity, t_i is the mean residence time in generation i, g is the gravitational acceleration, C_d is the Cunningham slip correction factor and λ is the mean free path of air molecules. In the alveolar region, $D_{eff,i}$ was

used as the airway diameter in eq. 5.68. The deposition probability by Brownian diffusion (DE_d) was calculated according to Ingham 1975 [189]:

$$DE_{d,i} = 1 - 0.819e^{-14.63\sigma} - 0.0976e^{-89.22\sigma} - 0.0325e^{-228\sigma} - 0.0509e^{-125.9\sigma^{2/3}} \quad (5.71)$$

with

$$\sigma = \frac{D_{mol} L_i}{u_i D_i^2} \quad (5.72)$$

and

$$D_{mol} = \frac{k_B T C_d}{3\pi\eta d_a}, \quad (5.73)$$

where D_{mol} is the Brownian diffusion coefficient, k_B is the Boltzmann constant and T is the absolute temperature. In the alveolar region, $(D_i+D_{eff,i})/2$ was used as airway diameter in eq. 5.72 [65]. The authors' rationale behind this choice was that while the alveoli increases the surface area for deposition, the larger effective diameter of the airway will also lead to a decreased deposition by diffusion.

The deposition equations above are applicable for all generations where $i \geq 2$, i.e. the nasal deposition probabilities are calculated by other equations. The nasal deposition probability by inertial impaction was approximated according to an empirical equation by Zhang and Yu 1993 [190]:

$$DE_{im,1} = \left(\frac{\left(d_a^2 Q\right)^\alpha}{C + \left(d_a^2 Q\right)^\alpha} \right)^\beta \quad (5.74)$$

where d_a is the aerodynamic diameter in µm, Q is the flow rate in cm^3/s and α, β and C are constants estimated by Zhang and Yu [190]. For the rat, these constant values are 2.553, 0.627 and 10^5, respectively. Except for eq. 5.74, MKS-units are used for all equations. The nasal deposition probability by diffusion was calculated as suggested by Cheng 1993 [191]:

$$DE_{d,1} = \begin{cases} 1.526\mu^{2/3} - 0.15\mu - 0.0342\mu^{4/3} & \text{for } \mu < 0.05 \\ 1 - \begin{pmatrix} 0.9104e^{-2.8278\mu} + 0.0531e^{-32.147\mu} \ldots \\ + 0.01528e^{-93.475\mu} + 0.00681e^{-186.805\mu} \end{pmatrix} & \text{for } \mu \geq 0.05 \end{cases} \quad (5.75)$$

with

$$\mu = \frac{8D_{mol}LW}{3QH}, \quad (5.76)$$

where L, W and H are the length, width and height of the nasal passage, respectively. The nasal deposition by gravitational sedimentation was assumed to be negligible compared to the other two deposition mechanisms (eqs. 5.74-5.75).

The resulting deposition probability in generation i (P_i) was subsequently given by [68]

$$P_i = 1 - (1 - DE_{im,i})(1 - DE_{s,i})(1 - DE_{d,i}). \quad (5.77)$$

Deposition in generation i during inhalation (DE_i^{in}) was calculated by

$$DE_i^{in} = f_i P_i \sum_{j=i}^{i\max} V_j \quad (5.78)$$

with

$$f_i = \prod_{j=1}^{i-1}(1-P_j) \tag{5.79}$$

where V_j is the volume of generation j and i_{max} is the last ventilated generation. Deposition in generation i during exhalation (DE_i^{ex}) was calculated by

$$DE_i^{ex} = f_{i+2}V_{i+1}P_i + P_i \sum_{j=i+2}^{i\max}\left(f_{j+1}V_j \prod_{k=i+1}^{j-1}(1-P_k) \right). \tag{5.80}$$

The aforementioned equation can be divided into two parts: 1) the first term in eq. 5.80 indicates the deposition (during exhalation in generation i) of particles that were in generation i + 1 at the end of inhalation, 2) the second term specifies the deposition of particles that were between generations i + 2 to i_{max} at the end of inhalation. Since the breath hold time between inhalation and exhalation is short compared to the breathing cycle, Lee *et al*. chose to assume that there was no deposition during breath holding. The resulting total deposition during a breath (DE_i^{tot}) is thus given by

$$DE_i^{tot} = DE_i^{in} + DE_i^{ex}, \tag{5.81}$$

and the deposition in a lung region (DE_{region}) between region j and k is then defined as

$$DE_{region} = \sum_{i=j}^{k}(DE_i^{in} + DE_i^{ex}). \tag{5.82}$$

Studies relying on computational simulations have suggested that penetration of particles into the alveoli not only rely on diffusion and sedimentation but there is an

additional mechanism: convective transport. In the absence of realistic models for describing this phenomenon Lee *et al*. assumed that deposition enhancement by this mechanism occurs for particles with d_a in the range $0.02 \leq d_a \leq 2.0$ μm. This was mathematically described as

$$DE_i^{tot} = \begin{cases} f_{conv} DE_i^{tot} & \text{for } i \geq 19 \\ DE_i^{tot} & \text{for } i < 19 \end{cases}, \tag{5.83}$$

with

$$f_{conv} = \begin{cases} 1 + \dfrac{\left(\log_{10}(d_a) - \log_{10}(2)\right)\left(\log_{10}(d_a) - \log_{10}(0.02)\right)}{2\left(\log_{10}(0.1) - \log_{10}(2)\right)\left(\log_{10}(0.1) - \log_{10}(0.02)\right)} & \text{for } 0.02 \leq d_a \leq 2 \\ 1 \quad \text{for } d_a < 0.02 \text{ or } d_a > 2 \end{cases}. \tag{5.84}$$

The resulting deposition fraction (*df*) was subsequently obtained by dividing the amount deposited (eq. 5.83) by the amount inhaled. The resulting *df* for the extrathoracic region (df_{ET}), tracheobronchial region (df_{TB}), alveolar region (df_{AL}) and all regions (df_{tot}) are shown in figure 5.17. The result of varying V_T (2.6, 3.9 and 5.2 cm^3) was investigated by calculating *df* for the three regions mentioned above while keeping f_{br} constant (97.4 min^{-1}). As can be seen in figure 5.18, the effect of changing V_T was most pronounced in the alveolar region. Increasing V_T has an effect both on the flow rate (eqs. 5.60 and 5.61) and the ventilation depth. In contrast, the f_{br} only affects the flow rate (eqs. 5.60 and 5.61). Hence, changing f_{br} (97.4, 195 and 390 min^{-1}) while keeping V_T constant (2.6 cm^3) should have a slightly different effect on *df*, which is shown in figure 5.19.

As can be understood from the equations governing the deposition by the three included deposition mechanisms, different mechanisms will be dominant in different

regions of the lung depending on *e.g.* the lung anatomy (D_i, L_i, φ_i and θ_i), regional flow velocity (u_i) and residence time (t_i). To investigate the importance of different mechanisms across the lung, the deposition probability by each mechanism was calculated for d_a in the range $0.001 \leq d_a \leq 10$ µm. Fig. 5.20a-c shows how DE_{IM}, DE_s and DE_D for each particle size changes with the lung generations. Similarly, figure 5.21a-c shows how DE_{IM}, DE_s and DE_D for each generation changes with d_a. Inertial impaction is particularly important in the tracheobronchial region (fig. 5.20a) with the exception of generation 2-3 where the branching angle $\theta = 0^{\circ}$, which precludes deposition by this mechanism. Fig. 5.21a highlights that larger particles are likely to deposit by inertial impaction, whereas small particles are unaffected. The latter is caused by small particles having low Stokes number (eq. 5.65), which implies smaller inertial effects and the particles thus tend to follow the streamlines. Gravitational sedimentation is an important mechanism for larger particles in the alveolar region (fig. 5.20b and fig 5.21b). This is an effect of the probability of this mechanism increasing with t_i, which is longer in the distal lung regions, and v_g, which increases with d_a (eq. 5.69). Brownian diffusion on the other hand is the dominant deposition mechanism for smaller particles (fig. 5.21c), especially in the alveolar region where u_i is lower (fig. 5.20c).

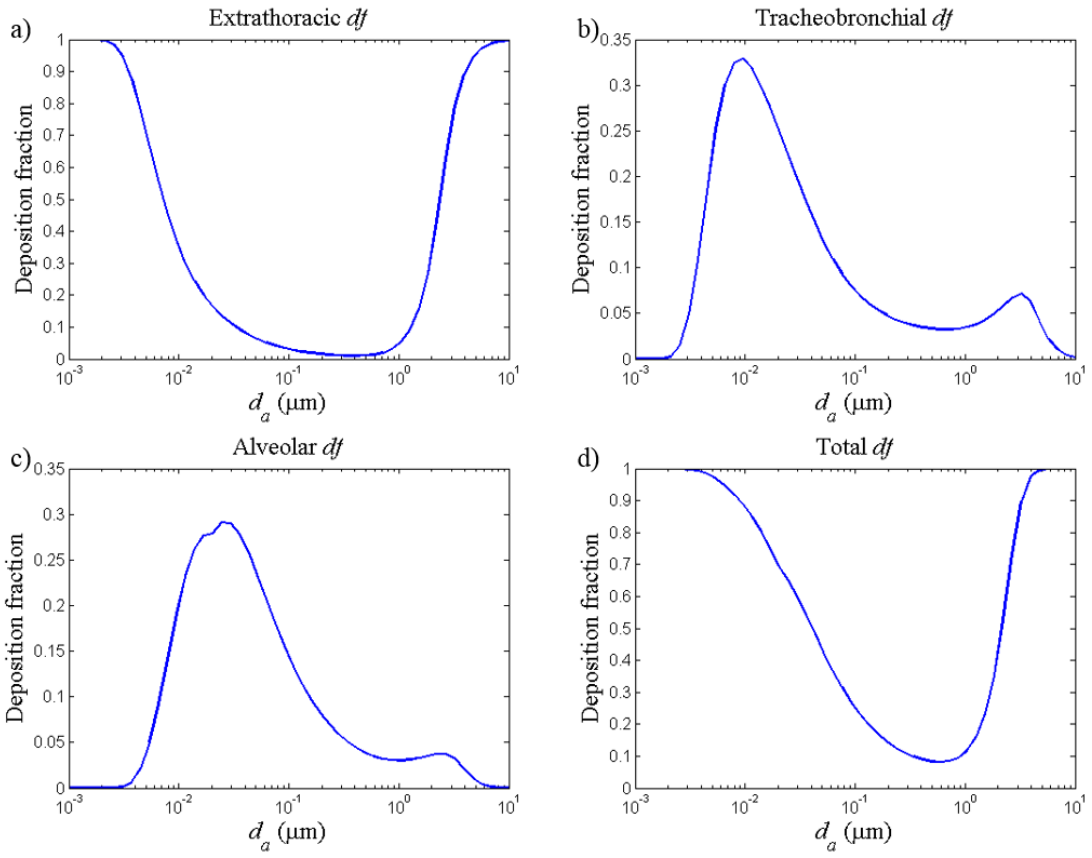

Figure 5.17 The deposition fractions (*df*) in a) the extrathoracic region, b) the alveolar region, c) the tracheobronchial region, and d) all three regions, i.e. total *df*, for normal breathing conditions (V_T = 2.6 cm^3 and f_{br} = 97.4 min^{-1}). The predictions were made after implementing the deposition model by Lee *et al*. [65]

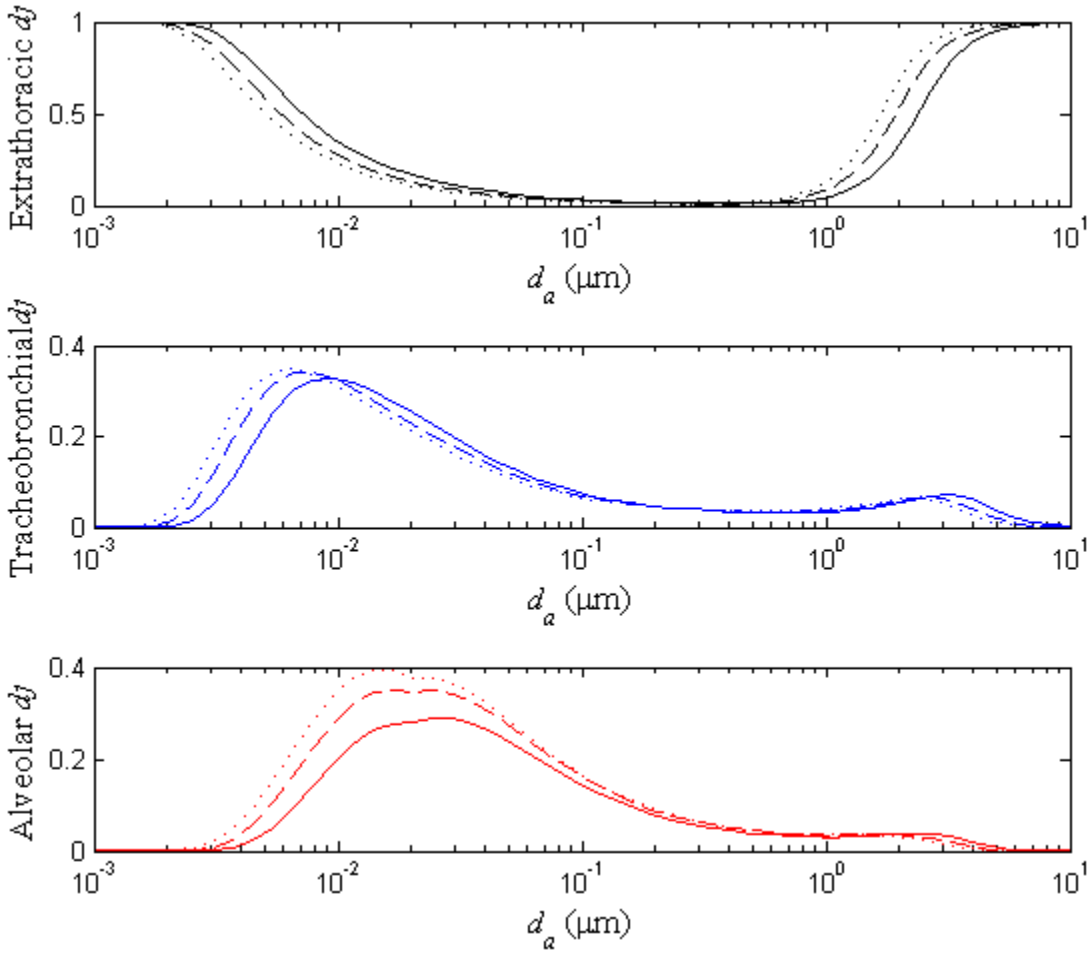

Figure 5.18 The effect of the tidal volume (V_T) on the deposition fraction (*df*) was investigated by simulating *df* for different V_T: 2.6 (solid line), 3.9 (dashed line) and 5.2 cm^3 (dotted line). The *df* was simulated in different regions: the extrathoracic- (upper panel), tracheobronchial- (middle panel) and alveolar region (lower panel).

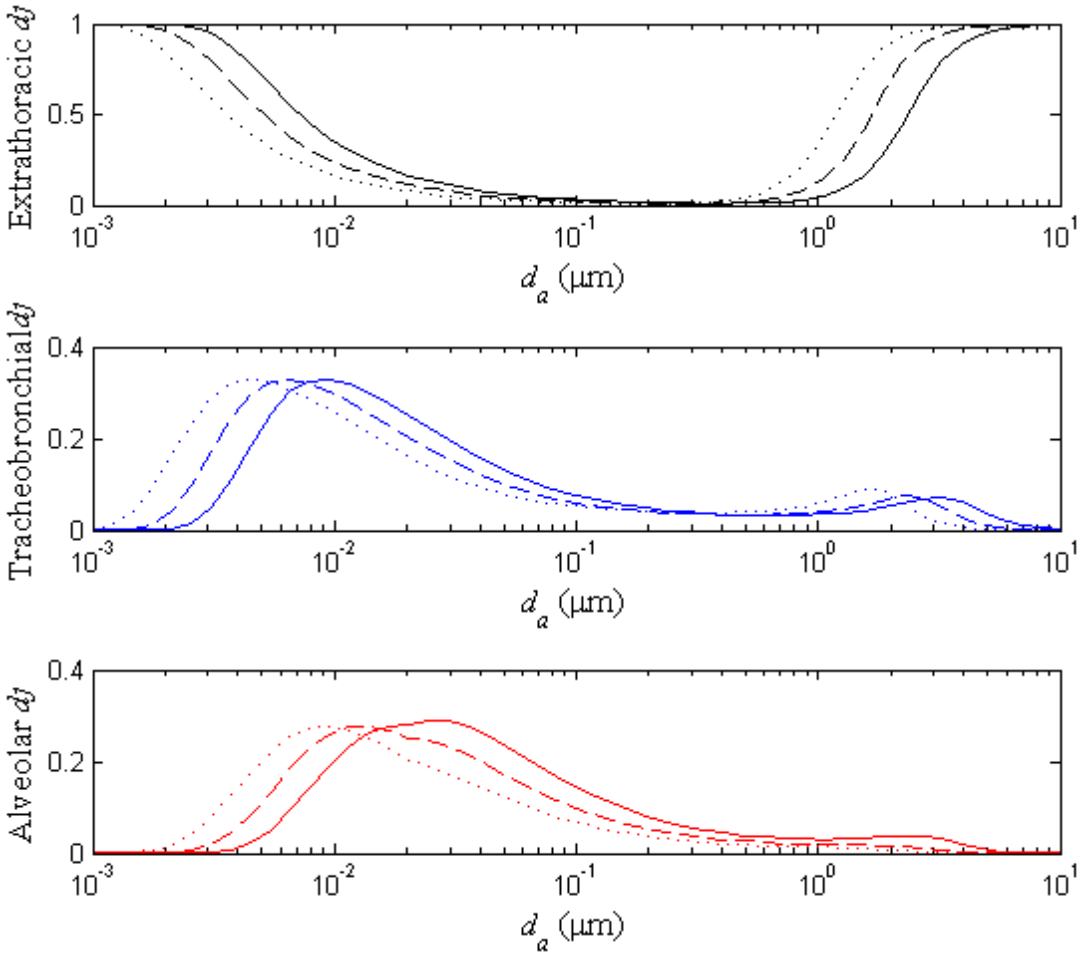

Figure 5.19 The effect of the breathing frequency (f_{br}) on the deposition fraction (*df*) was investigated by simulating *df* for different f_{br}: 97.4 (solid line), 195 (dashed line) and 390 min^{-1} (dotted line). The *df* was simulated in different regions: the extrathoracic- (upper panel), tracheobronchial- (middle panel) and alveolar region (lower panel).

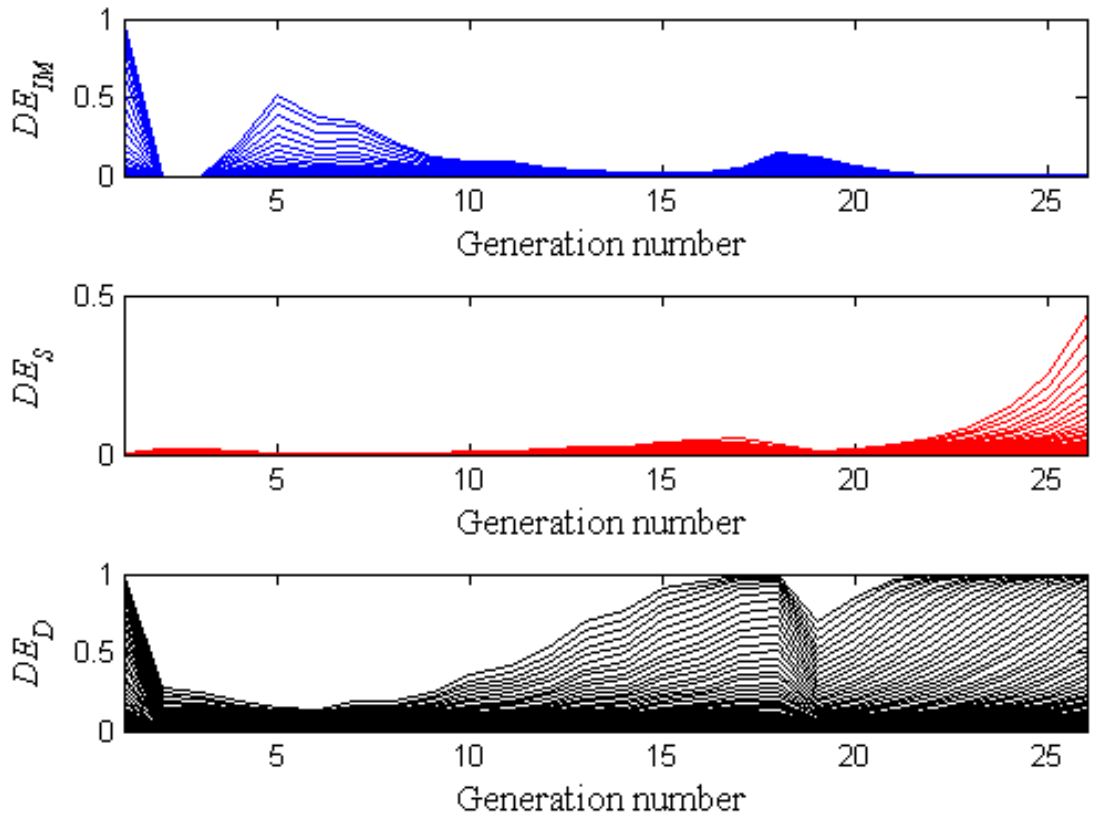

Figure 5.20 The probability of deposition by three deposition mechanisms: inertial impaction (DE_{IM}, upper panel), gravitational sedimentation (DE_S, middle panel) and Brownian diffusion (DE_D, lower panel) was investigated for each airway generation i where $i \in \{1, \ldots, 26\}$. Each line represents the deposition probability for a particle with a certain aerodynamic diameter (d_a), where d_a is in the range $0.001 \leq d_a \leq 10$ µm.

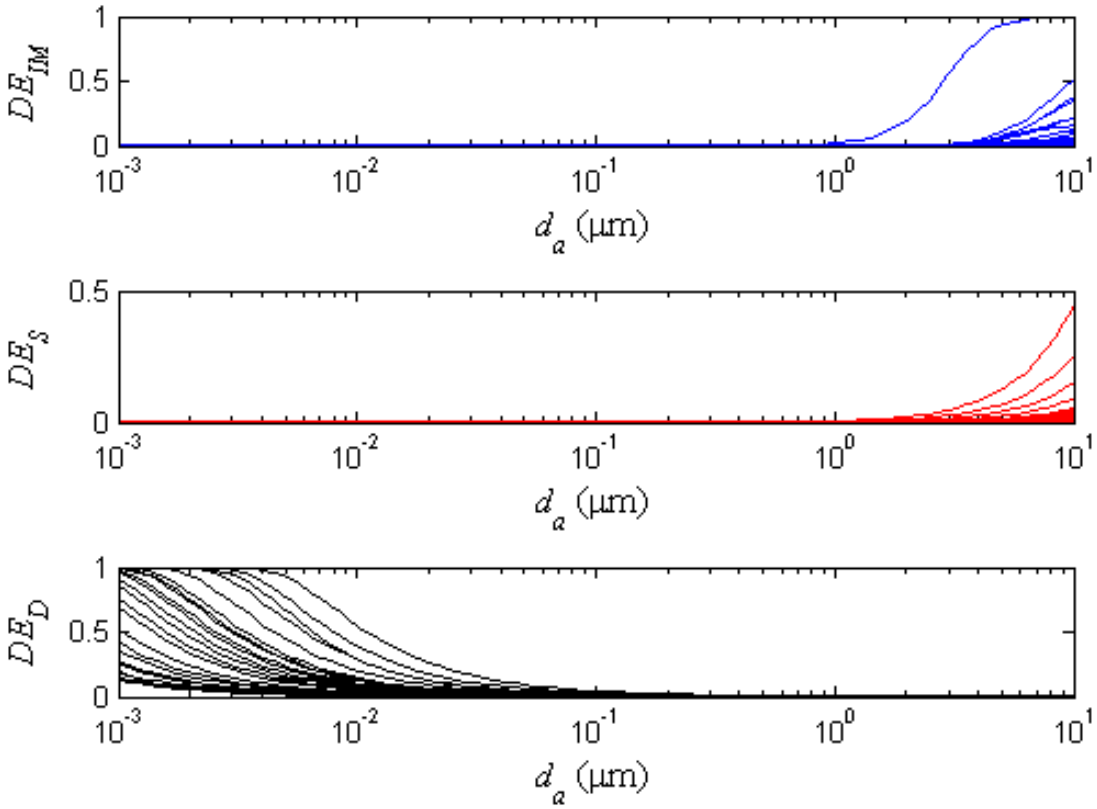

Figure 5.21 The probability of deposition by different deposition mechanisms: inertial impaction (DE_{IM}, upper panel), gravitational sedimentation (DE_S, middle panel) and Brownian diffusion (DE_D, lower panel) was investigated for a range of aerodynamic diameters (d_a) in the range $0.001 \leq d_a \leq 10$ µm. Each line represents the deposition probability in an airway generation i where $i \in \{1, \ldots, 26\}$.

Table 5.8 Lung structure of a rat lung at 81 postnatal days [65].

i	N_i	L_i (cm)	D_i (cm)	$D_{eff,i}$ (cm)	φ_i (◦)	θ_i (◦)
1	1	1.95	0.016[a], 5.7[b]		90	0
2	1	3	0.2700	0.2700	90	0
3	1	2.68	0.3153	0.3153	86	0
4	2	0.8079	0.2651	0.2651	90	15
5	3	0.3781	0.2343	0.2343	86	43
6	5	0.176	0.2030	0.2030	71	36
7	8	0.208	0.1630	0.1630	59	32
8	14	0.117	0.1340	0.1340	58	22
9	23	0.114	0.1230	0.1230	61	16
10	38	0.13	0.1120	0.1120	58	17
11	65	0.099	0.0950	0.0950	55	20
12	109	0.091	0.0870	0.0870	58	15
13	184	0.096	0.0780	0.0780	61	16
14	309	0.073	0.0700	0.0700	56	17
15	521	0.075	0.0580	0.0580	56	17
16	877	0.06	0.0490	0.0490	58	22
17	1477	0.055	0.0360	0.0360	57	24
18	2487	0.035	0.0200	0.0200	58	44
19	4974	0.0288	0.0189	0.0879	60	45
20	9948	0.0263	0.0179	0.0857	60	45
21	19896	0.0263	0.0170	0.0838	60	45
22	39792	0.024	0.0162	0.0820	60	45
23	79584	0.0219	0.0155	0.0804	60	45
24	159168	0.0201	0.0149	0.0789	60	45
25	318336	0.0184	0.0143	0.0776	60	45
26	636672	0.0168	0.0138	0.0764	60	45

Abbreviations: i is the lung generation number; N_i is the number of airways in generation i; L_i and D_i are the airway length and diameter, respectively; $D_{eff,i}$ is the effective diameter also considering the alveolar volume; φ_i and θ_i are the gravity and the branching angles, respectively. Generations 1, 2 and 3 represent the nose, the pharynx and the trachea, respectively. The nasal passage is described as a rectangular channel where the height and width are indicated by the superscripts a and b, respectively. The tracheobronchial and the alveolar region are defined as $i = 3, \ldots, 18$ and $i = 19, \ldots, 26$, respectively.

5.3.5.3 Repeated dosing of poorly and highly soluble compounds

As many inhaled drugs have a poor solubility and only a small volume of ELF is available for dissolution, an accumulation of drug might be expected after repeated dosing of this compound class. To theoretically explore this, repeated nose-only exposure (LDD_k = 100 nmol/kg, where $k \in \{1, \ldots, 5\}$ and τ = 24 h) was simulated for a poorly (C_s = 0.5 µM) and a highly soluble compound (C_s = 50 µM), respectively, using a moderate permeability (P_{app} = 5×10^{-6} cm/s). Otherwise, the drug- and formulation-specific properties for FP (table 5.4) were used. As mentioned in section 5.3.4.5, the permeability is expected to be lower centrally. The P was therefore set be a hundredfold higher in the peripheral lung as compared to the central lung (i.e. the peripheral P was set to $100\times P_{app}$). Since nasal absorption is absent for orally inhaled compounds in the clinic, the nasal blood flow was set to 0 to decouple the nose from the system and thereby mimic the clinical situation.

As can be seen in figure 5.22a, all solid drug particles of the poorly soluble drug will not be dissolved nor be removed by MCC during one dosing interval. Hence, an accumulation of solid drug particles will take place. Noteworthy is that the system appears to be close to steady-state conditions after five dosing intervals. In contrast, no solid drug remains at the end of one dosing interval for the highly soluble compound (fig. 5.22b). Obviously, the same patterns are seen in the simulations of the total lung concentrations (fig. 5.22c-d). For the poorly soluble compound, C_{ELF} in the central lung will be fairly high during the entire dosing interval (fig. 5.22e). A small accumulation is also present in the ELF, potentially leading to a slightly slower dissolution rate for repeated as compared to single dosing (eq. 5.20). For highly soluble compounds, the corresponding concentrations in the central ELF will initially be close to C_s and then rapidly decline (fig. 5.22f). As an accumulation does not take

place in the ELF, the dissolution rate will not be different for repeated and single dosing. Obviously, the same patterns are found in the plasma profiles. That is, a small accumulation is seen for the poorly soluble drug (fig. 5.22g), but not for the highly soluble drug (fig. 5.22h). Clearly, the different dissolution profiles are reflected in the plasma PK, where the poorly soluble compound has a flat PK-profile with small fluctuations. In contrast, the highly soluble compound has a relatively high peak concentration, which then rapidly declines leading to large fluctuations in the plasma profile. The different solubilities also lead to diverse receptor occupancy profiles. The poorly soluble drug only has small fluctuations in the receptor occupancy profile. Moreover, lung-selectivity is obtained over the entire dosing interval (fig. 5.22i). In contrast, the highly soluble compound has large fluctuations in receptor occupancy and lung-selectivity is only transiently obtained directly after dosing (fig. 5.22j).

There are few data available for validating predictions of PK after repeated nose-only exposure. Nevertheless, unpublished AstraZeneca data of one poorly soluble compound confirm that the systemic exposure, in terms of the maximum plasma concentration (C_{max}) and $AUC_{0\text{-}24h}$, was higher after repeated dosing compared to after a single dose. In line with the predictions, no difference in systemic exposure was found after single and repeated dosing of a highly soluble compound [164].

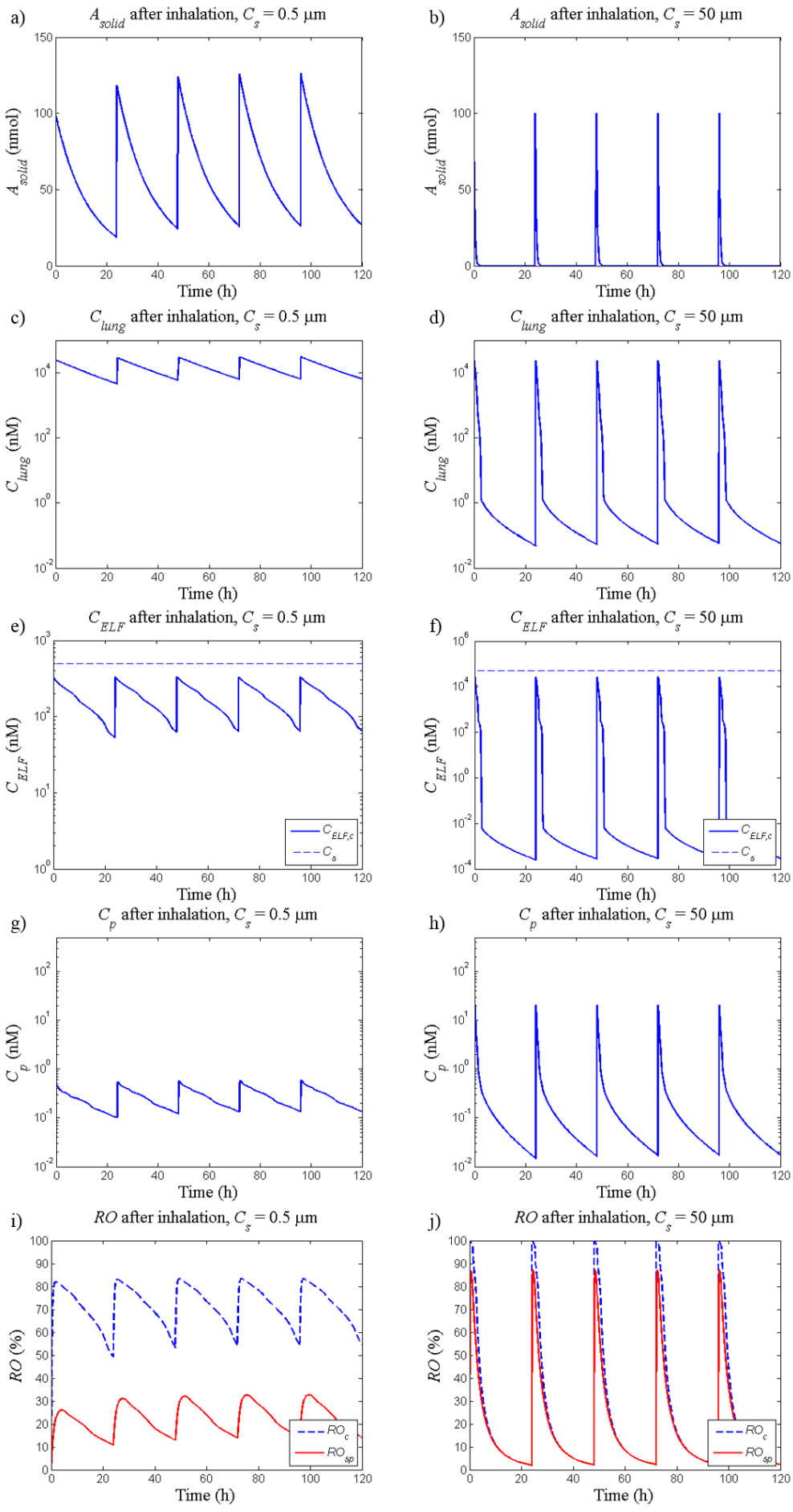
a)
A_{solid} after inhalation, C_s = 0.5 µm
A_{solid} (nmol)
Time (h)
b)
A_{solid} after inhalation, C_s = 50 µm
A_{solid} (nmol)
Time (h)
c)
C_{lung} after inhalation, C_s = 0.5 µm
C_{lung} (nM)
Time (h)
d)
C_{lung} after inhalation, C_s = 50 µm
C_{lung} (nM)
Time (h)
e)
C_{ELF} after inhalation, C_s = 0.5 µm
C_{ELF} (nM)
$C_{ELF,c}$
C_s
Time (h)
f)
C_{ELF} after inhalation, C_s = 50 µm
C_{ELF} (nM)
$C_{ELF,c}$
C_s
Time (h)
g)
C_p after inhalation, C_s = 0.5 µm
C_p (nM)
Time (h)
h)
C_p after inhalation, C_s = 50 µm
C_p (nM)
Time (h)
i)
RO after inhalation, C_s = 0.5 µm
RO (%)
RO_c
RO_{sp}
Time (h)
j)
RO after inhalation, C_s = 50 µm
RO (%)
RO_c
RO_{sp}
Time (h)

Figure 5.22 Simulations of repeated nose-only exposure. A lung deposited dose of 100 nmol/kg was administered every 24 hours. The left panel shows simulations of a poorly soluble drug (solubility, C_s = 0.5 µM), whereas the right panel shows the corresponding simulations of a highly soluble compound (C_s = 50 µM). The following variables are simulated: 1) solid amount of drug in the lung (A_{solid}), 2) total lung concentration (C_{lung}), 3) concentration in epithelial lining fluid in the central lung (C_{ELF}), 4) plasma concentrations (C_p), and 5) receptor occupancy in the central lung (RO_C, dashed blue line) and the spleen (RO_{sp}, red line).

5.3.5.4 Effect of increasing inhaled doses

As mentioned in section 2.2.4, meta-analyses have shown a relatively flat dose-response curve for efficacy measurements of inhaled corticosteroids. In contrast, a steeper dose-response curve has been noted for the side-effects. Taken together, these two relationships imply that although only a small clinical benefit is expected from increasing the inhaled dose, the risks of side-effects is considerably increased [47].

Simulations were used to investigate the dose-response relationship of inhaled corticosteroids with respect to both the local beneficial effects and the systemic side-effects. Firstly, a poorly soluble compound (C_s = 0.5 µM) with a moderate permeability ($P_{app} = 5\times10^{-6}$ cm/s) was administered repeatedly (k = 5, τ = 24 h) using a broad range of doses (LDD = 10, 50, 250, 750 and 1250 nmol/kg). RO_c and RO_{sp} was assumed to reflect the beneficial local effects and the systemic side-effects, respectively. Since nasal absorption is absent for orally inhaled compounds in the clinic, the nasal blood flow was set to 0 to decouple the nose from the system and thereby mimic the clinical situation. In line with the reasoning in section 5.3.5.3, P was set to be a hundredfold higher in the peripheral lung as compared to the central lung (i.e. the peripheral P was set to $100\times P_{app}$). Otherwise, the drug- and

formulation-specific parameters defined in table 5.4 were used. Noteworthy is that $F = 0$.

Secondly, a highly soluble compound with a moderate permeability ($P_{app} = 5\times10^{-6}$ cm/s) was used in the simulations (C_s = 50 µM). A broad range of *LDD* was used (*LDD* = 1, 5, 25, 125 and 250 nmol/kg). Except from C_s and *LDD*, all parameters and settings were identical in the two different simulation sets.

The simulations of a poorly soluble drug showed that the degree of lung-selectivity decreased at higher *LDD* (fig. 5.23a-e). Expressed differently, RO_{sp} was more sensitive to changes in *LDD* at higher doses since RO_c was already in the proximity of its maximum value. Increasing *LDD* at that stage should thus not be expected to provide a significantly better local effect but rather act by increasing the risk of side-effects. Furthermore, the model elucidated an interesting phenomenon: the ELF in the central region will be in the proximity of C_s throughout the entire dosing interval after repeated dosing of a high *LDD*. For poorly permeable compounds, this phenomenon will occur at lower *LDD* (simulations not shown). It thus follows that the maximum central lung tissue concentration (and thus RO_c) that can be obtained via flux *from the ELF* will be limited by the interplay between *e.g. P*, C_s, the particle size and the regional blood flow (i.e. Q_{bronch}). Under such circumstances, the small rise in RO_c that results from increasing the *LDD* will primarily be systemically driven as the input from the central ELF is close to its maximum.

As can be seen in figure 5.24a-e, the maximum RO_c was reached already at a low *LDD* for the highly soluble compound. The same pattern was subsequently noted; the degree of lung-selectivity decreased with increasing *LDD*. Thus, regardless of the solubility characteristics, the simulations at the higher end of the dose-spectrum were consistent with the dose-response relationships found in clinical studies.

It is worth noting that the lung-selectivity obtained for the highly soluble compound is the result of the dissolution process, the slow K_{off} (K_{off} = 0.51 h^{-1}) as well as the *P*. In order to investigate how the last two properties can affect the dose-response after repeated inhaled dosing of a highly soluble compound, two additional scenarios were explored. Firstly, K_{off} was set to be 10-fold lower (i.e. K_{off} = 0.051 h^{-1}). Secondly, the *P* was set to be 10-fold lower (i.e. $P_{app} = 0.5 \times 10^{-6}$ cm/s). Except from these changes, all drug- and formulation-specific input parameters as well as the choice of *LDD* remained unchanged.

As can be seen in figure 5.25a-e, a slow K_{off} acted by increasing the degree of lung-selectivity. Importantly, it prolonged the period during which lung-selectivity was obtained. In fact, for the three lower doses (*LDD* = 1, 5 and 25 nmol/kg) lung-selectivity was obtained throughout the entire dosing-interval. As in the previous simulations, the degree of lung-selectivity subsequently decreased with higher *LDD*. In this simulation set, K_{off} was lowered by a factor of 10 whereas K_d remained unchanged. Since K_d is defined as the ratio between K_{off} and K_{on} (eq. 4.8), it follows that K_{on} was 10-fold lower. The lower receptor occupancy levels seen in figure 5.25a-c as compared with figure 5.24a-c are thus the result of the lower K_{on} (the drug-receptor association is driven by $C_u(t)K_{on}R(t)$ as described in eq. 5.31).

Figure 5.26a-e presents the simulations in which a highly soluble compound with a 10-fold lower *P* was used. When comparing these simulations to the base-case (fig. 5.24a-e), it was found that the receptor occupancy profiles were similar at the three lowest doses used in this simulation study (*LDD* = 1, 5 and 25 nmol/kg). In contrast, at the two highest doses the effect of lowering *P* was more pronounced (fig. 5.24d-e and 5.26d-e for the base-case and the 10-fold lower *P*, respectively). As a result of the lower *P* and thus slower absorption from the airway lumen, high drug

concentrations will be maintained in the ELF over a prolonged time period. This effect will be particularly pronounced after a high *LDD* since the C_{ELF} will be in close proximity to C_s (i.e. it will be saturated with respect to drug) and thus significantly slow down the normally rapid dissolution process. Hence, the net effect of increasing *LDD* in combination with lowering *P* was a more sustained receptor occupancy profile with a prolonged period of lung-selectivity.

To summarise, in all simulations described in this subsection (figs. 5.23-5.26) the lung-selectivity decreases at high *LDD*. Expressed differently,

$$\lim_{LDD\to\infty} \frac{RO_c}{RO_{sp}} = 1. \qquad (5.85)$$

It is also clear that the ratio between RO_c and RO_{sp} will tend to infinity as *LDD* approaches 0, i.e.

$$\lim_{LDD\to 0} \frac{RO_c}{RO_{sp}} = \infty. \qquad (5.86)$$

Expressed differently, as *LDD* approaches 0 it follows that both RO_c and RO_{sp} tend to 0; i.e. an undesired situation where no pharmacological effect is exerted. This clearly emphasises the need to have a PK/PD model in place prior to making a dose optimisation in order to establish approximately what level of receptor occupancy is needed to exert the desired effect. Once this information is in place, it would be possible to apply constrained optimisation for dose optimisation purposes.

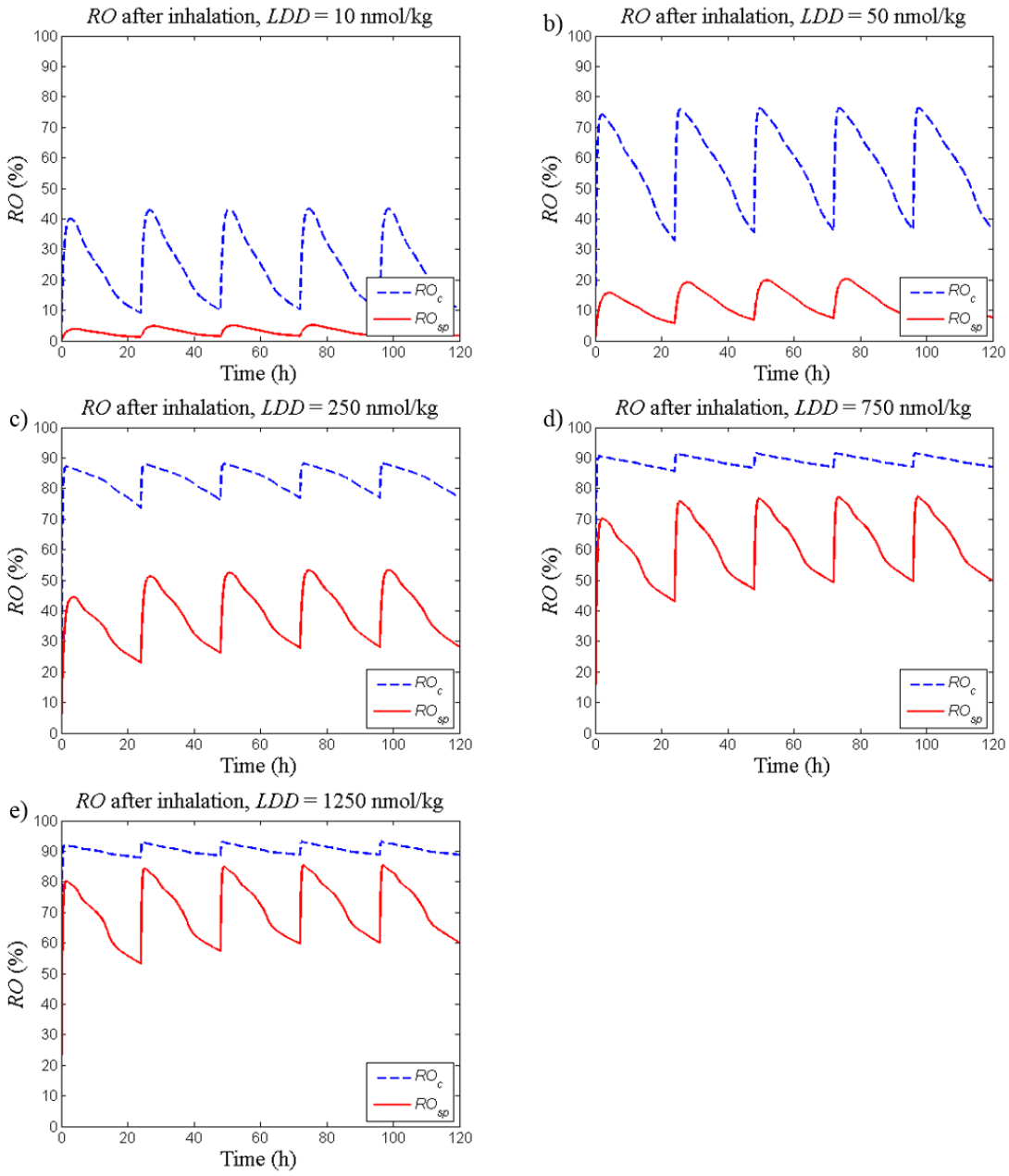

Figure 5.23 Simulations of receptor occupancy in the central lung (RO_c, dashed lines) and in the spleen (RO_{sp}, solid lines) after increasing lung deposited doses (*LDD*): a) 10 nmol/kg, b) 50 nmol/kg, c) 250 nmol/kg, d) 750 nmol/kg, and e) 1250 nmol/kg. A poorly soluble compound with moderate permeability was used in the simulations (solubility = 0.5 µM, permeability = 5×10^{-6} cm/s).

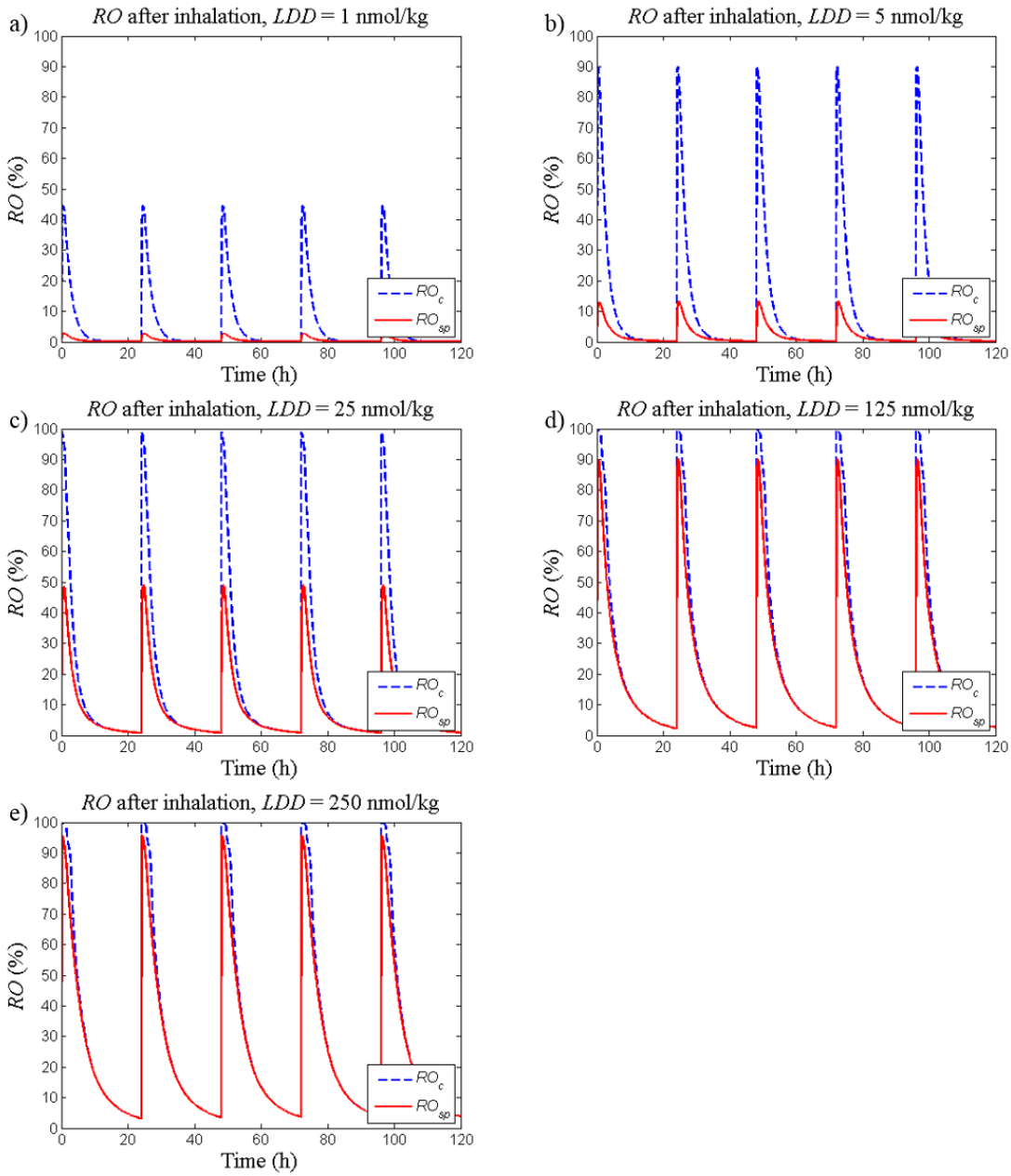

Figure 5.24 Simulations of receptor occupancy in the central lung (RO_c, dashed lines) and in the spleen (RO_{sp}, solid lines) after increasing lung deposited doses (*LDD*): a) 1 nmol/kg, b) 5 nmol/kg, c) 25 nmol/kg, d) 125 nmol/kg, and e) 250 nmol/kg. A highly soluble compound with moderate permeability was used in the simulations (solubility = 50 µM, permeability = 5×10^{-6} cm/s).

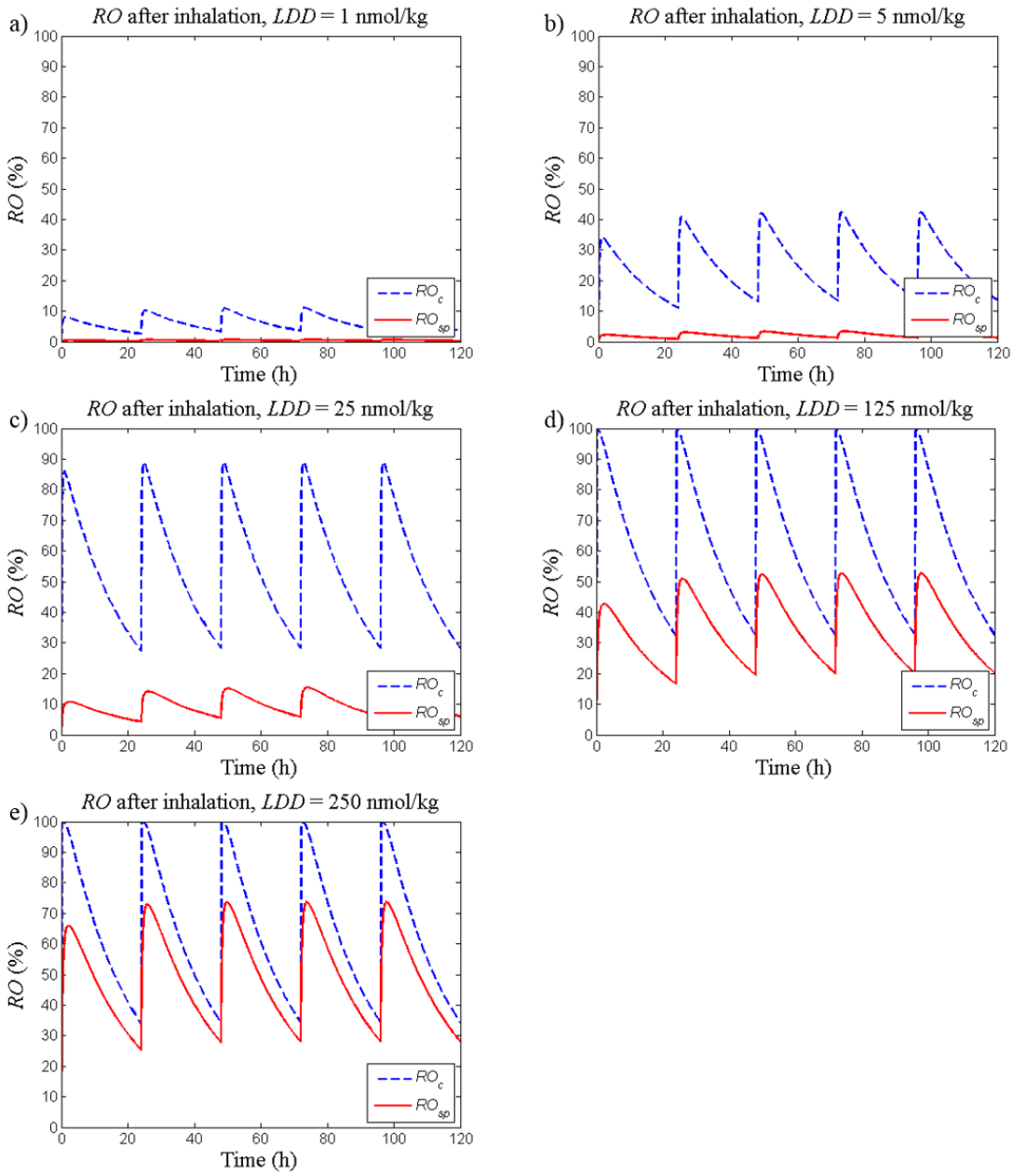

Figure 5.25 Simulations of receptor occupancy in the central lung (RO_c, dashed lines) and in the spleen (RO_{sp}, solid lines) after increasing lung deposited doses (*LDD*): a) 1 nmol/kg, b) 5 nmol/kg, c) 25 nmol/kg, d) 125 nmol/kg, and e) 250 nmol/kg. A highly soluble compound with moderate permeability and a slow dissociation rate constant (K_{off}) was used in the simulations (solubility = 50 µM, permeability = 5×10^{-6} cm/s, K_{off} = 0.051 h^{-1}).

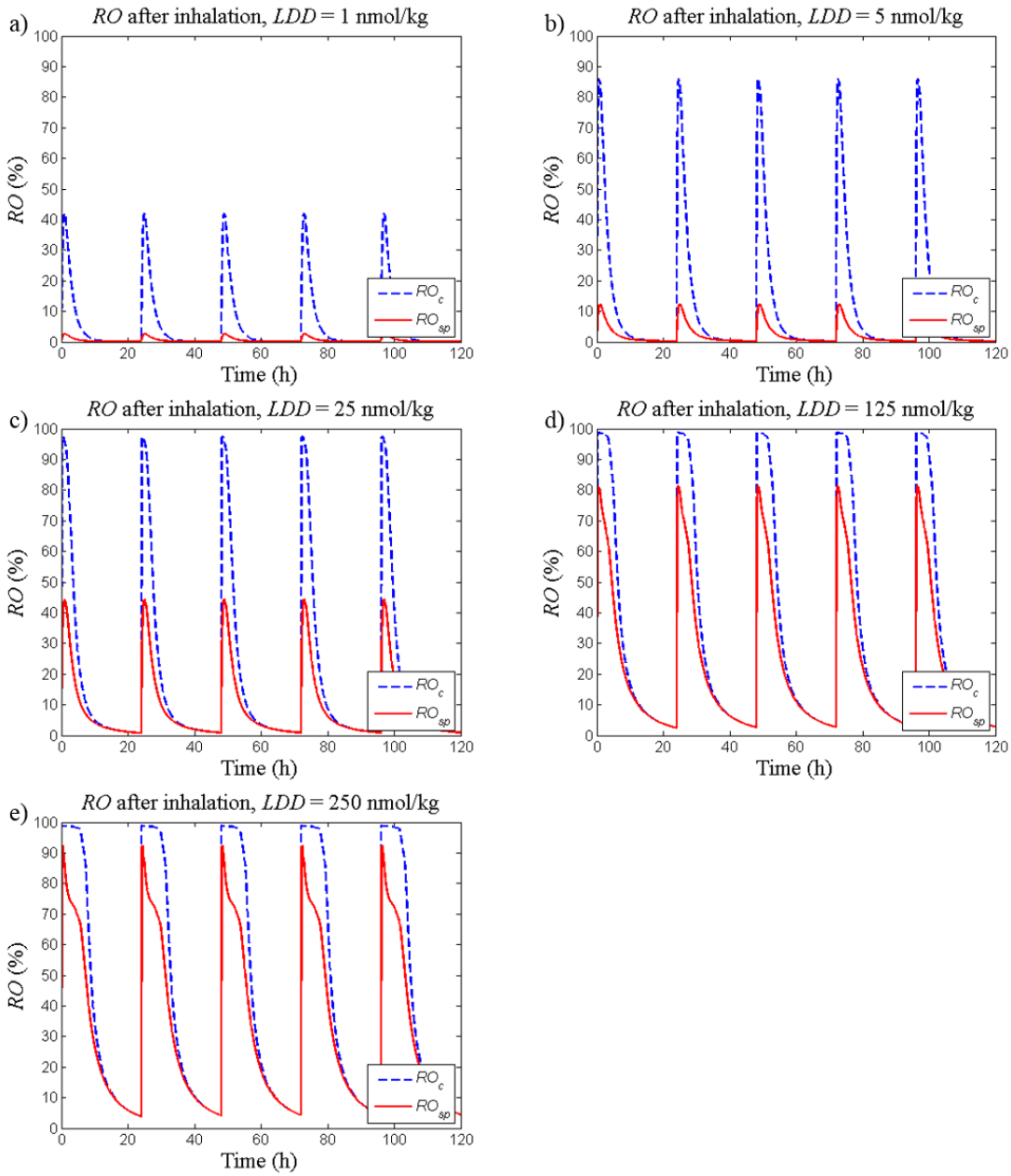

Figure 5.26 Simulations of receptor occupancy in the central lung (RO_c, dashed lines) and in the spleen (RO_{sp}, solid lines) after increasing lung deposited doses (*LDD*): a) 1 nmol/kg, b) 5 nmol/kg, c) 25 nmol/kg, d) 125 nmol/kg, and e) 250 nmol/kg. A highly soluble compound with a poor permeability was used in the simulations (solubility = 50 µM, permeability = 0.5×10^{-6} cm).

5.4 Discussion

This chapter presents the development of a mechanistic PBPK model including lung disposition for prediction of systemic and pulmonary PK for inhaled drugs, which was validated by experimental measurements of drug concentrations and receptor occupancy obtained from studies where FP was used as test compound. By virtue of being mechanistic, this model provides a tool to theoretically explore pulmonary drug disposition and how key processes in a physiological context produce lung-selectivity.

Two different compounds were used for evaluating the model: FP and budesonide. The model predictions for FP were consistent with experimental data collected from studies utilising the IV- as well as the inhaled route, which will be described in detail the subsequent paragraph. In contrast, regardless of the route of administration, there were discrepancies between model predictions and observations for budesonide. Since the model was predictive of FP, this systematic discrepancy for budesonide might suggest the presence of a drug-specific mechanism that is unaccounted for by the model. Indeed, as mentioned in section 5.3.2.1, a reversible fatty acid esterification of budesonide has been shown to take place both *in vitro* [175] and *in vivo* [79]. Upon characterisation of the PK of budesonide and its ester, budesonide-oleate, it was demonstrated that budesonide-oleate was rapidly formed both after IV-dosing and inhalation of budesonide in rats [79]. Since the resulting budesonide-oleate concentrations were in the proximity of the budesonide concentrations [79], the process of esterification and the subsequent hydrolysis is likely to have a pronounced effect on the PK of budesonide. This hypothesis has also been confirmed via semi-empirical modelling approaches [79,176]. Hence, the current model structure should not be expected to accurately describe the PK of budesonide. Further

research would thus be required to adequately describe this mechanism in a quantitative manner, which was not considered to fall within the scope of this thesis.

Data generated from IV-dosing as well as inhalation of FP were used for model validation, which thus allows the model to be used to compare the two administration routes. Model predictions of IV-administrations were consistent with experimental data (figs. 5.4a-d), supporting a perfusion rate-limited distribution. Notably, input parameters (*CL*, $V_{d,ss}$, K_{on} and K_{off}) obtained from the modelling of one data set (90 nmol/kg, IV) proved predictive of data from four other IV-dose levels (20, 150, 750 and 1000 nmol/kg), thus offering strong support and confidence in its predictive capability to determine systemic PK and receptor occupancy. Interestingly, inclusion of receptor binding was necessary for accurate predictions of spleen concentrations after IV-administration as well as nose-only exposure (fig. 5.4d and 5.5c, respectively), which verifies that FP has a high receptor-bound fraction as suggested from the results presented in section 3.3.2.3. Similarly, inclusion of the receptor-bound concentration was necessary for accurate predictions of C_{lung} after IV-administration of FP (fig. 5.4c). Taken together, this elucidates the potential pitfall of only relying on K_p-values when predicting tissue concentrations after low doses of highly potent compounds. Under such circumstances, under-predictions are inevitable as K_p-values do not account for receptor binding. In contrast, since C_{lung} after nose-only exposure was substantially higher than the receptor density (i.e. $C_{lung} >> B_{max}$, where B_{max} = 21 nM), the contribution of receptor binding to C_{lung} was negligible after inhaled drug delivery.

As the aqueous solubility of poorly soluble compounds, such as FP, tends to under-predict the *in vivo* dissolution rate [55], the single parameter C_s was estimated from observations of total drug concentrations in the lung made in one inhalation study

(11.3 nmol/kg, *LDD*). It is worth noting that the estimate of C_s (4530 [3845-5215] nM) was close to the measured FaSSIF-solubility (3120 nM) [164]. When the optimised model was tested on another data set (100 nmol/kg, *LDD*), it was shown to be predictive of the total lung concentrations with the exception of the last time point (fig. 5.5a). It should be noted that neither the particle size distribution nor the density was available for the study comprising of the higher *LDD*, which therefore was assumed to have the same formulation-specific properties as the low-dose study. The discrepancy between the predicted and observed C_{lung} at t = 24 h could thus possibly be explained by an inaccurately described particle size distribution. Nevertheless, it might also reflect limitations of the Nernst-Brunner equation for the alveolar region where the ELF layer might be smaller than the particle diameter.

Model predictions of plasma concentrations and systemic occupancy after nose-only inhalation agreed well with experimental data (figs. 5.5e-f). This consistency confirms that FP has a dissolution rate-limited absorption and underscores the importance of mechanistically describing the dissolution process for such compounds.

Validation of lung occupancy predictions was slightly more complex as these measurements reflect whole-lung occupancy. For comparison of observations and predictions, a weighted average accounting for the relative contribution of each pulmonary region was thus needed. Although exact determination of the tissue fractions cannot be made, the volume fraction of central lung ($f_{v,c}$) was approximated to be 0.19 (section 5.2.2.3). Given the uncertainty in $f_{v,c}$ and the slightly lower accuracy of lung occupancy measurements (section 3.4), a whole-lung occupancy prediction that qualitatively captures key features including lung-selectivity and late occupancy peak (fig. 5.5d) can be regarded as a good description of the data.

For validation purposes, emphasis was not placed on explaining the variability in the data, which is partly caused by the use of destructive sampling (one animal/time point). Apart from interindividual differences in model input parameters, a high variation in *LDD* is expected from preclinical studies utilising nose-only exposure systems. The latter can partly be explained by the individual animals having slightly different breathing patterns, the effect thereof on the deposition was illustrated by figs. 5.18 and 5.19. Since this is not monitored in preclinical studies, the validation instead focused on how well the model captured key features in the observations, both at a quantitative and a qualitative level.

Since the model proved to be predictive of FP, i.e. a neutral compound with a dissolution rate-limited absorption, it was used to theoretically explore various aspects of pulmonary drug disposition. As expected, simulations showed that lung-selectivity could not be obtained if the drug was administered via the IV-route. More interestingly, a previously unforeseen finding resulting from the simulation studies was that lung-selectivity is possibly unattainable in the well-perfused parts of the lung after inhaled drug delivery. This can be attributed to the high perfusion rate of the alveoli region (entire cardiac output, Q_{CO}), which thus rapidly equilibrates with the systemic circulation. In fact, the model predicted the tissue distribution half-life of FP in the peripheral lung to be below 2 s. However, lung-selectivity could be obtained in the central region after inhalation as its lower perfusion rate allows for a longer equilibration time. The receptor occupancy in the central lung (RO_c) was thus used as the pulmonary region for evaluation of lung-selectivity.

It was shown that a concentration-gradient, and thus lung-selectivity, was obtained during the dissolution phase (fig. 5.9a). It was also demonstrated that a low oral bioavailability and a high clearance were both important for obtaining a high degree

of lung-selectivity (simulations not shown). These three concepts have been demonstrated in an earlier simulation study by Hochhaus *et al*. [14]. Those simulations relied on a very simple model structure, in which the lung was described by a single compartment, the dissolution process by a rate constant, k_{diss}, and the receptor binding by a static E_{max}-model. The model presented in this thesis can thus explore further aspects of pulmonary drug disposition since it has: 1) a physiological parameterisation, 2) more sophisticated and mechanistic mathematical descriptions of drug disposition processes, and 3) a dynamic description of receptor binding, i.e. it is parameterised by the association rate constant (K_{on}) and the dissociation rate constant (K_{off}).

In line with results from previous research [14], this model also described the risk of only obtaining transient lung-selectivity after IT-administration of a dissolved drug without any additional mechanisms enhancing its lung-retention, i.e. a scenario resembling IV-administration where no lung-selectivity is obtained. Nevertheless, it was unravelled that a transient concentration-gradient can give rise to an extended period of lung-selectivity provided that the drug-receptor dissociation-rate is relatively slow (figs. 5.11a and 5.11e). The latter feature was unforeseen by earlier models since the receptor binding was described by a static E_{max}-model [14]. Interestingly, the lung-selectivity obtained via this mechanism could not be detected from the plasma profile after inhalation, which was close to identical to the corresponding profile obtained after administering the same dose as an IV-bolus (fig. 5.10). This example thus also serves to demonstrate that it might be inappropriate to interpret inhalation studies solely on the basis of plasma concentrations. Simulations in section 5.3.3.2 demonstrated how yet another drug-specific property, namely a poor permeability, can lead to a prolonged period of lung-selectivity after IT-

administration of a solution (fig. 5.9f). Besides, since a poor permeability results in a slower permeation into lung tissue and thus an increased drug concentration in the ELF (C_{ELF}, fig. 5.13c), this property might be even more interesting if the drug target resides in the airway lumen. According to model predictions, drug discovery projects with targets localised in the airway lumen would benefit from chemically design compounds that exhibit a poor permeability.

Moving back to lung-selectivity obtained by designing poorly soluble compounds and thereby creating a slow dissolution process. As mentioned in section 4.1, a more in-depth knowledge is needed to better understand the potential benefits and limitations of this strategy. Clearly, simulations indicate that this strategy is beneficial for highly potent compounds (figs. 5.9a, 5.22i, and 5.23a-e). Notably, at the other end of the spectrum are low-affinity compounds for which a low C_s might disrupt the opportunity of obtaining sufficiently high target site concentrations to elicit a pharmacological response. Simulations of repeated dosing of poorly soluble compounds elucidated this interesting phenomenon (fig. 5.23): the ELF in the central lung region will be in the proximity of C_s throughout the entire dosing interval after repeated doses of high *LDD*. The saturation of the ELF with respect to drug creates an interesting situation where the maximum central tissue concentration, and thus RO_C, that can be obtained *via flux from the airway lumen* is limited by an interplay between *e.g.* P, C_s, K_d and the regional blood flow (i.e. Q_{bronch}). Thus, after having saturated the ELF, RO_C can only increase via *flux from the systemic circulation*. That is, an undesirable situation has come to exist where the increase in the local effect is driven from the systemic side and a higher *LDD* will thus act by decreasing the degree of lung-selectivity. Again, this illustrates the importance of having an integrated understanding. Nevertheless, the strategy of designing compounds with a

poor solubility should primarily be considered if the chemical design also allows for a high affinity.

Simulations also demonstrated that particle size is an important determinant of the dissolution rate, which thus can be used to partly control the dissolution process (fig. 5.9c). Due to the enlarged surface area, smaller particles will dissolve more rapidly (eq. 5.19). Indeed, reducing the particle size has been documented to increase the *in vitro* dissolution rate as well as the oral bioavailability for poorly soluble compounds [192,193]. Nevertheless, the impact of changing the particle size is more complex for the inhaled route as compared with the oral route. This is attributed to the particle size also being an important determinant of the regional drug deposition. Thus, the dissolution process should not be considered in isolation when evaluating the consequences of changing the particle size. If a reduction of the particle size leads to a greater drug deposition in the more rapidly perfused distal airways, one could also expect *e.g.* less drug removal by MCC and a more rapid absorption from the lung to the systemic circulation. The latter was highlighted by simulations and discussions contained in section 5.3.4.3, which showed a more rapid pulmonary absorption of drug deposited in the distal airways. Accordingly, for several reasons, this is expected to be reflected in the plasma profile by a higher and earlier peak plasma concentration (C_{max}) as well as by a higher systemic bioavailability. However, when interpreting such data, it is thus difficult to separate the effect of a higher dissolution rate from the effects that are indirectly caused by a greater distal airway deposition. The presented mechanistic PBPK model, which describes the interplay between these different processes, could thus be a useful tool to understand the implications of changing a parameter, such as the particle size, that is expected to have a pronounced effect on several processes. This application can *e.g.* be useful for tailoring inhaled

drug formulations for clinical studies. It is worth mentioning that Usmani [194] has shown that inhalation of different sized particles of FP indeed produces different PK behavior. The smaller particles (1.5 µm MMAD) had a higher and earlier C_{max} as compared to the larger particles (6 µm MMAD). Furthermore, the systemic bioavailability was higher for the smaller particles. Both simulations and experimental data thus emphasise the importance of also considering formulation-specific parameters when designing preclinical- and clinical studies. By using a suboptimal particle size distribution, a compound might erroneously be considered to have PK-properties poorly suited for inhalation and/or to have a poor efficacy and safety profile. Clearly, the appropriate particle size distribution needs to be considered on a case-by-case basis depending on the compound as well as on the target.

Model predictions elucidated that a high nasal deposition, possibly accompanied by significant absorption, is expected following nose-only exposure studies (figs. 5.5g and 5.16a). While nasal absorption is absent for orally inhaled products in the clinic, simulations suggest that nasal uptake reduces the degree of lung-selectivity seen in preclinical models (figs. 5.9d-e). Accounting for this process might thus be important for interpretation and translation of preclinical data since drug candidates otherwise could be deselected based on false premises. Simulations indicated that the interplay between C_s and P will affect the degree of nasal absorption, where compounds with a high C_s and high P will be absorbed to a greater extent (fig. 5.14). A higher nasal MCC and a lower regional blood flow were also both shown to considerably decrease the extent of nasal absorption, suggesting that an even more careful characterisation of those two system-specific parameters would be informative for the model. It is worth noting that some drugs can cause vasoconstriction and thereby

reduce the nasal blood flow and thus the extent of nasal drug absorption, further emphasising the need for an integrated understanding of the entire system. If the technical challenges can be overcome, experiments addressing the extent of nasal absorption after nose-only exposure would indeed be useful.

As mentioned in section 2.2.4.1, meta-analyses of clinical studies have shown a relatively flat dose-response curve for inhaled corticosteroids [49,50]. In contrast, a steeper dose-response curve was found for the side-effects. This was theoretically investigated by model simulations, in which the nasal blood flow was set to zero to avoid nasal absorption and thereby mimic the clinical situation. Escalating *LDD*-levels were used in the simulations and RO_C and RO_{sp} were used as readouts for the local beneficial effect and the systemic side-effect, respectively. Regardless of the solubility characteristics of the compound (i.e. highly or poorly soluble), the model predictions for the *higher end* of the dose-spectrum were consistent with the dose-response relationships found in clinical studies (figs. 5.23-5.26). That is, at higher *LDD* RO_C was close to its maximum value whereas RO_{sp} still was increasing. Hence, these simulations combined with the results of the meta-analyses might imply a historical tendency to over-dose inhaled corticosteroids in clinical studies.

Furthermore, the two earlier examples illustrate how the model lends itself for translation. As it relies on a physiological parameterisation, translation from animal to human can be done by changing from nasal to oral inhalation and exchanging system- (rat vs. human physiology) and formulation-specific parameters (particle size etc.). Clearly, a deposition model specifically developed for humans should be used and the formulation-specific parameters should be adapted on a case-by-case basis for the compound of interest. This would thus be the next natural step for future research.

5.6 Summary

This chapter presents the development of a PBPK model, which places emphasis on mechanistically describing pulmonary drug disposition after inhalation. The model was validated by comparing model predictions to experimental measurements of drug concentrations and receptor occupancy after administration of FP via the IV- and inhaled route (figs. 5.4 and 5.5, respectively). The developed model was subsequently used to theoretically explore different aspects of pulmonary drug disposition and to identify key-determinants for lung-selectivity. Specific findings from this work include: 1) lung-selectivity possibly being unattainable in well-perfused parts of the lung, 2) preclinical inhalation studies might be contaminated by extensive nasal absorption (figs. 5.9d-e), and 3) identification of two more drug-properties that can be used to provide lung-selectivity, namely a slow K_{off} and a poor permeability (figs. 5.9b and 5.9f, respectively). It was also shown that the former property might be even more interesting for drug targets residing in the airway lumen (fig. 5.13c), thus providing a rational strategy for drug design. Several examples demonstrated the value of understanding the *interplay* between different processes instead of focusing on one in isolation, *e.g.* changing the particle size distribution will not only affect the dissolution rate, but also the deposition pattern and thus the absorption rate to the systemic circulation as well as the extent of drug removal by MCC. Clearly, this can have a pronounced effect on the pharmacodynamics of the drug.

In summary, the work contained in this chapter demonstrates the value of mechanistically describing the underlying processes of drug disposition in the lung to understand how the delicate interactions between drug-, formulation- and system-specific properties produce the final outcome of the system. The model can thereby

guide the design of compounds and inhaled drug formulations with optimal local pharmacology and provide a logic framework for translation of inhaled drug pharmacology.

Chapter 6 Conclusions

This thesis set out to explore how the free target site exposure to inhaled drug relates to various drug- and formulation-specific properties. This aspect of inhalation pharmacokinetics has indeed been recognised as challenging for various reasons including: 1) the easily accessible unbound blood concentration cannot be assumed to reflect the free lung target site exposure after topical administration, 2) it is not possible to directly measure unbound drug concentrations locally in the lung tissue, and 3) pulmonary drug disposition is known to be a complex interplay between numerous processes, thus making the development and the subsequent validation of predictive models for inhaled drugs more demanding.

The difficulties associated with both measuring and predicting the unbound drug concentration(s) at the target site(s) after inhalation have had negative implications for drug discovery and drug development programmes, which have been struggling to identify rational strategies for chemical- and formulation design as well as for targeting appropriate dose ranges for clinical studies. The ultimate aim of this thesis has therefore been to increase the understanding of how different drug- and formulation-specific properties, or the combination thereof, relate to the level and time course of free lung target site exposure. As declared in the introduction chapter, several objectives were set in order to reach this aim:

1. To continue and complete an ongoing development of an *in vivo* receptor occupancy methodology for an inhaled target, the glucocorticoid receptor (GR).

2. To apply the developed *in vivo* receptor occupancy methodology to characterise and compare the time course of receptor occupancy after intravenous- and inhaled drug delivery.
3. To characterise the binding kinetics of a GR agonist using the intravenous route.
4. To develop a mechanistic, mathematical framework to predict the time course of target site exposure to unbound drug and receptor occupancy after inhalation, taking into account the physiology of the species and processes judged to be important for pulmonary drug disposition.
5. To apply the developed model to understand what drug- and formulation-specific properties, or combinations thereof, that give rise to lung-selectivity in terms of local and systemic receptor occupancy.

The following paragraphs aim to briefly describe how each of these above-mentioned objectives were fulfilled.

In chapter 3, the development of an *in vivo* receptor occupancy methodology for the GR was presented. This method is novel in terms of measuring GR occupancy strictly *in vivo* and by the analytical technique used for tracer quantification (LC-MS/MS). An interesting feature is that it allows for simultaneous assessment of GR occupancy in the lung and in a reference organ for the systemic exposure (the spleen), which thus provides a quantitative readout of the degree of lung-selectivity that is achieved by inhaled drug delivery. After having established the experimental *in vivo* protocol, the method was evaluated by assessing its capability of establishing a dose-receptor occupancy relationship of intravenously administered fluticasone propionate (FP; 20, 150 and 750 nmol/kg). It proved capable of demonstrating such a

relationship (figs. 3.6a-b) and, as expected from IV-dosing, the receptor occupancies were of similar magnitude in the lung and the spleen (fig. 3.7). The method was also applied to study the time course of receptor occupancy after IV-administration of FP (90 nmol/kg, fig. 3.10).

In chapter 4, the developed methodology was used to characterise the time course of receptor occupancy after nose-only exposure of FP formulated as a dry powder (*LDD*, 11.3 nmol/kg, fig. 4.9). The receptor occupancy profiles that followed from drug delivery via the inhaled and intravenous route were shown to have distinct differences. Firstly, the observed receptor occupancy peak occurred at the first time point after IV-administration (t = 0.5 h), whereas the corresponding peak after nose-only exposure was found at t = 4 h. Secondly, the receptor occupancy rapidly declined after IV-dosing and had returned to baseline within 7 hours after dosing. In contrast, the receptor occupancy profile was relatively flat after topical administration. Furthermore, the drug-concentration profiles (lung, plasma and spleen) were distinctly different after dosing via the inhaled and intravenous route. The PK-data from the nose-only exposure studies (fig. 4.10) followed a pattern expected from a poorly soluble inhaled drug: a large amount of unabsorbed drug in the lung over several hours after dosing accompanied by low drug levels in plasma. Furthermore, the plasma profile was flat as compared to the corresponding profile resulting from IV-dosing, which indicates a slow absorption of drug to the systemic circulation.

In chapter 4, the binding kinetics of two GR agonists (FP and budesonide) were characterised using the intravenous route. For the first time, the binding kinetics parameters, K_{on} and K_{off}, for these two substances were estimated based on *in vivo* data. The parameter estimation was performed in Phoenix™ and an exhaustive

search algorithm subsequently confirmed that the minimum objective function had been found by the optimisation algorithm (within the expected parameter space). Combined with the data on systemic and pulmonary receptor occupancy after nose-only exposure of FP, the estimates of K_{on} and K_{off} provided an opportunity to, for the first time, validate model predictions of free lung target site exposure to inhaled drug.

Chapter 5 described the development of a whole-body rat physiologically based pharmacokinetic (PBPK) model, which placed emphasis on mechanistically describing important processes for pulmonary drug disposition after inhalation. The following processes were included: regional drug deposition, mucociliary clearance (MCC), drug dissolution and flux to/from the systemic circulation. Furthermore, the model dynamically described receptor binding and thus allowed for the evaluation of lung-selectivity in terms of local versus systemic receptor occupancy. The model was subsequently evaluated without parameter re-estimation with FP using drug- and formulation-specific properties from experiments or literature sources as input parameters. Since, to the best of my knowledge, experimental methods currently do not allow for *quantitative* measurements of the solubility (C_s) in the ELF, C_s was the sole parameter to be estimated in the model. Data on drug concentrations in different biological matrices (lung, plasma and spleen) and receptor occupancy measurements were available for model validation with respect to both the intravenous and the inhaled route. Importantly, the validation data set comprised data generated across a broad dose-range in particular after intravenous- (20, 90, 150, 750 and 1000 nmol/kg) but also after inhaled drug delivery (*LDD*, 11.3 and 100 nmol/kg). The model accurately described the PK and receptor binding of intravenously administered FP (fig. 5.4). Furthermore, the model predictions of the PK and receptor occupancy after nose-only exposure agreed well with experimental data (fig.

5.5). The model predictions could thereby confirm that FP has a dissolution rate-limited drug absorption and highlight that drug in the solid state does not contribute to receptor occupancy.

In chapter 5, the developed PBPK model was subsequently applied to assess how different drug- and formulation-specific properties, or combinations thereof, could give rise to lung-selectivity in terms of receptor occupancy. Interestingly, model predictions suggested that lung-selectivity is possibly unattainable in the well-perfused parts of the lung. This, previously unforeseen, finding can be attributed to the high perfusion rate of the alveolar region, which thus rapidly equilibrates with the systemic circulation.

This model thus elucidated the difficulties of obtaining lung-selectivity in the alveolar region. In retrospect, this is perhaps not surprising given the features of this region (large surface area, high vascularization). It is even less surprising when considering the properties of the investigated compounds (high permeability, neutral). Equally important, it cannot be excluded that other mechanisms unaccounted for by this model might offer the prospect of lung-selectivity in the alveolar region. Nevertheless, a general finding is that the anatomy of this region significantly impairs the prospect of obtaining lung-selectivity.

Lung-selectivity could be obtained in the less perfused central lung region, which was thus used as the pulmonary region for evaluation of lung-selectivity. Several strategies for obtaining lung-selectivity were identified: 1) slow drug dissolution, 2) slow drug-receptor dissociation as reflected by a slow K_{off}, and 3) poor permeability. Nevertheless, it cannot be emphasised enough that one property should not be considered in isolation, as the final outcome of the system will be the result of the *interplay* between different processes and properties. An illustrative example is that

lung retention by having a low C_s, and thus a slow dissolution rate, should only be considered for highly potent compounds to ensure that sufficiently high drug concentrations can be obtained at the target site. Poorly soluble compounds with low potency should thus not be progressed into extensive animal testing or clinical trials. The particle size distribution provides another manifestation of the interplay between different processes. If needed, decreasing/increasing the particle size might be used to change the dissolution rate. However, as outlined in the discussion in chapter 5, the particle size is expected to have a pronounced effect on several processes including the regional deposition pattern (fig. 5.17). Assume a situation where the pharmacological effect of a poorly soluble and highly potent inhaled drug candidate is planned to be evaluated using a nose-only exposure system. Results from earlier inhalation PK-studies, which used a particle size distribution with larger particles (aerodynamic diameter, $d_a \sim N(5,\ 0.5)$ µm), indicated a very slow dissolution rate. Hence, the particle size needs to be reduced to obtain target site concentrations that are sufficiently high to exert a pharmacologically meaningful effect. Since the target of the drug is known to reside primarily in the central airways, the deposition pattern should also be taken into account when choosing an appropriate particle size distribution for the PD-study. Hence, the PBPK model presented in this thesis provides drug discovery with an important tool for identifying a particle size distribution, which satisfies these requirements. This example thus serves to illustrate how a mechanistic PBPK model can be used to theoretically explore the wider implications of changing a parameter such as the particle size and thereby *e.g.* aid the formulation design.

Earlier research has also evaluated lung-selectivity in terms of pulmonary and systemic receptor occupancy [14]. The simulation study conducted by Hochhaus *et*

al. [14] relied on a very simple model structure, in which the lung was described by a single compartment, the dissolution process by a rate constant, k_{diss}, and the receptor binding by a static E_{max}-model. Despite its simplicity, the previously published model could identify that lung-selectivity is attained during the dissolution phase. Furthermore, it demonstrated that low oral bioavailability and high clearance are both important for obtaining a high degree of lung-selectivity. The model presented in this thesis thus builds and expands on these concepts and differentiates from the earlier work through introduction of: 1) physiological parameterisation, 2) more sophisticated and mechanistic mathematical descriptions of pulmonary drug disposition processes, and 3) dynamic description of receptor binding. The added sophistication allows for the possibility to evaluate more aspects of pulmonary drug disposition, which thereby have led to previously unforeseen findings including lung-selectivity possibly being unattainable in well-perfused lung regions and that slow drug-receptor dissociation can be a drug property yielding lung-selectivity. Furthermore, by virtue of being mechanistic and relying on a physiological parameterisation, model predictions were shown to agree with concepts of pulmonary drug disposition that earlier have been proposed and/or demonstrated in the literature such as: 1) MCC having a larger impact on slowly dissolving compounds, which has been suggested by *e.g.* Edsbäcker *et al*. [8] and shown by model predictions in fig. 5.12, 2) pulmonary absorption being more rapid in the alveolar region, which was demonstrated by Gerde *et al*. [152,153], suggested from results obtained from animal studies conducted by Schanker *et al*. [195,196] and shown by model predictions in fig. 5.13d, and 3) extensive nasal absorption taking place after nose-only exposure as shown in fig. 5.9d. Despite its important implications, the third concept has not received much attention in the literature.

However, this methodological insufficiency has been reported by Sakagami *et al.* [10]. Clearly, this issue would benefit from further experimental investigation to quantify how much nasal absorption contributes to the systemic exposure and thereby 'contaminates' the results obtained from nose-only exposure studies. If an extensive nasal absorption is confirmed to take place, it would have important implications for the interpretation of preclinical inhalation studies utilising nose-only exposure. In this context, it is important to underline that nasal absorption will not be an issue for orally inhaled products in the clinic and it is thus a finding that will not translate from animal to man. Clearly, not accounting for this process might lead to inappropriate ranking of compounds from PK- as well as PD-studies.

By having incorporated a mechanistic model that describes regional drug deposition, this work opens up interesting opportunities for: 1) targeting specific lung regions that are held to be particularly important for treating a given disease or condition, and/or 2) precluding deposition in lung regions devoid of drug target (*e.g.* if the target density is denser in the central lung such a strategy could minimise unnecessary systemic absorption). Clearly, a regionally targeted drug treatment requires in-depth knowledge about the drug target location and, in many instances, this is not known. This example thus serves to highlight the importance of understanding the target biology and its location. Furthermore, it also demonstrates how a modelling exercise can lead to further questions, opening for inter-disciplinary collaborations to break new ground.

To summarise, the PBPK model presented in this thesis provides a tool to theoretically explore various aspects of pulmonary drug disposition, including how the extent and time course of free target site exposure to inhaled drug relates to different drug- and formulation-specific properties; i.e. the aim of this thesis. The

model can thereby guide the chemical design of compounds and tailor inhaled drug formulations for clinical trials. Furthermore, it can provide a logical framework for translation of inhaled drug pharmacology. These application areas would be instrumental to any drug discovery or development programme targeting the lung via the inhaled route.

6.1 Future research and limitations

As discussed above, the PBPK model presented in this thesis represents an advancement of earlier simulation models and has thereby contributed to increasing the knowledge about pulmonary drug disposition. Nevertheless, several aspects of inhalation PK still remain to be explored, some of which may be relevant to incorporate in a PBPK model.

As mentioned in the previous section, the model lends itself to translation from animal to man since it is based on a physiological parameterisation. Translation to man can be done by changing the inhalation manoeuvre (from nasal to oral inhalation) and exchanging system-specific properties (from rat to human physiology). Clearly, a deposition model specifically developed for humans needs to be implemented prior to performing this research activity. Furthermore, the formulation-specific properties should be adapted on a case-by-case basis for the compound as well as the target of interest. The aforementioned steps would thus lead to a new mechanistic framework for translating inhaled drug pharmacology. A translation relying on mechanistic, instead of empirical, principles would provide a step-change for drug discovery and drug development programmes, which thus is expected to be a highly prioritised area for future research.

Whilst the focus of this work has been on increasing the understanding of inhalation pharmacokinetics in healthy lungs, it opens up for interesting opportunities to advance the understanding of how inhaled drugs will behave in diseased lungs. By virtue of being mechanistic, the developed model has the potential to assess how the pathophysiology of a disease might affect processes of pulmonary drug disposition and thereby possibly alter the extent and/or time-course of the free drug concentration at the site of the disease. A recent review pointed out that the impact of pulmonary diseases on the fate of inhaled compounds is still a large underdeveloped area and such questions needs to be addressed to optimise inhaled therapies [16].

Clearly, a mechanistic model has the potential to provide an integrated understanding of how the pathophysiology of a given pulmonary disease affects the local pharmacokinetics of inhaled drugs. This can be exemplified by obstructive airway diseases such as asthma, where an enhanced deposition in the tracheobronchial region is expected due to airway narrowing [16]. An altered deposition pattern in asthmatic patients might not only lead to a higher drug concentration centrally, but it may well for instance: 1) reduce the systemic bioavailability following inhalation as a higher fraction of the dose can be cleared by the MCC, and 2) reduce the maximum plasma concentration following inhalation. The second feature would have been caused by a slower drug absorption in the tracheobronchial- as compared to the alveolar region. This is in line with model simulations in this thesis, which suggest that the pulmonary absorption is more rapid in the alveolar region (fig. 5.13). Both these features have been observed when comparing plasma profiles between healthy volunteers and asthmatic patients [197]. On the other hand, the rate of the MCC has been reported to be significantly slower in asthmatic patients as compared to healthy volunteers [198]. Incorporating the

pathophysiology of pulmonary diseases might thus aid the understanding of how lung diseases impact the fate of inhaled compounds and thereby e.g. tailor inhaled doses and formulation designs to fit the diseased population. Closely investigating the pathophysiology of pulmonary diseases and subsequently incorporating the information within a mechanistic modelling framework would thus be an interesting area for future research. In the current model structure, the lung is divided into a tracheobronchial and an alveolar region. The anatomical model of the airway structure in [65] has 24 airway generations (excluding the nose and pharynx), thus making it possible to have up to 24 lung compartments. Increasing the number of pulmonary compartments would open up for incorporating more detailed information on regional physiological and anatomical differences as well as predicting drug concentrations in more defined regions. Clearly, a model with a higher regional resolution would be interesting, particularly if the drug target was known to be confined to a limited space in the lung. Nevertheless, the development of such a model would also require more detailed information on the regional differences and the modeller would need to make informed decisions on *e.g.* how to scale the permeability and blood perfusion across the lung. This leads the discussion to another interesting topic for future research: experimental characterisation of pulmonary permeability and, perhaps even more importantly, how it changes across the lung. Since both the type and the height of the epithelium changes across the lung [11], it is unlikely that one experimental assay, such as the Calu-3 cell line, would be representative of the permeability throughout the entire organ.

The model structure presented in this thesis was developed for predicting the PK of neutral compounds, such as FP, and does not therefore account for lung-retention caused by basicity. Even though basicity is a commonly used strategy for obtaining

lung-retention , the mechanism by which this occurs is still poorly understood. Recent research utilising empirical modelling demonstrated that a fraction of a dissolved, basic compound (olodaterol) was slowly absorbed from the lung [199]. The delayed absorption was proposed to be caused by lysosomal trapping. To the best of my knowledge, the temporal dynamics of this mechanism has not yet been investigated in the literature. Clearly, the field of inhalation PK would benefit from thoroughly investigating the mechanism(s) by which lung retention by basicity occurs at a *quantitative* level and subsequently develop a mechanistic model based on this information. This can be seen as a necessary step for progressing the understanding of the PK-behaviour of basic inhalation compounds and to thereby draw conclusions on how to optimise the chemical- and formulation-design of this compound class.

Another area, which would benefit from future research, is pulmonary drug dissolution. Firstly, measurement of compound solubility is an ongoing challenge and contemporary assays cannot provide quantitative measurements of the solubility in ELF, but should only be used to rank compounds with respect to solubility [200]. A quantitatively informative assay would require both a biorelevant dissolution medium as well as conditions similar to those seen *in vivo* (*e.g.* to mimic the thin fluid layer). Model predictions made in this thesis demonstrated that the solubility is an important parameter for predicting the pulmonary PK and the development of assays for measuring this property is thus an important avenue for future research. Secondly, the use of the Noyes-Brunner equation might be limited in the alveolar region where the particle diameter potentially exceeds the thickness of the ELF-layer. Due to the surfactant content, there should not be a wetting problem in this region and smaller particles are expected to be surrounded by the ELF. However,

depending on the thickness of the layer and the particle size, it may still limit the legitimate use of the Noyes-Brunner equation. To assess these limitations, more complex dissolution models involving partial differential equations might be needed. To the best of my knowledge, such models have not yet been developed, but it is plausible that the development of more advanced models might improve the predictions of drug dissolution in the alveolar region.

In preclinical research, the effect of an anti-inflammatory inhaled drug is often investigated by firstly inducing inflammation, *e.g.* by instillation of Sephadex as described by Källström *et al*. [147]. An interesting area for future research would be to mechanistically describe these challenge models and subsequently combine PBPK model predictions of free target site concentrations in appropriate lung regions with a either a PK/PD- or a systems pharmacology model to describe the drug effect. Clearly, several obstacles need to be overcome before reaching this goal. Perhaps the biggest challenge would be to produce time-resolved data of relevant biomarkers and thereby enable a mechanistic description of the challenge model as well as the pharmacological effect of the treatment. However, overcoming these challenges would provide a step-change in the understanding of contemporary preclinical PD-models and possibly also provide an opportunity for optimising the design of these studies.

6.2 Personal reflections

This thesis not only concerns modelling of inhalation pharmacokinetics, but also touches upon a broader topic relevant to the entire field of pharmacokinetics: the distinct differences between descriptive, non-mechanistic modelling and predictive, mechanistic modelling.

Pharmacokinetics is a field where experimental assays are continuously developed with the purpose of carefully characterising drug candidates with respect to various drug- and formulation-specific properties. Yet, the field has been dominated by non-mechanistic modelling approaches, precluding any possibilities to incorporate these invaluable experimental results in the modelling. Clearly, descriptive models are indisputably useful for *e.g.* describing drug concentration profiles, quantifying interindividual variability and predicting plasma pharmacokinetic profiles of *a particular* compound. It should be noted that the latter application area requires identical formulation-specific properties and its predictive capability across a broad range of doses is highly dependent on the study design, such that nonlinearities are detected. In this context, it cannot be emphasised enough that the choice of modelling approach should be made based on the purpose of the modelling exercise. Nevertheless, putting informative experimental results aside and instead relying on non-mechanistic approaches is not likely to advance our mechanistic understanding of the underlying drug disposition processes. From my viewpoint, this implies that scientific progress can be made by moving towards predictive, mechanistic modelling. By using the proposed approach, the drug- and formulation-specific properties will not merely be characterised but also be incorporated into a mechanistic model to progress our understanding. This brings the discussion back to inhalation pharmacokinetics: the utility of using the inhaled route for local as well as

systemic drug delivery suggests that the proposed shift towards predictive, mechanistic modelling is even more important for this particular niche of pharmacokinetics. That is, a thorough mechanistic understanding is required to enable identification of appropriate strategies in terms of chemical- and formulation design to *either*: 1) efficiently deliver drug to the systemic circulation, *or* 2) create a lung-selective drug exposure.

During this proposed journey, we will inevitably experience that our mechanistic inhalation model occasionally fails to predict the fate of compounds. However, this should not be seen as a failure but as a result *per se* as it serves to identify yet another gap in our knowledge and thus points us towards mechanisms, which would benefit from further exploration. Modelling should thus be an iterative process, which, combined with cleverly designed experiments, can advance our understanding of drug disposition processes. Clearly, identification of knowledge gaps is crucial for any researcher. In my mind, an approach leading to the identification of knowledge gaps should doubtlessly be favoured over the previously used non-mechanistic modelling approaches, which cannot progress our understanding of the underlying processes.

Easy as it may sound, introducing a new way of *approaching* a problem and suggesting an approach, which might not necessarily provide the solution but point us towards our knowledge gaps will doubtlessly face resistance within the scientific community of pharmacokinetics. It thus needs to be communicated that this modelling approach serves a slightly different purpose than the one previously used: instead being a tool for describing observed data, it is a tool for increasing our understanding of how the dynamic behaviour of the system responds to changes in various properties. Once proven predictive, this new approach thus opens up for

opportunities to rationally guide the chemical- and formulation design. However, it takes courage to leave an established approach, which is not likely to be questioned by a project team within pharmaceutical industry. This paradigm shift would thus, except from an effective communication, also require a project team, which is open for approaching the problem from a different angle. If the team ends up in a situation where the model predictions do not agree with the observed data, they might need to challenge their current understanding of the processes involved in pulmonary drug disposition and/or the pharmacological response of the investigated compound class. This approach thus requires one of the toughest, yet one of the most important, requirements on successful researchers: a humble attitude towards our limitations and knowledge gaps. By honestly and accurately identifying these, we open up for progressing the science.

Up until now, the focus has been on identifying knowledge gaps in the mechanistic understanding of the underlying processes of drug disposition and/or the pharmacological response of an investigated compound class. However, another aspect, which is equally important for the progression of systems models in general and mechanistic inhalation models in particular, is the technical development. The shift from simple, empirical models to more sophisticated, mechanistic models not only requires in-depth knowledge about the underlying processes but also places higher demands on the technical implementation both in terms of mathematics and programming. In the ideal situation, the progression of the biological knowledge and the technical development will go hand in hand, enabling us to benefit the most from both activities.

Personally, the shift from empirical to mechanistic models has changed my attitude towards modelling and how it can be used to rationally guide the chemical- and formulation design.

Chapter 7 References

[1]Sanders, M. Inhalation therapy: an historical review. *Primary care respiratory journal : journal of the General Practice Airways Group* **16**, 71-81 (2007).

[2]Bäckman, P., Adelmann, H., Petersson, G. & Jones, C.B. Advances in inhaled technologies: understanding the therapeutic challenge, predicting clinical performance, and designing the optimal inhaled product. *Clinical pharmacology and therapeutics* **95**, 509-520 (2014).

[3]Rosenfeld, G.C. & Loose, D.S. Toxicology: I. Principles and Terminology. In *Pharmacology*(eds. Rosenfeld, G.C. & Loose, D.S.) 320-322 (Lippincott Williams & Wilkins, New York, 2007).

[4]Olsson, B., et al. Pulmonary Drug Metabolism, Clearance, and Absorption. In *Controlled Pulmonary Drug Delivery*(eds. Smyth, H. & Hickey, A.) 21-50 (Springer, 2011).

[5]Winkler, J., Hochhaus, G. & Derendorf, H. How the Lung Handles Drugs: Pharmacokinetics and Pharmacodynamics of Inhaled Corticosteroids. *Proceedings of the American Thoracic Society* **1**, 356-363 (2004).

[6]Forbes, B., et al. Challenges in inhaled product development and opportunities for open innovation. *Adv. Drug Deliv. Rev.* **63**, 69-87 (2011).

[7]Cooper, A.E., Ferguson, D. & Grime, K. Optimisation of DMPK by the inhaled route: challenges and approaches. *Curr. Drug Metab.* **13**, 457-473 (2012).

[8]Edsbacker, S., Wollmer, P., Selroos, O., Borgstrom, L., Olsson, B. & Ingelf, J. Do airway clearance mechanisms influence the local and systemic effects of inhaled corticosteroids? *Pulm. Pharmacol. Ther.* **21**, 247-258 (2008).

[9]Sakagami, M. In vivo, in vitro and ex vivo models to assess pulmonary absorption and disposition of inhaled therapeutics for systemic delivery. *Advanced drug delivery reviews* **58**, 1030-1060 (2006).

[10]Sakagami, M., Kinoshita, W., Sakon, K. & Makino, Y. Fractional contribution of lung, nasal and gastrointestinal absorption to the systemic level following nose-only aerosol exposure in rats: a case study of 3.7- micro m fluorescein aerosols. *Archives of toxicology* **77**, 321-329 (2003).

[11]Patton, J.S. & Byron, P.R. Inhaling medicines: delivering drugs to the body through the lungs. *Nature reviews* **6**, 67-74 (2007).

[12]Weber, B. & Hochhaus, G. A pharmacokinetic simulation tool for inhaled corticosteroids. *The AAPS journal* **15**, 159-171 (2013).

[13]Chaudhuri, S.R., Lukacova, W.S. & Woltosz, W.S. Simulating the Disposition of Budesonide from Dry Powder Inhalers (DPIs) and Nebulizer. (2013).

[14]Hochhaus, G., Mollmann, H., Derendorf, H. & Gonzalez-Rothi, R.J. Pharmacokinetic/pharmacodynamic aspects of aerosol therapy using glucocorticoids as a model. *J. Clin. Pharmacol.* **37**, 881-892 (1997).

[15]Borghardt, J.M., Weber, B., Staab, A. & Kloft, C. Pharmacometric Models for Characterizing the Pharmacokinetics of Orally Inhaled Drugs. *AAPS J.* (2015).

[16]Wang, Y.B., Watts, A.B., Peters, J.I. & Williams, R.O.,3rd. The impact of pulmonary diseases on the fate of inhaled medicines--a review. *Int. J. Pharm.* **461**, 112-128 (2014).

[17]Martonen, T., Fleming, J., Schroeter, J., Conway, J. & Hwang, D. In silico modeling of asthma. *Adv. Drug Deliv. Rev.* **55**, 829-849 (2003).

[18]Derendorf, H., Nave, R., Drollmann, A., Cerasoli, F. & Wurst, W. Relevance of pharmacokinetics and pharmacodynamics of inhaled corticosteroids to asthma. *Eur. Respir. J.* **28**, 1042-1050 (2006).

[19]Global Initiative for Asthma (GINA). What's new in GINA 2015? **2016** (2015).

[20]Global Initiative for Chronic Obstructive Lung Disease (GOLDCOPD). At-A-Glance Outpatient Management Reference for Chronic Obstructive Pulmonary Disease (COPD). **2016** (2016).

[21]Patton, J.S., Fishburn, C.S. & Weers, J.G. The lungs as a portal of entry for systemic drug delivery. *Proceedings of the American Thoracic Society* **1**, 338-344 (2004).

[22]Schulz, H. & Mühle, H. Respiration. In *The Laboratory Rat*(ed. Krinke, G.J.) 323-344 (Academic Press, San Diego, 2000).

[23]Staub, C.N. Pulmonary and Bronchial Circulations. In *Basic Respiratory Physiology*(ed. Staub, C.N.) 105-127 (Churchill Livingstone Inc., London, 1991).

[24]Rhoades, R.A. Pulmonary Circulation and Ventilation-Perfusion. In *Medical Physiology. Principles for Clinical Medicine*(eds. Rhoades, R.A. & Bell, R.D.) 361-373 (Wolters Kluwer | Lippincott Williams & Wilkins, Philadelphia, 2009).

[25]Finlay, W.H. Introduction to the Respiratory Tract. In *The Mechanics of Inhaled Pharmaceutical Aerosols: An Introduction*(ed. Finlay, W.H.) 93-105 (Academic Press, San Diego, 2001).

[26]Flieder, D.B. Normal Anatomy, Tissue Artifacts, and Incidental Structures. In *Pulmonary Pathology*(eds. Zander, S.D. & Farver, C.F.) 1-8 (Churchill Livingstone, Philadelphia, 2008).

[27]Wang, C. Morphometry of the Human Respiratory System. In *Inhaled Particles*(ed. Wang, C.) 7-30 (Elsevier, London, 2005).

[28]Zhai, S. Pharmacokinetics of Isolated Lung Perfusion with Antitumor Agens. In *Handbook of Anticancer Pharmacokinetics and Pharmacodynamics*(eds. Figg, D.W. & McLeod, H.L.) 363-373 (Springer Science+Business Media, New York, 2004).

[29]Massaro, E.J. Structure and function of the respiratory tract. In *Handbook of Human Toxicology*(ed. Pinkerton, K.E., et al) 469-491 (CRC Press, USA, 1997).

[30]Gehr, P. Annexe A. Anatomy and morphology of the respiratory tract. *Ann. ICRP* **24**, 121-166 (1994).

[31]van der Vliet, A. Antioxidant Defenses in the Lung. In *Comparative Biology of the Normal Lung*(ed. Parent, R.A.) 489-510 (Academic Press, London, 2015).

[32]Gustafsson, D.L. & Bradshaw-Pierce, E.L. Fundamental Concepts in Clinical Pharmacology. In *Principles of Anticancer Drug Development*(eds. Hidalgo, M., Eckhardt, S.G., Garret-Mayer, E. & Clendeninn, N.J.) 37-62 (Springer, New York, 2010).

[33]Ruiz-Garcia, A., Bermejo, M., Moss, A. & Casabo, V.G. Pharmacokinetics in drug discovery. *J. Pharm. Sci.* **97**, 654-690 (2008).

[34]Rowland, M. & Tozer, T.N. Absorption and Distribution. In *Clinical Pharmacokinetics. Concepts and Applications*(eds. Rowland, M. & Tozer, T.N.) 11-52 (William & Wilkins, Philiadelphia, 1995).

[35]Brenner, G.M. & Stevens, C.W. Principles of Pharmacology. In *Pharmacology*(eds. Brenner, G.M. & Stevens, C.W.) 2-45 (Elsevier, Philadelphia, 2013).

[36]Peters, S.A. Drug absorption and gut bioavailability. In *Physiologically-Based Pharmacokinetic (PBPK) Modeling and Simulations: Principles, Methods, and Applications in the Pharmaceutical Industry*(ed. Peters, S.A.) 47 (Wiley, 2012).

[37]Rowland, M. & Tozer, T.N. Physiologic Concepts and Kinetics. In *Clinical Pharmacokinetics. Concepts and Applications*(eds. Rowland, M. & Tozer, T.N.) 109-202 (William & Wilkins, Philiadelphia, 1995).

[38]Lalonde, R.L. Pharmacodynamics. In *Applied Pharmacokinetics & Pharmacodynamics. Principles of Therapeutic Drug Monitoring*(eds. Burton, M.E., Shaw, L.M., Schentag, J.J. & Evans, W.E.) 60-81 (Lippincott Williams & Wilkins, Philadelphia, 2006).

[39]Meibohm, B. & Derendorf, H. Basic concepts of pharmacokinetic/pharmacodynamic (PK/PD) modelling. *Int. J. Clin. Pharmacol. Ther.* **35**, 401-413 (1997).

[40]Rajman, I. PK/PD modelling and simulations: utility in drug development. *Drug Discov. Today* **13**, 341-346 (2008).

[41]Danhof, M., Alvan, G., Dahl, S.G., Kuhlmann, J. & Paintaud, G. Mechanism-based pharmacokinetic-pharmacodynamic modeling-a new classification of biomarkers. *Pharm. Res.* **22**, 1432-1437 (2005).

[42]Derendorf, H. Pharmacokinetic and pharmacodynamic properties of inhaled corticosteroids in relation to efficacy and safety. *Respir. Med.* **91 Suppl A**, 22-28 (1997).

[43]Labiris, N. & Dolovich, M. **Pulmonary drug delivery. Part I: Physiological factors affecting therapeutic effectiveness of aerosolized medications**. *British Journal of Clinical Pharmacology* **56**, 588-599 (2003).

[44]Cooper, A., Ferguson, D. & Grime, K. Optimisation of DMPK by the inhaled route: challenges and approaches. *Current drug metabolism* **13**, 457-473 (2012).

[45]Rohatagi, S., Derendorf, H. & Zech, K. Risk-benefit value of inhaled corticosteroids: a pharmacokinetic/pharmacodynamic perspective. *Chest* **123**, 430S-1S (2003).

[46]Agu, R.U., Ugwoke, M.I., Armand, M., Kinget, R. & Verbeke, N. The lung as a route for systemic delivery of therapeutic proteins and peptides. *Respiratory research* **2**, 198-209 (2001).

[47]Barnes, P.J. Inhaled Corticosteroids. *Pharmaceuticals (Basel)* **3**, 514-540 (2010).

[48]Global Initiative for Asthma (GINA). Global strategy for Asthma Management and Prevention, Global Initiative for Asthma (GINA) 2015. **2015** (2015).

[49]Powell, H. & Gibson, P.G. Inhaled corticosteroid doses in asthma: an evidence-based approach. *Med. J. Aust.* **178**, 223-225 (2003).

[50]Adams, N.P. & Jones, P.W. The dose–response characteristics of inhaled corticosteroids when used to treat asthma: An overview of Cochrane systematic reviews. *Respir. Med.* **100**, 1297-1306 (2006).

[51]Barnes, P.J. Corticosteroids. In ***Asthma and COPD: Basic Mechanisms and Clinical Management***(eds. Barnes, P.J., Drazen, J., Rennard, S.I. & Thomson, N.C.) 639-654 (Academic Press, USA, 2009).

[52]Moynihan, A.H. & Crean, A.M. Drug partitioning and transport across biological barriers. In *The physicochemical basis of pharmaceutical*(eds. Moynihan, A.H. & Crean, A.M.) 212-254 (Oxford University Press, Oxford, 2009).

[53]Bosquillon, C. Drug transporters in the lung—do they play a role in the biopharmaceutics of inhaled drugs? *J. Pharm. Sci.* **99**, 2240-2255 (2010).

[54]Marques, M.R.C., Loebenberg, R. & Almukainzi, M. Simulated Biological Fluids with Possible Application in Dissolution Testing. *Dissolution Technologies* **18**, 15-28 (2011).

[55]Jones, H. & Rowland-Yeo, K. Basic concepts in physiologically based pharmacokinetic modeling in drug discovery and development. **2**, 1-12 (2013).

[56]Widdicombe, J.G. Airway liquid: a barrier to drug diffusion? *The European respiratory journal* **10**, 2194-2197 (1997).

[57]Wurthwein, G. & Rohdewald, P. Activation of beclomethasone dipropionate by hydrolysis to beclomethasone-17-monopropionate. *Biopharm. Drug Dispos.* **11**, 381-394 (1990).

[58]Nave, R., Fisher, R. & McCracken, N. In vitro metabolism of beclomethasone dipropionate, budesonide, ciclesonide, and fluticasone propionate in human lung precision-cut tissue slices. *Respir. Res.* **8**, 65-9921-8-65 (2007).

[59]Labiris, N. & Dolovich, M. Pulmonary drug delivery. Part I: Physiological factors affecting therapeutic effectiveness of aerosolized medications. *British Journal of Clinical Pharmacology* **56**, 588–599. (2003).

[60]NCRP. Deposition, retention and dosimetry of inhaled radioactive substances. **125** (1997).

[61]Hofmann, W. Modelling inhaled particle deposition in the human lung—A review. *J. Aerosol Sci.* **42**, 693-724 (2011).

[62]Rosati, J.A., Isaacs, K.K. & Martonen, T.B. Mechanisms of Particle Deposition. In *Aerosols Handbook. Measurement, Dosimetry and Health Effects*(eds. Ruzer, L.S. & Harley, N.H.) 47-74 (CRC Press, New York, 2013).

[63]Yeh, H.C., Phalen, R.F. & Raabe, O.G. Factors influencing the deposition of inhaled particles. *Environ. Health Perspect.* **15**, 147-156 (1976).

[64]Ramachandran, R. Chapter 10: Particle Motion in a Viscous Medium. In *Occupational Exposure Assessment for Air Contaminants*(ed. Ramachandran, R.) 129-148 (CRC Press, Roca Baton, 2005).

[65]Lee, D. & Wexler, A.S. Particle deposition in juvenile rat lungs: A model study. *J. Aerosol Sci.* **42**, 567-579 (2011).

[66]Schmid, O., Bolle, I., Harder, V., Karg, E., Takenaka, S. & Schulz,H.,Ferron,G.A. Model for the deposition of aerosol particles in the respiratory tract of the rat. I. Nonhygroscopic particle deposition. *Journal of aerosol medicine and pulmonary drug delivery* **21**, 291-307 (2008).

[67]Thomas, J.,W. Gravity Settling of Particles in a Horizontal Tube. *Journal of the Air Pollution Control Association* **8**, 32-34 (1958).

[68]Gerrity, T.R., Lee, P.S., Hass, F.J., Marinelli, A., Werner, P. & Lourenco, R.V. Calculated deposition of inhaled particles in the airway generations of normal subjects. *Journal of Applied Physiology* **47**, 867-873 (1979).

[69]Hofmann, W., Asgharian, B., Bergmann, R., Anjilvel, S. & Miller, F.J. The effect of heterogeneity of lung structure on particle deposition in the rat lung. *Toxicological sciences* **53**, 430-437 (2000).

[70]Asgharian, B. & Anjilvel, S. A multiple-path model of fiber deposition in the rat lung. *Toxicol. Sci.* **44**, 80-86 (1998).

[71]Munkholm, M. & Mortensen, J. Mucociliary clearance: pathophysiological aspects. *Clin. Physiol. Funct. Imaging* **34**, 171-177 (2014).

[72]Kirch, J., et al. Mucociliary clearance of micro- and nanoparticles is independent of size, shape and charge--an ex vivo and in silico approach. *J. Control. Release* **159**, 128-134 (2012).

[73]Edsbäcker, S. Uptake, Retention, and Biotransformation of Corticosteroids in the Lung and Airways. In *Inhaled Steroids in Asthma. Optimizing Effects in the Airways*(eds. Schleimer, R.P., O'Byrne, P.M., Szefler, S.J. & Brattsand, R.) 213-246 (Marcel Dekker, New York, 2002).

[74]Lansley, A.B. Mucociliary clearance and drug delivery via the respiratory tract. *Adv. Drug Deliv. Rev.* **11**, 299-327 (1993).

[75]Thorsson, L., Edsbacker, S., Kallen, A. & Lofdahl, C.G. Pharmacokinetics and systemic activity of fluticasone via Diskus and pMDI, and of budesonide via Turbuhaler. *Br. J. Clin. Pharmacol.* **52**, 529-538 (2001).

[76]Derendorf, H., Hochhaus, G., Möllman, H. & Krishnaswami, S. Systemic Disposition and Effacts of Inhaled Corticosteroids. In *Inhaled Steroids in Asthma. Optimizing Effects in the Airways*(eds. Schleimer, R.P., O'Byrne, P.M., Szefler, S.J. & Brattsand, R.) 247-272 (Marcel Dekker, New York, 2002).

[77]Backstrom, E., et al. Development of a Novel Lung Slice Methodology for Profiling of Inhaled Compounds. *J. Pharm. Sci.* (2015).

[78]Brattsand, R. & Miller-Larsson, A. The role of intracellular esterification in budesonide once-daily dosing and airway selectivity. *Clin. Ther.* **25 Suppl C**, C28-41 (2003).

[79]Jendbro, M., Johansson, C., Strandberg, P., Falk-Nilsson, H. & Edsbaecker, S. Pharmacokinetics of budesonide and its major ester metabolite after inhalation and intravenous administration. *Drug metabolism and disposition: the biological fate of chemicals* **29**, 769-776 (2001).

[80]Hogger, P. & Rohdewald, P. Binding kinetics of fluticasone propionate to the human glucocorticoid receptor. *Steroids* **59**, 597-602 (1994).

[81]Wong, B.A. Inhalation exposure systems: design, methods and operation. *Toxicol. Pathol.* **35**, 3-14 (2007).

[82]Driscoll, K.E., et al. Intratracheal instillation as an exposure technique for the evaluation of respiratory tract toxicity: uses and limitations. *Toxicol. Sci.* **55**, 24-35 (2000).

[83]Alexander, D., et al. Association of Inhalation Toxicologists (AIT) working party recommendation for standard delivered dose calculation and expression in non-clinical aerosol inhalation toxicology studies with pharmaceuticals. *Inhalation toxicology* **20**, 1179-1189 (2008).

[84]Forbes, B., et al. Challenges in inhaled product development and opportunities for open innovation. *Advanced drug delivery reviews* **63**, 69-87 (2011).

[85]Smith, D.A., Di, L. & Kerns, E.H. The effect of plasma protein binding on in vivo efficacy: misconceptions in drug discovery. *Nat. Rev. Drug Discov.* **9**, 929-939 (2010).

[86]MacIntyre, A.C. & Cutler, D.J. The potential role of lysosomes in tissue distribution of weak bases. *Biopharm. Drug Dispos.* **9**, 513-526 (1988).

[87]Rennard, S.I., et al. Estimation of volume of epithelial lining fluid recovered by lavage using urea as marker of dilution. *J. Appl. Physiol. (1985)* **60**, 532-538 (1986).

[88]Meibohm, B., et al. A pharmacokinetic/pharmacodynamic approach to predict the cumulative cortisol suppression of inhaled corticosteroids. *J. Pharmacokinet. Biopharm.* **27**, 127-147 (1999).

[89]Mollmann, H., et al. Pharmacokinetic/pharmacodynamic evaluation of systemic effects of flunisolide after inhalation. *J. Clin. Pharmacol.* **37**, 893-903 (1997).

[90]Mollmann, H., et al. Pharmacokinetic and pharmacodynamic evaluation of fluticasone propionate after inhaled administration. *Eur. J. Clin. Pharmacol.* **53**, 459-467 (1998).

[91]Conte, J.E.,Jr, Golden, J.A., Kipps, J. & Zurlinden, E. Intrapulmonary pharmacokinetics of linezolid. *Antimicrob. Agents Chemother.* **46**, 1475-1480 (2002).

[92]Kikuchi, E., Kikuchi, J., Nasuhara, Y., Oizumi, S., Ishizaka, A. & Nishimura, M. Comparison of the pharmacodynamics of biapenem in bronchial epithelial lining fluid in healthy volunteers given half-hour and three-hour intravenous infusions. *Antimicrob. Agents Chemother.* **53**, 2799-2803 (2009).

[93]Hochhaus, G. & Mollmann, H. Pharmacokinetic/pharmacodynamic characteristics of the beta-2-agonists terbutaline, salbutamol and fenoterol. *Int. J. Clin. Pharmacol. Ther. Toxicol.* **30**, 342-362 (1992).

[94]Bonate, P.L. The Art of Modeling. In *Pharmacokinetic-Pharmacodynamic Modeling and Simulation*(ed. Bonate, P.L.) 1-60 (Springer, London, 2011).

[95]Godfrey, K. Introduction to Compartmental Modelling. In *Compartmental models and their application*(ed. Godfrey, K.) 1-11 (Academic Press Inc., London, 1983).

[96]Rowland, M. & Tozer, T.N. Distribution kinetics. In *Clinical Pharmacokinetics. Concepts and Applications*(eds. Rowland, M. & Tozer, T.N.) 313-339 (Williams & Wilkins, Philadelphia, 1995).

[97]Gabrielsson, J. & Weiner, D. Pharmacokinetic Concepts. In *Pharmacokinetic & Pharmacodynamic Data Analysis: Concepts and Applications*(eds. Gabrielsson, J. & Weiner, D.) 11-224 (Swedish Pharmaceutical Press, Stockholm, 2007).

[98]Peters, S.A. Physiogically-Based Modeling. In *Physiogically-Based Pharmacokinetic (PBPK) Modeling and Simulation*(ed. Peters, S.A.) 13-13-16 (Wiley, 2012).

[99]Peters, S.A. Hypothesis generation and pharmacokinetic precictions. In *Physiologically-Based Pharmacokinetic (PBPK) Modeling and Simulations: Principles, Methods, and Applications in the Pharmaceutical Industry*(ed. Peters, S.A.) 273 (Wiley, 2012).

[100]Rowland, M., Peck, C. & Tucker, G. Physiologically-based pharmacokinetics in drug development and regulatory science. *Annu. Rev. Pharmacol. Toxicol.* **51**, 45-73 (2011).

[101]Pang, K.S., Sun, H. & Chow, E.C.Y. Chapter 5: Impact of Physiological Determinants: Flow, Binding, Transporters and Enzymes on Organ and Total Body Clearance. In ***Enzyme- and Transporter-Based Drug-Drug Interactions:*** *Progress and Future Challenges*(eds. Pang, K.S., Rodrigues, A.D. & Peter, R.M.) 114-107-150 (Springer, 2009).

[102]Badhan, R.K.S., Chenel, M. & Penny, J.I. Development of a physiologically-based pharmacokinetic model of the rat central nervous system. *Pharmaceutics* **6**, 97-136 (2014).

[103]Peters, S.A. Physiological model for distribution. In *Physiologically-Based Pharmacokinetic (PBPK) Modeling and Simulations: Principles, Methods, and Applications in the Pharmaceutical Industry* (ed. Peters, S.A.) 111 (Wiley, 2012).

[104]Jones, H.M., Gardner, I.B. & Watson, K.J. Modelling and PBPK Simulation in Drug Discovery. *The AAPS Journal* **11**, 155-166 (2009).

[105]Rodgers, T. & Rowland, M. Physiologically based pharmacokinetic modelling 2: predicting the tissue distribution of acids, very weak bases, neutrals and zwitterions. *Journal of pharmaceutical sciences* **95**, 1238-1257 (2006).

[106]Graham, S.G. Prediction of drug distribution in rat and human. , 18 (2012).

[107]Mager, D.E. & Ramanathan, M. Preclinical Pharmacokinetics. In *Handbook of pharmaceutical biotechnlogy*(ed. Gad, S.C.) 272-253-273 (Wiley, New Jersey, 2007).

[108]Rowland Yeo, K., Jamei, M., Yang, J., Tucker, G.T. & Rostami-Hodjegan, A. Physiologically based mechanistic modelling to predict complex drug-drug interactions involving simultaneous competitive and time-dependent enzyme inhibition by parent compound and its metabolite in both liver and gut -The effect of diltiazem on the time-course of exposure to triazolam. *European Journal of Pharmaceutical Sciences* **39**, 298-309 (2010).

[109]Nestorov, I.A., Aarons, L.J., Arundel, P.A. & Rowland, M. Lumping of whole-body physiologically based pharmacokinetic models. *J. Pharmacokinet. Biopharm.* **26**, 21-46 (1998).

[110]Chis, O., Banga, J.R. & Balsa-Canto, E. Structural Identifiability of Systems Biology Models: A Critical Comparison of Methods. *PLoS ONE* **6**, e27755 (2011).

[111]Bellman, R. & Åström, K.J. On structural identifiability. *Math. Biosci.* **7**, 329-339 (1970).

[112]Vanrolleghem, P. & De Pauw, D. Practical aspects of sensitivity analysis for dynamic models. (2003).

[113]Saltelli, A. Global sensitivity analysis: An introduction. , 27-43 (2004).

[114]Snelder, N., et al. PKPD modelling of the interrelationship between mean arterial BP, cardiac output and total peripheral resistance in conscious rats. *Br. J. Pharmacol.* **169**, 1510-1524 (2013).

[115]van Aalderen, W.M.C. & Sprikkelman, A.B. Inhaled corticosteroids in childhood asthma: the story continues. *Eur. J. Pediatr.* **170**, 709-718 (2011).

[116]Barnes, P.J. Anti-inflammatory actions of glucocorticoids: molecular mechanisms. *Clin. Sci. (Lond)* **94**, 557-572 (1998).

[117]Derendorf, H., et al. Receptor-based pharmacokinetic-pharmacodynamic analysis of corticosteroids. *Journal of clinical pharmacology JID - 0366372* , 115-123 (0329).

[118]Ramakrishnan, R., DuBois, D.C., Almon, R.R., Pyszczynski, N.A. & Jusko, W.J. Fifth-generation model for corticosteroid pharmacodynamics: application to steady-state receptor down-regulation and enzyme induction patterns during seven-day continuous infusion of methylprednisolone in rats. *J. Pharmacokinet. Pharmacodyn.* **29**, 1-24 (2002).

[119]Steiniger, B., Kniess, T., Bergmann, R., Pietzsch, J. & Wuest, F.R. Radiolabeled glucocorticoids as molecular probes for imaging brain glucocorticoid receptors by means of positron emission tomography (PET). *Mini Rev. Med. Chem.* **8**, 728-739 (2008).

[120]Hochhaus, G., Gonzalez-Rothi, R.J., Lukyanov, A., Derendorf, H., Schreier, H. & Dalla Costa, T. Assessment of glucocorticoid lung targeting by ex-vivo receptor binding studies in rats. *Pharm. Res.* **12**, 134-137 (1995).

[121]Fish, L., et al. An improved method of determining *ex vivo* glucocorticoid receptor occupancy using [3H]Dexamethasone in rats. **1** (2007).

[122]Chernet, E., et al. Use of LC/MS to assess brain tracer distribution in preclinical, in vivo receptor occupancy studies: Dopamine D2, serotonin 2A and NK-1 receptors as examples. *Life Sci.* **78**, 340-346 (2005).

[123]Miller, T.R., et al. Use of the H3 receptor antagonist radioligand [3H]-A-349821 to reveal in vivo receptor occupancy of cognition enhancing H3 receptor antagonists. *Br. J. Pharmacol.* **157**, 139-149 (2009).

[124]Kapur, S., Barlow, K., VanderSpek, S.C., Javanmard, M. & Nobrega, J.N. Drug-induced receptor occupancy: substantial differences in measurements made in vivo vs ex vivo. *Psychopharmacology (Berl)* **157**, 168-171 (2001).

[125]Friden, M., Wennerberg, M., Antonsson, M., Sandberg-Stall, M., Farde, L. & Schou, M. Identification of positron emission tomography (PET) tracer candidates by prediction of the target-bound fraction in the brain. *EJNMMI Research* **4**, 50 (2014).

[126]Boger, E., et al. A novel in vivo receptor occupancy methodology for the glucocorticoid receptor: toward an improved understanding of lung pharmacokinetic/pharmacodynamic relationships. *J. Pharmacol. Exp. Ther.* **353**, 279-287 (2015).

[127]Edman, K., et al. The discovery of potent and selective non-steroidal glucocorticoid receptor modulators, suitable for inhalation. *Bioorg. Med. Chem. Lett.* **24**, 2571-2577 (2014).

[128]Boger, E. Development of target occupancy methodologies for the study of pulmonary drug delivery and target engagement. (2012).

[129]Need, A.B., et al. The relationship of in vivo central CB1 receptor occupancy to changes in cortical monoamine release and feeding elicited by CB1 receptor antagonists in rats. *Psychopharmacology (Berl)* **184**, 26-35 (2006).

[130]Need, A.B., McKinzie, J.H., Mitch, C.H., Statnick, M.A. & Phebus, L.A. In vivo rat brain opioid receptor binding of LY255582 assessed with a novel method using LC/MS/MS and the administration of three tracers simultaneously. *Life Sci.* **81**, 1389-1396 (2007).

[131]Nirogi, R., et al. In-vivo rat striatal 5-HT4 receptor occupancy using non-radiolabelled SB207145. *J. Pharm. Pharmacol.* **65**, 704-712 (2013).

[132]Farde, L., Wiesel, F.A., Halldin, C. & Sedvall, G. Central D2-dopamine receptor occupancy in schizophrenic patients treated with antipsychotic drugs. *Arch. Gen. Psychiatry* **45**, 71-76 (1988).

[133]Wadenberg, M.L., Kapur, S., Soliman, A., Jones, C. & Vaccarino, F. Dopamine D2 receptor occupancy predicts catalepsy and the suppression of conditioned avoidance response behavior in rats. *Psychopharmacology (Berl)* **150**, 422-429 (2000).

[134]Johnson, M. Fluticasone propionate: safety profile. *Cutis* **57**, 10-12 (1996).

[135]Laerd Statistics. One-way ANOVA. **2015**.

[136]Trujillo-Ortiz, A. Levenes Test. **2015** (2003).

[137]Schaaf, M.J. & Cidlowski, J.A. Molecular mechanisms of glucocorticoid action and resistance. *J. Steroid Biochem. Mol. Biol.* **83**, 37-48 (2002).

[138]Miller, A.H., Spencer, R.L., Stein, M. & McEwen, B.S. Adrenal steroid receptor binding in spleen and thymus after stress or dexamethasone. *Am. J. Physiol.* **259**, E405-12 (1990).

[139]Tozer, N.T. & Rowland, M. Chapter 5: Disposition Following Intravenous Bolus. In *Introduction to Pharmacokinetics and Pharmacodynamics: The Quantitative Basis of Drug Therapy* (eds. Troy, D.B. & Klingler, A.) 63-104 (Lippincott Williams & Wilkins, Philadelphia, 2006).

[140]Gearhart, J.M., Jepson, G.W., Clewell, H.J., Andersen, M.E. & Conolly, R.B. Physiologically based pharmacokinetic and pharmacodynamic model for the inhibition of acetylcholinesterase by diisopropylfluorophosphate. *Toxicology and applied pharmacology* **106**, 295-310 (1990).

[141]Chen, A. & Kaufman, S. Splenic blood flow and fluid efflux from the intravascular space in the rat. *The Journal of physiology* **490**, 493-499 (1996).

[142]Brown, R.P., Delp, M.D., Lindstedt, S.L., Rhomberg, L.R. & Beliles, R.P. Physiological parameter values for physiologically based pharmacokinetic models. *Toxicology and industrial health* **13**, 407-484 (1997).

[143]Matic, G., Trajkovic, D., Damjanovic, S. & Petrovic, J. Modifications of rat liver glucocorticoid receptor by insulin-induced hypoglycemia. *Biochim. Biophys. Acta* **1051**, 192-198 (1990).

[144]Siller, H., Taylor, J.D. & Middleton, B. Two-start design within a Sephadex inflammatory model – A means to generate reliable ED50 data whilst significantly reducing the number of animals used. *Pulm. Pharmacol. Ther.* **25**, 223-227 (2012).

[145]Hamm, T.E., Vasbinder, M.A. & King-Herbert, A. Toxicology. In *The Laboratory Rat*(eds. Suckow,M.A.,Weisbroth,S.H. & Franklin, C.L.) 803-817 (Elsevier Academic Press, Burlington, 2005).

[146]Esmailpour, N., Hogger, P. & Rohdewald, P. Binding kinetics of budesonide to the human glucocorticoid receptor. *Eur. J. Pharm. Sci.* **6**, 219-223 (1998).

[147]Kallstrom, L., Brattsand, R., Lovgren, U., Svensjo, E. & Roempke, K. A rat model for testing anti-inflammatory action in lung and the effect of glucocorticosteroids (GCS) in this model. *Agents Actions* **17**, 355-357 (1986).

[148]AstraZeneca. AZ data on file.

[149]Agoram, B. Evaluating Systems Pharmacology Models Is Different From Evaluating Standard Pharmacokinetic-Pharmacodynamic Models. *CPT Pharmacometrics Syst. Pharmacol.* **3**, e101-. Epub 2014 Feb 19 doi:10.1038/psp.2013.77 (2014).

[150]Dunning, M.B. Respiratory physiology. In *Physiology secrets*(ed. Raff, H.) 91-123 (Hanley&Belfus, Philadelphia, 2003).

[151]Tronde, A. & Bosquillon,C., Forbes,B. The Isolated Perfused Lung for Drug Absorption Studies. In *Drug Absorption Studies In Situ, In Vitro and In Silico Models*(ed. Ehrhardt,C., Kim,K.J.) 135-135-163 (Springer, New York, 2008).

[152]Gerde, P., Muggenburg, B.A., Hoover, M.D. & Henderson, R.F. Disposition of polycyclic aromatic hydrocarbons in the respiratory tract of the beagle dog. I. The alveolar region. *Toxicol. Appl. Pharmacol.* **121**, 313-318 (1993).

[153]Gerde, P., Muggenburg, B.A., Thornton-Manning, J.R., Lewis, J.L., Pyon, K.H. & Dahl, A.R. Benzo[a]pyrene at an environmentally relevant dose is slowly absorbed by, and extensively metabolized in, tracheal epithelium. *Carcinogenesis* **18**, 1825-1832 (1997).

[154]Anjilvel, S. & Asgharian, B. A multiple-path model of particle deposition in the rat lung. *Fundamental and applied toxicology* **28**, 41-50 (1995).

[155]Pesic, J., et al. In Vivo Assessment Of Mucociliary Clearance In Rodents Via SPECT Imaging After Instillation And Inhalation Of A 99mTc-Labelled Colloid. *C37.COPD: WHAT IS NEW IN IMAGING?* , A4327-A4327 (2014).

[156]Creutzenberg, O., Muhle, H. & Bellmann, B. Nasal Retention and Clearance of Wood Dust in Rats. *Ann. Occup. Hyg.* **38**, 895-901 (1994).

[157]Chanoine, F., Grenot, C., Heidmann, P. & Junien, J.L. Pharmacokinetics of butixocort 21-propionate, budesonide, and beclomethasone dipropionate in the rat after intratracheal, intravenous, and oral treatments. *Drug Metabolism and Disposition* **19**, 546-553 (1991).

[158]Brunner, E. & Nernst, W. Theorie der Reaktionsgeschwindigkeit in heterogenen Systemen. *Zeitschrift für physikalische Chemie, Stöchiometrie und Verwandtschaftslehre* **47**, 56-102 (1904).

[159]Noyes, A. & Whitney, W.R. The rate of solution of solid substances in their own solutions. *J. Am. Chem. Soc.* **19**, 930-934 (1897).

[160]Kesisoglou, F. & Wu, Y. Understanding the effect of API properties on bioavailability through absorption modeling. *The AAPS journal* **10**, 516-525 (2008).

[161]Gaohua, L., et al. Development of a Multicompartment Permeability-Limited Lung PBPK Model and Its Application in Predicting Pulmonary Pharmacokinetics of Antituberculosis Drugs. *CPT: Pharmacometrics & Systems Pharmacology* , n/a-n/a (2015).

[162]Wang, J. & Flanagan, D.R. General solution for diffusion-controlled dissolution of spherical particles. 1. Theory. *J. Pharm. Sci.* **88**, 731-738 (1999).

[163]Spencer, R.L., Young, E.A., Choo, P.H. & McEwen, B.S. Adrenal steroid type I and type II receptor binding: estimates of in vivo receptor number, occupancy, and activation with varying level of steroid. *Brain Res.* **514**, 37-48 (1990).

[164]AstraZeneca. Internal data.

[165]Peters, S.A. Physiological models for absorption. In *Physiologically-Based Pharmacokinetics (PBPK) Modeling and Simulation*(ed. Peters, S.A.) 44-88 (Wiley, 2012).

[166]Galia, E., Nicolaides, E., Hörter, D., Löbenberg, R., Reppas, C. & Dressman, J.B. Evaluation of Various Dissolution Media for Predicting In Vivo Performance of Class I and II Drugs. *Pharm. Res.* **15**, 698-705 (1998).

[167]Jones, J.H. & Longworth, K.E. Comparative Biology of Airway Lining Fluid. In *Treatise on Pulmonary Toxicology, Volume I: Comparative Biology of the Normal Lung*(ed. Parent, R.A.) 621 (CRC Press, 1992).

[168]Nie, Y.C., et al. Anti-inflammatory effects of naringin in chronic pulmonary neutrophilic inflammation in cigarette smoke-exposed rats. *Journal of medicinal food* **15**, 894-900 (2012).

[169]Weiler, E. & Farbman, A.I. Proliferation in the rat olfactory epithelium: age-dependent changes. *J. Neurosci.* **17**, 3610-3622 (1997).

[170]Arundel, P.A. A multicompartment model generally applicable to physiologically-based pharmacokinetics. , 129-133 (1997).

[171]Campbell, J.L., Andersen, M.E. & Clewell, H.J. A hybrid CFD-PBPK model for naphthalene in rat and human with IVIVE for nasal tissue metabolism and cross-species dosimetry. *Inhalation Toxicology* **26**, 333-344 (2014).

[172]Yeh, H.C., Schum, G.M. & Duggan, M.T. Anatomic models of the tracheobronchial and pulmonary regions of the rat. *The Anatomical record* **195**, 483-492 (1979).

[173]Jones, J.H. & Longworth, K.E. Chapter 19: Gas Exchange at Rest and During Exercise in Mammals. In *Treatise on Pulmonary Toxicology, Volume I: Comparative*

Biology of the Normal Lung (ed. Parent, R.A.) 271-307 (CRC Press, Florida, USA, 1992).

[174]Schreider, J.P. Nasal Airway Anatomy and Inhalation Deposition in Experimental Animals and People. In *Nasal Tumors in Animals and Man*(eds. Reznik, G. & Stinson, S.F.) 1-26 (CRC Press, Florida, USA, 1983).

[175]Tunek, A., Sjodin, K. & Hallstrom, G. Reversible formation of fatty acid esters of budesonide, an antiasthma glucocorticoid, in human lung and liver microsomes. *Drug Metab. Dispos.* **25**, 1311-1317 (1997).

[176]Edsbacker, S. & Jendbro, M. Modes to Achieve Topical Selectivity of Inhaled Glucocorticosteroids - Focus on Budesonide . **1**, 71-82 (1998).

[177]Li, D. & Kerns, E.H. Permeability Methods. In *Drug-like Properties: Concepts, Structure Design and Methods: from ADME to Toxicity Optimization*(eds. Li, D. & Kerns, E.H.) 287-296 (Elsevier, UK, 2008).

[178]Harrison, T.W., Wisniewski, A., Honour, J. & Tattersfield, A.E. Comparison of the systemic effects of fluticasone propionate and budesonide given by dry powder inhaler in healthy and asthmatic subjects. *Thorax* **56**, 186-191 (2001).

[179]Brutsche, M.H., et al. Comparison of pharmacokinetics and systemic effects of inhaled fluticasone propionate in patients with asthma and healthy volunteers: a randomised crossover study. *Lancet* **356**, 556-561 (2000).

[180]Melchor, R., Biddiscombe, M.F., Mak, V.H., Short, M.D. & Spiro, S.G. Lung deposition patterns of directly labelled salbutamol in normal subjects and in patients with reversible airflow obstruction. *Thorax* **48**, 506-511 (1993).

[181]Pires, A., Fortuna, A., Alves, G. & Falcao, A. Intranasal drug delivery: how, why and what for? *J. Pharm. Pharm. Sci.* **12**, 288-311 (2009).

[182]Huang, C.H., Kimura, R., Nassar, R.B. & Hussain, A. Mechanism of nasal absorption of drugs I: Physicochemical parameters influencing the rate of in situ nasal absorption of drugs in rats. *J. Pharm. Sci.* **74**, 608-611 (1985).

[183]Corbo, D.C., Liu, J.C. & Chien, Y.W. Characterization of the barrier properties of mucosal membranes. *J. Pharm. Sci.* **79**, 202-206 (1990).

[184]Greiff, L., Wollmer, P., ErjefÃ¤lt, I., Pipkorn, U. & Persson, C.G. Clearance of 99mTc DTPA from guinea pig nasal, tracheobronchial, and bronchoalveolar airways. *Thorax* **45**, 841-845 (1990).

[185]Gerde, P., Muggenburg, B.A. & Henderson, R.F. Disposition of polycyclic aromatic hydrocarbons in the respiratory tract of the beagle dog. III. Mechanisms of the dosimetry. *Toxicol. Appl. Pharmacol.* **121**, 328-334 (1993).

[186]Brodin, B., Steffansen, B. & Nielsen, C. Passive diffusion of drug substances: the concepts of flux and permeability. In *Molecular Pharmaceutics*(eds. Brodin, B., Steffansen, B. & Nielsen, C.) 135-152 (Pharmaceutical Press, UK, 2010).

[187]Finlay, W.H. Lung Deposition Simulation. In *Pharmaceutical Inhalation Aerosol Technology*(ed. Hickey, A.J.) 155-170 (Marcel Dekker, Inc., New York, 2004).

[188]Zhang, L., Asgharian, B. & Anjilvel, S. Inertial Deposition of Particles in the Human Upper Airway Bifurcations. *Aerosol Science and Technology* **26**, 97-110 (1997).

[189]Ingham, D.B. Diffusion of aerosols from a stream flowing through a cylindrical tube. *J. Aerosol Sci.* **6**, 125-132 (1975).

[190]Zhang, L. & Yu, C.P. Empirical Equations for Nasal Deposition of Inhaled Particles in Small Laboratory Animals and Humans. *Aerosol Science and Technology* **19**, 51-56 (1993).

[191]Cheng, Y.S. Condensation detection and diffusion size separation techniques. In *Aerosol Measurement, Principles, Techniques and Applications*(eds. Baron, P.A. & Willeke, K.) 427-451 (Van Nostrand Reinhold, New York, 1993).

[192]Kesisoglou, F., Panmai, S. & Wu, Y. Nanosizing--oral formulation development and biopharmaceutical evaluation. *Adv. Drug Deliv. Rev.* **59**, 631-644 (2007).

[193]Sun, J., et al. Effect of particle size on solubility, dissolution rate, and oral bioavailability: evaluation using coenzyme Q(10) as naked nanocrystals. *Int. J. Nanomedicine* **7**, 5733-5744 (2012).

[194]Usmani, O.S. Exploring Aerosol Absorption in Humans: Pharmacokinetics of Monodisperse Fluticasone Propionate. **1**, 155-162 (2014).

[195]Brown, R.A.,Jr & Schanker, L.S. Absorption of aerosolized drugs from the rat lung. *Drug Metab. Dispos.* **11**, 355-360 (1983).

[196]Schanker, L.S., Mitchell, E.W. & Brown, R.A.,Jr. Species comparison of drug absorption from the lung after aerosol inhalation or intratracheal injection. *Drug Metab. Dispos.* **14**, 79-88 (1986).

[197]Diderichsen, P.M., Cox, E., Martin, S.W., Cleton, A. & Ribbing, J. Characterizing systemic exposure of inhaled drugs: application to the long-acting beta2-agonist PF-00610355. *Clin. Pharmacokinet.* **52**, 443-452 (2013).

[198]Del Donno, M., Bittesnich, D., Chetta, A., Olivieri, D. & Lopez-Vidriero, M.T. The effect of inflammation on mucociliary clearance in asthma: an overview. *Chest* **118**, 1142-1149 (2000).

[199]Borghardt, J.M., Weber, B., Staab, A., Kunz, C., Formella, S. & Kloft, C. Investigating pulmonary and systemic pharmacokinetics of inhaled olodaterol in healthy volunteers using a population pharmacokinetic approach. *Br. J. Clin. Pharmacol.* **81**, 538-552 (2016).

[200]AstraZeneca. Internal expertise. (2016).

Appendix A
Matlab code used for simulating repeated dosing

Main script:

```
% Main script used for simulating repeated dosing.
% It uses; pbpk_repeated_ode.m (contains ODEs)
% init_repeated.m (contains input parameters)
% computeClung.m (calculates Asolid, Clung and RO)

% Deposition model by Lee et al. is implemented

% Define solubility (Cs) in nM
Cs =5000;

% Define aerodynamic diameters in um
diameter=[6 3.9 2.4 1.5 0.92 0.59 0.39 0.2]; % Aerodynamic diameters

% Define mass fraction (f_m) corresponding to each aerodynamic
diameter
f_m=[0.1736 0.3008 0.2605 0.1760 0.0733 0.0091 0.0032 0.0035]; %
Mass fraction

% Define tau and the lung deposited dose (LDD)
tao=24; % tau in h
ldd=100; LDD in nmol/kg

% Gather all ldd in a vector to enable repeated dosing
LDD=[ldd ldd]

k=length(LDD) % Number of dosing occasions

% Load input parameters from file
% init_repeated automatically calculates deposition fractions for
the
% given aerodynamic diameters defined in 'diameter'
[ data ] = init_repeated( Cs, LDD, diameter, f_m);

% Assign how Papp relates to the permeability in the central and
% peripheral lung using p_c and p_p, respectively
% p_c=1 --> no difference; p_c=100 --> 100-fold lower
% p_p=1 --> no difference; p_p=0.01 --> 100-fold higher
p_c=1;
p_p=0.01;

% Error messages
msg = 'You cannot use more than 8 different particle sizes';
if max(length(diameter),length(f_m))>8
    error(msg)
    break
end

msg2 = 'The code currently supports up to 11 dosing occasions';
if k > 11
    error(msg2)
    break
```

```
end

x0 = data.x0;
Y = [];
T = [];

% Information needed for calculating indices for updating initial
% conditions (x0) in conjunction with repeated dosing

n_eq=3*length(diameter); %nr of eq to be added at each dosing
occasion
step=n_eq-1;

% Indices for updating x0
index1=[49:n_eq:49+24*(k-2)] % Start values
index2=[72:n_eq:72+24*(k-2)] % End values

tic;
for i = 1:k
%i = 1
    dt = [(i-1)*tao, i*tao];
    options=odeset('RelTol',1e-8);
    [t,y] = ode15s(@(t,x) pbpk_repeated_ode( t, x, data, tao, p_c,
p_p, k), dt, x0, options );
    Y = [Y; y];
    T = [T; t];
    x0 = y(end,:); % Update x0 by extracting the value of each state
y at
% t_end, i.e. y(t_end),last sim time point

    % Update initial values of radii from 0 to data.r_set prior to
simulating % dosing occasion i+1
    if i == 1 && k>=2
        x0(index1(1):index2(1))=[data.r_set data.r_set data.r_set];
    elseif i == 2 && k>=3
        x0(index1(2):index2(2))=[data.r_set data.r_set data.r_set];

    elseif i == 3 && k>=4
        x0(index1(3):index2(3))=[data.r_set data.r_set data.r_set];

    elseif i == 4 && k>=5
        x0(index1(4):index2(4))=[data.r_set data.r_set data.r_set];

    elseif i == 5 && k>=6
        x0(index1(5):index2(5))=[data.r_set data.r_set data.r_set];

    elseif i == 6 && k>=7
        x0(index1(6):index2(6))=[data.r_set data.r_set data.r_set];

    elseif i == 7 && k>=8
        x0(index1(7):index2(7))=[data.r_set data.r_set data.r_set];

    elseif i == 8 && k>=9
        x0(index1(8):index2(8))=[data.r_set data.r_set data.r_set];

    elseif i == 9 && k>=10
        x0(index1(9):index2(9))=[data.r_set data.r_set data.r_set];

    elseif i == 10 && k>=11
```

```
        x0(index1(10):index2(10))=[data.r_set data.r_set
data.r_set];
    end
end

% Simulate solid amount of drug (Asolid), receptor occupancy (RO)
and total lung conc (Clung_tot)
[Asolid_p, Asolid_c, Asolid_tot, RO_c, RO_sp, RO_ave,
Clung_tot]=computeClung( T, Y, data, tao, k);
toc


%% Figures

close all

figure(1)
semilogy(T,Y(:,7),'b-','LineWidth',1.5); hold on
ylabel('\it{C_p}\rm (nM)','FontName','Times New
Roman','FontSize',18);
xlabel('Time (h)','FontName','Times New Roman','FontSize',18);
title(['\it{C_p}\rm after inhalation, \it{C_{s}}\rm = ', num2str(Cs)
' nM'],'FontName','Times New Roman','FontSize',18); % after
inhalation
set(gca,'fontsize',12,'LineWidth',1.4)
axis([0 tao*k 0.0001 100]) %

figure(2)
plot(T,RO_c,'b--',T,RO_sp,'r-','LineWidth',1.5); hold on
legend('\it{RO_c}\rm','\it{RO_{sp}}\rm','Location','SouthEast');
ylabel('\it{RO}\rm (%)','FontName','Times New Roman','FontSize',18);
xlabel('Time (h)','FontName','Times New Roman','FontSize',18);
title(['\it{RO}\rm  after inhalation, \it{C_{s}}\rm = ', num2str(Cs)
' nM'],'FontName','Times New Roman','FontSize',18);
set(gca,'fontsize',12,'LineWidth',1.4)
axis([0 tao*k 0 100])

figure(3)
semilogy(T,Clung_tot,'b-','LineWidth',1.5); hold on
ylabel('\it{C_{lung}}\rm (nM)','FontName','Times New
Roman','FontSize',18);
xlabel('Time (h)','FontName','Times New Roman','FontSize',18);
title(['\it{C_{lung}}\rm after inhalation, \it{C_{s}}\rm = ',
num2str(Cs) ' nM'],'FontName','Times New Roman','FontSize',18); %
after inhalation
set(gca,'fontsize',12,'LineWidth',1.4)
xlim([0 k*tao])
ylim([1e-2 1e5])
```

Function containing coupled ODEs

```
% Coupled ODEs in the PBPK model
% pbpk_repeated_ode( t, x, data, tao, p_c, k)
% t=time; x=states; data=input parameters generated from
init_repeated.m;
% tao=tau; p_c=factor assigning how much lower the permeability is
in the
% central as compared to Papp; p_p=factor assigning how much
% lower the permeability is in the peripheral as compared to
Papp;k=number of dosing occasions

function [ xDot ] = pbpk_repeated_ode( t, x, data, tao, p_c, p_p, k)
Cs = data.Cs; % Solubility (nM)
fu_f = data.fu_f; % Unbound fraction in the fluid
factor_s = data.factor_s; %

n_p=length(data.f_m); % number of particle sizes, double definition
temp
r_n=length(data.f_m); % number of particle sizes
all_r=n_p*3; % number of particle sizes multiplied by number of
regions

% Initialise ODE vector xDot
% 24 ODEs describing tissue conc, receptor binding etc. + k*all_r
ODEs
% describing change of radii
xDot = zeros(24+(k*all_r),1);

%% Based on number of dosing occasions (k), automatically generate
index for the ODEs describing radii
%  in the nose, central lung and peripheral lung

% Step 1: Generate first index for each dosing occastion
nose_r_index = [25, (25+n_p*3):all_r:((k-1)*n_p*3)+25];
cent_r_index = [25+n_p, ((25+n_p)+n_p*3):all_r:((k-
1)*n_p*3)+25+n_p];
peri_r_index = [25+(n_p*2), ((25+(n_p*2))+n_p*3):all_r:((k-
1)*n_p*3)+25+(n_p*2)];

% Step 2: Create full set for each dosing occasion based on n_p (nr
of
% particle size classes)
nose_r_index = (nose_r_index')*ones(1,n_p) + ones(k,1)*(0:7); % Add
0:7 to the first index of each dosing occasion
cent_r_index = (cent_r_index')*ones(1,n_p) + ones(k,1)*(0:7);
peri_r_index = (peri_r_index')*ones(1,n_p) + ones(k,1)*(0:7);

% Step 3: Define the states describing the radius in the nose (r_n),
% the central lung (r_c) and the peripheral lung (r_p)
r_n = x(nose_r_index);
r_c = x(cent_r_index);
r_p = x(peri_r_index);

% Define the states describing the fluid concentrations
c_fluid = [x(22), x(23), x(24)]; % nose, central, peripheral

xb = 1.5e-6; % Break-point for the radius in dm (150 nm)
```

```
s = xb/factor_s;

% Create empty matrices for
% 1) dissolution of drug
diss_cent = zeros(k,n_p); %Central lung
diss_nose = zeros(k,n_p); %Nose
diss_peri = zeros(k,n_p); %Peripheral lung

% 2) transport of drug to gut absorption compartment with drug
% coming from either the nose (gut_n) or the central lung (gut_c)
gut_n = zeros(k,n_p);
gut_c = zeros(k,n_p);

% 3) ODEs describing change of radius in  the nose (rnDot),
% the central lung (rcDot) and the peripheral lung (rpDot)
rnDot = zeros(k,n_p);
rcDot = zeros(k,n_p);
rpDot = zeros(k,n_p);

% Create matrix of tau to use as input to equations
% Rows for dosing occasion (k) and columns for particle sizes (n_p)
Tau = (((1:k)-1)'*ones(1,n_p))*tao;

% Simulations of:

% 1) dissolution processes
diss_nose = noseEquation(c_fluid(1), r_n, data.N_n, t, Tau, data);
diss_cent = centEquation(c_fluid(2), r_c, data.N_c, t, Tau, data);
diss_peri = periEquation(c_fluid(3), r_p, data.N_p, t, Tau, data);

% 2) transport of drug to the gut absorption compartment
gut_n = gutEquation(r_n, ones(k,1)*data.r_set, data.N_n,
ones(k,1)*data.A_0_F, data.k_mcc_n, t, Tau, data);
gut_c = gutEquation(r_c, ones(k,1)*data.r_set, data.N_c,
ones(k,1)*data.A_0_F, data.k_mcc,   t, Tau, data);

% 3) size of radius during dissolution
rnDot = (Cs- (fu_f*c_fluid(1)) )*data.D/data.p  .*
mRadiusTerm(r_n,xb,s);
rcDot = (Cs- (fu_f*c_fluid(2)) )*data.D/data.p  .*
mRadiusTerm(r_c,xb,s);
rpDot = (Cs- (fu_f*c_fluid(3)) )*data.D/data.p  .*
mRadiusTerm(r_p,xb,s);

% Define ODEs describing change of radius wrt both index and
equations
xDot(nose_r_index) = rnDot;
xDot(cent_r_index) = rcDot;
xDot(peri_r_index) = rpDot;

% ODEs for organs: x(1)=Cspleen; x(2)=Crichly; x(3)=Cpoorly;
x(4)=Cadi;
% x(5)=C_gut; x(6)=Chepatic; x(7)=Cartery; x(8)=Cvein
xDot(1) = ( data.Q_s*(x(7) -(data.b_p*x(1)/data.Kp_s)) -
data.V_s*(data.Kon*(x(1)/data.Kp_s_u)*(data.Bmax_sp-x(11)) -
data.Koff*x(11)) )/data.V_s;
xDot(2) = ( data.Q_richly*(x(7) -(data.b_p*x(2)/data.Kp_richly)) -
data.V_richly*(data.Kon*(x(2)/data.Kp_richly_u)*(data.Bmax_all-
x(12)) -data.Koff*x(12)) )/data.V_richly;
```

```
xDot(3) = ( data.Q_poorly*(x(7) -(data.b_p*x(3)/data.Kp_poorly)) -
data.V_poorly*(data.Kon*(x(3)/data.Kp_poorly_u)*(data.Bmax_all-
x(13)) -data.Koff*x(13)) )/data.V_poorly;
xDot(4) = ( data.Q_adi*(x(7) -(data.b_p*x(4)/data.Kp_adi)) -
data.V_adi*(data.Kon*(x(4)/data.Kp_adi_u)*(data.Bmax_all-x(14)) -
data.Koff*x(14)) )/data.V_adi;
xDot(5) = ( data.Q_g*(x(7) -(data.b_p*x(5)/data.Kp_g))
+data.ka*x(17)  -
data.V_g*(data.Kon*(x(5)/data.Kp_g_u)*(data.Bmax_all-x(15)) -
data.Koff*x(15)) )/data.V_g;
xDot(6) = ( data.Q_g*(data.b_p*x(5)/data.Kp_g) + data.Q_h*x(7)
+data.Q_s*(data.b_p*x(1)/data.Kp_s)-
(data.Q_h+data.Q_s+data.Q_g)*(data.b_p*x(6)/data.Kp_h) -
data.V_h*(data.Kon*(x(6)/data.Kp_h_u)*(data.Bmax_all-x(16)) -
data.Koff*x(16)) )/data.V_h;
xDot(7) = (data.Q_CO*( (data.b_p*x(21)/data.Kp_l) -x(7)) )
/data.V_art ; %C_artery
xDot(8) = (-data.CL_eh*x(8) -data.Q_richly*(x(8)-
(data.b_p*x(2)/data.Kp_richly)) -data.Q_poorly*(x(8)-
(data.b_p*x(3)/data.Kp_poorly)) -
(data.Q_h+data.Q_g+data.Q_s)*(x(8)-(data.b_p*x(6)/data.Kp_h) )...
- data.Q_bronch*(x(8)-(data.b_p*x(20)/data.Kp_l)) -data.Q_n*(x(8)-
(data.b_p*x(19)/data.Kp_n)) -data.Q_adi *(x(8) -
(data.b_p*x(4)/data.Kp_adi) ))/data.V_vein; %C_vein

% ODEs for binding kinetics
xDot(9) =data.Kon*(x(20)/data.Kp_l_u)*(data.Bmax-x(9)) -
data.Koff*x(9); % RD_C
xDot(10) =data.Kon*(x(21)/data.Kp_l_u)*(data.Bmax-x(10)) -
data.Koff*x(10); % RD_P
xDot(11) =data.Kon*(x(1)/data.Kp_s_u)*(data.Bmax_sp-x(11)) -
data.Koff*x(11); % RD_spleen
xDot(12) =data.Kon*(x(2)/data.Kp_richly_u)*(data.Bmax_all-x(12)) -
data.Koff*x(12); % RD_richly
xDot(13) =data.Kon*(x(3)/data.Kp_poorly_u)*(data.Bmax_all-x(13)) -
data.Koff*x(13); % RD_poorly
xDot(14) =data.Kon*(x(4)/data.Kp_adi_u)*(data.Bmax_all-x(14)) -
data.Koff*x(14); % RD_adi
xDot(15) =data.Kon*(x(5)/data.Kp_g_u)*(data.Bmax_all-x(15)) -
data.Koff*x(15); % RD_gut
xDot(16) =data.Kon*(x(6)/data.Kp_h_u)*(data.Bmax_all-x(16)) -
data.Koff*x(16); % RD_hepatic

% ODE describing change of drug amount in the gut absorption
compartment
xDot(17) = sum(sum(gut_c)) + sum(sum(gut_n)) -data.ka*x(17);

% x(18) is not coupled to anyother ODE and xDot(18) can thus be used
for looking at specific questions
xDot(18) = sum(sum(diss_cent))+sum(sum(diss_peri)); %

% ODEs for the nose, central lung tissue and peripheral lung tissue
xDot(19) = ( data.A_nose*data.P*(fu_f*x(22)-x(19)/data.Kp_n_u) +
data.Q_n* (x(7)-(data.b_p*x(19)/data.Kp_n)) )/data.V_n; %C_diss_nose
xDot(20) = ( data.A_c*data.P/p_c*(fu_f*x(23)-x(20)/data.Kp_l_u)
+data.Q_bronch *(x(7) -(data.b_p*x(20)/data.Kp_l)) -
data.V_lung_C*(data.Kon*(x(20)/data.Kp_l_u)*(data.Bmax-x(9)) -
data.Koff*x(9)) )/data.V_lung_C;
xDot(21) = ( data.A_p*data.P/p_p*(fu_f*x(24)-x(21)/data.Kp_l_u) +
data.Q_CO*(x(8)-(data.b_p*x(21)/data.Kp_l))-
```

```
data.V_lung_P*(data.Kon*(x(21)/data.Kp_l_u)*(data.Bmax-x(10)) -
data.Koff*x(10)) )/data.V_lung_P;

% ODEs for lining fluids
% x(22)=C_fluid_nose
xDot(22) =( (   sum(sum(diss_nose)) -data.A_nose*data.P*(fu_f*x(22)-
x(19)/data.Kp_n_u)) )/data.V_n_fluid;
% x(23)=C_ELF_C
xDot(23) =( sum(sum(diss_cent))...
           -data.A_c*data.P/p_c*(fu_f*x(23)-
x(20)/data.Kp_l_u))/data.V_ELF_C;
% x(24)=C_ELF_P
xDot(24) =( sum(sum(diss_peri))-data.A_p*data.P/p_p*(fu_f*x(24)-
x(21)/data.Kp_l_u))/data.V_ELF_P;
end
```

Functions called by pbpk_repeated_ode.m

Function for simulating drug dissolution in the nose

```
% Simulation of drug dissolution in the nose
% noseEquation(con, rad, N_part,t, t0, data)
% Input needed: con=Cfluid(t), rad=radius(t), N_part=number of
particles
% t=time, t0=tau, data=input parameters

function [c] = noseEquation(con, rad, N_part,t, t0, data)

c = (data.Cs- (data.fu_f*con) ).*(N_part.*exp(-data.k_mcc_n*(t-
t0))*data.D*4*pi.*rad);
```

Function for simulating drug dissolution in the central lung

```
% Simulation of drug dissolution in the central lung
% centEquation(con, rad, Npart, t, t0, data)
% Input needed: con=Cfluid(t), rad=radius(t), N_part=number of
particles
% t=time, t0=tau, data=input parameters

function [c] = centEquation(con, rad, Npart, t, t0, data)

c = (data.Cs-(data.fu_f*con) ).*(Npart.*exp(-data.k_mcc*(t-
t0))*data.D*4*pi.*rad);
```

Function for simulating drug dissolution in the peripheral lung

```
% Simulation of drug dissolution in the peripheral lung
% periEquation(con, rad, Npart, t, t0, data)
% Input needed: con=Cfluid(t), rad=radius(t), N_part=number of
particles
% t=time, t0=tau, data=input parameters

function [c] = periEquation(con, rad, Npart, t, t0, data)
c = (data.Cs- (data.fu_f*con) ).*(Npart.*data.D*4*pi.*rad);
```

Function for dealing with the numerically instability caused by 1/r(t) in the ODE describing the change of the radius , dr/dt

```
function [y] = mRadiusTerm(x,xb,s)

% x=radius; xb=break point; s=radius in circle defined as
xb/factor.s

y = -(x > xb)./(max(x,xb));

x_l= xb-s*cos(pi/2-atan(1/(xb^2)));

y_l = -1./xb+s*sin(pi/2-atan(1/(xb^2))); %

u=x-x_l;

% Compute angles
l1 = sqrt(x_l.^2+y_l^2); % pythagoras theorem, using that [xb yb] is
known
```

```
l2 = s; % radius in circle
l3 = sqrt(l1.^2-l2^2); % pythagoras theorem
gamma = atan(l2./l3);
kappa = atan(y_l./x_l);
beta = -gamma + kappa; %

x_f = x_l+sin(beta)*s; %


y = y + (x > x_f & (x <= xb)).*(y_l - sqrt(s^2-u.^2));

y = y + (x <= x_f & (x <= xb)).*(tan(beta)*x);
```

Function for calculating the total lung concentration (C_{lung}), the solid amount of drug (A_{solid}) and receptor occupancy (RO)

```
function [Asolid_p, Asolid_c, Asolid_tot, RO_c, RO_sp, RO_ave,
Clung_tot] = computeClung( t, y, data, tao, k)

% Calculation of total lung conc, receptor occupancy and solid
amount of
% drug

Cs = data.Cs;
fu_f = data.fu_f;
factor_L = data.factor_L;%
factor_s = data.factor_s;%

% Calculate occupancy
RO_c=100*y(:,9)./data.Bmax; %Receptor occupancy central lung
RO_p=100*y(:,10)./data.Bmax; %Receptor occupancy peripheral lung
RO_sp=100*y(:,11)./data.Bmax_sp; %Receptor occupancy spleen

% Calc of weighted average lung occupancy
f_cv=0.19; %Fraction calculated based on surface area and height of
epithelium
f_pv=1-f_cv; %fraction central lung volume
RO_ave=100*(f_pv*y(:,10)+f_cv*y(:,9))./data.Bmax;

% Initial amount in each particle at t=0 (nmol)
A_0=data.A_c0;

% Equations for A_solid in the central lung (A_solid_c),
% peripheral lung (A_solid_p),nose (A_solid_n)

n_p=length(data.f_m);
all_r=n_p*3;

nose_r_index = [25, (25+n_p*3):all_r:((k-1)*n_p*3)+25];
cent_r_index = [25+n_p, ((25+n_p)+n_p*3):all_r:((k-
1)*n_p*3)+25+n_p];
peri_r_index = [25+(n_p*2), ((25+(n_p*2))+n_p*3):all_r:((k-
1)*n_p*3)+25+(n_p*2)];

nose_r_index = (nose_r_index')*ones(1,n_p) + ones(k,1)*(0:7);
cent_r_index = (cent_r_index')*ones(1,n_p) + ones(k,1)*(0:7);
peri_r_index = (peri_r_index')*ones(1,n_p) + ones(k,1)*(0:7);

r_n = y(nose_r_index);
r_c = y(cent_r_index);
r_p = y(peri_r_index);

A_solid_c=[];

for j=1:k

    for i=1:n_p
    A_solid=data.N_c(j,i)*exp(-data.k_mcc*(t-tao*(j-
1)))*A_0(i).*((y(:,cent_r_index(j)+(i-
1))./data.x0(cent_r_index(1)+(i-1))).^3);
```

```
    A_solid_c(:,i,j)=A_solid;
    end

end

A_solid_p=[];
for j=1:k

    for i=1:n_p
    A_solid=data.N_p(j,i)*A_0(i).*((y(:,peri_r_index(j)+(i-
1))./data.x0(peri_r_index(1)+(i-1))).^3);
    A_solid_p(:,i,j)=A_solid;
    end

end

A_solid_n=[];
for j=1:k

    for i=1:n_p
    A_solid=data.N_n(j,i)*exp(-data.k_mcc_n*(t-tao*(j-
1)))*A_0(i).*((y(:,nose_r_index(j)+(i-
1))./data.x0(nose_r_index(1)+(i-1))).^3);
    A_solid_n(:,i,j)=A_solid;
    end

end

% Summarize over particle sizes and dosing occasions
per=sum(A_solid_p,2); % Sum the amount across all particle sizes for
each t
Asolid_p=sum(per,3);

cen=sum(A_solid_c,2); % Sum the amount across all particle sizes for
each t
Asolid_c=sum(cen,3);

% Summarize total solid amount of drug
Asolid_tot=Asolid_p+Asolid_c;

% Calculate total lung conc
% y(23) = C_ELF_c; y(24) = C_ELF_p
Alung_tot= (y(:,20).*data.V_lung_C) + (y(:,21).*data.V_lung_P) +
(y(:,23).*data.V_ELF_C) + (y(:,24).*data.V_ELF_P) + Asolid_tot;
%Total amount of drug in the lung
Clung_tot = Alung_tot/(data.V_lung+data.V_ELF_C+data.V_ELF_P);
%Total lung concentration, perhaps
V_lung_tot=V_lung+v_fluid(1)+v_fluid(2)

end
```

Function gathering all drug-, formulation- and system-specific parameters

```
function [ data ] = init_repeated( Cs, LDD, diameter, f_m,
parameters )
% Initial parameters are stored in data
% [ data ] = init_repeated ( Cs, LDD, diameter, f_m, parameters )
% Input needed: solubility (Cs); LDD=lung deposited dose;
% diameter=aerodynamic diameters; f_m=mass fractions of each
particle size
% class; parameters is not default input, only to be used in case of
% MC-simulations wrt the binding kinetics parameters

k=length(LDD); % Number of doses
data.factor_s = 4;%

data.Cs = Cs; % Solubility (nM)
data.f_m=f_m; % Mass fractions of each particle size

% Intravenous (iv) and intraarterial (ia) dosing
data.dose_iv=0; % IV-bolus dose
data.dose_ia=0; % ia dose

% System-specific parameters
data.k_mcc_n=0.2079;
data.k_mcc=0.0472;

% Input parameters
data.my=13.82816; %mol/(dm*h)
data.MW=500.6; % g/mol
data.p_g=715; %Density (g/dm3)
data.D=13.26*10^(-5)/(data.my^1.14*(data.MW/data.p_g)^0.589);
%Diffussion coefficient
data.p=1.430*10^9 ; %Density (nmol/dm3)

data.fu_f=1; % fu_fluid
data.Papp=46.9; %Papp (10^(-6) cm/s)
data.P_app=data.Papp*10^(-6);
data.P=3600/10*data.P_app; %Papp unit conversion
data.fu=0.016; % Unbound fraction in plasma
data.b_p=0.95; % Blood-plasma ratio
data.ka=5; % Absorption rate constant
data.F=0; % Oral bioavailability

% Binding kinetics FP
data.Kd_FP=0.0150934; %(nM) Value from modeling of FP-IV
data.Koff=0.510892; %(h-1) Value from modeling of FP-IV
data.Kon=data.Koff/data.Kd_FP;

if nargin > 4
    data.Koff = parameters(1);
    data.Kd_FP = parameters(2);
end

% Receptor density
data.Bmax=21; %Receptor density in the lung (nmol/L)
data.Bmax_sp=31.5; %Receptor density in the spleen (nmol/L)
data.Bmax_all=23; %Mean value brain Bmax
```

```
%Kp-values FP
data.Vu_lung=213.4;
data.kp_factor=1.93;
data.Kp_h=data.kp_factor*5.293087;
data.Kp_s=data.kp_factor*2.686034;
data.Kp_richly=data.kp_factor*4.8;
data.Kp_poorly=data.kp_factor*3.990;
data.Kp_l=data.Vu_lung*data.fu;
data.Kp_g=data.kp_factor*10.50719;
data.Kp_adi=data.kp_factor*65.32998;
data.Kp_n=data.Vu_lung*data.fu;

%Kp,u-values
data.Kp_h_u=data.Kp_h/data.fu;
data.Kp_s_u=data.Kp_s/data.fu;
data.Kp_richly_u=data.Kp_richly/data.fu;
data.Kp_poorly_u=data.Kp_poorly/data.fu;
data.Kp_l_u=data.Kp_l/data.fu;
data.Kp_g_u=data.Kp_g/data.fu;
data.Kp_adi_u=data.Kp_adi/data.fu;
data.Kp_n_u=data.Kp_n/data.fu;

% Blood flows
% 1) Fraction of cardiac-output, fi. From Gearhart et al. 1990
unless stated otherwise
data.f_n=0.0015; % A hybrid CFD-PBPK model
data.f_h=0.024;  % Brown et al.
data.f_s=0.0715 ; % Kaufman et al 1996
data.f_richly=0.5096; % Sum of Qrichly+Qkidney+Qbrain Gearthart et
al.
data.f_g=0.14; % Delp et al
data.f_bronch=0.021; %Brown et al.
data.f_adi=0.009302; %Arundel:0.4 mL/min of 43 mL/min as QCO.
data.f_poorly=1-
(data.f_h+data.f_s+data.f_richly+data.f_bronch+data.f_g+data.f_adi+d
ata.f_n);
data.f_tot=data.f_h+data.f_s+data.f_richly+data.f_poorly+data.f_bron
ch+data.f_g+data.f_adi+data.f_n;

% 2) Blood-flows, Qi
data.Q_CO=20.77; % Gearthart et al 1990 (4.57 L/h / 220 g rat)
data.Q_n=data.Q_CO*data.f_n;
data.Q_h=data.Q_CO*data.f_h;
data.Q_s=data.Q_CO*data.f_s;
data.Q_g=data.Q_CO*data.f_g;
data.Q_richly=data.Q_CO*data.f_richly;
data.Q_poorly=data.Q_CO*data.f_poorly;
data.Q_bronch=data.Q_CO*data.f_bronch;
data.Q_adi=data.Q_CO*data.f_adi;

% Surface areas
data.A_nose=4*10.4*10^(-2) ; %Surface area nasal cavity, 10.4 cm2,
250 g rat.
data.A_c=1.08/0.330 ; % dm2, 108 cm2, tracheobronchial airways, 330
g rat
data.A_p=38.70/0.14 ; % dm2, 3870 cm2, alveolar region, 140 g rat

% Tissue volumes, Vi
data.v_fluid=lining_fluid; %v_fluid(1)=V_ELF_C;
v_fluid(2)=V_ELF_P;v_fluid(3)=V_lining_nose;
```

```
data.V_ELF_C=data.v_fluid(1);%A_c*5*10^(-5); %Assuming ELF thickness
5 um and continuous distribution
data.V_ELF_P=data.v_fluid(2);%A_p*d_peri*10^(-5); %Assuming ELF
thickness 0.07 um and continuous distribution
data.V_n_fluid=data.A_nose*5*10^(-5);

data.V_h=0.04; %Gearthart et al
data.V_s=0.002; %Brown et al.
data.V_art=0.02; %Gearhart et al
data.V_vein=0.04; %Gearhart et al
data.V_richly=0.0388; %Vrichly=Vkidney+Vrichly+Vbrain, Gearhart et
al
data.V_g=0.0259 ; %From Delp et al
data.V_adi=0.040; %Arundel 10 mL/250 g rat
data.V_lung=0.004127-(data.V_ELF_C+data.V_ELF_P); %4.127 g/kg from
100 animals, mean BW: 0.285 kg, removing VELF
data.V_n=data.A_nose*61*10^(-5); % Volume nasal mucosa, 0.2538 mL,
comparison ET-volume taken from GastroPlus 0.046 mL TEMP!
data.V_poorly=1-
(data.V_h+data.V_s+data.V_art+data.V_vein+data.V_richly+data.V_lung+
data.V_g+data.V_adi+data.V_n+data.V_n_fluid+data.V_ELF_C+data.V_ELF_
P);

% Calculation of central and peripheral lung tissue volumes
data.lung_vol=lung_volume(data.V_lung); %lung_vol(1)=V_lung_C;
lung_vol(2)=V_lung_P
data.V_lung_C=data.lung_vol(1); %Volume of central lung tissue
data.V_lung_P=data.lung_vol(2); %Volume of peripheral lung tissue

% Calculation of CL_blood based on CL_plasma and B:P-ratio
% Extrahepatic CL to add up to obs CL
data.CL_pl=10.95; %Plasma CL
data.CL_bl=data.CL_pl/data.b_p; %CL blood
data.CL_eh=data.CL_bl;
data.CL_h=0;

%Initial geometric radius expressed in dm
x=diameter;

p_g=data.p_g/1000; % Normalise to g/cm3
n=length(x);

% Calculation of geometric radius (note: x is diameter)
r=[];
for i=1:n
    r(i)=x(i)/2*10^(-5)/sqrt(p_g);
end

% Define vector data.x0 of initial values

% Step 1: Initiate vector of 24 zeros for the 24 first states
(tissue conc, RD etc.)
set_1=zeros(1,24); % 24 zeros
set_initial=set_1;

% Step 2: Extract states where x(0) can be different from 0
set_initial(7)=data.dose_ia/data.V_art; % C_arterial(0)
set_initial(8)=data.dose_iv/data.V_vein; % C_vein(0)
set_initial(18)=0; % Agut(0)
```

```
% Step 3: Define initial values of geometric radii
data.r_set=r;

% Step 4: Define data.x0, length of data.x0 defined by number of
dosing
% occasions, k
data.x0=zeros(1,(24+k*24));
data.x0(1,1:(24+n*3))=[set_initial data.r_set data.r_set
data.r_set];

% Calculate number of particles initially deposited in the nose
(data.N_n),
% central (data.N_c) and peripheral lung (data.N_p)

data.N_n=[];
data.N_c=[];
data.N_p=[];

for i=1:k
data.N_n(i,:)=number_n_test(LDD(i), data.f_m, diameter, data.p_g,
data.p);
data.N_c(i,:)=number_c_test(LDD(i), data.f_m, diameter, data.p_g,
data.p);
data.N_p(i,:)=number_p_test(LDD(i), data.f_m, diameter, data.p_g,
data.p);
end

% Possibility to check data.N_x
data.N_n;
data.N_c;
data.N_p;

[row col]=size(data.N_n);

% Initial amount in each particle at t=0 (nmol)
data.A_c0=amount_particle(diameter, data.p_g, data.p);

% Include F here to account for bioavailability
data.A_0_F=data.A_c0.*data.F;

% k=number of dosing occasions;n=number of particle size classes

data.m_cen=zeros(k,n); % Changed from 8 to n
for j=1:k
    for i=1:n
        data.m_=data.A_c0(i)*data.N_n(j,i);
        data.m_cen(j,i)=data.m_;
    end
    data.dep_n(j)=sum(data.m_cen(j,:));
end

data.m_c_lung=zeros(k,n);

for j=1:k
    for i=1:n
        data.m_=data.A_c0(i)*data.N_c(j,i);
        data.m_c_lung(j,i)=data.m_;
    end
```

```
    data.dose_c(j)=sum(data.m_c_lung(j,:));
end

data.m_p_lung=zeros(k,n);

for j=1:k
    for i=1:n
        data.m_=data.A_c0(i)*data.N_p(j,i);
        data.m_p_lung(j,i)=data.m_;
    end
data.dose_p(j)=sum(data.m_p_lung(j,:));
end

for j=1:k
data.dd_region(j,:)=[data.dep_n(j) data.dose_c(j) data.dose_p(j)];
end% deposited dose in each region

end



function [lining_fluids]=lining_fluid()
% Returns lining fluid volumes [V_ELF_C,V_ELF_P,V_n_fluid]
format long
% Surface areas
A_nose=4*10.4*10^(-2) ; %Surface area nasal cavity, 10.4 cm2, 250 g
rat.
A_c=1.08/0.330 ; % dm2, 108 cm2, tracheobronchial airways, 330 g rat
A_p=38.70/0.14 ; % dm2, 3870 cm2, alveolar region, 140 g rat

% Tissue volumes, Vi
d_peri=0.07; %Byron and Patton
V_ELF_C=A_c*5*10^(-5); %Assuming ELF thickness 5 um and continuous
distribution
V_ELF_P=A_p*d_peri*10^(-5); %Assuming ELF thickness 0.07 um and
continuous distribution
V_n_fluid=A_nose*5*10^(-5);
lining_fluids=[V_ELF_C,V_ELF_P,V_n_fluid];
end

function [V_lung_k]=lung_volume(V_lung)
% Returns regional tissues volumes based on total tissue volume
% (V_lung), [V_lung_C V_lung_P]
% V_lung=0.004127; %4.127 g/kg from 100 animals, mean BW: 0.285 kg
format long
f_cv=0.19; %Fraction calculated based on surface area and height of
epithelium
f_pv=1-f_cv; %fraction central lung volume

% Calculation of central and peripheral lung tissue volumes
V_lung_C=f_cv*V_lung; %Volume of central lung tissue
V_lung_P=f_pv*V_lung; %Volume of peripheral lung tissue

V_lung_k=[V_lung_C V_lung_P];
end
```

Functions called by init_repeated.m

Function used for calculating the amount in each particle

```
function [A_zero]=amount_particle(diameter, p_g, p_mol)
% Calculation of amount in each particle at t=0
% [A_zero]=amount_particle(diameter, p_g, p_mol)
% diameter=aerodynamic diameter (um); p_g=density in g/dm3

x=diameter;

p_g=p_g/1000; % Normalise to g/cm3
n=length(x);

% Calculation of geometric radius (note: x is diameter)
r=[];
for i=1:n
    r(i)=x(i)/2*10^(-5)/sqrt(p_g);
end

% Calculate volumes
V=zeros(1,8);
for i=1:8
V_=(4*pi*r(i)^3)/3;
V(i)=V_;
end

A_zero=zeros(1,8);
for i=1:8
A_=V(i)*p_mol;
A_zero(i)=A_;
end
```

Function used for calculating the number of particles in the central lung (same principle applied for both lung regions and the nose)

```
function [N_zero_c]=number_c_test(LDD, f_m, x, p_g, p_mol)
% Calculation of numbers of particles deposited centrally
% [N_zero_c]=number_c_test(LDD, f_m, x, p_g, p_mol)
% LDD = lung deposited dose; f_m = mass fraction; x = aerodynamic
diameter
% (um); p_g = density in g/dm3; p_mol = density in nmol/dm3

p_g=p_g/1000; % Normalise to g/cm3
n=length(x);

% Calculation of geometric radius (note: x is diameter)
r=[];
for i=1:n
    r(i)=x(i)/2*10^(-5)/sqrt(p_g);
end
r;

% Extract deposition fraction given aerodynamic diameter x
% 1) Define breathing conditions for deposition model
V_T=2.6; % Tidal volume (mL) Lee et al.
f_br=97.4; % Breathing frequency (min-1)
```

```
% 2) Run deposition model (for simplicity, the model code for the
deposition is attached as a separate appendix)
[et tb a] = get_df_lee(x, V_T, f_br);

% Probability of peripheral deposition
f_dep=a;
% Probability of central deposition
f_dep_c=tb;
% Probability of nasal deposition
f_dep_n=et;

% Calculate prob of lung deposition in both c and p lung
lung_dep=zeros(1,n);
for i=1:n
    lung_dep_=f_m(i)*f_dep(i)+f_m(i)*f_dep_c(i);
    lung_dep(i)=lung_dep_;
end
lung_dep_sum=sum(lung_dep);

% Density
p=p_g; % g/dm3
p_mol=p_mol; % Density (nmol/dm3)

% Calculate volumes
V=zeros(1,n);
for i=1:n
V_=(4*pi*r(i)^3)/3;
V(i)=V_;
end

dose_inh=LDD/lung_dep_sum; % Calc of inhaled dose

% Calculate number of particles initially deposited centrally
N_zero_c=zeros(1,n);
for i=1:n
N_=f_m(i)*f_dep_c(i)*dose_inh/(V(i)*p_mol);
N_zero_c(i)=N_;
end

m_zero=zeros(1,n);
for i=1:n
    m_=N_zero_c(i)*V(i)*p_mol;
    m_zero(i)=m_;
end
total_m_cen=sum(m_zero);
end
```

Appendix B

Matlab implementation of regional drug deposition (Lee *et al*)

Main function for calculating drug deposition

```
function [df_et df_tb df_al] = get_df_lee(da, V_T, f_br)
% Input: areodynamic diameter, da, [um]; tidal volume, V_T [mL]
% and breathing frequency, f_br [min-1]
% default values V_T=2.6 mL; f_br=97.4 min-1

% Function for calculating deposition in the lung after rodent
inhalation
% "Particle deposition in juvenile rat lungs: A model study" by Lee
et al.
% Anatomy values for 81-day old rats
% To couple to repeated dosing

load('anat_2.mat') % anatomy data from Lee et al.

% The model automatically transforms the anatomy based on V_T and BW
ANAT = anat_2;

% Extract anatomical input from the data set
i_gen=ANAT(:,1);
N_i=ANAT(:,2);
L_i=ANAT(:,3);
D_i=ANAT(:,4);
D_i_eff=ANAT(:,5);
V_i=ANAT(:,6);
cum_Vi=ANAT(:,7);
phi=ANAT(:,8); % Angle 1
theta=ANAT(:,9); % Angle 2

% Conversion from degrees to radians
phi=phi.*(pi/180);
theta=theta.*(pi/180);

%% Breathing conditions and anatomy

%V_T=2.6; %Tidal volume [cm3] from Lee et al.
%f_br=97.4; % Breathing frequency (1/min) from Lee et al.
V_min=V_T*f_br; % Minute respiration [cm3/min]
Q=V_min*2/60; % Inhalation flow rate according to Schmid et al;
Q=2*Vmin [cm3/s]

BW=381; %BW [g]

% Function for transforming volumes, diameters and length
% Possible to exclude transformation of i=1:2 (Schmid et al)
[L_i_scaled, D_i_scaled, f_scale, D_i_eff_scaled, imax, cum_Vi_2,
V_i_2]=calcV(D_i,L_i,N_i,V_T,BW,D_i_eff,cum_Vi,V_i);

% Anatomy data for the nose; transformation based on f_scale
L_n=1.95*f_scale; % Length, cm. Lee et al
H_n=0.016*f_scale; % Height, cm. Lee et al.
W_n=5.7*f_scale; % Width, cm. Lee et al.

% Unscaled values
```

```
L_i_unscaled=L_i;
D_i_unscaled=D_i;

% Choose input values
L_i=L_i_scaled;
D_i=D_i_scaled;
D_i_eff=D_i_eff_scaled;

%% Particle input parameters

% Unit particle density
po=1000; % 1 g/cm3 = 1000 kg/m3

%% Calculation of airflow (Q_i), velocity (v_i) and mean residence
time (t_i)

[v_i,t_i,Q_i]=airflow(L_i,D_i,N_i,Q);

% Transformation of v_i and Q_i to SI-units
v_i=v_i./100; % from cm/s to m/s
Q_i=Q_i./1e6; % from cm3/s to m3/s. Note, to nasal impaction, cm3/s
should be used, otherwise m3/s.

% Get deposition parameters
[Cd,vg,Dp,ne,pa,Dmol]= get_parameters(da,po); % Dmol = Dp

% Row 2 and 3 in IMP_i equals zero due to theta=0, sin(theta)=0
[stk,mu,re,eps]=Deposition_equation_parameters_lee(da,po,ne,v_i,D_i,
Dp,t_i,pa,vg,phi,D_i_eff,Cd);

% Deposition according to Lee et al.
[IMP_i, SED_i,DIF_i]=deposition_probability2(stk,re,theta,eps,D_i,
D_i_eff,L_i,v_i,Dmol);

% Calculate nasal deposition; (IMP_n remains to be implemented
properly)
[DIF_n IMP_n SED_n mu_n]=nose(L_n,W_n,H_n,Q_i(1),Dmol, da);

DEP_n=DIF_n + IMP_n + SED_n;

% Add nasal deposition to the pulmonary deposition fractions
IMP_i(1,:)=IMP_n;
SED_i(1,:)=SED_n;
DIF_i(1,:)=DIF_n;

%% Change size of V_i and cum_Vi if imax<26 (maximum nr of
generations)

V_i_2=V_i_2(1:imax);
cum_Vi_2=cum_Vi_2(1:imax);
IMP_i=IMP_i(1:imax,:);
SED_i=SED_i(1:imax,:);
DIF_i=DIF_i(1:imax,:);

%% Calculate resulting deposition fractions

 [ df, DEP_in, DEP_ex, f_conv ] = dfCalc2( IMP_i, SED_i, DIF_i,
V_i_2, da, imax );
```

```
size(df);

df_et=sum(df(1:2,:));
df_tb=sum(df(3:18,:));
df_al=sum(df(19:26,:));

end
```

Functions called by get_df_lee.m

Function for scaling the anatomy

```
function [L_i_scaled, D_i_scaled, f_scale, D_i_eff_scaled, imax,
cum_Vi_2, V_i_2]=calcV(D_i,L_i,N_i,V_T,BW,D_i_eff,cum_Vi,V_i)
% Calculation of scaled lengths (L_i_scaled), diameters (D_i_scaled)
% and volumes (V_i_scaled) based on the scale factor f_scale, which
is
% calculated based on BW and tidal volume (V_T)
% Note that V_i_scaled(1) needs to be calc separately since it is
not a cylinder
% Schmid et al only scales i=3:26 whereas Lee scales i=1:26

% Calculation of scale factor (f_scale)
TLC=0.032*BW^1.05; % Total lung capacity [cm3]
f_scale=((0.4*TLC+0.5*V_T)/TLC)^(1/3); %Scale factor

% Calculation of scaled volumes, i=1:2 not scaled by Schmid et al
% Lee appears to have scaled the nose and the pharynx as well

L_i_scaled=L_i.*f_scale;
%L_i_scaled(1:2)=L_i(1:2); % Schmid et al
D_i_scaled=D_i.*f_scale;
%D_i_scaled(1:2)=D_i(1:2); % Schmid et al
D_i_eff_scaled=D_i_eff.*f_scale;

r_i=D_i_scaled./2;
A=pi.*(r_i).^2;

V_i_scaled=N_i.*A.*L_i_scaled;

%V_i_scaled(1:2)=V_i(1:2); % Schmid et al

% Scaled nose and pharynx volumes
V_i_scaled(1)=0.1770*(f_scale^3);
V_i_scaled(2)=0.17180*(f_scale^3);

% Calculation of last ventilated generation, imax

% 1) Calculate cumulative lung volume, sum_Vi
sum_Vi=[];
for i=1:length(V_i)
    sum_Vi(i)=sum(V_i_scaled(1:i));
end

% 2) Test logical conidition: V_T > sum_Vi
true=V_T>sum_Vi;
[min_value index]=min(true); %index gives generation when V_cum >
V_T

if index==1 % If V_T never exceeds sum_Vi all generations are
ventilated
    imax=26;
else
    imax=index;
end

% 3) Adapt volume of imax such that sum_Vi=V_T by changing L_imax
```

```
% as done by Schmid et al
V_i_scaled(imax)=V_T-sum_Vi(imax-1);
L_i_imax=V_i_scaled(imax)/(N_i(imax)*A(imax));
L_i_scaled(imax)=L_i_imax;

% Update cumulative V, i.e. sum_V_i
for i=1:length(V_i)
    sum_Vi(i)=sum(V_i_scaled(1:i));
end
sum_Vi=sum_Vi;

% Change name of variables
cum_Vi_2=sum_Vi;
V_i_2=V_i_scaled;

% If imax < 26, set arbitrarily V to i > imax (will not be used)

for i = 1:26
    if i<=imax
        cum_Vi_2(i)=cum_Vi_2(i);
    elseif i>imax
        cum_Vi_2(i)=cum_Vi_2(imax);
    end
end
```

Function for calculating air velocity, mean residence time and flow

```
function [v_i,t_i,Q_i]=airflow(L_i_scaled,D_i_scaled,N_i,Q)
% Calcultion of air velocity (v) and residence time (t_i) in each
tube
% Prior to this, calculate the flow Qi for each generation i
% Use L_i_scaled and D_i_scaled as input

Q_i=Q./N_i; % Unit Q [cm3/s]
A_i=pi.*(D_i_scaled./2).^2; % [cm2] A=r^2*pi
v_i=Q_i./A_i; % [cm/s]
t_i=L_i_scaled./v_i; % Mathematically the same as below [s]

end

%V_scaled=N_i*A_i.*L_i_scaled;
%t_i=V_scaled./Q_i;
```

Function for getting parameters

```
function [Cd,vg,Dp,ne,pa,Dmol]= get_parameters(da,po)
% po=unit density; da=aerodynamic diameter
% cd=cummingham slip correction factor; vg=gravitational settling
velocity
% of a particle [m/s]; Dp=Dmol=particle diffusion constant [m2/s];
% ne=viscosity of air [kg/m/s]; pa=density of air (kg/m3)
% Use SI-units consistently

da=da.*10^-6; % Transformation from um to m

k = 1.38064852*10^-23 ; % boltzmann constant [m^2·kg/(s^2·K)]
T = 273.15+37.5; %311.05; % absolute temp, 37.5 degree Celcius
(range 37-37 degree C)
```

```
ne = 1.9224364E-5;% viscosity of air at 37.5 dgr C [kg/m/s]
(1.846*10^-5 kg/m/s at 300K)
g = 9.81;% gravitational acceleration [m/s^2]
pa = 1.1372; % density of air 37.5 degr C [kg/m3];
http://www.gribble.org/cycling/air_density.html
lamda=0.066*10^-6; % 0.066 um,
http://myweb.uiowa.edu/tpeters/IH1/Aerosols/AerosolFormulae.pdf

% Calculations
Cd= 1 + (lamda./da).*(2.514+0.8*exp(-0.55*(da./lamda))); % from Lee
et al.
Dp =(k*T.*Cd)./(3*pi*ne.*da); % particle diffusion constant [m2/s]
vg = (po.*((da.^2).*g.*Cd)./(18*ne)); % gravitational settling
velocity of a particle
Dmol=(k*T.*Cd)./(3*pi*ne.*da); %Brownian diffusion coefficient
[m2/s]

end
```

Function for calculating parameters necessary for the deposition equations

```
function
[stk,mu,re,eps]=Deposition_equation_parameters_lee(da,po,ne,v_i,D_i,
Dp,t_i,pa,vg,phi,D_i_eff,Cd)
% calculation of deposition parameters: eps, mu reynolds number and
stokes
% number

% D_i_eff to be used for calc of eps if i>18

% Unit transformations
% v_i already written in the correct units
da=da.*10^-6; % Transformation from um to m
D_i=D_i.*10^-2; % Transformation from cm to m
D_i_eff=D_i_eff.*10^-2; % Transformation from cm to m

stk=[];
mu=[];
re=[];
eps=[];

for j=1:length(da)
    for i=1:length(v_i)

            stk(i,j)=po*(da(j)^2)*v_i(i)/(9*ne*D_i(i));
            re(i,j)=pa*D_i(i)*v_i(i)/ne;
           mu(i,j)=Dp(j)*t_i(i)/(D_i(i)^2);
        if i <= 18
            eps(i,j)=3*vg(j)*t_i(i)*sin(phi(i))/(4*D_i(i));
        else
            eps(i,j)=3*vg(j)*t_i(i)*sin(phi(i))/(4*D_i_eff(i));
        end
    end
end

end

% eps = par in sedimentation equation
```

```
% mu = par in diffusion equation (not used by Lee et al but by
Schmid)
% re = Reynolds number
% stk= stokes number
```

Function used for calculating the deposition probability for the three included deposition mechanisms: inertial impaction, gravitational sedimentation and brownian diffusion

```
function [DEP_i, SED_i,
DIF_i]=deposition_probability2(stk,re,theta,eps, D_i,
D_i_eff,L_i,v_i,Dmol)

% Unit transformations
D_i=D_i.*10^-2; % Transformation from cm to m
D_i_eff=D_i_eff.*10^-2; % Transformation from cm to m
L_i=L_i*10^-2; % Transformation from cm to m

DEP_i=[];
SED_i=[];
DIF_i=[];
test=[];
[n m]=size(stk); % n=number of gen; m=number of particle sizes

for j=1:m
    for i=1:n
        if stk(i,j)<0.04

DEP_i(i,j)=0.000654*exp(55.7*stk(i,j)^0.954)*re(i,j)^(1/3)*sin(theta
(i));
        else
DEP_i(i,j)=(0.19...
-0.193*exp(9.5*stk(i,j)^1.565))*re(i,j)^(1/3)*sin(theta(i));
        end
    end
end

for j=1:m
    for i=1:n
        if i==1
            SED_i(i,j)=0;
        else
        SED_i(i,j)=2/pi*(2*eps(i,j)*(1-eps(i,j)^(2/3))^(1/2)...
        -(eps(i,j)^(1/3))*(1-eps(i,j)^(2/3))^(1/2)...
            +asin(eps(i,j)^(1/3)));
        test(i,j)=asin(eps(i,j)^(1/3));
        end
    end
end

% In the alveoli region (i>=19) D=(D_i+D_i_eff)/2
D_i_d=D_i;
D_ex=(D_i+D_i_eff)/2;
D_i_d(19:26)=D_ex(19:26);

for j=1:m
    for i=1:n
    delta(i,j)=Dmol(j)*L_i(i)/(v_i(i)*(D_i_d(i)^2));
```

```
    DIF_i(i,j)=1-0.819*exp(-14.63*delta(i,j))-0.0976*exp(-
89.22*delta(i,j))-0.0325*exp(-228*delta(i,j))...
        -0.0509*exp(-125.9*delta(i,j)^(2/3));
    end
end
```

Function for calculating drug deposition in the nose

```
function [DIF_n IMP_n SED_n mu_n]=nose(L,W,H,Q1,Dmol,da)

% Unit transformation from cm to m (L,W and H are given in cm)
L=L*0.01;
W=W*0.01;
H=H*0.01;

mu_n=8*Dmol.*L*W./(3*Q1*H);

[xx n_da]=size(da);

DIF_n=zeros(1,n_da);
for i=1:n_da
    if mu_n(i) < 0.05
        DIF_n(i)=1.526*mu_n(i)^(2/3)-0.15.*mu_n(i)-
0.0342.*mu_n(i)^(4/3);
    else
        DIF_n(i)=1-( 0.9104*exp(-2.8278.*mu_n(i)) + 0.0531*exp(-
32.147.*mu_n(i))...
        +0.01528*exp(-93.475.*mu_n(i)) + 0.00681*exp(-
186.805.*mu_n(i)));
    end
end

% Impaction, simplified formula

al=2.553;
beta=0.627;
C=10^5;

Q1_im=Q1*1e6; % m3/s to cm3/s

da2Q=(da.^2).*Q1_im;
% units da [um], Q [cm3/s]; Hence, da does not need unit
transformation

IMP_n=(da2Q.^al./(C+(da2Q.^al))).^beta;

% Nasal deposition by sedimentation negligible
[n,m]=size(IMP_n);
SED_n=zeros(n,m);
```

Function used for calculating the resulting deposition fraction

```
function [ df, DEP_in, DEP_ex, f_conv ] = dfCalc2( IMP, SED, DIF, V,
da, imax )
% Calculation of resulting deposition fractions

% Calculation of resulting probability P
P = 1-(1-IMP).*(1-SED).*(1-DIF);
```

```
% Convection factor for the alveolar region (i=19:26) Lee et al.
f_conv = 1+0.5*(log10(da)-log10(2)).*(log10(da)-
log10(0.02))./((log10(0.1)-log10(2))*(log10(0.1)-log10(0.02)));
f_conv(da < 0.02) = 1;
f_conv(da > 2) = 1;

N_g = imax; % Nr of generations
N_p = size(P,2); % Nr of particle sizes

% Augment P to compute fi, set the first row to 0
% --> first row in fi should equal 1 (nothing has deposited when
entering the nose)
P_hat = [zeros(1,N_p); P];

% fi should consist of 27 rows (N_g+1)
f = zeros(N_g+1,N_p);

% prod returns the product of each column
for i = 1:(N_g+1)
    f(i,:) = prod([ones(1,N_p);1-P_hat(1:i,:)]);
end

% Clone V into a matrix
V = V(:)*ones(1,N_p);

% Create alpha, see definition below
% fi(1)=1; fi(2)=(1-P1); fi(3)=(1-P1)(1-P2) etc.
% term 2 exhalation starts with: f(i+3)*V(i+2)
% term 1 exhalation starts with: f(i+2)*V(i+1)
alpha = [f(3:end,:).*V(2:end,:)];

% Exhalation, no deposition in gen 26
x = zeros(N_g, N_p);

% x defines all that flows, the probability for deposition is taken
into account afterwards in DEP_ex: DEP_ex(i)=P(i)*x(i)

% At i = 25 alpha(25) = fi(27)*Vi(26), i.e. (1-P1)...(1-P26)*Vi(26)
% --> x(26,:) = 0
% --> x(25,:) = (1-P26)*0        + (1-P1)...(1-P26)*Vi(26)
% --> x(24,:) = (1-P25)*x(25,:)  + fi(26)*Vi(25)
% --> x(23,:) = (1-P24)*x(24,:) + fi(25)*Vi(24)

for i = N_g-1:-1:1 % 25 to 1

    x(i,:) = (1-P(i+1,:)).*x(i+1,:) + alpha(i,:);

end

DEP_ex = x.*P;

% Inhalation
% Create vector of cumulative volumes (take away V that stays in
each generation)
sum_V=zeros(length(N_g),1);
for i = 1:N_g
    V2=flipud(V(:,1));
    sum_V(i)=sum(V2(1:(N_g+1-i)));
end
```

```
DEP_in = zeros(N_g, N_p);
for j = 1:N_p
    DEP_in(:,j) = f(1:end-1,j).*P(:,j).*sum_V';
end

% Result:
df = (DEP_in + DEP_ex)/sum(V(1:imax,1));
df(19:imax,:) = df(19:imax,:).*(ones((imax-18),1)*f_conv);
```

Appendix C

Summary of PBPK model ODEs

This appendix summarises the ODEs used in the PBPK model. Please note that all abbreviations are provided at the end of this appendix.

ODEs describing the change of drug concentrations in the systemic tissues and the blood:

$$V_{sp}\frac{dC_{sp}}{dt}=Q_{sp}\left(C_A(t)-\frac{RC_{sp}(t)}{K_{p,sp}}\right)-V_{sp}\left(K_{on}\left(B_{\max,sp}-RD_{sp}(t)\right)\frac{C_{sp}(t)}{K_{p,u,sp}}-K_{off}RD_{sp}(t)\right),\quad C_{sp}(0)=0$$

$$V_{ri}\frac{dC_{ri}}{dt}=Q_{ri}\left(C_A(t)-\frac{RC_{ri}(t)}{K_{p,ri}}\right)-V_{ri}\left(K_{on}\left(B_{\max,ave}-RD_{ri}(t)\right)\frac{C_{ri}(t)}{K_{p,u,ri}}-K_{off}RD_{ri}(t)\right),\quad C_{ri}(0)=0$$

$$V_{po}\frac{dC_{po}}{dt}=Q_{po}\left(C_A(t)-\frac{RC_{po}(t)}{K_{p,po}}\right)-V_{po}\left(K_{on}\left(B_{\max,ave}-RD_{po}(t)\right)\frac{C_{po}(t)}{K_{p,u,po}}-K_{off}RD_{po}(t)\right),\quad C_{po}(0)=0$$

$$V_{adi}\frac{dC_{adi}}{dt}=Q_{adi}\left(C_A(t)-\frac{RC_{adi}(t)}{K_{p,adi}}\right)-V_{adi}\left(K_{on}\left(B_{\max,ave}-RD_{ri}(t)\right)\frac{C_{adi}(t)}{K_{p,u,adi}}-K_{off}RD_{adi}(t)\right),\quad C_{adi}(0)=$$

$$V_h\frac{dC_h}{dt}=Q_hC_A(t)+Q_g\frac{RC_g(t)}{K_{p,g}}+Q_{sp}\frac{RC_{sp}(t)}{K_{p,sp}}-(Q_h+Q_{sp}+Q_g)\frac{RC_h(t)}{K_{p,h}}\ldots$$

$$-V_h\left(K_{on}\left(B_{\max,ave}-RD_h(t)\right)\frac{C_h(t)}{K_{p,u,h}}-K_{off}RD_h(t)\right),\quad C_h(0)=0$$

$$V_g\frac{dC_g}{dt}=Q_g\left(C_A(t)-\frac{RC_g(t)}{K_{p,g}}\right)+k_aA_{gut}(t)-V_g\left(K_{on}\left(B_{\max,ave}-RD_g(t)\right)\frac{C_g(t)}{K_{p,u,g}}-K_{off}RD_g(t)\right),\quad C_g(0)=$$

$$V_A\frac{dC_A}{dt}=Q_{CO}\left(\frac{RC_{lung,p}(t)}{K_{p,lung}}-C_A(t)\right),\quad C_A(0)=0$$

$$V_{ve}\frac{dC_{ve}}{dt}=-\sum_{i=1}^{5}Q_i\left(C_{ve}(t)-\frac{RC_i(t)}{K_{p,i}}\right)-(Q_h+Q_{sp}+Q_g)\left(C_{ve}(t)-\frac{RC_h(t)}{K_{p,h}}\right)-CLC_{ve}(\mathrm{t}),\quad C_{ve}(0)=0$$

where *i* assigns the following five tissue compartments: nose, central lung, richly perfused tissue, poorly perfused tissues and adipose tissue.

ODEs describing pulmonary and nasal drug disposition

a) ODEs describing the change of drug concentrations in the lining fluids

There are eight different particle size classes in the model, hence the ODEs describing the change of concentration in the nasal lining fluid ($C_{fluid,n}$), the central epithelial lining fluid ($C_{fluid,c}$) and the peripheral epithelial lining fluid ($C_{fluid,p}$) will be as follows:

$$V_{fluid,n}\frac{dC_{fluid,n}}{dt}=\sum_{i=1}^{8}\left(N_{n,i}(t)4\pi r_{n,i}(t)D(C_s-C_{fluid,n}(t)f_{u,fluid})\right)...$$
$$-PA_{surf,n}\left(C_{fluid,n}(t)f_{u,fluid}-\frac{C_n(t)}{K_{p,u,n}}\right),\quad C_{fluid,n}(0)=0$$

$$V_{fluid,c}\frac{dC_{fluid,c}}{dt}=\sum_{i=1}^{8}\left(N_{c,i}(t)4\pi r_{c,i}(t)D(C_s-C_{fluid,c}(t)f_{u,fluid})\right)...$$
$$-PA_{surf,c}\left(C_{fluid,c}(t)f_{u,fluid}-\frac{C_{lung,c}(t)}{K_{p,u,lung}}\right),\quad C_{fluid,c}(0)=0$$

$$V_{fluid,p}\frac{dC_{fluid,p}}{dt}=\sum_{i=1}^{8}\left(N_{p,i}4\pi r_{p,i}(t)D(C_s-C_{fluid,p}(t)f_{u,fluid})\right)...$$
$$-PA_{surf,p}\left(C_{fluid,p}(t)f_{u,fluid}-\frac{C_{lung,p}(t)}{K_{p,u,lung}}\right),\quad C_{fluid,p}(0)=0$$

b) ODEs describing the change of drug concentrations in the nose and lung

The ODEs describing the concentration in the central lung tissue ($C_{lung,c}$), the peripheral lung tissue ($C_{lung,p}$) and the nose (C_n).

$$V_{lung,c}\frac{dC_{lung,c}}{dt}=PA_{surf,c}\left(C_{fluid,c}(t)f_{u,fluid}-\frac{C_{lung,c}(t)}{K_{p,u,lung}}\right)+Q_{br}\left(C_A(t)-\frac{RC_{lung,c}(t)}{K_{p,lung}}\right)...$$
$$-V_{lung,c}\left(K_{on}\left(B_{\max,lung}-RD_c(t)\right)\frac{C_{lung,c}(t)}{K_{p,u,lung}}-K_{off}RD_c(t)\right),\quad C_{lung,c}(0)=0$$

$$V_{lung,p}\frac{dC_{lung,p}}{dt}=PA_{surf,p}\left(C_{fluid,p}(t)f_{u,fluid}-\frac{C_{lung,p}(t)}{K_{p,u,lung}}\right)+Q_{CO}\left(C_{ve}(t)-\frac{RC_{lung,p}(t)}{K_{p,lung}}\right)...$$
$$-V_{lung,p}\left(K_{on}\left(B_{\max,lung}-RD_p(t)\right)\frac{C_{lung,p}(t)}{K_{p,u,lung}}-K_{off}RD_p(t)\right),\quad C_{lung,p}(0)=0$$

$$V_n\frac{dC_n}{dt}=PA_{surf,n}\left(C_{fluid,n}(t)f_{u,fluid}-\frac{C_{lung,n}(t)}{K_{p,u,n}}\right)+Q_n\left(C_A(t)-\frac{RC_n(t)}{K_{p,n}}\right),\quad C_n(0)=0$$

c) ODE describing the change of the radius:

$$\frac{dr_{j,i}}{dt} = \frac{D}{\rho} f(r_{j,i})(C_s - C_{fluid,j}(t) f_{u,fluid}), \quad r_{j,i}(0) = r_i$$

where *j* assigns the region (i.e. nose, central lung or peripheral lung) and *i* assigns the particle size class. A detailed description of $f(r_{j,i})$ is provided in section '5.2.1.3 Dissolution of drug', particularly by eq. 5.23.

ODE describing the change of drug amount in the gut absorption compartment A_{gut}:

$$\frac{dA_{gut}}{dt} = k_{mcc,lung} \times F \times A_{solid,c}(t) + k_{mcc,nasal} \times F \times A_{solid,n}(t) - k_a A_{gut}(t), \quad A_{gut}(0) = 0$$

ODE describing receptor binding in tissue compartment *i*:

$$\frac{dRD_i(t)}{dt} = \left(K_{on}\left(B_{\max,i} - RD_i(t)\right)\frac{C_i(t)}{K_{p,u,i}} \right) - K_{off} RD_i(t)$$

where *i* assigns the following tissues: central lung, peripheral lung, liver, spleen, gut, richly perfused tissues, poorly perfused tissues and adipose tissue.

Abbreviations:

C_x=concentration of drug in tissue compartment *x*; V_x=tissue volume of *x*; Q_x=blood flow to *x*; *R*=blood/plasma ratio; $K_{p,x}$= tissue-plasma partition coefficient; K_{on}=association rate constant; K_{off}=dissociation rate constant; $B_{max,x}$=receptor density in *x*; $K_{p,u,x}$=tissue-to-unbound plasma partition coefficient; RD_x=concentration of drug-receptor complex in *x*; A_{gut}=the amount of drug in the gut absorption compartment; k_a=oral absorption rate constant; $k_{mcc,lung}$=mucociliary clearance rate constant in the lung; $k_{mcc,nasal}$=mucociliary clearance rate constant in the nose; *F*=oral bioavailability; $N_{j,i}$=number of particles of size class *i* in region *j*; A_i=amount of drug in a particle of size class *i*; $r_{j,i}$=radius of a particle of size class *i* in region *j*; *CL*=clearance; $C_{fluid,j}$=concentration of drug in the epithelial lining fluid (ELF) or the nasal lining fluid; $f_{u,fluid}$=unbound fraction in ELF or the nasal lining fluid; *D*=diffusion coefficient; C_s=solubility of the drug; $A_{surf,j}$=surface area in region *j*; ρ=particle density

Subscripts:

sp=spleen; ri=richly perfused tissues; po=poorly perfused tissues; adi=adipose tissues; h=hepatic; g=gut; A=arterial; ve=venous; lung,p=peripheral lung tissue; lung,c=central lung tissue; n=nose; CO=cardiac output; c=central; p=peripheral